



HAL
open science

Anisotropic 1D/2D NMR in Molecular Analysis

Philippe Lesot, Roberto R. Gil

► **To cite this version:**

Philippe Lesot, Roberto R. Gil. Anisotropic 1D/2D NMR in Molecular Analysis: Contributions and Opportunities of Anisotropic 1D/2D NMR to Recent Analysis of Small Organic Molecules. K. Ivanov; P.K. Madhu; G. Rajalakshmi. Two-Dimensional (2D) NMR Methods, Wiley, pp.209-296, 2023, 10.1002/9781119806721.ch9 . hal-04218745

HAL Id: hal-04218745

<https://hal.science/hal-04218745>



Submitted on 12 Jan 2024

HAL is a multi-disciplinary open access archive for the deposit and dissemination of scientific research documents, whether they are published or not. The documents may come from teaching and research institutions in France or abroad, or from public or private research centers.

L'archive ouverte pluridisciplinaire **HAL**, est destinée au dépôt et à la diffusion de documents scientifiques de niveau recherche, publiés ou non, émanant des établissements d'enseignement et de recherche français ou étrangers, des laboratoires publics ou privés.

Anisotropic 1D/2D NMR in Molecular Analysis


“Contributions and Opportunities of Anisotropic 1D/2D NMR to Recent Analysis of Small Organic Molecules”

Philippe Lesot^{1,*}  and Roberto R. Gil² 

¹Université Paris-Saclay, RMN en Milieu Orienté, ICMMO, UMR CNRS 8182, Bât. 410, F-91405 Orsay cedex, France.

²Department of Chemistry, Carnegie Mellon University, Pittsburgh, PA, USA.

 **Philippe Lesot:** orcid.org/0000-0002-5811-7530

 **Roberto R. Gil:** orcid.org/0000-0002-8810-5047

E-mail: philippe.lesot@university-paris-saclay.fr

Abstract

Contrarily to isotropic solutions, the molecular tumbling regime no longer exists in oriented solvents/media made of lyotropic liquid crystals (LLCs) or compressed/stretched gels. Under this condition, any analyte dissolved in these systems (chiral or not) adopt an orientational order with respect to the magnetic field of a NMR spectrometer. This leads to very informative intramolecular anisotropic NMR interactions such as the residual dipolar coupling (RDC), the chemical shift (RCSA) and finally the residual quadrupolar coupling (RQC) for spin $I > \frac{1}{2}$, that can be successfully exploited for many applications useful to chemists. In this Chapter 12, the various key theoretical and practical/technical aspects are presented as well as the spectral specificities of 1D/2D multinuclear NMR in weakly aligned chiral solvents (both LLCs and gels) using a large collection of chemically different organic analytes. Some additional concepts related to stereochemistry analysis (as chirality, prochirality or enantiotopicity) and their spectral consequences in anisotropic NMR are also examined. For illustrating the outstanding analytical potential of the anisotropic NMR spectroscopy, the most significant and contributive applications, such as the determination of enantiopurity of chiral mixtures, the study of the site-specific natural isotopic fractionation, the analysis of prochiral compounds or molecular dynamic processes. A special attention will be paid also to the recent and creative approaches developed for the structure and configuration elucidation based on RDC, RCSA and RQC observables or their combination. Key or pioneering examples will be examined.

Keywords:

Anisotropic NMR interactions,
Chirality,
Configuration
Enantiodiscrimination,
Oriented solvents,
Stereochemistry,
Structure analysis.

Table of contents

1. Introduction

2. Advantages of oriented solvents

2.1 Description of orientational order parameters

2.2 The GDO concept

3. Description of useful anisotropic NMR parameters

3.1 Residual dipolar coupling (RDC)

3.2 Residual chemical shift anisotropy (RCSA)

3.3 Residual quadrupolar coupling (RQC)

3.4 Spectral consequences of enantiodiscrimination

- *Chirality and prochirality*

- *NMR in LLCs*

4. Adapted 2D NMR tools

4.1 Spin-1/2 based 2D experiments

4.2 Spin-1 based 2D experiments

5. Examples of polymeric liquid crystals

5.1 Polypeptide or polyacetylene-based systems

5.2 Compressed and stretched gels

5.3 Polynucleotide-based chiral oriented media

5.4 Some practical aspects of polymer-based LLCs preparation

6. Contribution to the analysis of chiral or prochiral molecules

6.1 Analysis and enantiopurity determination of chiral mixtures

- *Proton NMR*

- *Carbon-13 NMR*

- *Deuterium NMR*

- *Combined anisotropic ^2H and ^{13}C NMR*

6.2 Discrimination of enantiotopic elements in prochiral structures

6.3 Dynamic analysis by ^2H NMR

- *Case of cis-decalin*

- *Determination of the activation barrier energy*

- *Reaction monitoring*

- *Ultrafast 2D NMR*

7. Structural value of anisotropic NMR parameters

7.1 From molecular constitution to configuration of complex molecules

- *Principle and process*

- *Hyphenated protocols*

7.2 Contribution of spin-1/2 NMR

- *Examples using (^{13}C - ^1H)-RDC*

- *Examples using ^{13}C -RCSA*

7.3 Configuration determination using spin-1 NMR analysis

- *Analysis of scalemic mixtures by ANAD 2D NMR*

- *First analysis of natural drugs by ANAD 2D NMR*

7.4 Determining the absolute configuration of monostereogenic chiral molecules

8. Conformational analysis in oriented solvents

9. Anisotropic ^2H 2D NMR applied to molecular isotope analysis

9.1 The natural ($^2\text{H}/^1\text{H}$) isotope fractionation: principle

9.2 Case of prochiral molecules: the fatty acid family

9.3 New tools for fighting against counterfeiting

9.4 Exploring the ($^{13}\text{C}/^{12}\text{C}$) isotope fractionation

10. Anisotropic NMR in molecular analysis: what you should keep in mind?

11. References and further reading

1. Introduction

Due to its variety of analytical possibilities and methodologies developed over the last three decades in solid or liquid phase, NMR spectroscopy has become a powerful and indispensable tool in modern Chemistry. [Emsley *et al.*, 1995] In this **Chapter**, we will address an original aspect of modern NMR dedicated to the analysis of small (achiral, prochiral and chiral) molecules using (weakly-orienting) ordered media as alternative NMR solvents. Interestingly, this approach combines the use of residual anisotropic NMR interactions (tensorial properties) observed in oriented environments (liquid crystals, liquid-crystalline solution, ordered phases) and the spectral advantages of high-resolution liquid-state NMR. In the literature, there are numerous publications describing the analysis of mesogenic molecules forming generally nematics mesophases (thermotropics) or solutes aligned in oriented phases. Without wishing to be exhaustive, the readers may take a look at some “reference” books dealing with this subject. [Burnell and Delange, 2003; Dong, 2004, 2010, 2012; Emsley, 1975; Veracini, 1985] In this chapter, we will use various terms to define ordered media, such as, anisotropic solvents, ordered liquids, aligning media or a combination of them.

In isotropic solutions, small molecules tumble rapidly and randomly, adopting all possible orientations with respect to the external magnetic field \mathbf{B}_0 (of NMR spectrometer) with the same probability on the NMR timescale, *i.e.* it does not possess any orientational order. This molecular tumbling regime no longer exists in oriented media, leading to very informative molecular anisotropic NMR interactions. These new interactions, which no longer average out by molecular tumbling as in isotropic liquid phases, are: i) the residual dipolar coupling (noted RDC or D), ii) the chemical shift (δ^{aniso}) through the residual chemical shift anisotropy (noted RCSA or $\Delta\sigma$), and iii) finally the residual quadrupolar coupling (noted RQC or $\Delta\nu_Q$).

We will, first, present the specificities of anisotropic/oriented NMR using weakly aligning media as well as the tools (the “spectral toolkit”) and NMR approaches to extract and exploit the anisotropic information involved in the analysis of small organic molecules of synthetic or natural origin. Among weakly-aligning media as useful anisotropic NMR solvents (opposed to thermotropic liquid crystals), we will mainly present the case of polypeptide-based lyotropic liquid crystals (such as PBLG or PCBL) and the polymeric aligning gels (such as PMMA or PolyHEMA). Key experimental examples illustrating the principles of anisotropic NMR have been selected to show the diversity of analyzable compounds in these systems, associated with a description of spectral information visible on their anisotropic spectra.

Then we will describe the challenges and the analytical opportunities of NMR in oriented solvents (chiral and non-chiral), such lyotropic liquid crystals or stretched/compressed gels, through key illustrative applications. The examples proposed will show how anisotropic 1D and 2D NMR can solve many analytical problems encountered by a large community of chemists. Throughout this Chapter we will show how 2D NMR methodologies provide solutions for simplifying complex anisotropic 1D spectra.

Finally, and beyond the description of NMR results in terms of spin system analysis (AX, AB, A₃, ...) as well as magnetic or chemical equivalence, we will also refer to various stereochemical aspects encountered routinely in organic chemistry (chirality, prochirality, diastereotopic and enantiotopic groups, etc.). While some aspects will be proposed in this Chapter, a more precise description of these important concepts can be found in the “Bible” of stereochemistry written by Eliel and Wilen. **[Eliel and Wilen, 1994]**

2. Advantages of oriented solvents

Discovered in 1888, liquid crystals (LCs) are fascinating molecules. **[Renitzer, 1888]** They show an interesting state of matter between solids and liquids (see **Figure 1a**), providing NMR spectroscopists with a wide variety of anisotropic environments (aligning media), with the advantages of combining solid-state NMR (SS-NMR) properties (through the detection of anisotropic observables) with those of liquid-state NMR (highly fluid solvents leading to high-resolution spectra). **[Dong, 2010; Emsley, 1975; Veracini, 1985]** In other words, NMR parameters only observed in solid state can be measured with the resolution obtained in liquid state. This unique “anisotropy-fluidity” combination is at the origin of a strong analytical potential that can be successfully exploited in modern molecular analysis.

Regardless of how the molecular order is created, the use of NMR in oriented media provides a possible access to: i) the determination the constitution, the configuration and the preferred conformation/s of the aligned guest molecules, ii) the study the orientational behaviour of solutes in relation to the solute-solvent interactions, and iii) the evaluation of the enantiomeric purity of a mixture of chiral molecules (enantiomers or enantio-isotopomers) or the discrimination of enantiotopic element in prochiral molecules if the oriented system is chiral, for instance.

The analytical success of anisotropic NMR lies in the ability of the liquid crystal mesophases (chiral or non-chiral) or the strained (stretched or compressed) aligning gels to orient a solute

homogeneously and uniformly inside the magnetic field (\vec{B}_0) of the NMR spectrometer. These unique properties lead to exploitable high-resolution NMR spectra, that can be combined with the ability to spectrally discriminate enantiomers (chiral molecules) or enantiotopic elements (prochiral molecules) if the aligning system is homochiral (eg. enantiopure). Herein, achiral and chiral liquid crystals will be denoted ALCs and CLCs, respectively.

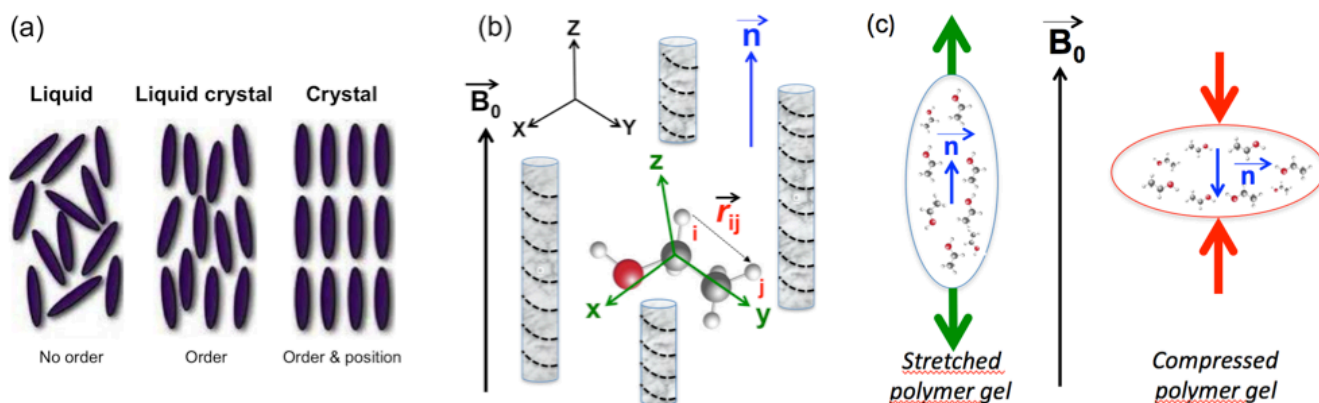


Figure 1. (a) Schematic description of the molecular orientational order in an isotropic liquid (no order, $S = 0$), a nematic liquid crystal (only order, $0 < S < 1$) and a crystalline solid (position and order with $S = 1$). (b) Example of a reference axis system (x , y and z) attached to a molecule dissolved in a chiral polymer-based LLC, and used for the description of molecular order. (c) Model description of stretched or compressed gels inducing a molecular order. **Figure partially adapted from Refs. [Lesot et al., 2020-a; Gil et al., 2017-a] with permission.**

A large collection of weakly aligning systems has been designed over the last two decades, both for water- and organo-soluble compounds. [Lesot et al., 2020-a; Tjandra and Bax 1997-a] These molecular systems are very interesting because they produce a weak degree of solute alignment, leading to residual anisotropic NMR interactions of small magnitude, in the order of 10^{-3} - 10^{-4} respect to the values observed in solid state. Contrarily, thermotropic liquid-crystalline phases, another family (historical) of oriented media, show a degree of order ~ 0.15 respect to solid state. Weak alignment reduces the complexity of NMR spectra and so the difficulty to record them. Among weakly-aligning mesophases, a special attention has been paid to the design of many chiral polymer-based liquid crystals (see Figure 1b), as well as the development of mechanically controlled compressed or stretched achiral gels (see Figure 1c). [Gayathri et al., 2010; Kuchel et al., 2006; Kummerlöwe et al., 2010] Compared to thermotropics, the lyotropic systems allow an easy control of global orientation of solutes by adjusting: i) the temperature of the sample, ii) the concentration of components of the mesophase, iii) the nature of the helical polymer, and iv) the polarity of the co-solvent (organo-soluble polymer). These four parameters afford a full control and easy optimization of the

properties of the mesophase in terms of solute orientation but also of difference in orientation (chiral molecules) if the system is enantiodiscriminating. For aligning gels, which are not chiral, the degree of alignment generally depends on: i) the cross-link density of the polymer gel, [Luy, 2005; Gil, 2008] and ii) the degree of stretching or compression which with the exception of polyacryamide gels, is reversible and can be tuned up and down at the user's whim. [Gayathri et al., 2010; Kuchel et al., 2006; Kummerlöwe et al., 2010]

2.1 Description of orientational order parameters

Phenomenologically, molecular orientation can be described using the Saupe's order matrix, a second-rank tensor (3×3) noted $\mathbf{S}_{\alpha\beta}$ or $\{S_{\alpha\beta}\}$ or \hat{S} , associated with a molecular (orthogonal) axis system x, y, z , whose internal elements ($\alpha\beta \equiv x, y, z$) can be individually expressed as: [Emsley, 1975]

$$S_{\alpha\beta} = \frac{1}{2} \langle 3 \cos \theta_Z^\alpha \cos \theta_Z^\beta - \delta_{\alpha\beta} \rangle. \quad (1)$$

In **Eq. 1**, $\delta_{\alpha\beta}$ is the Kronecker function ($\delta = 1$ if $\alpha = \beta$, and $\delta = 0$ if $\alpha \neq \beta$) and θ_Z^α are the angles between the axes, x, y and z and the Z axis of laboratory axis system (X, Y, Z). As a consequence, all order-dependent NMR interactions are tensorial properties related to these order parameters.

The Saupe's matrix has two important properties: i) it is symmetric ($S_{\alpha\beta} = S_{\beta\alpha}$) since the orientation can have two opposite directions, ii) it is traceless, i.e., the sum of its diagonal elements is null ($\sum S_{\alpha\alpha} = 0$), because no order exists in isotropic liquids. Expressed in an arbitrarily defined reference axis system (RAS) (see **Figure 1b**), the number of independent elements in $S_{\alpha\beta}$ is dependent on the symmetry of the analyte, as well as whether the oriented solvent is chiral or not. [Merlet et al., 1999-a] For instance, five (non-zero) order parameters are needed to describe the orientational behaviour of chiral molecules of C_1 symmetry, both in ALCs and CLCs. In contrast, for C_s -symmetry prochiral (rigid) molecules, three (non-zero) order parameters are needed in ALCs to describe their orientational ordering, but five are needed in CLCs. As we will discuss in **Section 3.4**, three other molecular symmetries (C_{2v} , D_{2d} and S_4) are also affected by the chirality of the solvent, thus leading to important spectral consequences.

From the matrix elements of $S_{\alpha\beta}$, we can derive any local order parameters, S_{ij} , associated with any internuclear direction, i - j , (the vector \vec{r}_{ij}) expressed in the molecular reference axis system (RAS) initially defined, (x, y, z) , (see **Figure 1b**) on the basis of the so-called director cosines following **Eq. 2: [Emsley, 1975; Lesot et al., 2020-a]**

$$S_{ij} = \sum_{\alpha, \beta=x,y,z} \cos \theta_{ij\alpha} \cos \theta_{ij\beta} S_{\alpha\beta} \quad (2)$$

Interestingly, the local order term, S_{ij} , can be also described as a simple trigonometric function defined as:

$$S_{ij} = \frac{1}{2} \langle 3 \cos^2 \theta_{ij}^{B_0} - 1 \rangle \quad (3)$$

where $\theta_{ij}^{B_0}$ is the angle between a given i - j internuclear vector (\vec{r}_{ij}) and the \vec{B}_0 axis. **Figure 2a** shows the variation of term, $3(\cos^2 \theta_{ij}^{B_0} - 1)/2$, vs. the $\theta_{ij}^{B_0}$ angle. As schematically

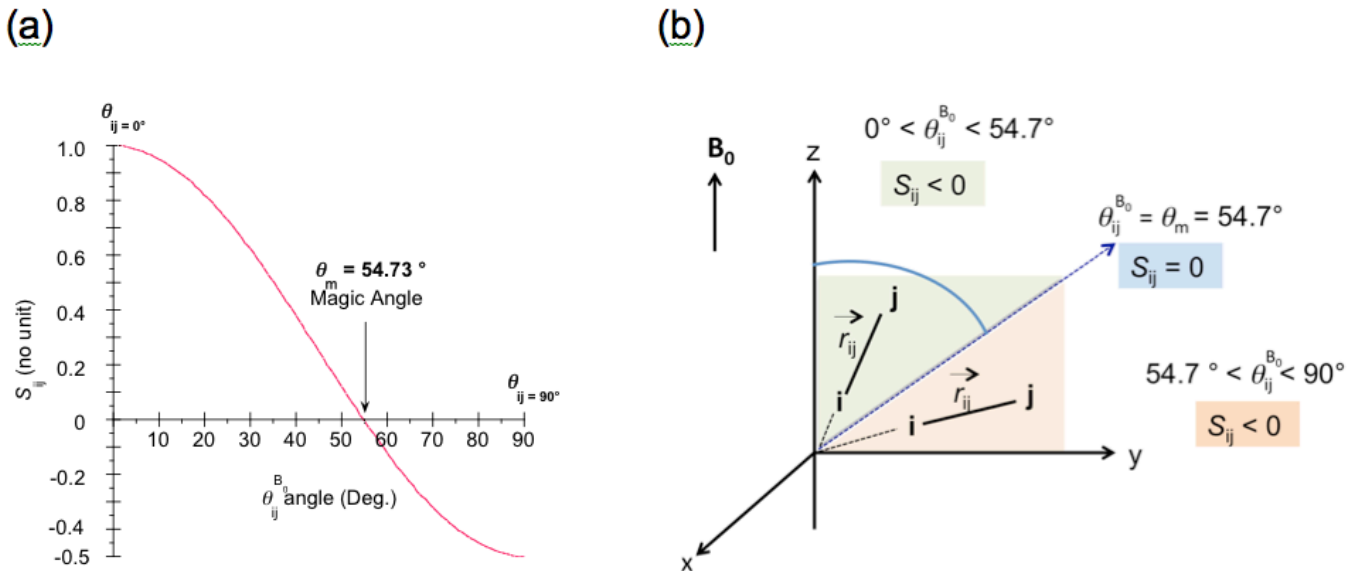


Figure 2. (a) Variation of the trigonometric term, $(3\cos^2\theta_{ij}^{B_0} - 1)/2$, versus angle $\theta_{ij}^{B_0}$. Note the famous magic angle, θ_m , for which the local order parameter, S_{ij} , is null. At $\theta_{ij}^{B_0} = \theta_m$, any $(^1\text{H}-^1\text{H})$ -RDCs or ^2H -RDCs are equal to zero. (b) Vectorial description of the position of an internuclear vector i - j (noted also \vec{r}_{ij}) relative to the axis \vec{B}_0 .

described in **Figure 2b**, the S_{ij} values are positive between $[0^\circ \leq \theta_{ij}^{B_0} < 54.73^\circ]$, negative between $[54.73^\circ < \theta_{ij}^{B_0} \leq 90^\circ]$, and null when $\theta_{ij}^{B_0} = 54.73^\circ$ (the so-called magic angle).

Remarkably, at $\theta_{ij}^{B_0} = \theta_m$, any RDC or RQC values are equal to zero (as in liquids), even if molecules are oriented in the field \mathbf{B}_0 .

Note, finally, that the Saupe matrix, $S_{\alpha\beta}$, can be also diagonalized. This matrix, noted $S_{\alpha'\beta'}$, expressed in the unique principal axis system (PAS) of the molecule (noted x' , y' , z') contains only three parameters, $S_{x'x'}$, $S_{y'y'}$ and $S_{z'z'}$ and as previously is traceless, $S_{x'x'} + S_{y'y'} + S_{z'z'} = 0$.

2.2 The GDO concept

In 2001, the concept of generalized degree of order (GDO) in the principal axis system has been introduced to describe the orientational order of an analyte using a single value (scalar quantity). GDO is defined as follows: [Tolman et al., 2001; Kramer et al., 2004]

$$\text{GDO} = \frac{|\mathbf{A}|}{|\mathbf{A}_{\max}|} = \sqrt{\frac{3}{2}} |\mathbf{A}| \quad (4)$$

where $|\mathbf{A}|$ is the norm of the alignment tensor, $\hat{\mathbf{A}}$, and $|\mathbf{A}_{\max}|$ represents the maximum order for a static molecule (solid state). Note here that the relation between the order matrix, noted, $\hat{\mathbf{S}}$, and the alignment tensor, noted $\hat{\mathbf{A}}$, is simply defined as $\hat{\mathbf{A}} = \frac{2}{3} \hat{\mathbf{S}}$. [Kramer et al., 2004] Since in the principal axis system (x' , y' , z'), only the diagonal elements of $\hat{\mathbf{A}}$ are non-zero, the above equation is reduced to:

$$\text{GDO} = \sqrt{\frac{3}{2}} \sqrt{|A_{x'x'}^2 + A_{y'y'}^2 + A_{z'z'}^2|} \quad (5)$$

For a static molecule, the GDO is equal to 1. The GDO is an indication of the degree of alignment induced by the orienting media. It cannot be calculated but it can be determined experimentally by first obtaining the alignment tensor \mathbf{A} from fitting anisotropic data (RDCs, RCSAs, RQCs) to the correct 3D structure. It is important to highlight that the degree of alignment also depends on the shape and size of the molecule. Molecules that are very small and close to a spherical shape align poorly. However, for a molecule that aligns well, the GDO is a good indication of the strength of alignment of a particular orienting media. The bigger the GDO, the stronger the alignment is. Aligning gels have a GDO in the order of 10^{-4} , while LLCs phase such PBLG it is in the order of 10^{-3} , compared to solid state (static molecule). If we know the order of the GDO we can predict the maximum value of RDCs, RCSAs and/or RQCs

that we should expect to observe experimentally. For instance, the maximum possible $^1D_{CH}$ solid state for a CH bond is when the bond is parallel to the magnetic field \mathbf{B}_0 . This value is -45.38 KHz. In a gel, with a GDO of $7.0 \cdot 10^{-4}$, a simple calculation of $[-45.38 \text{ KHz} \times 7.0 \cdot 10^{-4}]$ tells us that the maximum expected $^1D_{CH}$ would be of ~ 31.8 Hz with $r_{CH} = \sim 1.5 \text{ \AA}$ (see **Table 1**). As mentioned above, this value will also depend on the size and shape of the molecule. In conclusion, if we know the solid-state value of RDCs, RCSAs and RQC, we can estimate their maximum value in solution if we know the GDO.

3. Description of useful anisotropic NMR parameters

For any magnetically active nuclei ($I \neq 0$), chemical shifts (due to electronic shielding), δ^{iso} and (homo- or heteronuclear) scalar couplings between inequivalent nuclei (due to magnetic mutual interaction through bonds), J_{ij} , observed in isotopic liquids are two important informative sources of molecular data.

As in NMR in liquids, all non-zero spin nuclei of molecules dissolved in oriented media are also potential NMR probes for the three key anisotropic NMR interactions: i) the RDC's associated with the mutual dipole-dipole interaction between magnetically active nuclei through space, ii) the chemical shift (δ^{aniso}) through the RCSA's originating from the specific electronic shielding of nuclei, and iii) finally the RQC's resulting from the interaction between the electric quadrupolar moment of quadrupolar nuclei (spin $I > \frac{1}{2}$) and an electric field gradient. The value of these anisotropic parameters depends on the average orientation (at NMR time scale) of the molecules (and associated local internuclear directions) with respect to external magnetic field \mathbf{B}_0 (see **Figure 1b,c**).

Generally, the anisotropy of scalar coupling, ΔJ , the last anisotropic interaction is not considered because the anisotropic component of J is not as strong as for the three other interactions ($\Delta\delta$, D and $\Delta\nu_Q$), and its potential analytical use is only limited to very particular nuclei such as Fluorine-19.

3.1 Residual dipolar coupling (RDC)

The homo- or heteronuclear dipolar coupling between two chemically non-equivalent coupled nuclei, i and j , (an AX or AB spin system) vanishes in isotropic solution because the bonded or

non-bonded internuclear vectors (r_{ij}), E.g., “i–j” or “i···j”, adopt all the possible orientations (defined by the angle θ_{ij}) with respect to \mathbf{B}_0 with the same probability (molecular isotropic tumbling) (see **Figure 3**). [Kummerlöwe *et al.*, 2009; Emsley, 1975] In contrast, in the presence of an anisotropic medium, only a fraction of the dipolar coupling is observed (about 10^{-3} - 10^{-4}), hence the term “residual interaction”. The resulting coupling is known as residual dipolar coupling (noted RDC), but contain the same information than the dipolar coupling.

Mathematical description of RDCs (whatever the pair of mutually interacting nuclei) is presented with key equations 4 and 5. If an internuclear scalar coupling exists between two bonded nuclei, i and j , (J_{ij}), the signal observed (for i and j) shows a total splitting (named also “total spin-spin coupling”) equal to $T_{ij} = J_{ij} + 2D_{ij}$ (see **Figure 3**). As S_{ij} can be positive, negative or null (magic angle), the RDC values can be negative, positive, or null,

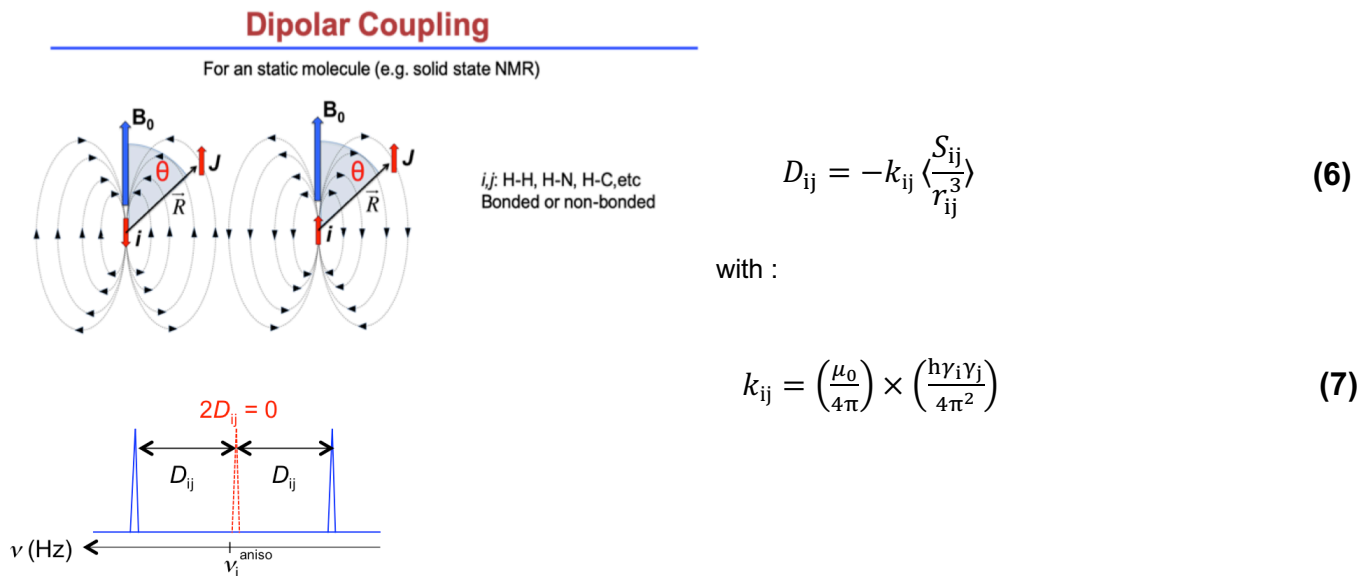


Figure 3. The origin of the dipolar coupling, D_{ij} , between two magnetically active nuclei, i and j , the spectral consequences for two inequivalent coupled nuclei (view on nucleus i), and associated equations to RDCs. In **Eq. 6**, S_{ij} and r_{ij} are the local order parameter of the internuclear direction, i – j , and the distance separating the two nuclei r_{ij} . In **Eq. 7**, μ_0 is the permeability constant in vacuum, and γ_i and γ_j are the gyromagnetic ratios of i and j . In the case of a mixture of enantiomers (R/S), a doubling of the spectral patterns (on *per* enantiomers) is expected to be observed if a spectral enantiodiscrimination occurs, while generally centered on the very close frequencies ($\delta^{\text{aniso}, R} \approx \delta^{\text{aniso}, S}$).

respectively. Depending on the magnitude and the sign of J_{ij} and D_{ij} , the final value of T_{ij} can be positive, negative or null. Note that in the literature, the total coupling, T_{ij} , can also be defined as $J_{ij} + D_{ij}$; this difference comes from the definition of dipolar coupling used (see **Eq. 6**). In this Chapter, we adopt the notation “ $2D_{ij}$ ” for the dipolar contribution to J_{ij} . RDCs provide information

of the relative orientation of internuclear vectors between an atomic pair (i and j) in a molecule. They can be bonded, such as C-H ($^1D_{CH}$), N-H ($^1D_{NH}$), C-F ($^1D_{CF}$), C-P ($^1D_{CP}$) bonds, but also non-bonded nuclei as geminal proton-proton pairs ($^{2,3}D_{HH}$), or two to three bonds carbon-proton pairs ($^{2,3}D_{CH}$). From a practical standpoint, the most widely used RDC for structural analysis of small molecules is the one-bond proton-carbon ($^1D_{CH}$), because it is easy to measure from F_2 - or F_1 -coupled HSQC 2D experiments. Although less often, geminal proton-proton RDCs ($^{2,3}D_{HH}$) and long-range 2-3 bond proton-carbon RDCs ($^{2,3}D_{CH}$) were occasionally used in addition to $^1D_{CH}$ data.

Other RDC's can be exploited if they are detected. E.g., $^1D_{CF}$ can be straightforwardly measured from the fluorinated carbon signal splitting in the $^{13}C\{-^1H\}$ 1D NMR spectra as the difference between the isotropic and anisotropic spectra. From **Eq. 6**, it can be noted that the magnitude of the RDC value, for a given θ angle and r_{ij} distance, will strongly depend on the term k_{ij} , that corresponds to the product of gyromagnetic ratio for two interacting nuclei and the inverse of the cube of the distance between them, $(r_{ij})^{-3}$. **Table 1** lists the most useful values of k_{ij} .

An interesting property of anisotropic NMR is that, different from the scalar coupling J , RDCs do not vanish under chemical equivalence. As a consequence, this unique property provides access to RDCs between equivalent nuclei, such as hydrogens inside a methyl group (A_3 spin system) and a methylene group (A_2 spin system), while their scalar coupling is not measured in NMR in liquids. For these both cases, purely dipolar splittings measured on the corresponding spectral patterns (a 1:2:1 triplet and a 1:1 doublet, respectively) is equal to $T_{ii} = 3D_{ii}$. These proton-proton RDCs within methyl or intramethylene groups can be easily measured in polypeptide/polyacetylenic-based systems but the situation is more difficult with aligning gels whose the degree of alignment is smaller (by at least a factor 10 or more) compared to previous systems. Indeed, if the spectral rules applied to analyze the anisotropic spectra are theoretically the same in the two families of orienting media, some practical differences can appear because all anisotropic interactions measured in alignment gels are generally one order of magnitude smaller than in PBLG, and leading to RDC values smaller than the linewidths for these particular cases. In general, any pair of protons close in space that have the same chemical shift, either by coincidence or by symmetry (A_2 , A_3 , ... A_n), will show a measurable RDCs in anisotropic conditions.

Table -1. Examples of k_{ij} values (with sign) involving nuclei ^1H , ^2H , ^{13}C , ^{19}F and ^{31}P , and ranked in decreasing order

Pair of interacting nuclei	k_{ij} values (kHz.A ³)	Sign ^a
^1H - ^1H	120.07	> 0
^1H - ^{19}F	199	> 0
^{19}F - ^{19}F	106.30	> 0
^1H - ^{31}P	48.62	> 0
^1H - ^{13}C	30.20	> 0
^{13}C - ^{19}F	28.41	> 0
^{31}P - ^{31}P	19.68	> 0
^1H - ^2H	18.44	> 0
^{13}C - ^{31}P	12.23	> 0
^{13}C - ^{13}C	7.59	> 0
^2H - ^{31}P	7.46	> 0
^2H - ^{13}C	4.64	> 0
^2H - ^2H	2.83	> 0

^a k_{ij} is negative when one of interacting atoms has a negative gyromagnetic ratio (E.g. ^{15}N).

Technically, one-bond (^{13}C - ^1H)-RDCs, ($^1D_{\text{CH}}$), are by far the easiest to measure on any NMR spectrometers with the help or not of adapted homo- or heteronuclear 2D experiments to extract information, even with small molar amounts of analyte. Followed by geminal (^1H - ^1H)-RDCs, ($^2D_{\text{HH}}$). Measuring other proton-proton RDCs is more challenging and barely used in structure elucidation of small molecules. One limitation exists, however, in the case of proton-deficient molecules. A peculiar situation in which ^{13}C -RCSAs play a relevant role because they can be measured for every carbon, even those not protonated, as we will show below.

3.2 Residual chemical shift anisotropy (RCSA)

In isotropic solutions, the chemical shift measured corresponds to the average value of the three main components of the chemical shift anisotropic tensor (see **Figure -4**). In the presence of an anisotropic medium, this average value is shifted, and the shift is known as RCSA. Same as RDCs, the RCSA values can be positive, negative or null, leading to a low- or high-field shift of resonances compared to isotropic ones. Mathematical descriptions of RCSAs (whatever the nuclei) are presented with the key equations **-8** to **10**. [Emsley, 1975; Lesot et al., 2020-a]

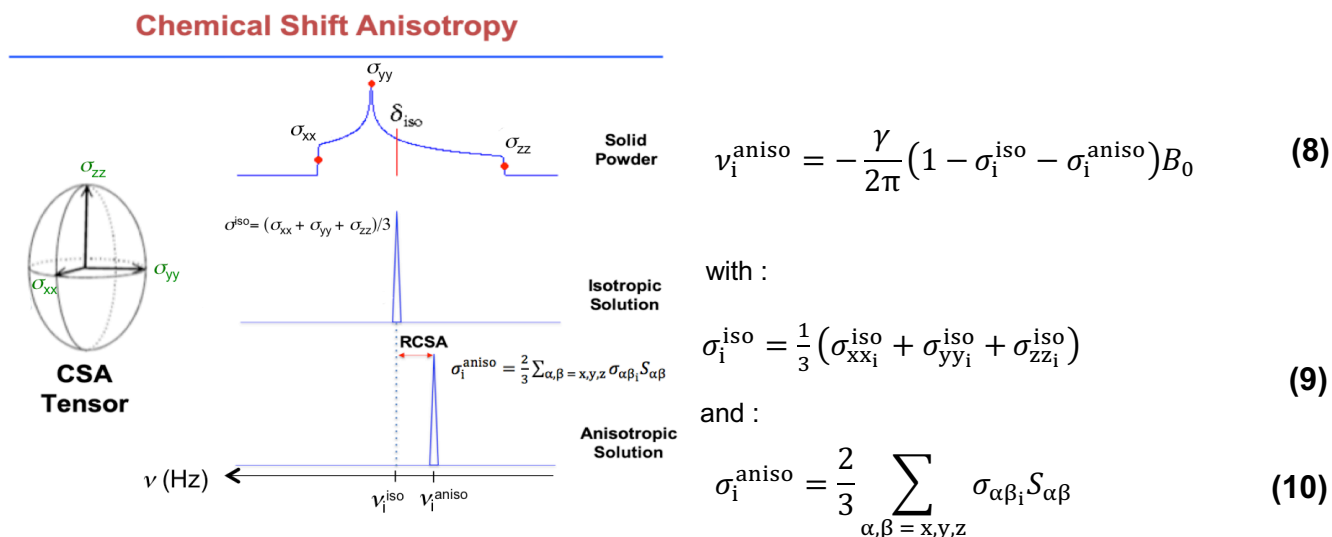


Figure 4. The origin of chemical shift anisotropy, σ^{aniso} , related to anisotropic distribution of electrons (CSA tensor), spectral consequences and associated equations to RCSAs. In **Eq. (8)**, γ is the gyromagnetic ratio of i , and σ^{iso} and σ^{aniso} are the isotropic and anisotropic terms contributing to the electronic shielding. In the case of a mixture of enantiomers (R/S), two shifted resonances are expected to be detected with $\nu^{aniso,R} \neq \nu^{aniso,S}$, if spectral enantiodiscrimination occurs. In the case of mixture of enantiomers, two resonances are expected to be detected, centred on $\nu^{aniso,R}$ and $\nu^{aniso,S}$ if a spectral enantiodiscrimination occurs.

According to IUPAC recommendations, [IUPAC 1972; 1976] the absolute magnetic shielding, σ (expressed in ppm), is the difference in shielding between the frequency of the bare nucleus, $\nu^{bare\ nucl.}$, and the frequency of the same nucleus in the species under investigation, $\nu^{spe.}$:

$$\sigma(\text{ppm}) = 10^6 \times \left(\frac{\nu^{bare\ nucl.} - \nu^{spe.}}{\nu^{bare\ nucl.}} \right) \quad (11)$$

This is the value that can be obtained when using chemical shift calculations by DFT, and the chemical shift (δ) is then determined using the σ calculated for TMS, for instance. The well-known chemical shift, δ (expressed in ppm), used by chemists in the, is the difference in shielding between the nucleus in the species under investigation, $\sigma_{spe.}$, and the shielding of the same nucleus in a reference compound, $\sigma_{ref.}$:

$$\delta(\text{ppm}) = 10^6 \times \left(\frac{\sigma_{ref.} - \sigma_{spe.}}{1 - \sigma_{ref.}} \right) = 10^6 \times \left(\frac{\nu^{spe.} - \nu^{ref.}}{\nu^{ref.}} \right). \quad (12)$$

Approximatively, we can write: $\delta(\text{ppm}) = 10^6 \times (\sigma_{ref.} - \sigma_{spe.})$

When talking about chemical shift, as reported in the NMR spectral data given in database of in scientific literature, the quantity δ (in ppm) is used, thus allows to compare the same information whatever the strength of the spectrometer (the Larmor frequency). The symbol σ is reserved to the absolute magnetic shielding constant.

Mathematically, the chemical shift is a tensorial property. It is not a number, and it is represented by a second-rank tensor (3×3 matrix). The value of the chemical shift depends on the orientation of the molecule respect to the magnetic field B_0 . This orientational dependence is known as chemical shift anisotropy (CSA). In solid state NMR, a powder pattern is observed, as shown in **Figure 4b**. As mentioned above, in solution, the isotropic chemical shift (δ^{iso}) is observed, corresponding to the average value of the three principal components of the chemical shift tensor $(\delta_{xx} + \delta_{yy} + \delta_{zz})/3$.

For a given pair of spins (E.g. C-H bond) with same or similar internuclear distance, the maximum RDCS value at the same degree of order will be nearly the same. In order for this value to significantly change, the internuclear distance has to change such as for the case of long-range RDCs (${}^{2,3}D_{CH}$), which are one order of magnitude smaller than the corresponding one-bond RDC (${}^1D_{CH}$). However, for RCSAs this is not the case. Its maximum value will depend on the anisotropy of the chemical shift tensor for each carbon in the molecule. If the value of the three components of the chemical shift tensor is the same ($\delta_{xx} = \delta_{yy} = \delta_{zz}$), the tensor will be spherical (zero anisotropy) and the RCSA will be null, no matter how strong is the anisotropy created by the alignment medium.

The anisotropy of a chemical shift tensor, in terms of the electronic shielding constant σ , is defined as:

$$\text{Anisotropy} = \sigma_{zz} - \left(\frac{\sigma_{11} + \sigma_{22}}{2} \right) \quad (13)$$

In practice, carbons with sp^3 hybridization show very poor anisotropy while sp and sp^2 carbons normally show strong anisotropy, as shown in **Figure 5**.

In anisotropic media, the maximum RCSA values observed correspond to the product $(\sigma_{zz} - \sigma^{iso}) \times GDO$ (see above), because, σ_{33} is the largest value of the CS tensor by convention. For example, a PMMA gel of 0.2 M% of cross-link density has a GDO value of 0.7×10^{-4} . For a sp^2 hybridized ${}^{13}C$ nuclei where the difference $(\sigma_{zz} - \sigma^{iso})$ is equal to ~ 200 ppm (E.g. carbonyl group or aromatic carbon atom), the maximal ${}^{13}C$ -RCSA value is equal to $200 \times 0.7 \times 10^{-4} = 0.14$

ppm, namely ~ 17.5 Hz at 125 MHz (11.75 T). For a CH_3 group is $(\sigma_{zz} - \sigma^{iso})$ is about ~ 20 ppm, and then max value of RCSA is ~ 1.75 Hz. In conclusion, RCSAs are very small and are in the range of ppb's. Hence, in order to accurately measure ^{13}C -RCSAs it is necessary to have a very high-resolution spectrum and the only way to achieve it is to run $^{13}\text{C}\{-^1\text{H}\}$ 1D NMR spectra.

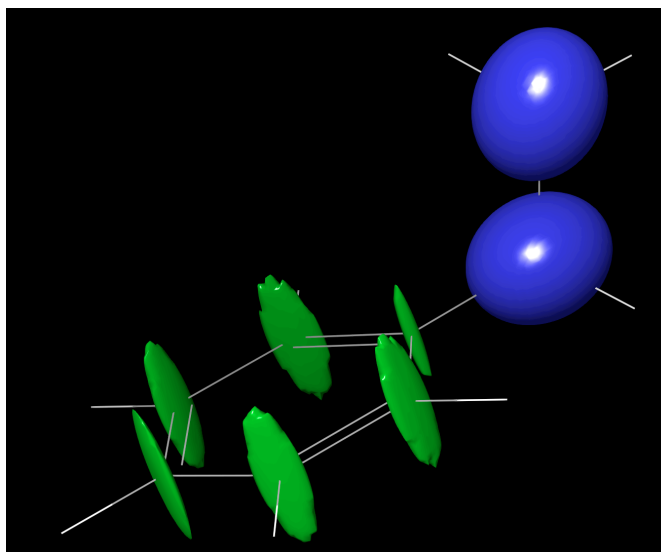


Figure 5. Isosurface plot of the ^{13}C chemical shift tensors of ethyl benzene (sp^2 in green and sp^3 in blue). The difference in size of the sp^2 and sp^3 carbons is because the CS tensor drawn in absolute chemical shielding units (ppm). The sp^3 carbon atoms are significantly more shielded than the sp^2 carbons, hence their larger size. Note the difference in shape between the aromatic carbons (flat ellipsoid) compared to the CH_2 and CH_3 carbons (more spherical ellipsoids).

As we will see in the section of application of RCSAs to the structural analysis of small molecules (see **Section 7.2**), the larger the GDO the better. Thus PBLG-based LLCs are ideal orienting media to measure RCSAs, since they have GDO values with one order of magnitude larger than aligning gels. In fact, it is like having a “magnifying glass” to particularly enhance the ^{13}C -RCSAs values of sp^3 carbons.

The same way that RDCs encode information about the relative orientation of internuclear vectors (E.g. C-H bonds), ^{13}C -RCSAs encode information about the relative orientation of alignment tensors. It is easy to visualize the relative orientation of highly anisotropic CS tensors, because of their ellipsoidal shape (see aromatic carbon atoms in **Figure 5**). However, the poorer the anisotropy, the more spherical the CS tensor is, and if there is not anisotropy at all, there is no way to determine the relative orientation of two spherical objects (two balls). In addition, as for RDCs, parallel CS tensors do not provide additional orientational information. As you can see in **Figure 5**, the six CS tensors for the aromatic ring counts as one. In case of a double bond, they will count as two. The only advantage from the assignment standpoint is that

if you have two double bonds (sp^2 - sp^2) with different relative orientation in space, the carbons that belong to the same double bond will have similar RCSAs values. Finally, judging from the orientation the CS tensors in ethyl benzene (**Figure 5**), the six aromatic carbons count as one (all parallel) since they provide the same orientational information, while the CS tensor of CH_2 and CH_3 carbon atoms show independent orientations of their σ_{zz} components.

From an experimental point of view, the main problem when measuring RCSAs are the interferences from isotropic chemical shift changes. Indeed, many factors can affect the value of the chemical shift such as temperature, concentration, pH, changes in magnetic susceptibility of the medium (solvent changes), etc. The bottom line here is that if the isotropic and anisotropic spectra are not acquired in the same exact experimental conditions, the change in chemical shift value will not only be due to RCSA. Errors introduced by isotropic chemical shift changes can be high because RCSAs are very small compared to RDCs. The following are different experimental scenarios for combinations of isotropic and anisotropic chemical shift changes: i) isotropic solvent A and then isotropic solvent B (isotropic shift), ii) isotropic solvent and then solvent/gel (isotropic shift), iii) isotropic solvent and then solvent/compressed gel (isotropic shift plus RCSAs), iii) isotropic shift not observed in stretched gels, iv) same gel from relaxed to compressed (RCSA data and predictable isotropic shifts that can be corrected), and v) same gel from relaxed to stretched (only RCSAs). In the session of applications of RCSAs we will show how this problem was trackled in order to accurately measure them.

Among the common magnetically active nuclei present in the majority of organic molecules (C, H, O, N), the ^{13}C nucleus is the most efficient nuclear spy as far as RCSA is concerned. Indeed, ^{13}C -RCSA can be measured for any type of carbons, even quaternary (sp^3), provided that the carbons show enough anisotropy. In practice, sp^2 - and sp -hybridized carbon atoms (aromatic rings, double bonds, carbonyls) provide the largest values of ^{13}C -RCSA. As we will see, ^{13}C -RCSA is very useful for discriminating enantiomers on the basis of difference of ^{13}C -RCSA, as well as revealed to be very useful for proton-deficient molecules where the number of CH vectors is not enough to determine alignment tensors using only RDCs.

3.3 Residual quadrupolar coupling (RQC)

For the same reasons explained for the dipolar coupling above, the quadrupolar coupling vanishes in isotropic solutions. In the presence of an (weakly orienting) anisotropic medium, a

fraction of it is observed (10^{-3} - 10^{-4}), and it is known as RQCs. As for RDCs, higher values are obtained with classical thermotropics.

Numerous quadrupolar nuclei exist and can be detected, but most of them present a strong quadrupolar moment, accelerating the relaxation process, leading in turn to low resolution NMR signals. Interestingly, deuterium atoms ($I = 1$), naturally present in any organic molecules, as the second isotope of hydrogen possess a rather small quadrupolar moment (see **Eq. 15**). They can be detected using modern NMR spectrometers with or without cryogenic probes. Evidently, using isotopically enriched molecules (deuterated analytes) is a spectral advantage in terms of sensitivity (100% instead of 1.5 10^{-2} %), but requires a molecular modification by chemical synthesis. Numerous synthetic approaches for introducing deuterium atoms (selectively or not) in achiral/prochiral/chiral molecules have been developed and are well documented. However, it is clear that they are not always possible or easy to make. Their description is over the scope of this Chapter, but readers can see Refs. [**Canet et al., 1995; Gao et al., 2018; Jackman et al., 2007; Meddour et al., 1994**]

Compared to the routine nuclei of spin one-half, the detection of deuterium nuclei gives access to the residual deuterium quadrupolar (^2H -RQC). These couplings originate from the interaction between the nuclear quadrupolar moment of a deuterium atom and an electric field gradient along the C-D bond.

Quadrupolar Coupling

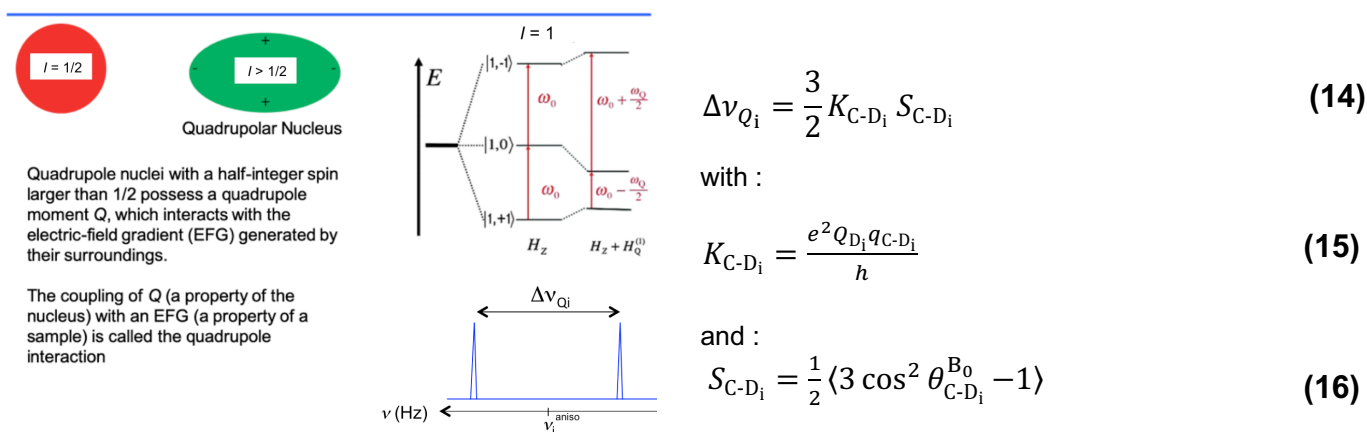


Figure 6. The origin quadrupolar coupling, $\Delta\nu_Q$, associated with a non-spherical distribution of electric charge inside of nuclei, energetic diagram in case of spin $I = 1$, as deuterium, example of an ^2H -QD, and associated equations to ^2H -RQCs. In **Eq. 12**, K_{C-D_i} is the quadrupolar coupling constant (QCC) for nucleus i (the C-D_{*i*} bond). In **Eq. 13**, Q_D is the nuclear electric quadrupolar moment and q_{C-D_i} is the electric field gradient of the C-D_{*i*} bond. The anisotropic chemical shift, $\nu_i^{\text{aniso}}(^2\text{H})$, correspond to the contribution of $\nu_i^{\text{iso}}(^2\text{H})$ and ^2H -RCSA terms. In the case of a mixture of monodeuterated enantiomers (*R/S*), two ^2H -QDs are expected to be detected while centered on $\nu^R \approx \nu_i^{\text{aniso},S}$, if spectral enantiodiscrimination occurs.

In case of an isolated deuterium site, we observe one quadrupolar doublet (^2H -QD) in a non-chiral phase. For two monodeuterated enantiomers dissolved in a discriminating chiral liquid crystal, two quadrupolar doublets are expected. Interestingly, the quadrupolar interaction is very sensitive to small difference of molecular orientation. Mathematical description of ^2H -RQCs is presented from key Eqs. **14** to **16** (see **Figure 6**).

When preparing samples for (^1H - ^1H)- and (^{13}C - ^1H)-RDCs and ^{13}C -RCSAs measurements in LLCs, the ^2H 1D-NMR spectrum of the deuterated solvent can be used to verify: i) if the sample is anisotropic, ii) the degree of anisotropy by looking at the value of the ^2H solvent signal splitting, and iii) the quality of the anisotropy by looking at the shape of the solvent signal.

3.4 Spectral consequences of enantiodiscrimination

Chirality and prochirality. Among exciting domains of modern organic chemistry, the asymmetric synthesis of active substances used in human health has a special place (mainly from the terrible case of Thalidomide at the end of 1950's, a chiral drug whose one of the enantiomers was teratogenic). The development of new (NMR) tools to analyze and spectrally discriminate enantiomers of chiral molecules is a continuous challenge. **[Wenzel, 2007; Wenzel and Chisholm, 2011]** In this Section, we describe the significant contribution of anisotropic NMR to this societal problem.

Enantiomers of chiral molecules are mirror-image objects by a plane of symmetry, but are not superimposable. Majority of chiral molecules possess a stereogenic center (as an asymmetric tetrahedral carbon atom, for instance) (see **Figure 7**), but it is not a prerequisite as observed in cases of planar chirality, axial chirality or atropisomerism.

In the domain of chiral analysis by NMR spectroscopy, the determination of enantiomeric purity of chiral mixtures is one of the main analytical challenges. **[Sylva, 2017; Wenzel, 2007, 2017]** The enantiopurity of a sample of chiral molecules can be simply evaluated by the enantiomeric excess ($ee(\%)$) defined as: **[Elieil and Wilen, 1994]**

$$ee(\%) = 100 \times \frac{|A^R - A^S|}{|A^R + A^S|} \quad (17)$$

where A^R and A^S are the areas of resonances (or group of resonances) for the R and S enantiomers. Peak areas can be determined by peak integration or signal deconvolution as featured in any NMR processing software. When ee is equal to 0% and 100%, the mixture is called "racemic" and "enantiopure", respectively. Otherwise, it is called "scalemic".

The concept of enantiotopicity and prochirality in chemistry is another important aspect of the molecular enantiomorphism. [Eliel and Wilen, 1994] Unlike chirality, which involves two non-superimposable constitutionally identical molecular 3D objects, prochirality involves intramolecular enantiotopic elements (generally bonded to prostereogenic centers), such as nuclei, groups of nuclei or internuclear directions, which are exchangeable by an improper symmetry operation (see **Figure 6**). [Eliel and Wilen, 1994]

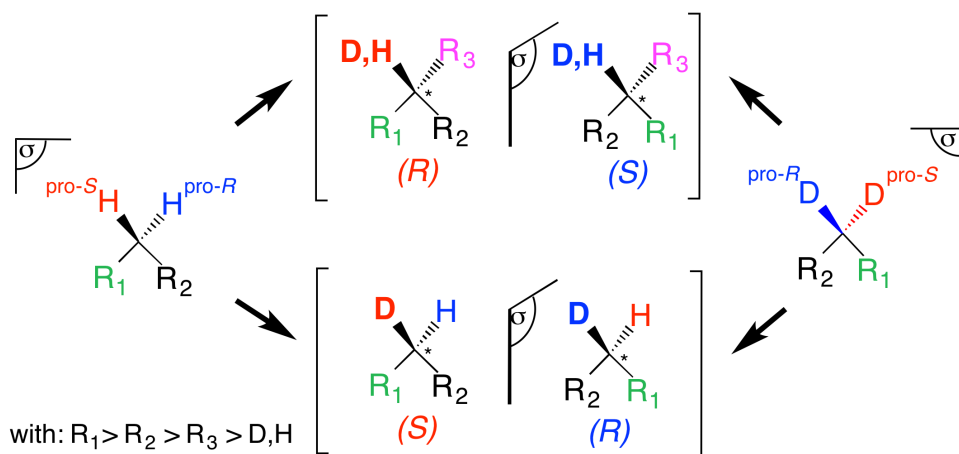


Figure 7. Examples of *R/S*-enantiomeric pairs of a model C_1 -symmetry chiral molecule (“classical” chirality and “(D/H) isotopic” chirality) with a single stereogenic center (tetrahedral carbon atom) deriving from their deuterated or hydrogenated prochiral precursors and characterized by methylene enantiotopic directions, pro-*R*/pro-*S*. **Figure adapted from Ref. [Lesot et al., 2020-c] with permission.**

NMR in CLCs. Contrarily to ALCs, distinct interactions of enantiomers (diastereomorphous interactions) with the enantiopure molecules of the chiral mesophase results in different average orientations of enantiomers with respect to the \mathbf{B}_0 magnetic field of the NMR spectrometer. Each orientation is described with the Saupe’s order matrix, noted $S_{\alpha\beta}^S$ and $S_{\alpha\beta}^R$ (see **Eq. 1**). [Emsley, 1975; Lesot et al., 1997] From an order-dependent NMR interaction point of view, each enantiomer presents a specific set of anisotropic observables ($RDC^{R \text{ or } S}$, $RDC^{R \text{ or } S}$ and $RQC^{R \text{ or } S}$) that (auto)-consistently characterize each isomer (see **Section 7**). In practice, independent and distinct NMR spectra associated to each enantiomer in the mixture are expected to be observed in CLCs. Illustrative examples will be presented below. Interestingly, the intensity of resonances for each *R*- or *S*-spectrum is proportional to the concentration of each enantiomer in the mixture, and hence using different enantiomeric amounts ($[R] \neq [S]$) facilitate the assignment of spectra.

The peculiar case of spectral discrimination of enantiotopic elements of prochiral molecules is another interesting analytical challenge for anisotropic NMR. Using group theory, it has been

demonstrated that for rigid molecules, the enantiotopic discrimination of prochiral solutes in CLCs for four molecular improper point groups, namely C_s , C_{2v} , D_{2d} and S_4 , originates from the reduction of their effective molecular symmetry when they interact with a chiral environment. [Merlet et al., 1999-a] Interestingly, these four symmetries correspond to rigid molecules having enantiotopic faces, groups of atoms, or internuclear directions. This reduction of the effective symmetry increases the number of non-zero independent order parameters of $S_{\alpha\beta}$ as well as the changes in the location of the PAS of the orientational order matrices, which allows enantiotopic element to be discriminated using NMR in CLCs. Experimentally, and contrarily to ALCs, the difference of orientation of enantiotopic elements (internuclear vectors) of C_s , C_{2v} , D_{2d} and S_4 symmetry molecules in CLCs leads to distinct anisotropic NMR observables ($RDC^{\text{pro-}R \text{ or } \text{pro-}S}$, $RDC^{\text{pro-}R \text{ or } \text{pro-}S}$ and $RQC^{\text{pro-}R \text{ or } \text{pro-}S}$). Hence originating different spectral patterns for each enantiotopic element, but not for the different homotopic elements (exchangeable by a C_n -symmetry axis as in case of methyl groups) of the structure. Here again, some key examples will be presented below.

4. Adapted 2D NMR tools

As in NMR of liquids (isotropic solvents), the analysis of complex anisotropic spectra can be simplified with the help of classical homo- or heteronuclear 2D NMR experiments (with or without specific adaptation) or specially designed anisotropic experiments. Numerous 2D experiments have been developed over the last two decades. In brief, we can mention the methodological developments around ^1H and ^{13}C NMR, such as the family of CLIP-CLAP HSQC or G-SERF 2D sequences), as well as for ^2H NMR (the family of QUOSY 2D sequences), both recorded on poly- or perdeuterated molecules, or at natural abundance level (see below).

4.1 Spin-1/2 based 2D experiments

$(^1\text{H}-^1\text{H})$ -RDCs and $(^1\text{H}-^{13}\text{C})$ -RDCs are two important sources of anisotropic information used in various applications as structure determination, but their measurement from complex 1D spectra are not always simple, and request 2D NMR sequences able to separate chemical shifts and homo or heteronuclear couplings on both spectral dimensions. " J -resolved"-type 2D schemes or more sophisticated schemes as the ^1H J -HSQC-BIRD correlation sequence [Thiele, 2012] or CLIP-CLAP HSQC 2D sequence [Enthart, 2008; Reinsperger, 2014] or which only the (one bond) coupling interaction evolves during the t_1 dimension are interesting

tools. Note that further spectral simplifications using a selective excitation of nuclear site of interest (family of homo or heteronuclear G-SERF experiments) are obtained (see **Figure 6**. [Farjon *et al.*, 2010; Giraud *et al.*, 2010; Lesot *et al.*, 2020-a]) A schematic description of these nD experiments and some other useful ones are depicted in **Figure 8**. [Aroulanda and Lesot, 2021]

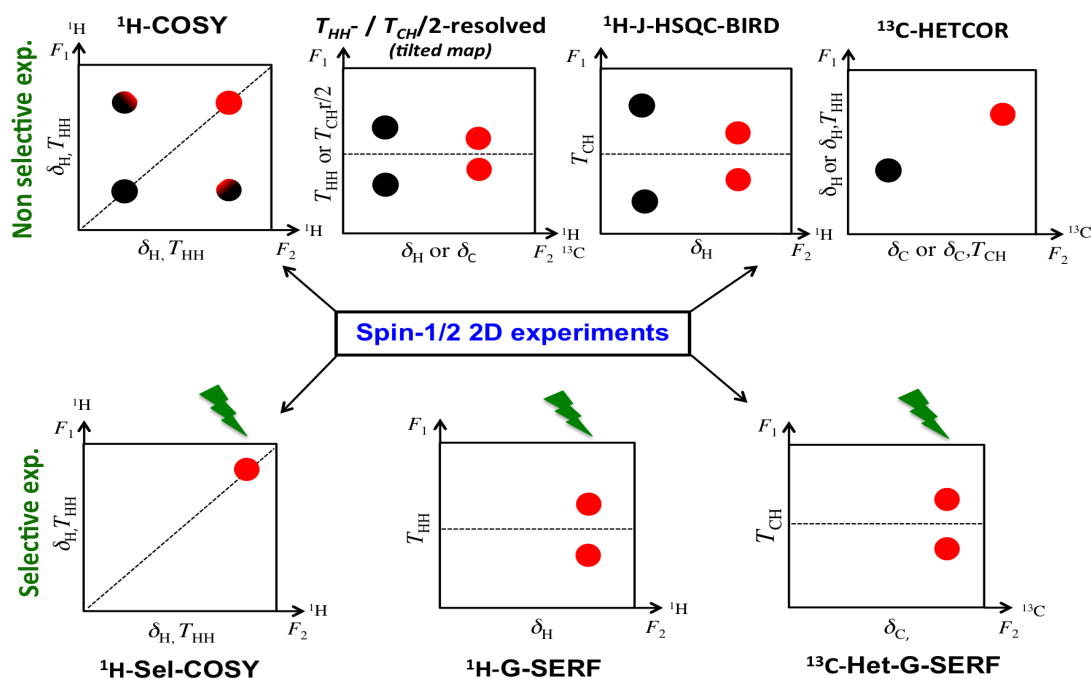


Figure 8. Schematic description of the main homo- and heteronuclear (^1H - ^1H or ^{13}C - ^1H pairs) experiments used for simplifying the analysis of anisotropic spin-1/2 spectra ($^1\text{H}/^{13}\text{C}$) without (top) and with selective excitation (bottom). **Figure adapted from Ref. [Aroulanda and Lesot., 2021] with permission.**

An exhaustive description of all these sequences are out of the scope of this book chapter, but clearly one of the most popular and established heteronuclear 2D experiments for the measurement of one-bond scalar coupling ($^1J_{\text{CH}}$) or the total spin-spin coupling ($^1T_{\text{CH}} = ^1J_{\text{CH}} + 2 \times ^1D_{\text{CH}}$), are the ^{13}C - ^1H CLIP-HSQC 2D experiment, [Enthart *et al.*, 2008] and some more sophisticated variations. [Reinsperger *et al.*, 2014; Becker *et al.*, 2015]

Extraction of isotropic and anisotropic spin-1/2 spectral data. To determine (^1H - ^1H)-RDCs or (^1H - ^{13}C)-RDCs or RDCs of any pair of homo- or heteronuclear magnetically inequivalent nuclei (X-X or X-Y), it is necessary to determine first the associated scalar couplings ($^nJ(^1\text{H}-^1\text{H})$, $^nJ(^1\text{H}-^{13}\text{C})$, $^nJ(\text{X}-\text{X})$ and $^nJ(\text{X}-\text{Y})$). Under this condition, the spectral data of the analyte must be extracted using isotropic and anisotropic environments. From a practical point of view, this is

generally achieved by preparing two distinct NMR samples, the first one using a liquid solvent, the second one using an anisotropic medium, both at the same sample temperature.

An interesting alternative to this two-step approach consists in measuring both types of data (J and D) in a single sample. The first one relies on the so-called variable angle spinning sample (VASS) NMR technique that orients the axis of alignment of a liquid crystal (the director, \vec{n}) at varying angles to the magnetic field by sample rotation, including the magic angle ($\theta_m = 54.7^\circ$) (see also **Figure 45**). For this specific angle, all anisotropic observables are averaged to zero and disappeared and scalar coupling can be measured (see **Fig. 2a**). [Courtieu *et al.*, 1994] Another approach using a compressed aligning gel (see above) is also possible, as reported in 2016, with DMSO-compatible using cross-linked poly(2-hydroxyethyl methacrylate) (poly-HEMA). [Gil-Silva *et al.*, 2016] In this case, the significant difference in bulk magnetic susceptibility between the DMSO inside and outside the gel allows the simultaneous extraction of isotropic and anisotropic NMR data from the same spectra. Extraction of data is obtained with F_1 coupled HSQC 2D experiment. The concept and example of 2D map are shown in **Figure 9**.

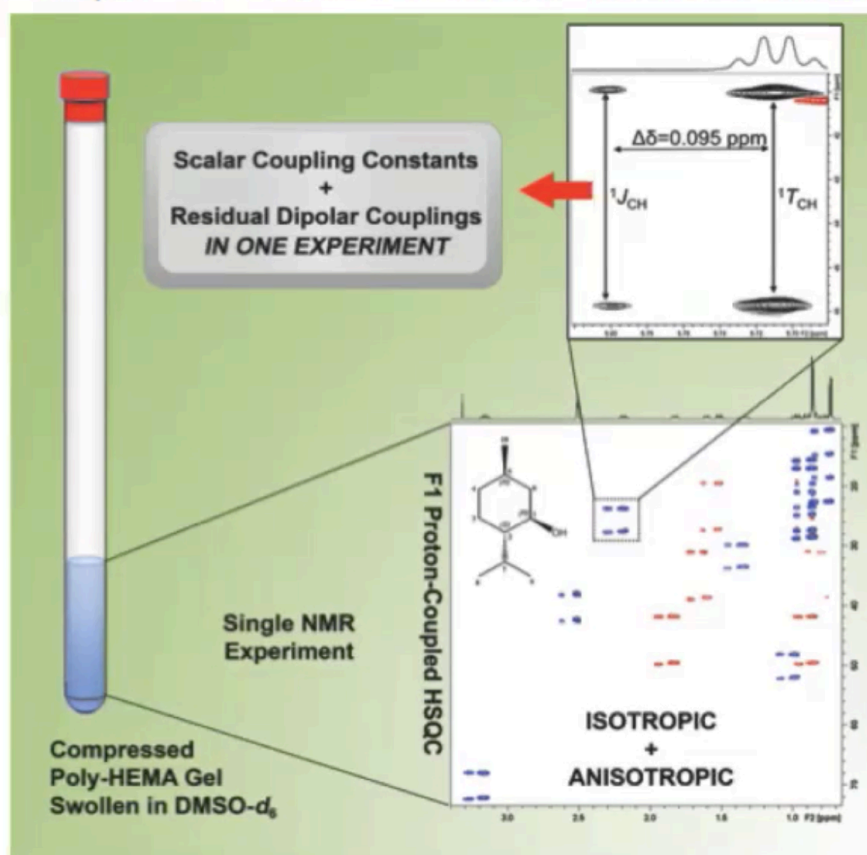


Figure 9. Principle of the simultaneous detection of isotropic and anisotropic data in a single 2D experiment. Figure adapted from Ref. [Gil-Silva *et al.*, 2016] with permission.

^1H J -HSQC-BIRD 2D experiment is a highly functional multipurpose HSQC 2D sequence with evolution of $^1J_{\text{CH}}$'s and $\delta(^1\text{H})$ in F_1 and F_2 dimensions, respectively. [Souza et al., 2017] Using simple switches, the user can activate different blocks of the pulse program shown in **Figure 10**, including the option of having homonuclear decoupling (pure-shift) or not during the acquisition period. Block A controls the $^1J_{\text{CH}}$ evolution in F_1 using a scaling factor. A factor of zero corresponds to no $^1J_{\text{CH}}$ evolution (^1H decoupling in F_1) and a regular HSQC experiment is collected. A value of 1 provides splitting in F_1 corresponding to the $^1J_{\text{CH}}$ value, and values other than one allows the user to collect experiments with J -scaling as it is normally done in the JBS-HSQC 2D experiment. Block C controls the chemical shift evolution in F_1 dimension via a chemical-shift scaling factor. A factor of zero produce a J -resolved experiment with no chemical shift information in F_1 , just the $^1J_{\text{CH}}$ splitting in F_1 at the corresponding ^1H signal in F_2 .

Figure 10b shows the J -resolved HSQC 2D spectrum of Artemisinin. [Navarro-Vazquez et al., 2018] As it can be seen, as long as there is good ^1H signals separation in F_2 dimension, $^1J_{\text{CH}}$ in isotropic conditions and $^1T_{\text{CH}}$ in anisotropic conditions permit the accurate extraction of $^1D_{\text{CH}}$ values. Since there is no chemical shift evolution in F_2 , the experiment is much faster since there is no need for many increments in F_1 to obtain an excellent degree of digital resolution in F_1 . Block B permits the measurement of long-range proton-carbon RDCs ($^{2,3}D_{\text{CH}}$) using the Selective J -Scaled (SJS) HSQC 2D experiments. [Trigo-Mouriño et al., 2011] Finally, a third approach using stable biphasic liquid-crystalline phases (combination of anisotropic and nearly isotropic domains) in a single sample has been also proposed in 2017 with the using a lyotropic system based on a helically-chiral polyisocyanide polymer. [Reller et al., 2017] In this last approach, spatially selectively excited ^{13}C - ^1H CLIP-HSQC 2D experiments (along the z -axis) are applied to the isotropic part and the anisotropic part of the sample, leading to 2D maps where $^1J_{\text{CH}}$ and $^1T_{\text{CH}}$ can be measured respectively. These specific selective experiments relies on the combined application of a pulsed field gradient along the z axis, and a shaped pulse for a spatial selection of a certain volume of the sample at a predefined position of the sample (the isotropic and anisotropic part).

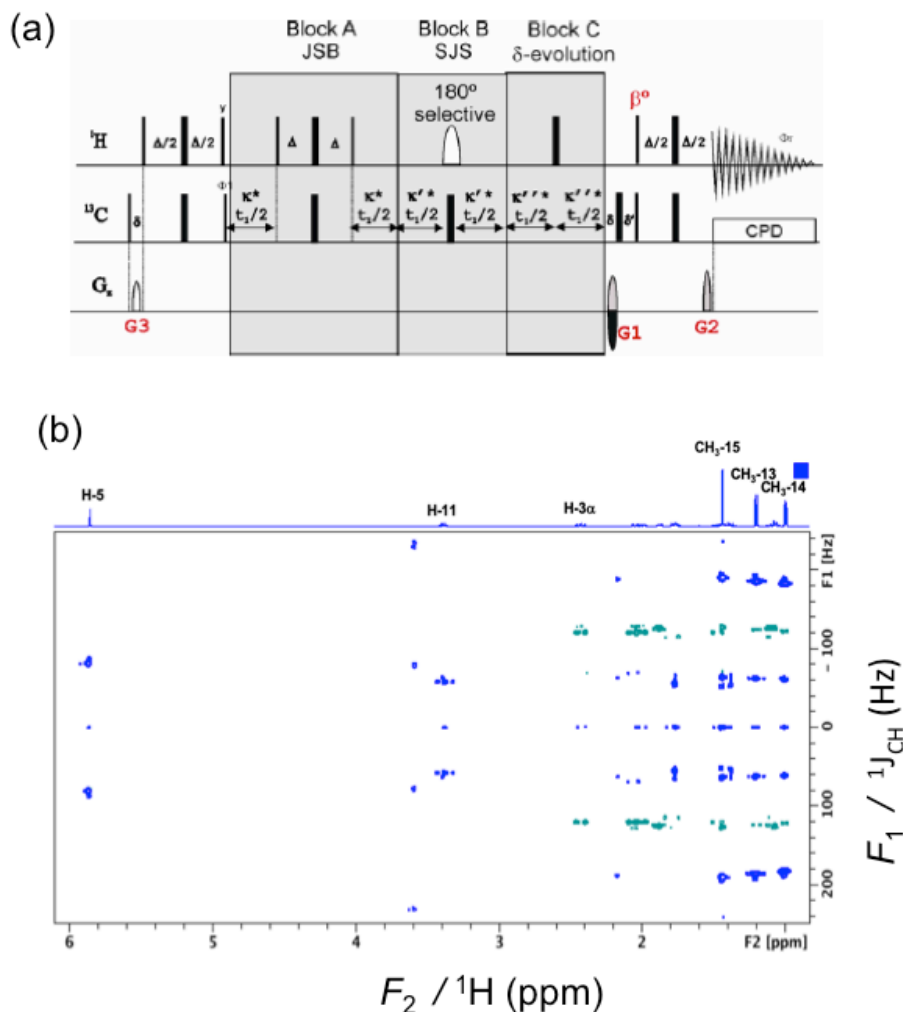


Figure 10. (a) Pulse diagram of the multipurpose HSQC 2D. G1, G2, G3 are z-axis pulse gradients. The delays Δ are adjusted according to the magnitude average values of expected couplings (J or T). (b) Example of anisotropic J -resolved HSQC 2D spectrum of Artemisinin aligned in a PMMA/ CDCl_3 gel using the compression device. **Figure reproduced from Ref. [Navarro-Vazquez et al., 2018] with permission.**

4.2 Spin-1 based 2D experiments

^2H -RQC is another powerful source of anisotropic information very useful in various applications involving enantiotopic or enantiomeric discriminations (enantiopurity determination or isotopic profile) as well as the structure determination as recently reported. [Aroulanda, 2021; Lesot, 2020; Luy, 2010] The interest of ^2H -RQCs lies in the magnitude of the observed ^2H -quadrupolar splittings compared to (^1H - ^1H)-RDCs or (^{13}C - ^1H)-RDCs, for instance, and in the great sensitivity to small differences of molecular orientations (see Eq. 14). This anisotropic interaction reveals to be extremely efficient for spectral enantiodiscrimination when using monodeuterated analytes because we obtain simple deuterium spectra with an optimal sensitivity. However, this approach

needs the chemical transformation of the molecule, which can be time consuming or difficult, and only one site can be spectrally observed. These two drawbacks vanished when detecting all deuterium sites by recording the ^2H spectra at natural abundance level (or NAD NMR). Although of low sensitivity, NAD 1D/2D NMR is generally possible, even using routine NMR spectrometers operating at low field (5.9 T) [Lesot *et al* 1997; Merlet *et al* 1998,]. The use of high-field NMR in combination with ^2H cryogenic probes significantly its sensitivity.

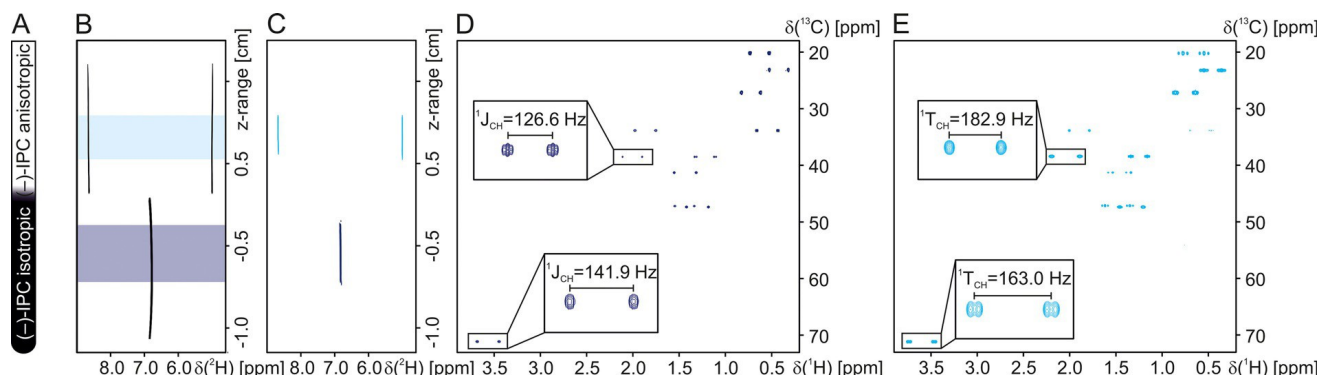


Figure 11. (a) Principle of biphasic LLC NMR samples where the anisotropic part (upper part) and quasi-isotropic (lower part) are clearly identified. (b and c) Phase encoded deuterium 2D spectrum selectively excited regions in a biphasic lyotropic liquid crystal. (d and e) Same as (b and c) but with the spatially selectively excited ^{13}C - ^1H CLIP-HSQC 2D spectra applied to the quasi-isotropic part and the anisotropic part, respectively. **Figure extracted from Ref. [Reller *et al.*, 2017] with permission.**

As we simultaneously detect all monodeuterated species of the mixture molecular isotopomers, various ^2H autocorrelation experiments, called “QUOSY” for QUadrupolar Order Spectroscopy, have been developed to simplify the analysis of complex NAD 1D spectra. [Merlet, 1999-b] Obviously, all these 2D experiments designed for recording anisotropic ^2H spectra at natural abundance can be applied to study poly- or perdeuterated solutes, as well. Among this class of specifically designed ^2H 2D experiments, the most interesting one is the tilted Q-resolved 2D experiment (phased or not) that allows the full separation of ^2H anisotropic chemical shifts, $\delta^{\text{aniso}}(^2\text{H})$, and the residual quadrupolar couplings, $\Delta\nu_{\text{Q}}(^2\text{H})$, in two spectral

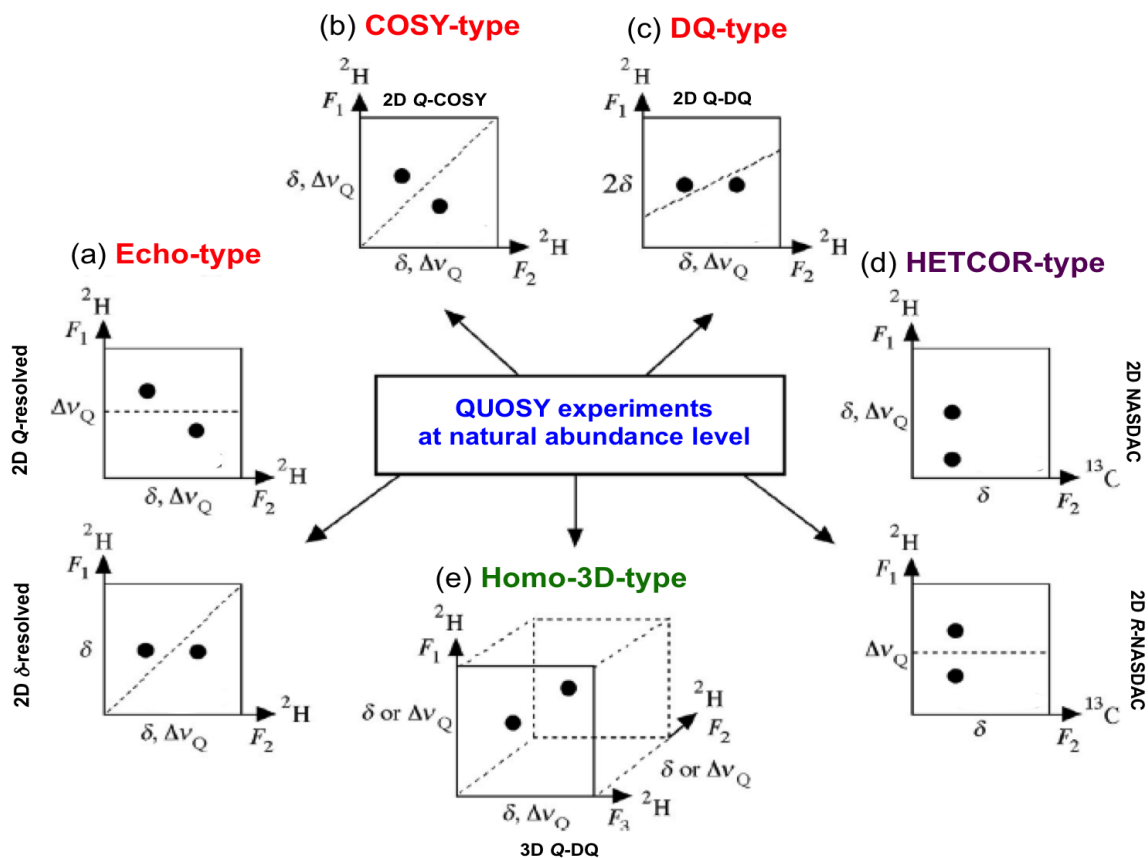


Figure 12. Schematic description of homo- and heteronuclear ^2H QUOSY 2D/3D experiments: (a) Echo-type scheme (Q-resolved and δ -resolved sequences), (b) COSY-type scheme (Q-COSY), (c) Double quantum-type scheme (Q-DQ), (d) HETCOR-type 2D schemes (CDCOM, NASDAC and 2D Refocussed-NASDAC sequences) and (e) homonuclear 3D-type scheme (3D Q-DQ sequence). **Figure adapted from Ref. [Lesot, 2017] with permission.**

dimensions of the map (F_2 and F_1). Homonuclear 3D experiments (as 3D Q-DQ) [Lafon, 2005] were also designed, as well as heteronuclear versions of QUOSYs experiments. The latter correlates (one-bond scalarly or dipolarly coupled) ^{13}C and ^2H nuclei either in deuterated molecules (“CDCOM” 2D experiments: Carbone-Deuterium Correlation in Oriented Media) [Lafon, 2004; Auger, 1998] or even at natural abundance level (“NASDAC” experiment: Natural Abundance Spectroscopy Deuterium and Carbon), allowing the detection of ^2H and ^{13}C isotopologues without any isotopic enrichment [Lesot, 2012b]. A schematic description of these nD experiments and other also developed are depicted in **Figure**

5. Examples of polymeric liquid crystals

Anisotropic NMR using liquid crystals as solvents has a long history since the first anisotropic NMR spectra recorded in achiral and chiral oriented systems have been described by Saupe and Englert in 1963 (nematic thermotropic) and Sackmann, Meiboom and Snyder in 1968

(cholesteric thermotropic), respectively; namely in the early stage of NMR developments. **[Saupe and Englert, 1963; Sackmann et al]**

From mid-1990, a paradigm shift occurred with the first uses of lyotropic (organosoluble or water compatible) weakly orienting (chiral or not) solvents. **[Bayle et al. 1992; Tjandra et al. 1996; Tjandra and Bax, 1997-a]** Contrarily to thermotropics, these lyotropic phases are made up of molecular components that do not possess intrinsic mesogenic properties, but when mixed with suitable (organic) solvents under appropriate conditions (concentration, temperature and pressure) lead to a uniform/homogeneous oriented medium in the magnetic field of the spectrometer. Interestingly, such aligning systems lead to weakly oriented solutes (10^{-3} to 10^{-5}) where the (high-resolution) 1D/2D NMR spectra resembles generally to ones recorded in isotropic solvents.

Among organo-compatible, weakly aligning enantiodiscriminating mesophases, a special attention has been paid to rod-like systems made of α -helicoidally chiral polymers (see **Figure 1b**) and stretched or compressed oriented gels (see **Figure 1c**).

5.1 Polypeptide or polyacetylene-based systems

Many LLCs are generally made by a helically chiral homopolymer, where $\text{Length}^{\text{poly}} \gg \text{Diameter}^{\text{poly}}$. The stereogenic center can be present in the central backbone (as polypeptidic polymers with achiral side chains), on the flexible side chain (as polyacetylenic or poly(arylisocyanide) polymers) or simultaneously on both these structural elements (polypeptides bearing a chiral side chain) (see **Figure 9a**).

Among the most investigated homopolypeptide polymers (used as efficient enantiodiscriminating CLCs) and applied in many different applications (in particular at Orsay), we can mention the case of poly- γ -benzyl-*L*-glutamate (PBLG) or poly- ϵ -carbobenzyloxy-*L*-lysine (PCBLL) for each the absolute configuration (AC) is of *L*-type (see **Figure 13a**). **[Aroulanda et al., 2001-a]** Evidently, the enantiomers of these polymers (PBDG, PCBDL, ...) are also enantiodiscriminating systems, but with inverted results in terms of enantio-orientation. Interestingly, mixtures prepared by mixing equal amounts by weight of polypeptides (close DP) of same nature but with opposite absolute configuration (E.g. PBLG and its enantiomer PBDG) lead to achiral liquid crystals (ALCs) where enantiodiscrimination phenomenon vanishes. In these achiral mesophases, noted « PBG », both enantiomers exchange rapidly, between the (*L*)- and (*D*)-helical vicinities of each polypeptide on the NMR time scale. These results in identical average magnetic interactions for enantiomers, and no difference on their NMR

spectra are therefore expected. [Canlet *et al.*, 2010] Another source of new chiral lyotropic liquid crystals consists simply in mixing two chiral polymers of the same family (with the same absolute configuration but with side chains chemically different, as polypeptides PBLG *et* PCBLL). [Lesot *et al.*, 2008-b] Depending of the peptide unit ratio of each polymer in the mixture, a control of the orientation and enantiodiscrimination is possible. As previously, a

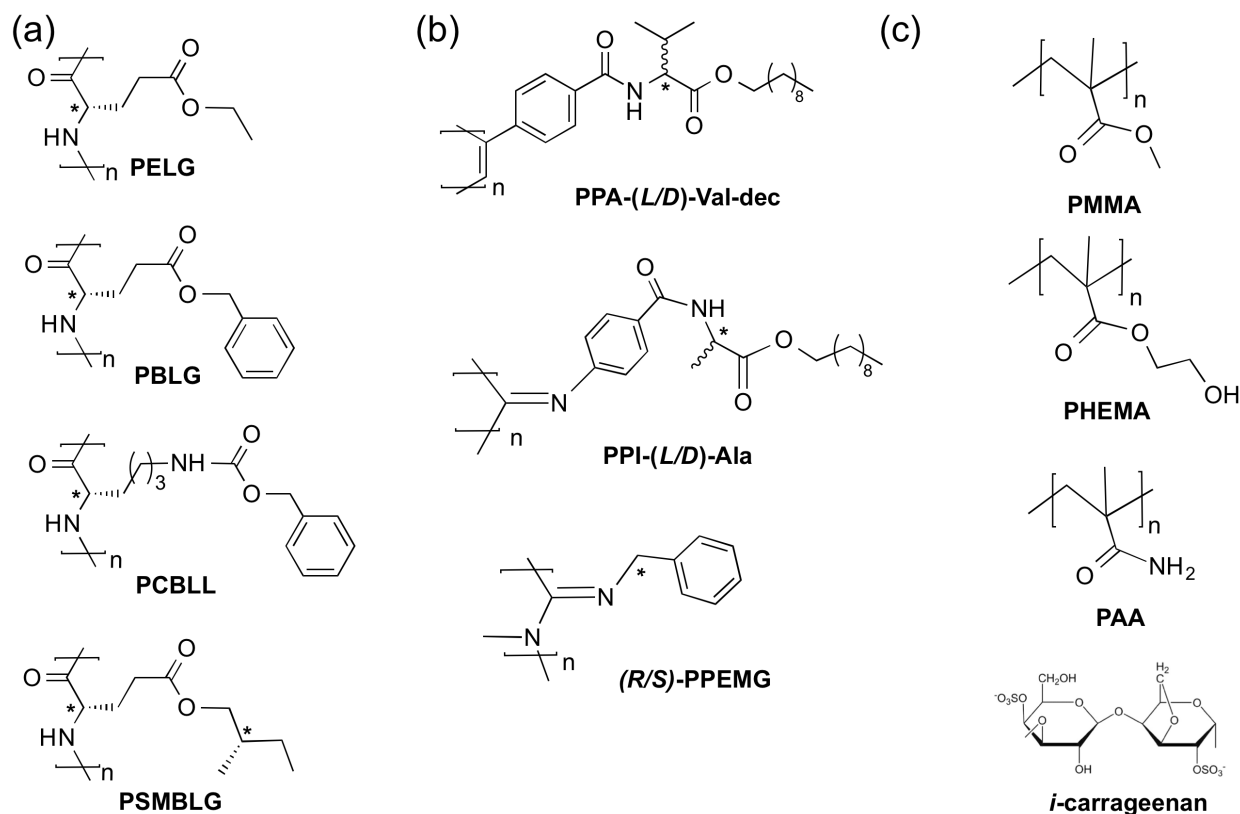


Figure 13. (a) Examples of structures of polypeptide-based helical polymers with a L-configuration for the repeating unit (PELG, PBLG, PCBLL, PSMBLG). (b) Other examples of non-polypeptide helical polymers (PPA-(L/D)-Val, PPI-(L/D)-Ala, (R/S)-PPEMG). In these polymers, the stereogenic center is located on the side-chain. (b) Examples of polymers involved compressed/stretched gels (PMMA, PHEMA, PPA, i-carrageenan). These latter are compatible with chlorinated solvents, but also DMSO, that is not the case with polypeptide-based phases.

mixture of two polymers with their respective enantiomers leads to an achiral oriented media. [Serhan *et al.*, 2016] Over the last decade, innovative and original enantiodiscriminating polypeptide-based polymers have been reported such as helical chiral systems made of (see **Figure 13b**): i) poly- β -phenethyl-L-aspartate (PPLA), [Schwab *et al.*, 2017] ii) poly- β -benzyl-L-aspartate (PBLA), [Hirschmann *et al.*, 2019] iii) poly- γ -*p*-biphenylmethyl-L-glutamate (PBPLMG), [Jeziorowski, 2018] and iv) poly- γ -(S)-2-methylbutyl-L-glutamate (PSMBLG). [Hansmann *et al.*, 2017] The idea related to the use of PSMBLG is to reinforce the

enantio-recognition efficiency and increase spectral enantio-separations by adding a second asymmetric center in the side chain. Finally, we can also mention the design of a polypeptide co-polymer (a polymer bearing two types of sidechain) made phenethyl and benzylpolyaspartate. [Schwab *et al.*, 2018, 2017] Note that this list is not exhaustive but gives a brief overview of the diversity of chiral helical polymers.

5.2 Compressed and stretched gels

During the development of anisotropic media for proteins, methods to generate alignment by compressing a polyacrylamide (PA) gel were simultaneously proposed in 2000. [Sass *et al.*, 2000; Tycko *et al.*, 2000] The method was referred to as strain-induced alignment (SAG). These approaches were inspired by an early work by Deloche and Samulski, [Deloche and Samulski, 1981] which correlates the ^2H residual quadrupolar coupling vs. elasticity by stretching elastomers swollen in deuterated solvents in a solid-state NMR instrument. The only limitation of PA gels is that they are not elastic (no reversible compression) and they are only compatible with water. However, in 2013, the first report on the application of RDCs to the structure analysis of a small organic molecule in a PA gel was described using sodium cholate (see Figure 14a) as analyte. [Mangoni *et al.*, 2003]

In 2004, a very ingenious approach in which a cylindrical polystyrene gel stick (~3 mm of diameter and ~10 mm in length) was inserted in a regular 5-mm o.d. NMR tube was reported. [Luy *et al.*, 2004] Then, CDCl_3 was added and the gel was allowed to swell. Once the gel touched the wall of the NMR tube, it continued swelling axially and over time its self-stretches

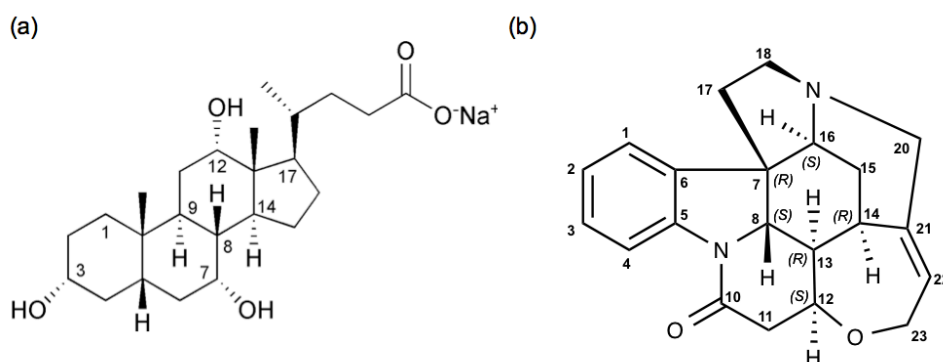


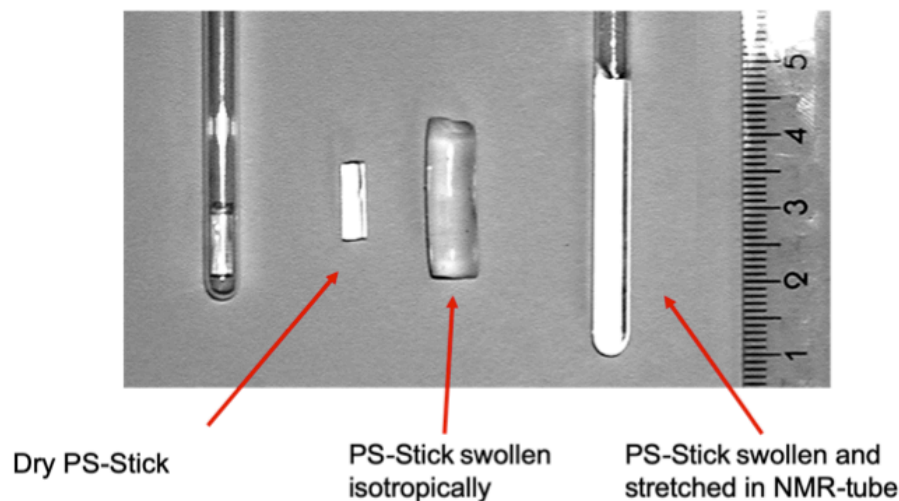
Figure 14. (a) Structure of sodium cholate. (b) Structure of strychnine, a (toxic) natural compounds abundantly used as model molecule in the framework of the structure/configuration analysis.

inside the NMR tube generating anisotropy. Over a period of several days, the ^2H residual quadrupolar coupling reached a maximum value of 25 Hz that did not change further. Once the maximum degree of alignment is reached, it cannot be varied, but it was reported that the degree of alignment can be tuned by changing the cross-link density of the polymer gel. As a proof of concept, they aligned strychnine (see **Figure 14b**) and collected RDCs. This seminal piece of work that opened many further developments in the field of NMR in anisotropic media. In a follow-up article, more detailed study on the aligning properties of the polystyrene gels was presented, [**Luy et al., 2005**] continued with the development of other polymer gels compatible with different organic solvents, such as polydimethylsiloxane (PDMS), [**Freudenberger et al., 2004**] poly(vinyl acetate) (PVAc), [**Freudenberger et al., 2005**] polyacrylonitrile (PAN), [**Kummerlöwe et al., 2007**] gelatin from commercial “gummy bears” with enantiodiscrimination properties, [**Kobzar et al., 2005**] noncovalently and covalently cross-linked polyurethane gels, [**Kaden et al., 2012**] and poly(ethylene oxide) (PEO). [**Merle et al., 2013**] Other interesting systems as copolymeric polyacrylamide gel, the first alignment medium compatible with DMSO have been proposed in 2005 [**Harbez et al., 2005**] or chemically cross-linked poly(methyl methacrylate) (PMMA) compatible with CDCl_3 in 2008 [**Gil et al., 2008**] as a self-stretched gel; as well as poly(2-hydroxyethyl methacrylate) (HEMA) gel compatible with DMS, [**Gil-Silva et al., 2016**] poly[di(ethylene glycol) methyl ether methacrylate] (poly(DEGMEMA)) gel compatible with methanol, [**Garcia et al., 2017**] all designed to work with the compression device, which was first developed for PMMA gels (see **Figure 15a**). [**Gayathri et al., 2010**]

As far as we know, these are the aligning gels developed so far since 2004. The PEO gels are compatible with solvents of any polarity, including water. In 2021, was developed cross-linked poly-(4-acrylomorpholine) (p-AM) blended with PMMA to add mechanical robustness. [**Farley et al., 2021**] This new gel is fully compatible with water and was designed to be used with the compression devices. Its analytical value was illustrated in the case of strychnine hydrochloride and a cyclic peptide.

The self-stretching method was not practical at all, and its limitation led to the design of stretching and compression devices. The first device reported in 2006 to generate anisotropy in

(a)



(b)

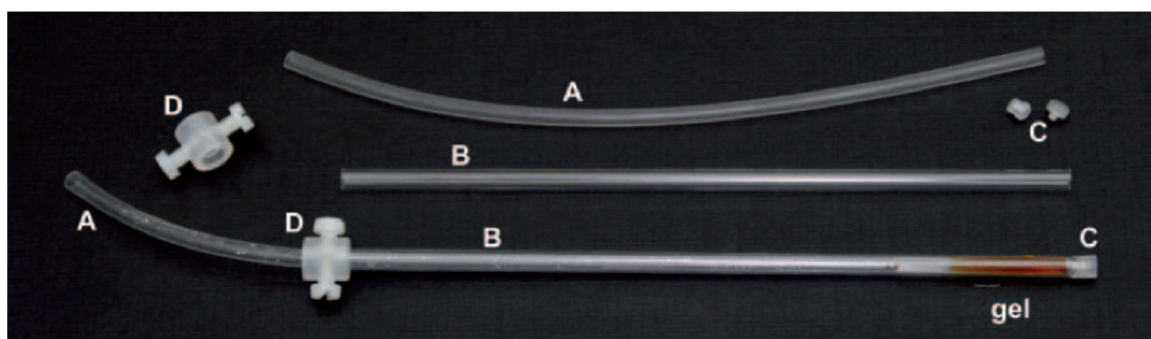


Figure 15. (a) Pictures of swollen gels (PS-stick) with and without stretching (b) Example of stretching apparatus for 5-mm o.d. standard high-resolution NMR probe heads. The flexible Kalrez 8002UP tube (A) is placed inside a cut-open 5-mm o.d. NMR tube (B) and fixed with a specially designed PCTFE screw (C) at the bottom. A PCTFE device with nylon screws (D) is used to fix the stretched tube at the top. Inside the assembled apparatus a reddish-brown PAN/DMSO gel is ready to be stretched. **Figure reproduced from reference [Kummerlöwe et al., 2010; Luy et al., 2004] with permission.**

stretched gelatin uses a silicon-rubber tube inside and open-ended NMR tube. [Kuchel et al., 2006] The silicon rubber is compatible with polar solvents like water or DMSO, but not with apolar organic solvents like chloroform; this device was then modified and replaced the silicon rubber by a Kalrez 8002 perfluoroelastomer. [Dupontelastomers] Figure 15b shows a picture of the stretching apparatus. The only shortcoming of this device is the reluctance of many users to insert an open-ended tube into the NMR probe for fear of accidental leaking. But the degree of alignment can be tune at the user's whim. In Figure 16 is shown an example of the CLIP-CLAP HSQC 2D experiment (case of the quinine in PDMS) with $^1T_{CH}$ values measured in F_2 at different degrees of stretching (see insets). [Kummerlöwe et al., 2010]

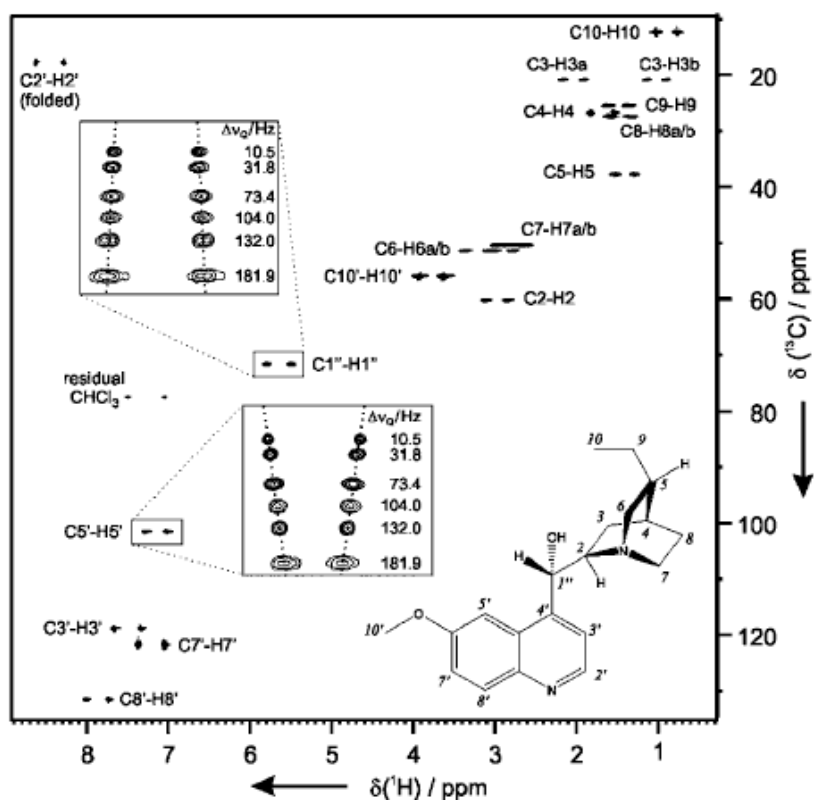


Figure 16. Arbitrary scaling of RDCs in gels with halogenated solvents using a Kalrez 8002UP tubing and observed on CLIP-HSQC 2D spectrum of hydroquinidine in a PDMS/ CDCl_3 gel. Insets show two signals ($\text{C1}''\text{-H1}''$ and $\text{C5}'\text{-H5}'$) at various stages of stretching with peaks separated in the vertical direction according to the corresponding quadrupolar splitting $\Delta\nu_Q$ of the solvent CDCl_3 . The linear dependence between observed $^1\text{T}_{\text{CH}}$ couplings and quadrupolar splittings is evident. **Figure extracted from Ref. [Kummerlöwe et al., 2010] with permission.**

In 2010, a fast and tunable alignment by reversible compression/relaxation of PMMA gels was reported using a compression device, [Gayathri et al., 2010] which was later extended to other polymer gels, such as poly-HEMA, [Gil-Silva et al., 2016] poly-EDGMEMMA, [Garcia et al., 2017] and poly-(4-acrylomorpholine). [Farley et al., 2021]

The original (home-made) compression device consisted in swelling a cylindrical gel rod of ~ 2 mm in diameter and 25 - 30 mm in length inside a regular 5-mm o.d. NMR tube. The gel swells up to a diameter of ~ 4 mm and a length of ~ 40 mm, but it does not touch the walls of the tube. Then, a Shigemi plunger is inserted and the gel is compressed to the desired degree of anisotropy (see **Figure 17**).

The compression device evolved into a more sophisticated design to precisely lock the position of the plunger (see **Figure 18a**), and it is commercially available. [New Era Enterprise] The Teflon piston, which is threaded, can be easily adjusted to any degree of compression with

high accuracy. It is important highlight that when the gel is fully relaxed, there is space between the gel and the wall of the NMR tube. That space is filled with solvent. The ^2H

^1D NMR spectrum of the relaxed gel shows signal of the solvent peak from outside and inside the gel. Both signals are from the solvent in isotropic conditions. The gel buckles upon compression, and the signal from outside gets reduced but never disappeared. The compression generates a ^2H -RDC, indicating that anisotropy was created inside the gel.

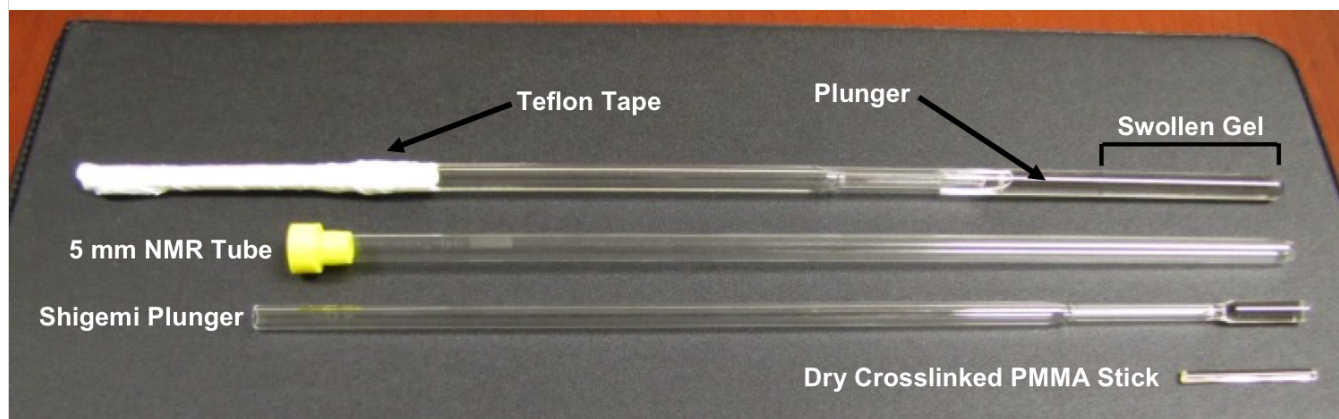


Figure 17. First compression device. The plunger (here a Shigemi plunger) is hold tight inside the tube using teflon tape. **Figure reproduced from Ref. [Gayathri *et al.*, 2010] with permission.**

5.3 Polynucleotide-based chiral oriented media

Helical polymers can be constituted by the repetition of a single monomeric unit (homopolymer) or of two different units (copolymer) but also by the linking of various units (without repetition) as in the case of polynucleotides. The use of polynucleotide chiral polymers made of short chiral LLC made of short DNA-fragment was reported and showed an interesting enantiodiscrimination potential when combined with ^1H NMR [Sau and Ramanathan, 2009] or ^2H - $\{^1\text{H}\}$ NMR of labelled molecules. [Lesot *et al.*, 2011] DNA strands are known to provide cholesteric oriented systems. [Brandes and Kearns, 1986; Strzelecka and Rills, 1987] From a practical point of view, if those systems may provide convenient oriented media for NMR studies, they are generally not commercially available (fragmentation of DNA (200 - 300 base pairs) by sonication), and their preparation (such as control of pH, ionic balance, and sample homogeneity) is sometime tricky. An example of exciting applications of ^2H - $\{^1\text{H}\}$ NMR in DNA/water-based LLCs phase will be presented in **Section 6.3.** [Chan-Huot *et al.*, 2013]

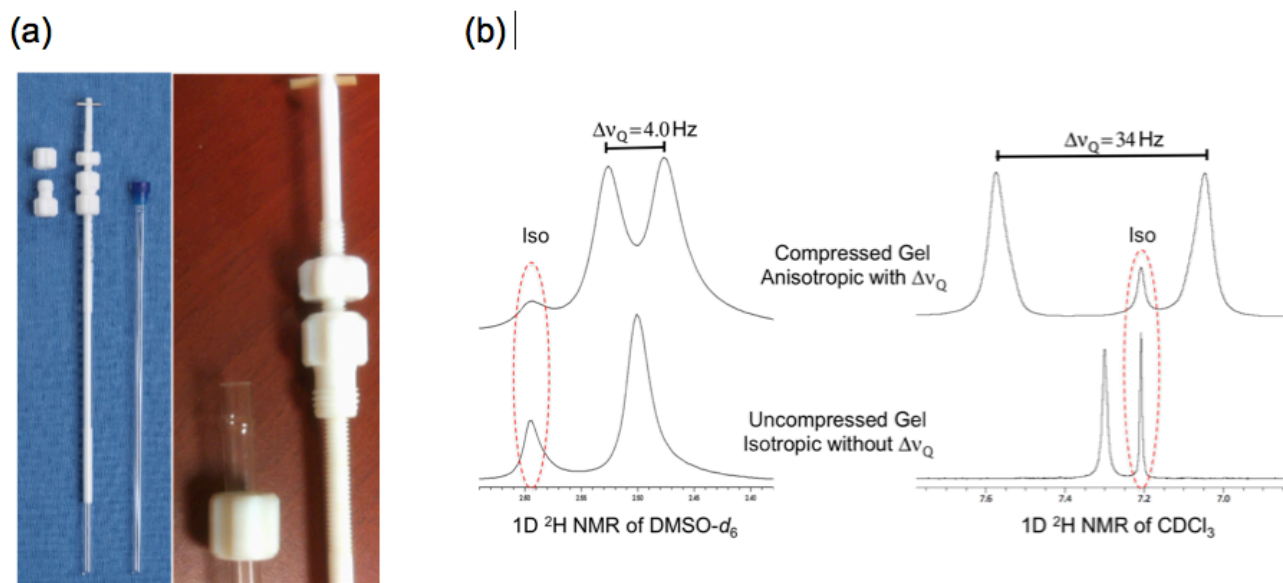


Figure 18. (a) More recent version of the compression device. The plunger is made out of Teflon and it is locked into a special tube to maintain the anisotropy at a constant degree of alignment. (b) Example of ^2H 1D NMR spectrum of $\text{DMSO-}d_6$ in a poly-HEMA gel (left) and of CDCl_3 in a PMMA gel (right). For each gel, the bottom trace corresponds to the fully relaxed gel and the top trace to the gels fully compressed. When the gel is relaxed, two signals are observed, one from inside and other from outside the gel. Both are in isotropic condition. The gel buckles upon compression and not matter how much is compressed, there are always pocket of solvent outside the gel, but the signal from inside the gel show the ^2H residual quadrupolar coupling, indicating that anisotropy was created upon compression.

Without being exhaustive, it is relevant to mention that the description of experimental spectral enantiodiscriminations of small chiral molecules in water-based chiral LLCs were first discovered and reported by Tracey and Diehl in 1975. [Tracey and Diehl, 1975] Despite this, the number of very efficient systems (easy to prepare) proposed so far remains rather limited. For instance, we can mention: a) the potassium *N*-dodecanoyl-L-alaninate based system, [Tracey and Radley, 1984] b) the glucoPON/hexanol/buffered water, [Solgadi 2004] and c) alanine derivated system. [Baczko et al., 2004] However, these systems did not meet a large success for routine applications, mainly due to their difficulties of preparation (their availability / phase homogeneity) and their efficiency.

5.4 Some practical aspects of polymer-based LLCs preparation

Classical oriented lyotropic solutions are prepared by mixing appropriate amounts of analyte and mesogen molecules for thermotropic systems, and analyte and polymer for lyotropic phases. In all cases, the molar ratio analyte/mesogen or analyte/polymer/co-solvent must be determined to avoid biphasic systems (a mixture of oriented and non-oriented molecules), or

destroy the liquid crystallinity of the sample. These ratios are very different with respect to the type of liquid crystals and molecules involved.

Importantly, the oriented lyotropic solutions must be orientationally homogeneous (no concentration gradient) and the molecules oriented uniformly along the magnetic field \mathbf{B}_0 in order to record high-resolution NMR spectra. Typical linewidths in a range of 1-5 Hz can be obtained depending upon the choice of the type of liquid crystal (degree of order), the experimental conditions (concentration viscosity and temperature) and the quality of the sample preparation. For thermotropics, homogenization can be reached by repeated cycles of heating the mixtures to the isotropic phase, physical shaking and then cooling back to the nematic phase inside the magnetic field. For lyotropics, as polymeric aligned systems, a series of centrifugations of the sample at rather low speed (~500 rpm) during a dozen of seconds is useful (to accelerate the dissolution process or avoid matter gradients). Between each series, the 5-mm o.d. NMR tube in the centrifuge (up/down) is inverted. The thermic equilibration of the sample is then performed inside the magnet during a few minutes (see **Figure 19a**). Depending on the nature of the liquid crystals, NMR samples can be spun at moderate rates (10 - 20 Hz).

At the last stage, the use of a simple polarizer (two polarized slabs) allows to controlling if the system is biphasic or not (dark zone) and uniformly oriented in the tube. Analysis of ^2H signal(s) (lineshape and quadrupolar splitting of QD(s)) of deuterated co-solvents (organic or not) present in the oriented sample allows another simple control of the quality of aligning phase, and to verify if the system is not biphasic (presence of signal $\delta^{\text{iso}}(^2\text{H})$). A fine approach based on the use of gradient NMR experiments to obtain a ^2H “image” of the sample can provide also such information. **[Trigo-Mouriño et al., 2013]** Depending on the nature of the liquid crystals, NMR samples can be spun at moderate rates (10 - 20 Hz).

Finally, whatever their nature, the samples can be then shimmed to reduce the homogeneities of the external magnetic field. Automatic shimming procedures (on a selective resonance of the ^1H or ^2H spectra) can even be applied.

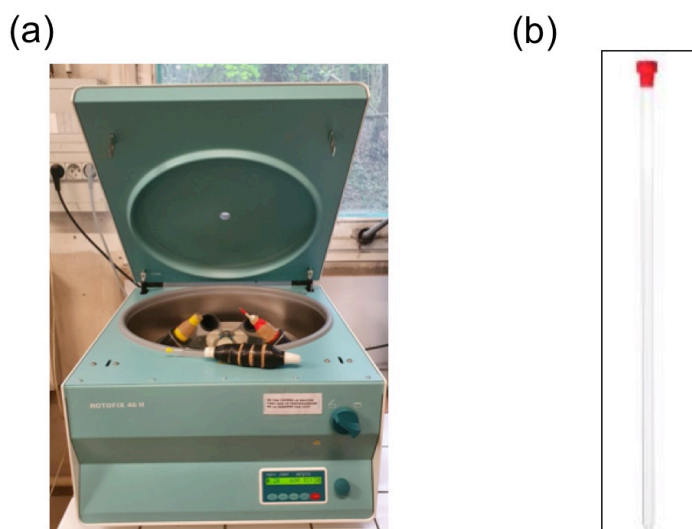


Figure 19. Example of modern (commercially available) centrifuge (a) used for preparing classical 5. mm o.d. NMR tubes (b) containing polymer-based LLCs (as PBLG, PELG, or PLA), for instance. The tube support (home-made) has been adapted to protect the NMR tube during its rotation (~500 rpm) in the centrifuge (**Picture from P. Lesot**).

6. Contribution to the analysis of chiral and prochiral molecules

Strictly imposed by the American Food and Drug Administration (FDA) [**FDA**] or European control rules (Registration, Evaluation and Authorization of CHemicals (REACH) [**REACH**] this control is crucial for pharmaceutical laboratories, whose number one priority is to develop enantiopure bioactive drugs since two enantiomers can induce very different pharmacological effects/responses. Hence, enantiomers can be used to efficiently treat different diseases, as in the case of “*Ritalin*”. In other cases, the less active enantiomer can generate undesired side effects, but remains harmless to human health. On the other hand, the simultaneous presence of the two forms in the drug composition can be highly dramatic as in the case of “*Thalidomide*” mentioned above. Indeed, while one of the enantiomers has a sedative effect and prevents nausea, the other has teratogenic properties leading to irreversible fetal malformations.

From the NMR spectroscopic point of view, enantiomers have identical magnetic properties. Therefore, this approach, alone, is unable to separate their signals when dissolved in a non-chiral media. In contrast, the magnetic properties of diastereoisomers are different in any environment, whether chiral or not. To discern enantiomers by NMR, it is therefore necessary to make them react (diastereoisomers) or interact (diastereomeric adducts) with an enantiomerically pure chiral entity or environment. In this field, NMR in chiral oriented environment provides new and original solutions, thus giving a suitable alternative to classical methods either chromatographic (GC, HPLC) or spectral (isotropic NMR). [**Wenzel, 2007**]

Enantiomorphism covers both the concept of chirality and prochirality, associated respectively with enantiomers of chiral compounds or enantiotopic elements in prochiral molecules. Prochiral molecules are simply defined as any molecule that can be transformed into a chiral one by a single isotopic substitution. Chirality can therefore originate from isotopic substitution around a stereogenic center or not, and called isotopic chirality (see **Figure 7**). [Elieil and Wilen, 1994] In this section, again, we describe the significant contribution of anisotropic NMR to the discrimination of enantiotopic elements in prochiral molecules, and its possible applications.

6.1 Analysis and enantiopurity determination of chiral mixtures

When the enantiodiscrimination mechanisms involved in CLCs are effective, a doubling of resonances (for each enantiomer or enantiotopic elements) is expected compared to NMR spectra recorded in ALCs. As a consequence of this additional spectral complexity in CLCs, all routine magnetically active nuclei (C, H, O, N) are more or less suitable NMR spies to use to reveal spectral differentiations in weakly aligning CLCs.

For almost all organic molecules, we can pay attention to ^1H and its first isotope, ^2H , as well as ^{13}C nuclei, mainly; each of them having its own advantages and drawbacks depending of the spin I , the gyromagnetic ratio, γ , and the relative natural abundance. Quadrupolar nuclei, ^{14}N and ^{17}O , can be theoretically used. However, their quadrupolar properties and their spin (large Q value (see **Eq. 13**) reducing drastically the T_1 , T_2 relaxation times and the spin $5/2$ for ^{17}O) make them rather poor analytical probe. When present in compounds, other nuclei of spin $I = 1/2$, like ^{19}F or ^{31}P can be also successfully exploited. Below we discuss the potential of ^1H , ^2H and ^{13}C NMR.

Proton NMR. *A priori*, hydrogen atoms appear to be the simplest nuclear spies for revealing spectral enantiodiscriminations based on differences in (^1H - ^1H)-RDC values (see **Eq. 4**), because ^1H -RCSAs are generally rather small and rarely exploitable. The analytical advantages of this nucleus are its high isotopic abundance (99.985%), its large gyromagnetic constant (γ) and its spin $I = 1/2$. However, even for small-size molecules, a dense homonuclear network made of (long and short range) (^1H - ^1H)-RDCs exists, and the contribution of long- and short-range couplings (J and D) generally leads to weakly-resolved ^1H spectral patterns, rather difficult to decipher compared to isotropic ^1H spectra. Some exceptions can be found with (ideal)

compounds, such as in case of *S*-enriched mixture of 3-butyn-2-ol dissolved in PBLG where all (*R*)- and (*S*)-resonances of the methyl group are nicely resolved and RDCs can be easily determined (see **Figure 20**).

Note finally that in case of compressed or stretched polymeric gels for which the degree of solute orientation is one of order magnitude less than in polypeptide-based oriented phases, it is sometimes difficult to obtain clear and resolved spectral patterns and so extract reliable proton dipolar information. In practice, using aligning gels for the extraction of (^{13}C - ^1H)-RDCs from the total spin-spin coupling, $T(^{13}\text{C}$ - $^1\text{H})$, is much simpler.

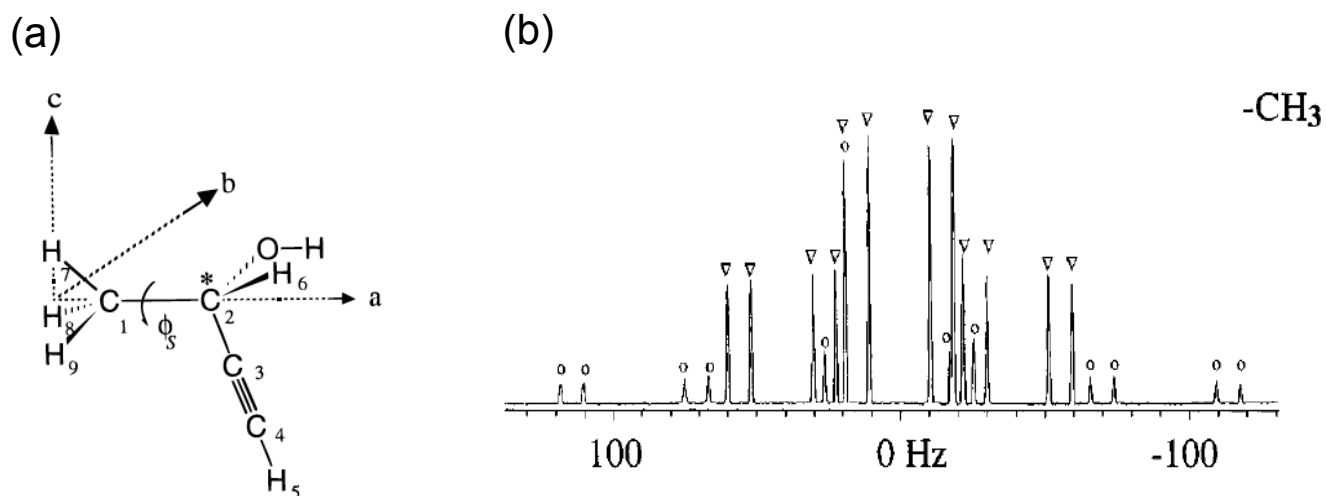


Figure 20. (a) Structure of 3-butyn-2-ol. (b) 400.1 MHz ^1H 1D-NMR signal of methyl group ($ee(S) = 72\%$) in PBLG/ CDCl_3 phase. For each enantiomer, the spectral pattern is made of two A_3MX spin system, namely a dipolar triplet (CH_3) coupled with methyne hydrogens 5 and 6. Note the difference of intensity of the two A_3MX systems due to the ee used. **Figure adapted from Ref. [Lesot *et al.*, 1997] with permission.**

To overcome the complexity of low-resolution proton 1D spectra, 2D approaches have been explored to improve the resolution of ^1H NMR spectra of enantiomeric mixtures in CLCs. Most of these methods rely on the ability of separating the evolution of chemical shifts and spin-spin coupling interactions, combined with the selection of part of spectral information using selective irradiation. All these anisotropic experiments derived from the first ^1H SERF 2D experiments introduced in 1995. [Facke and Berger, 1995] Then, numerous Improvements to the original SERF pulse sequence were proposed to obtain cleaner and simpler spectra to analyze. Among them we can mention: i) the experiments capable of providing pure absorption 2D spectra (SERFph), [Beguin *et al.*, 2009] ii) the combination of these phased SERF with the VASS method [Beguin *et al.*, 2006] where the sample spins at a given angle, [Courtieu *et al.*, 1994] iii) the implementation of spatially-encoded selective spin echoes in order to visualize the whole total coupling network involving a given proton site in a single T -edited 2D

spectrum. [Farjon et al., 2011] An example of spatially-encoded selective spin echoes 2D spectra is illustrated in **Figures 21b,c,d**. The resulting maps show a series of multiplets that are often reduced to simple doublets and appear for each enantiomer at the resonance frequency of each coupling partner of the probed proton site. This allows for a straightforward assignment and measurement of the ^1H - ^1H total couplings and a possible measurement the ee of mixture.

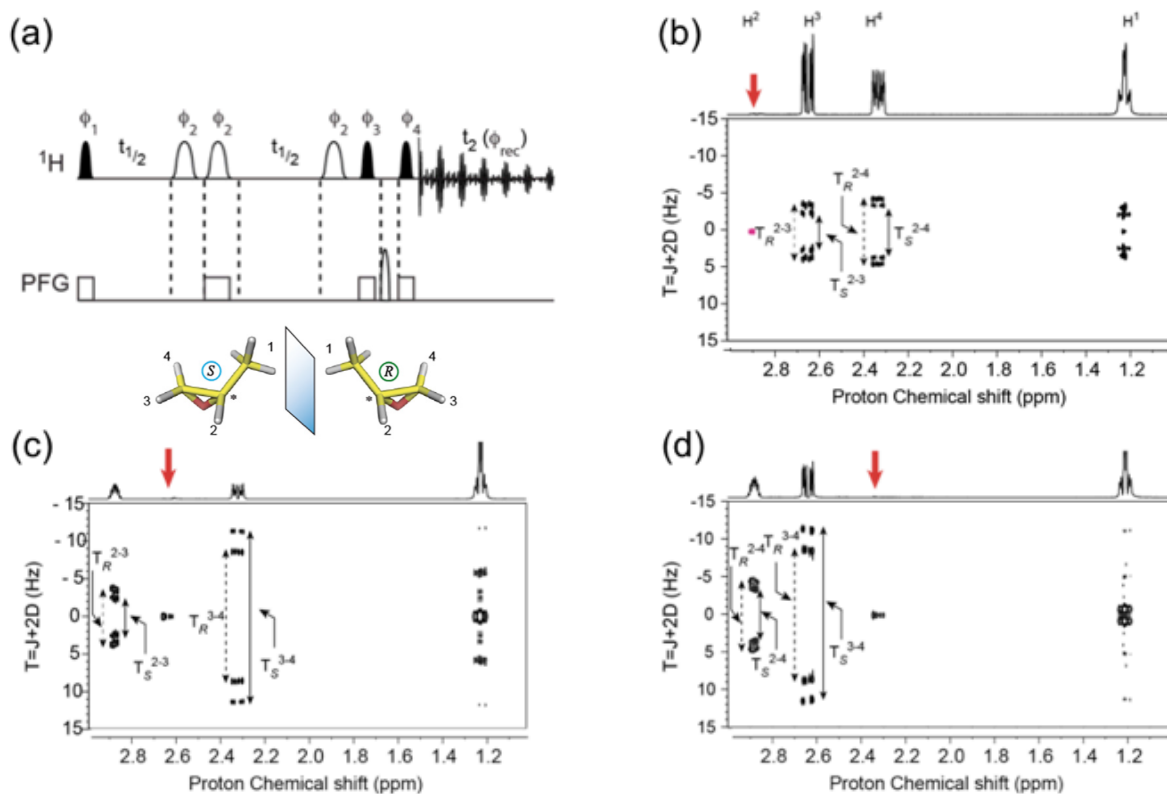


Figure 21. (a) Schematic pulse diagram of the ^1H G-SERF 2D experiment. (b to c) Examples of ^1H G-SERF spectra applied on (\pm)-1,2-epoxypropane in PBLG/ CDCl_3 for the edition of the total couplings involving proton sites, H^2 (b) H^3 (c) and H^4 (d). Figure partially adapted from Ref. [Lesot et al., 2020; Merlet et al., 2011] with permission.

Carbon-13 NMR. Exploiting the potential of anisotropic interactions (^{13}C -RCSA or ^{13}C - ^1H RDCs) associated with carbon-13 nuclei is at the origin of many applications: from the determination of enantiomeric purity, [Lesot et al., 1995; Meddour et al., 1997; Tzvetkova et al., 2011] to the analysis of ($^{13}\text{C}/^{12}\text{C}$) isotopic ratios, as demonstrated in 2021. [Lesot et al., 2021] Although ^{13}C and ^1H are nuclei of spin 1/2, the main difference with ^1H is the low ^{13}C natural abundance of 1.1%. Interestingly, the detection of low abundance nuclei like ^{13}C leads to simpler NMR spectra (compared to ^1H) to analyze, particularly when all protons are decoupled using classical composite pulse decoupling (CPD) sequences such as the WALTZ-16

sequence. [Shaka et al., 1983] In this case, the spectrum is a sum of independent resonances associated to each ^{13}C - ^{12}C isotopologue of a molecule, while the probability to detect a pair of ^{13}C - ^{13}C isotopologues ($1.1\% \times 1.1\% = 0.01\%$) is too low to be simply detected (INADEQUATE 2D NMR). Another specific advantage of ^{13}C nuclei is its large range of chemical shifts ($\delta^{\text{iso or aniso}}(^{13}\text{C}) = 0 - 250$ ppm ppm, instead of a range of $\delta^{\text{iso or aniso}}(^1\text{H}) = 0$ to 15 ppm). This occurrence considerably enlarges the distribution of ^{13}C resonances or ^{13}C spectra patterns in the ^{13}C -(^1H) ^{13}C spectra, respectively, thus facilitating their assignment or analytical deciphering (coupling measurements).

Among drawbacks associated with this nucleus, it could be mentioned the lowest sensitivity compared to ^1H ($\gamma(^{13}\text{C}) = \gamma(^1\text{H})/4$), as well as longer longitudinal relaxation times, $T_1^{\text{iso or aniso}}(^{13}\text{C})$, notably with quaternary ^{13}C atoms. In fact, the relative sensitivity at natural abundance $^1\text{H}/^{13}\text{C} = 5,666:1$. However, it should be noticed that: i) with the anisotropic ^{13}C NMR, $T_1^{\text{aniso}}(^{13}\text{C})$ are shorter than $T_1^{\text{iso}}(^{13}\text{C})$ measured in isotropic NMR due to viscosity of the solvent, and ii) the use of new cryogenic ^{13}C NMR probes (that reduce the electronic noise) allows to compensate the problem of sensitivity due to low γ and natural abundance, even with a small amount of analyte. [Kovacs et al., 2005; Marathias et al., 2010]

When chiral oriented solvents are used, spectral enantiodiscrimination can be detected by proton-coupled ^{13}C NMR on the basis of a difference of (^{13}C - ^1H)-RDCs, and the *ee* easily measured on isolated sites in the molecule (few or no long-range RDCs). This situation is often observed with (more or less isolated) methyl groups as in case of 2-bromopropionic acid as illustrated in **Figure 22a**. Here for each enantiomer, the ^{13}C spectral pattern is associated with an A_3MX spin system with X: ^{13}C , and A_3 and M: ^1H , but only one isomer shows a total non-zero ^{13}C - ^1H coupling. [Lesot et al., 1995-a] **Figure 22b** shows proton-coupled ^{13}C signal of diastereotopic (inequivalent sites in α -position of the asymmetric carbon) hydrogens of the methylene group of β -trichloromethyl- β -propiolactone. The (*R*)- and (*S*)-spectral patterns are typically two ABX spin systems with X: ^{13}C and A and B: $^1\text{H}_a$ and $^1\text{H}_b$) with two distinct (^{13}C - ^1H)-RDC values. [Lesot et al., 1995-b] As we will see in the next Section with other examples, the analysis of NAD signals of this CH_2 lead to the detection of four ^2H -QDs, revealing *de facto* the inequivalence of diastereotopic ^1H sites through the detection of their four associated ^2H diastereo-isotopomers.

The ^{13}C NMR approach is often limited when a significant number of long-range (^{13}C - ^1H)-RDCs contributing to signal of interest. As mentioned previously, the use of heteronuclear

(selective or not) 2D experiments such as *J*-resolved, CLIP-CLAP HSQC or ^1H F_1 -Coupled *J*-Scaled BIRD filtered HSQC (JSB-HSQC) 2D experiments can overcome this problem. [Enthart *et al.*, 2008; Reinsperger *et al.*, 2014; Thiele and Bermel, 2012]

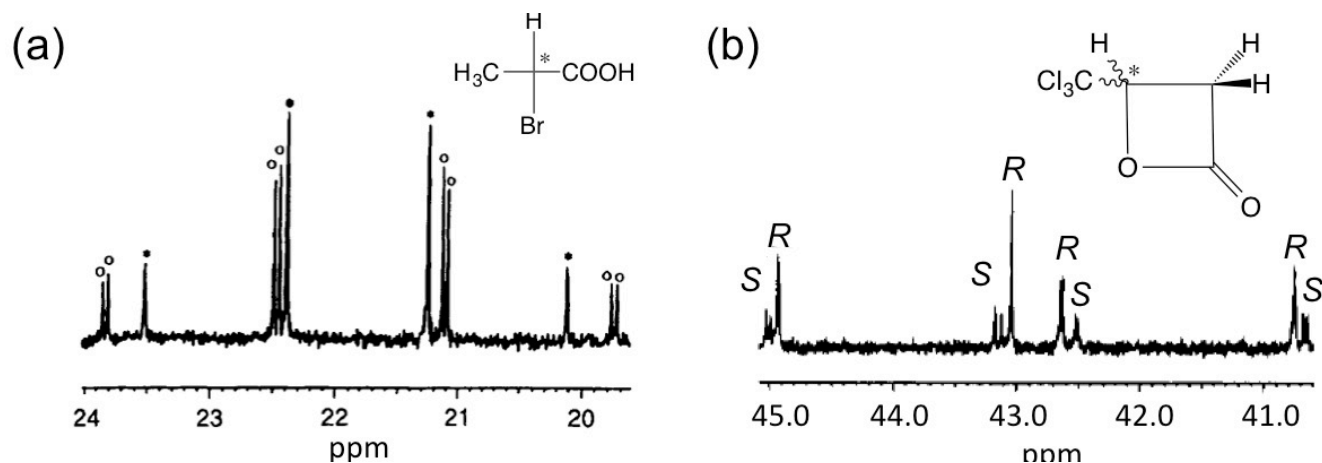


Figure 22. (a) 100.3 MHz ^{13}C spectral pattern of methyl group (A_3X spin system with $X = ^{13}\text{C}$) of (\pm)-2-bromopropionic acid showing. (b) ^{13}C spectral pattern (ABX spin system with $X = ^{13}\text{C}$) of methylene group of β -trichloromethyl- β -propiolactone ($ee(R) = 40\%$) in PBLG. Both examples recorded in the PBLG phase show clear enantiodiscriminations. **Figure adapted from Refs. [Lesot *et al.*, 1995-a,b] with permission.**

Simpler spectral analyses and successful results are generally obtained when all protons are decoupled ($^{13}\text{C}\{-^1\text{H}\}$ NMR), because discrimination is detected only on the basis of differences in ^{13}C -RCSA values. Thus, all inequivalent $^{13}\text{C}\{-^1\text{H}\}$ signals of a chiral molecule give rise to a single resonance in ALCs, and two resonances in a CLC, one for each enantiomer, if the enantiodiscrimination phenomenon occurs as seen in the simple case of (\pm)-phenethyl alcohol recorded at 16.5 T (176.1 MHz for ^{13}C) (see **Figure 23a**). [Lesot *et al.*, 2021] For this molecule, differences in ^{13}C -RCSA values, $\Delta(\text{RCSA})$, observed at this magnetic field strength (see **Eq.8**) vary within a range of 8 (sp^3) to 16 Hz (sp^2). Among other remarkable, more complex, examples of spectral $^{13}\text{C}\{-^1\text{H}\}$ enantiodiscriminations, we can mention the case of enantiomers of planar chirality as chromium tricarbonyl complexes ($(\eta^6\text{-arene})\text{X}(\text{CO})_3$ with $\text{X} = \text{Cr}$) obtained with new asymmetric synthesis reactions (see **Figure 23b**). [Lafon *et al.*, 2005]

Figure 23c presents a more atypical case of chirality (atropoisomerism) with the 1,1'-bi(2-naphthol) (BINOL), whose 80% of ten ^{13}C sites (sp^2 carbon atoms) in PBLG are enantiodiscriminated with a difference in ^{13}C -RCSA values of about 10-17 Hz (9.4 T). [Meddour *et al.*, 1997] Interesting results were also obtained with (\pm)-2,2'-dimethyl-1,1'-binaphthyl [Lesot *et al.*, 2003], as well as the possibility to differentiate enantiomers of chiral molecules having a heteronuclear stereogenic center, as it is the case of chiral sulfoxides (see **Figure 23d**).

In all cases, the large number of enantiodifferentiated ^{13}C sites allows to select the optimal carbon site both in terms of spectral R/S separations and signal-to-noise ratios (SNR) for a robust determination of the enantiopurity (ee) of chiral mixtures.

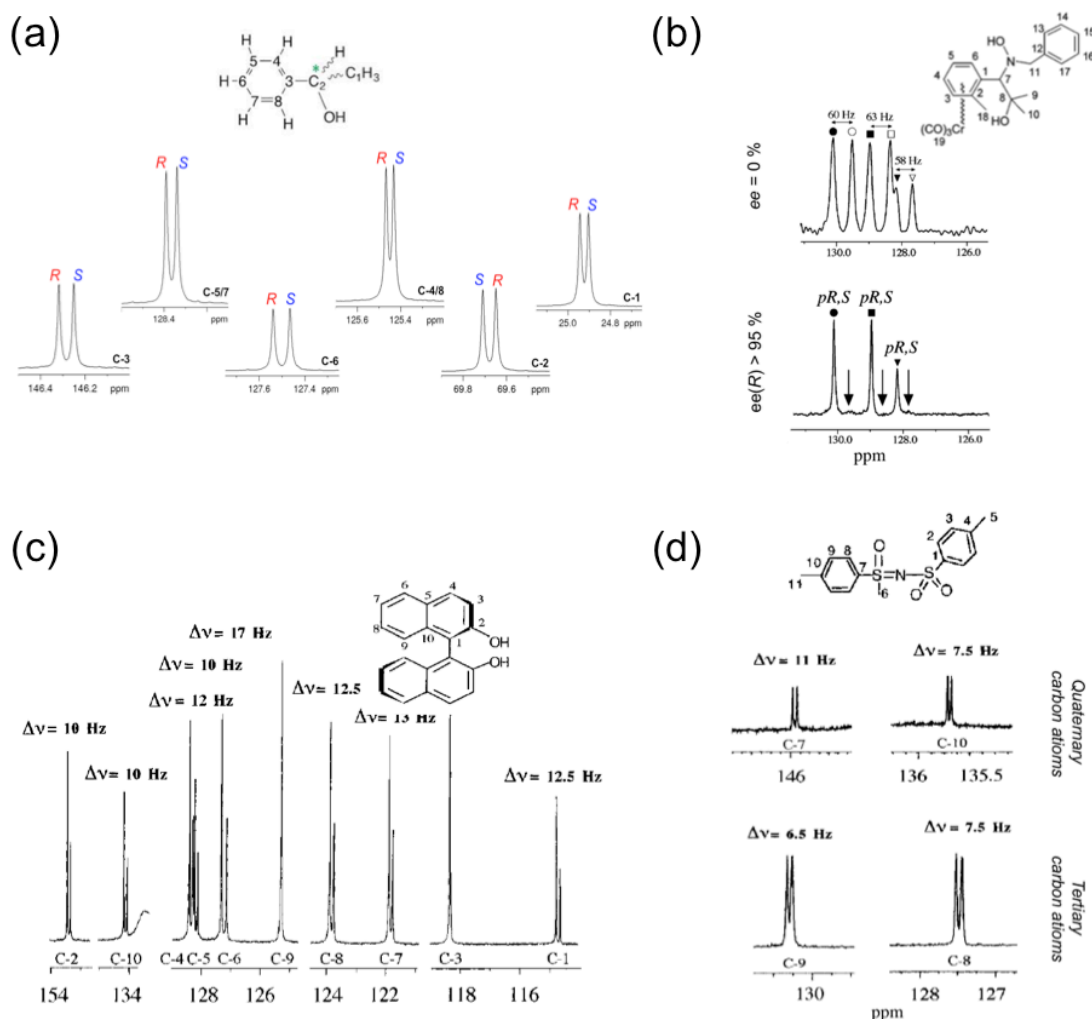


Figure 23. Selected examples of ^{13}C - $\{^1\text{H}\}$ enantiodiscriminations (on sp^2 and sp^3 carbon atoms) associated with various types of chirality: (a) 176.1 MHz ^{13}C - $\{^1\text{H}\}$ 1D spectrum of (\pm)-phenethyl alcohol in the PBLG/ CDCl_3 phase showing an enantiodiscrimination on all ^{13}C sites. (b) Three differentiated aromatic ^{13}C - $\{^1\text{H}\}$ signals (100.3 MHz) of the *N*-(2-methyl-2-hydroxy-1-((2-methylphenyl) chromium tricarbonyl) propyl)-*N*-benzyl-hydroxylamine, a chiral (η^6 -arene) chromium tricarbonyl complex recorded in PBLG, in racemic (top) and enantiopure series (bottom). (c) Eight (over ten) 100.3 MHz ^{13}C - $\{^1\text{H}\}$ 1D spectrum of 1,1'-bi(2-naphthol) ($ee(R) = 31\%$) in PBLG/DMF- d_7 . (d) Four (aromatic) enantiodiscriminated ^{13}C - $\{^1\text{H}\}$ 1D signals of (\pm)-*S*-methyl-*S*-*P*-tolyl-*N*-tosylsulfoximine in PBLG. **Figure adapted from Refs. [Lafon et al., 2005, Lesot et al, 2021-a; Meddour et al., 1997] with permission.**

In collaboration with many chemists, this tool has been successfully applied in the evaluation of enantioselectivity in various asymmetric synthesis cases: i) monofluorination reactions on propargylic compounds, ii) double diastereoselection in [2 + 3] cycloaddition reactions of chiral oxazoline *N*-oxides and their application to the kinetic resolution of a racemic α,β -unsaturated δ -lactone, [Dirat et al., 2010] iii) intramolecular hydroamination catalyzed by ate and neutral rare-

earth complexes, [Queffelec *et al.*, 2011] iv) aza-Michael additions of *O*-benzylhydroxylamine to *N*-alkenyloxazolidinones catalyzed by samarium iodobinaphtholat. [Didier *et al.*, 2011]

Finally, it is interesting to note that by increasing the spectrometer's magnetic field strength by a factor of 2 (18.8 T), the enantiodifferences of all examples presented here will simply double (see **Eq. 8**), facilitating the integration or the deconvolution of the *R/S* enantiomers resonances.

Deuterium NMR. Deuterium nuclei, the second isotope of hydrogen, is naturally present in all hydrogenated compounds at very low natural abundance level ($1.55 \times 10^{-2}\%$) and resonate at a lower Larmor frequency ($\gamma(^2\text{H}) = \gamma(^1\text{H})/6.515$). However, same as for anisotropic ^{13}C NMR, the use of high field NMR spectrometers combined with ^2H cryogenic probes compensate enough the very low sensitivity of this nucleus to be analytically exploited. This sensitivity limitation is no longer a problem for ^2H isotopically enriched compounds.

Contrarily to ^{13}C and ^1H , ^2H nuclei ($I = 1$) possess a quadrupolar moment, Q , specific to "quadrupolar" nuclei with spin $I > \frac{1}{2}$ (see **Eq. 15**), giving rise to a measurable ^2H -RQC (see **Eq. 14**) in oriented media. This new property represents an analytical advantage for various reasons. First, due to its spin number, any ^2H signal is featured by a quadrupolar doublet (^2H -QD) that distribute the signal on only two components ($2I$ transitions), except if $\theta_{\text{CD}}^{\text{B}_0}$ is aligned on θ_m (see **Eq. 16**). Second, the magnitude of the quadrupole moment, Q , that governs the efficiency of quadrupolar relaxation mechanisms, is small enough to lead to resolved and sharp spectral lines, unlike the majority of quadrupolar nuclei. Third, the range of magnitude of ^2H -RQCs ($|\Delta\nu_{\text{Q}}| = 0$ to 1 - 2 kHz) in weakly aligning media compensate for the low distribution of ^2H chemical shifts (0 to 15 ppm), thus limiting the peak overlaps. Last but not least, the ^2H quadrupolar interaction is very sensitive to a difference of orientation of the C-D bond, since the K_{CD} varies from 150 to 300 kHz depending on the hybridization state of the deuteron and the neighbouring substituents, which one order of magnitude large than the corresponding (^{13}C - ^1H)-RDCs for the same bond. All these reasons make proton-decoupled ^2H NMR a very attractive tool. Finally, and contrary to ^{13}C NMR, the possible exploitation of ^2H - ^1H scalar and dipolar couplings is extremely rare due to their low amplitude (0-1 Hz) measured in weakly aligned media, since they directly depend on the products of their corresponding gyromagnetic constants.

From the first results reported in 1992, [Bayle et al., 1992] a large collection of deuterated compounds has been tested to establish the analytical potential of $^2\text{H}\{-^1\text{H}\}$ 1D NMR using polypeptide-based CLCs as enantiodiscriminating media. The experimental results were successful for almost all of the classes of organic chiral compounds tested, including the cases of chiral compounds by virtue of the isotopic substitution (D/H), as well as for enantiomers with a large variety of structures and functional groups (alcohol, amines, carboxylic acids, esters, ethers, epoxides, tosylates, chlorides, bromides). Even cyclic hydrocarbons were successfully discriminated. [Canet et al., 1995; Lesot et al., 2003] Clearly, the method revealed to be efficient regardless the molecular structure: rigid, semi-rigid or flexible, with however significant variations in RQC differences ($|\Delta\Delta\nu_Q|$), which generally depend on the distance of deuterated site to the stereogenic center in more or less flexible compounds. [Lesot et al., 2003]

Four typical examples of $^2\text{H}\{-^1\text{H}\}$ 1D spectra of mono- or dideuterated chiral molecules aligned in PBLG are shown in **Figure 23**, clearly illustrating the ^2H enantiodiscrimination power in a structurally diverse group of chiral compounds (tetrahedral chirality, axial chirality, C_3 chirality, isotopic chirality).

As mentioned in **Section 3.3**, the introduction of a deuterium probe in a target molecule without a real guarantee of success can be seen by organic chemists as a severe technical limitation of ^2H -NMR in CLCs applied. A first alternative consists on discriminating deuterated enantiomers prepared *in situ* by ^2H NMR in CLCs, like in the case of compounds bearing a labile hydrogen (OH or NH) since their isotopic labelling can be achieved by a simple deuterium exchange in the presence of MeOD or D_2O . [Palomino et al., 2012] In the case of amides and amines the labile site is generally in a slow exchange regime at room temperature. [Phillips and Sharman, 2004] The case of chiral alcohols is more difficult. Indeed, at room temperature, the labile deuterons in -OD hydroxyl group are often in a fast exchange regime, from one enantiomer to the other (or with the media), preventing generally their visualization. This exchange can be significantly slowed down by decreasing the sample temperature. [Palomino et al., 2012]

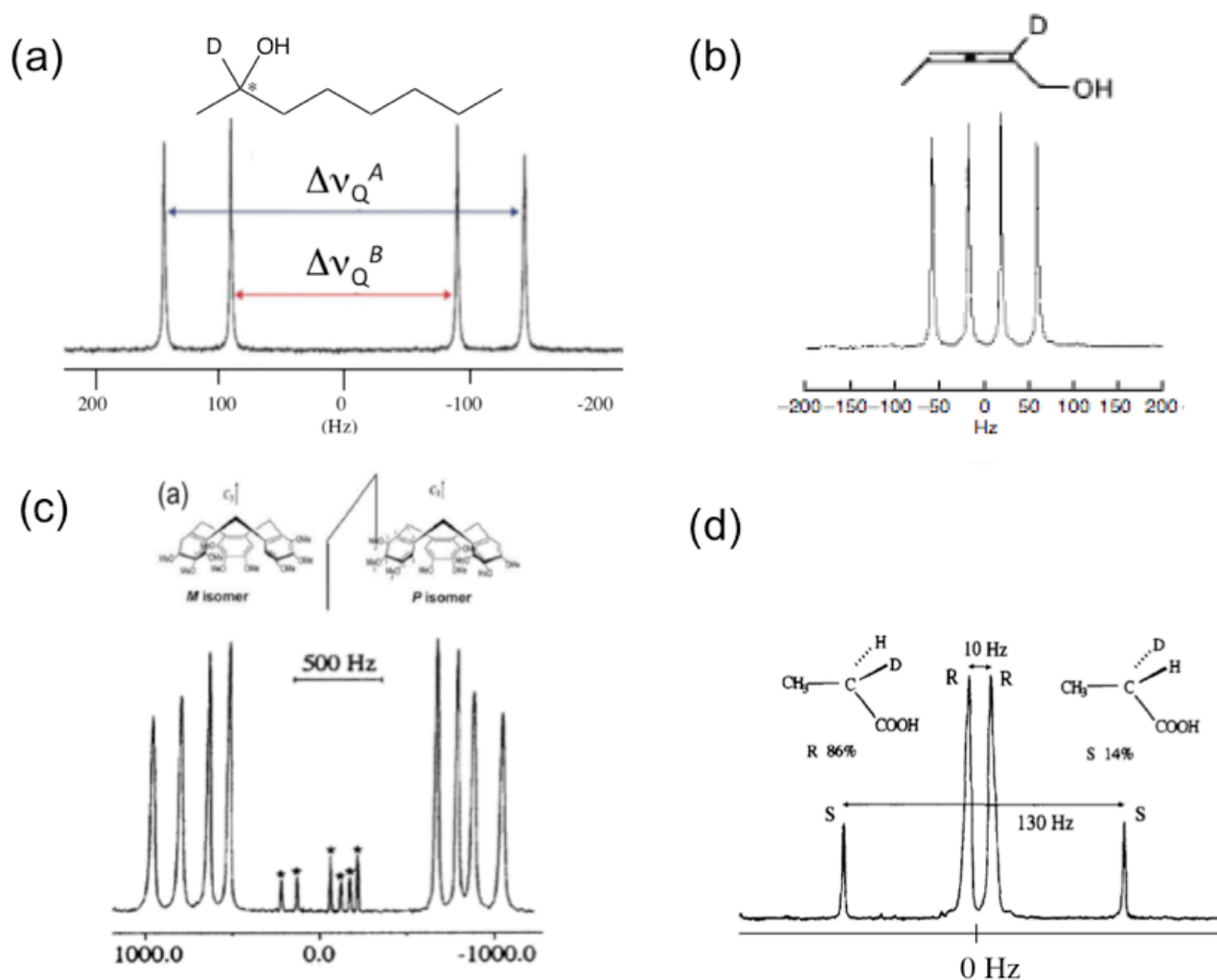


Figure 24. Selected examples of enantiodiscriminations observed by $^2\text{H}\{-^1\text{H}\}$ 1D NMR of deuterated chiral molecules dissolved in a PBLG phase: (a) (*R/S*)-2-deutero-octan-2-ol, (b) (*R/S*)-2-deutero-2,3-pentadiene-1-ol, (c) (*M/P*)- (\pm) -nonamethoxy-CTV hexadeuterated (methylene groups), and (d) *R*-enriched mixture of 2-deutero-propionic acid ($ee(R) = 63\%$). Note that in panel (c) four ^2H -QDs are observed due to the diastereotopicity of the deuterium sites in three equivalent methylene groups. **Figure adapted from Refs. [Lesot et al., 2002; Meddour et al., 1994, 1998; Smadja et al., 1997] with permission.**

To avoid any step of isotopic enrichment, *ex-* or *in-situ*, the ideal alternative remains to be the detection of all natural monodeuterated isotopomers of a molecule by $^2\text{H}\{-^1\text{H}\}$ NMR, as shown using achiral thermotropics or lyotropic chiral liquid crystals. [Khetrapal et al., 1998, Lesot et al., 1998] The advent of high-field NMR spectrometers equipped with fully digital consoles and cryogenic ^2H NMR probes (not a prerequisite) led to a successful application of anisotropic NAD NMR. [Kovacs et al., 2005] Combined with the use of ^2H QUOSY-type 2D experiments (see **Section 2**), it is possible to record NAD spectra for the analysis of complex (chiral) molecules with significant MW, such as natural products (see **Section 7.3**) with reasonable amounts of solute ($4 - 6 \times 10^{-4}$ mol). [Merlet et al., 1999b; Lesot and Courtieu, 2009]

Figure 25a shows a typical example of NAD- $\{^1\text{H}\}$ 1D spectrum recorded with the (\pm)-hept-3-yn-2-ol (seven non chemically equivalent sites, except the hydroxyl group) in PBLG, where numerous components of 14 ^2H -QDs of analyte are overlapped, leading to 1D spectra not trivially analyzable, even with this small molecule. The recording of a ANAD Q-resolved 2D spectrum followed by tilting the 2D map allows a simple analysis of various enantio-isotopomers by separating the $\delta^{\text{aniso}}(^2\text{H})$ and $\Delta\nu_Q(^2\text{H})$ in F_2 and F_1 dimension, respectively (see **Figure 25a**) [Lesot and Lafon, 2008-a]. As it can be seen, the methyl group shows two ^2H -QDs evidencing the discrimination of associated enantio-isotopomer. From practical aspects, the detection of enantiodiscriminations on methyl groups, where three equivalent enantio-isotopomer contribute to the signal (A_3), it is highly advantageous in terms of sensitivity and subsequent robustness of ee determination. As speculated for the methylene group of β -trichloromethyle- β -propiolactone, the diastereotopic sites in methylene 6,6' give rise to eight ^2H -QDs, evidencing of the discrimination of enantio- and diastereo-isotopomers associated with this CH_2 group.

Interestingly, these results permit the enantioselectivity of the alkyne zipper reaction, leading to hept-6-yn-2-ol from the hept-3-yn-2-ol, a possible chiral building block for preparing the dolatrienoic acid used to build the south fragment of dolastatine-14. [Parenty et al., 2012] The analyses of the NAD signals of the methyl of precursor and those associated with one of the diastereotopic deuterons of the methylene group 3 for product, both in racemic and enantioenriched series, have established unambiguously that the reaction was a racemisation-free process (ee over 95%) (see **Figure 25b**). Other examples of NAD spectra will be presented in the applications presented in the next sections.

Note here that some attempts to measure ^2H -RQCs in compressed gels compatible with chloroform (PMMA) and DMSO (poly-HEMA) [Gayathri et al., 2010; Gil-Silva et al., 2016] failed due to strong polymer background signal of ^2H NMR at natural abundance, and limited volume inside the gel (~300 mL) to dissolve large amounts of analyte. Finally, and contrarily to ^{13}C -RCSAs, it is important to note that the magnitude of ^2H -RQCs (as RDCs) is absolutely not affected by the strength of the magnetic field used.

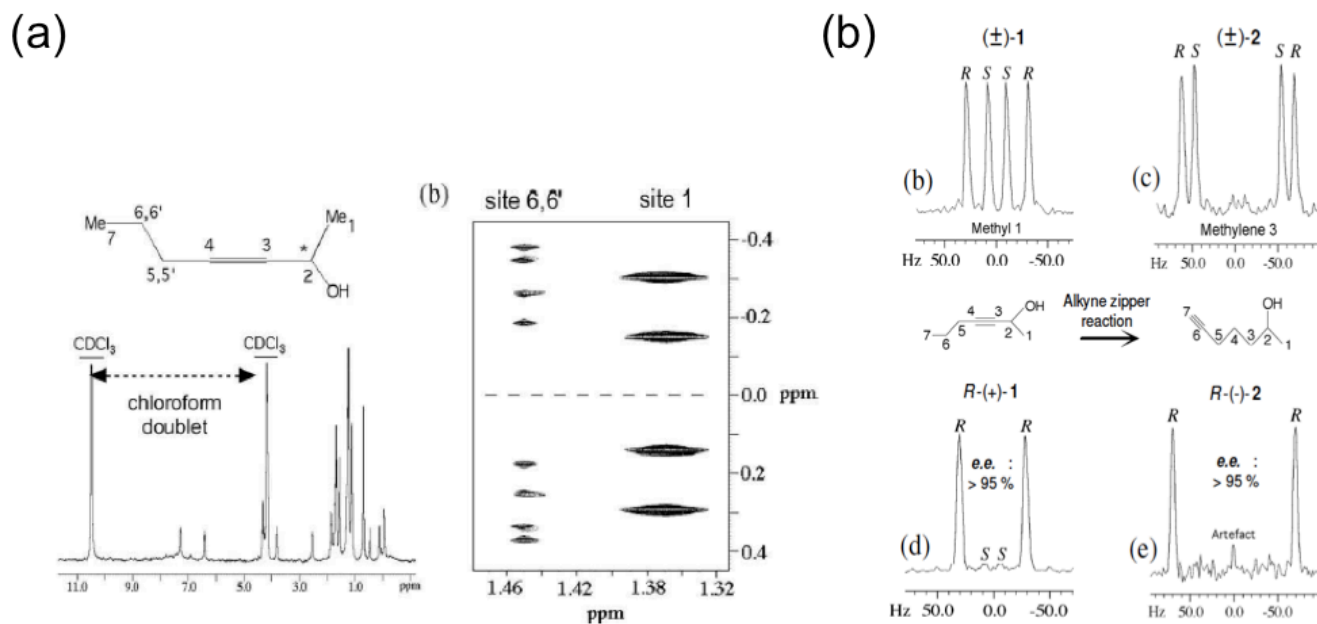


Figure 25. (a) Example of NAD- $\{^1\text{H}\}$ 1D spectrum of (\pm)-hept-3-yn-2-ol in PBLG/ CHCl_3 . Note the NAD signal of chloroform used as organic co-solvent. (b) Zoom on the Q-resolved 2D experiment of (\pm)-hept-3-yn-2-ol showing enantiodiscrimination on methyl and methylene group. (b) 61.4 MHz NAD signals of (b and c) methyl group 1 of **1** and (d and e) one of two deuterons in methylene group 3 of **2** in racemic (top) and enriched series (bottom) in PBLG/ CHCl_3 . **Figure partially adapted from Refs. [Lesot and Lafon, 2008-a; Parenty et al., 2002] with permission.**

Combined anisotropic ^2H and ^{13}C NMR. As demonstrated previously, the use of ^2H homonuclear QUOSY 2D experiments greatly simplifies the analysis of overcrowded ANAD spectra. However, the assignment of ^2H -QDs based on ^2H chemical shifts is not always simple due to the rather low dispersion of ^2H chemical shifts.

An interesting alternative approach to this limitation is to acquire anisotropic ^2H - ^{13}C heteronuclear correlation spectra using pulse sequences derived from the original ^2H - ^{13}C HETCOR experiment, [Lafon, et al. 2004; Lesot et al., 2012] but other schemes have been also proposed, [Sandström et al., 2000; Auger et al., 1998] including in solid NMR. [Robyr et al., 2000] Using polypeptide-based CLCs and deuterated analytes, the 2D experiment was renamed as Carbon-Deuterium Correlation in Oriented Media (CDCOM) (see **Figure 26a,c**). [Lafon et al., 2004] In this experiment, the ^2H magnetization is transferred to ^{13}C so that one-bond ^2H - ^{13}C correlations appear in the direct domain at the chemical shift of each carbon nucleus. The resulting spectra provide significant resolution enhancements in the direct domain (F_2) as a result of the larger chemical shift dispersion of ^{13}C nuclei (in ppm) compared to ^2H .

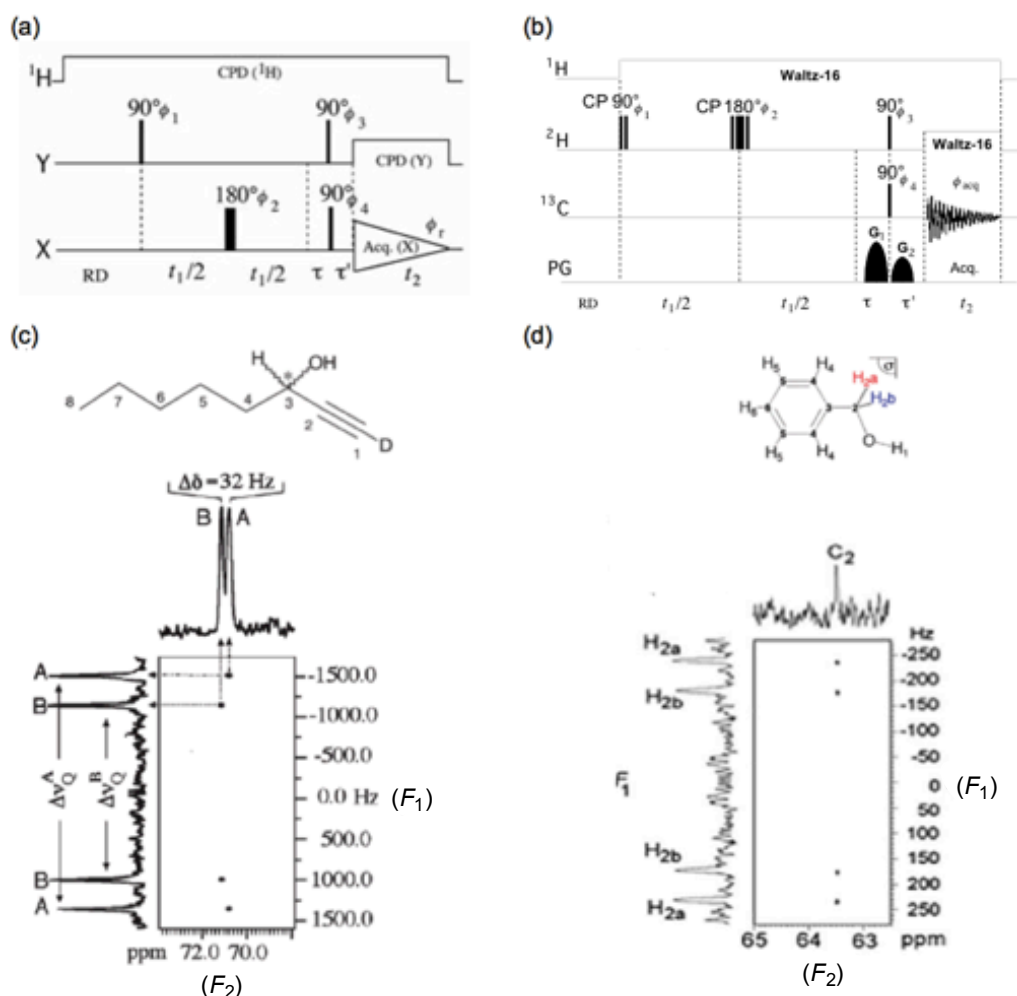


Figure 26. (a and b) Pulse diagram of the CDCOM (HETCOR-type scheme with X: ^{13}C and Y = ^2H) and R-NASDAC 2D experiments, respectively. (c) The CDCOM 2D spectrum of (\pm)-[1- ^2H]-1-octyn-3-ol in PBLG phase recorded at 9.4 T (400.1 and 61.4 MHz) and showing the simultaneous ^{13}C and ^2H enantiodiscrimination (F_2 and F_1). (d) The R-NASDAC 2D spectrum (900.1 and 225.6 MHz) of benzyl alcohol in PBLG and showing the detection of ^2H -X enantio-isotopomers with X: ^{13}C . **Figure adapted from Refs. [Lafon et al., 2004, Lesot et Lafon, 2012, 2014] with permission.**

It has been demonstrated that the anisotropic ^{13}C -detected ^2H - ^{13}C HETCOR 2D sequence displays higher sensitivity than HMQC or HSQC-based 2D sequences, either detecting ^2H or ^{13}C nuclei. [Lesot et al., 2012, 2014]

In the same spirit, but experimentally more difficult, it is possible to detect isotopomers containing both deuterium and carbon nuclei at their natural abundance level ($1.55 \times 10^{-2} \% \times 1.1 \%$) using NASDAC and R-NASDAC 2D experiments (see **Figure 26b**). This optimized version of the ^2H - ^{13}C correlation 2D experiments (HECTOR-type) are able to eliminate all ^2H - ^{12}C and ^1H - ^{13}C isotopomers, and so detecting 1 out of 600,000 molecules. [Lesot et al., 2012] A first example was reported in the case of the ^2H - ^{13}C isotopomer of the small prochiral

molecule benzyl alcohol in PBLG. The differentiation of two ^2H - ^{13}C enantio-isotopomers associated to the methylene group of benzyl alcohol is shown in **Figure 26d**. Finally, the comparison of the F_2 projection of anisotropic NASDAC 2D and $^{13}\text{C}\{-^1\text{H}\}$ 1D spectra allows the determination of the ^2H to ^{13}C isotopic effect on $\delta(^{13}\text{C})$, without deuteration of the analyte.

6.2 Discrimination of enantiotopic elements in prochiral structures

So far, only a few isotropic NMR methodologies were proposed for resolving signals of enantiotopic elements in prochiral molecules. We can mention the use of cryptan ligands, leading to distinct isotropic chemical shifts in prochiral carboxylic acids. **[Bilz et al., 1997]** When successful, differences in interactions between the enantiotopic elements and the enantiopure agent are usually too small to produce significant difference in terms of chemical shifts or scalar couplings. Here again, anisotropic NMR in CLCs has provided new effective alternative for spectrally discriminating enantiotopic elements (see **Section 3.4**).

The spectral discrimination of enantiotopic elements can be achieved using various the NMR approaches already described for enantiomers: ^{13}C NMR, $^{13}\text{C}\{-^1\text{H}\}$ NMR and $^2\text{H}\{-^1\text{H}\}$ NMR, the ^1H NMR being the less adapted tool. **Figures 27a** and **27b** show two examples of enantiotopic discrimination using ^{13}C NMR and $^{13}\text{C}\{-^1\text{H}\}$ NMR, respectively. **[Aroulanda et al., 2001-b; Lafon et al., 2004]** In the case of ethanol (C_s symmetry), the proton-coupled the observed ^{13}C spectral pattern corresponds to an AXYM_3 (with $A = ^{13}\text{C}$ and $\text{XYM}_3: ^1\text{H}$) spin system with two distinct ($^{13}\text{C}\text{-}^1\text{H}$)-RDCs associated with the $^{13}\text{C}\text{-}^1\text{H}$ enantiotopic directions bonded on the prostereogenic center. Details can be found in ref. **[Aroulanda et al., 2001-b]** The analysis of $^{13}\text{C}\{-^2\text{H}\}$ spectrum of perdeuterated diphenylmethanol (another C_s -symmetry molecule) is simpler, since the doubling of $^{13}\text{C}\{-^2\text{H}\}$ resonances of four aromatic sites revealed directly their spectral enantiodiscrimination. Outstandingly, up to 23 Hz of differences in ^{13}C -RCSAs are observed. Using $^{13}\text{C}\{-^1\text{H}\}$ NMR, an identical result would be obtained with a regular sample (not labelled) of diphenylmethanol or the isotopic chiral analogous when only one of aromatic groups is deuterated. **[Lesot et al., 2004-a]**

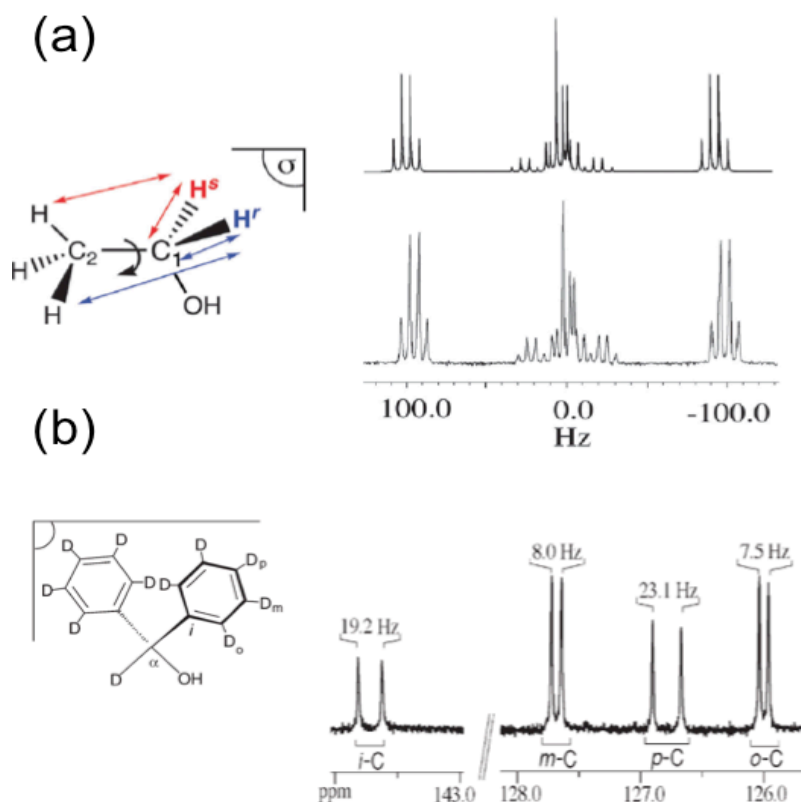


Figure 27. (a) Experimental (bottom) and simulated (top) proton-coupled ^{13}C signal of the C-1 carbon of ethanol. The spectral pattern corresponds to a AXYM_3 spin system. Note the spectral desymmetry due to a second order effect. (b) $^{13}\text{C}\{-^2\text{H}\}$ 1D signals of aromatic carbons of perdeuterated diphenylmethanol (C_s symmetry). Both spectra were recorded at 100.3 MHz in PBLG. **Figure partially adapted from Refs. [Aroulanda et al., 2001-b; Lafon et al., 2004] with permission.**

The use of ^2H 1D/2D NMR in CLCs is another excellent tool for revealing enantiotopic discriminations in prochiral deuterated compounds. First tested on isotopically enriched C_s -symmetry molecules like benzyl alcohol, [Meddour et al., 1994] ethanol [Aroulanda et al., 2001-b] or perdeuterated diphenylmethanol, [Lafon et al., 2004] but also compounds of C_{2v} symmetry (acenaphthen). [Merlet et al., 1999-a] This approach has been extended to the detection of deuterium atoms at natural abundance level. In this case, and contrary to enantiomers, only the monodeuterated enantio-isotopomers (isotopic chirality) of a mixture (associated with a pair of hydrogenated enantiotopic sites) will be discriminated, giving rise to two ^2H -DQs observable when the enantiodiscrimination occurs (see **Figure 7**). It is important to understand here that the discrimination of enantiomers of isotopic chirality is a consequence of the discrimination of enantiotopic elements in the prochiral parent molecule. With this approach, it has been possible to experimentally validate the theoretical arguments predicting that all prochiral molecules of C_s , C_{2v} , D_{2d} and S_4 possess enantiotopic directions discriminable in CLCs. [Merlet et al., 1999-a] **Figures 28a** and **28b** show two typical examples of enantiotopic

discriminations in D_{2d} and S_4 prochiral molecules using $^2\text{H}\{-^1\text{H}\}$ NMR. [Aroulanda et al., 2011; Lesot et al., 2015-a] Note that molecules of S_4 symmetry are rather rare in Nature.

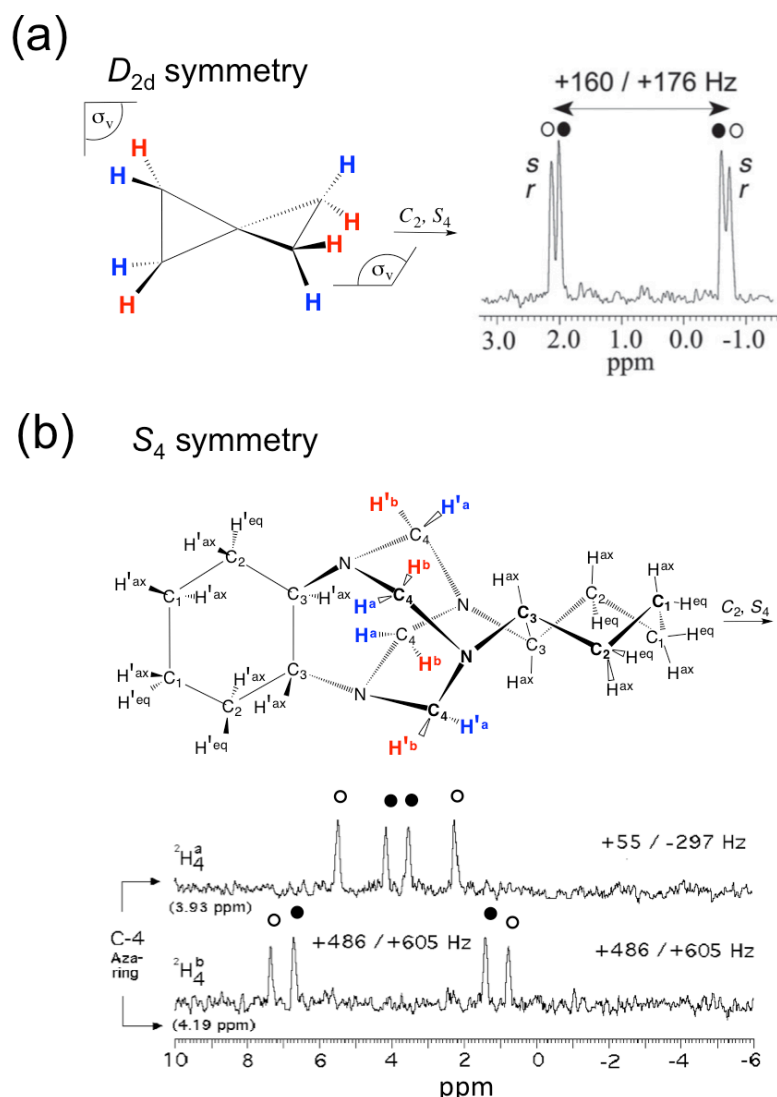


Figure 28. Two examples of D_{2d} and S_4 molecules possessing enantiotopic sites (red/blue) and their associated NAD- $\{^1\text{H}\}$ enantiodiscriminated signal: (a) spiropentane (D_{2d}) and (d) icosane (S_4). The doubling of ^2H -QDs indicates the discrimination of deuterated enantio-isotopomers. **Figure from Refs. [Aroulanda et al., 2011] and [Lesot et al., 2015-a] with permission.**

All examples shown so far were obtained with polypeptide-based LLCs co-dissolved in a broad range of organic solvents, but the enantiotopic discrimination phenomenon has been also revealed using other chiral weakly orienting media. We can mention chiral systems made of: i) DNA-based water compatible LC in case of dideuterated glycine (see **Figure 29a**), [Lesot et al., 2011-a] ii) polyacetylene-based LC in case of perdeuterated C_S -symmetry analyte (ethanol,

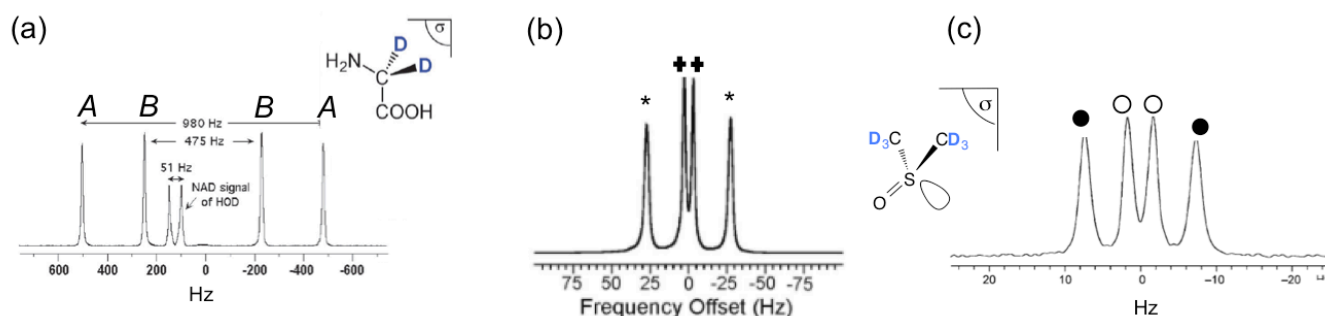


Figure 29. Three examples of enantiotopic discriminations in C_s symmetry prochiral molecule by ^2H NMR: (a) glycine- d_2 in DNA/water based CLC, (b) DMSO- d_6 in a stretched gelatin gel, and (c) DMSO- d_6 in a polysaccharide-based stretched gel (i-carrageenan). **Figure from Refs. [Lesot et al., 2011-a; Naumann and Kuchel, 2008, 2009] with permission.**

benzyl alcohol, DMSO) but also of C_{2v} symmetry (acenaphthen), [Lesot et al., 2019] as well as compressed gelatin gels [Naumann and Kuchel, 2008] or cross-linked gelatin. [Kummerlöwe et al., 2009] Finally, polysaccharide-based stretched gels (i-carrageenan) using DMSO- d_6 as prochiral probe (see Figure 29b). [Naumann and Kuchel, 2009]

Before closing this section, it is noteworthy to examine the intriguing case of malononitrile ($\text{H}_2\text{C}(\text{CN})_2$) (MLN), a rigid C_{2v} -symmetry molecule with a non-prostereogenic tetrahedral center. [Aroulanda et al., 2001] For chemists, MLN could be defined as “pro-prochiral”, because *a priori* two chemical steps would be needed to convert it into a chiral structure. From a symmetry point of view, MLN can be also defined as non-prochiral, because it may be superimposed upon itself by an overall rotation, thus producing a structure that is indistinguishable from the original. Finally, from a more stereochemical side, if the (bonded) ^{13}C - ^1H internuclear directions are homotopic and cannot be differentiated in a CLC, the $^{13}\text{C}\cdots^1\text{H}$ (non-bonded) internuclear directions are enantiotopic (exchangeable by a plane), and so expected to be spectrally distinguished in a CLC. Experimentally, a typical second-order spectral pattern (AXX' spin system) was observed for ^{13}C signals (C-2/C-3) of nitrile group in the PBLG chiral phase showing the enantiodiscrimination of these directions. This pattern disappears in the PBG-based ALC. Amazingly, the spectral differentiation of enantiotopic directions in MLN, a C_{2v} symmetry molecules without a prostereogenic tetrahedral center, has validated a stereochemical hypothesis made by Mislow and Raban in 1967. [Mislow and Raban, 1967] Indeed, it had been speculated that “for molecules of the type “CXXYY”..., the two X groups as well as the Y groups are equivalent and cannot be distinguished in chiral or achiral experimental conditions. However, the relationships between X and Y groups are not all equivalent. The four X-Y relationships may be ordered into two enantiotopic sets of two equivalent relationships”.

These results validate also a more recent concept of stereogenicity defined by Fujita in 1990, who considers that “the compounds (CX_2Y_2) can be regarded as prochirals, since the four edges (X-Y) construct an enantiospheric $C_{2v}(C_1)$ orbit”. [Fujita, 2000] Clearly, a fundamental stereochemical issue about the definition of prochirality and the concept of enantiomorphism is raised here. Indeed, MLN can be regarded as a prochiral compound when interacting with the CLC, while for organic chemists, this molecule is not!

6.3 Dynamic analysis by 2H NMR

The study of conformational dynamic processes (as intramolecular interconversion or exchange processes) in achiral or chiral, flexible molecules allows to understand their molecular internal motions. [Luz et al., 2003, 1983] In particular, from the analysis of NMR spectra, we can determine, for instance, exchange or interconversion rate constants, which themselves depend on the magnitude of the barrier to interconversion, ΔH^\ddagger , and the sample temperature. [Bain, 2003] This can be done using isotropic or anisotropic NMR, chiral or not chiral oriented media. However, the combination of NMR and chiral anisotropic environments makes possible to study dynamic processes involving enantiomeric molecular forms or enantiotopic elements in prochiral molecules, [Lesot et al., 2006; Lafon et al., 2007] since in both cases their spectral discrimination is possible. These exchange processes are, obviously, invisible in achiral (oriented) media.

Among the NMR tools described above, $^2H\{-^1H\}$ NMR possess three advantages for such investigations: i) simple high-resolution spectra dominated by the 2H quadrupolar interaction, ii) the phenomenon can be clearly identified, and iii) spectral separations between exchanging 2H anisotropic signals can be much larger than those observed in isotropic 2H or ^{13}C NMR, thus allowing a much wider dynamic process range to be studied. Two examples are proposed here: the case of (\pm)-*cis*-decalin and (\pm)-1-bromo-2-methyl-3-deuterio-5-(1'-naphthyl)benzene).

Case of *cis*-decalin. *Cis*-decalin (CDC) can be described as a chiral compound without any stereogenic center while possessing a two-fold rotational symmetry axis (see **Figure 30a, top**). Interestingly, this molecule is submitted to a possible interconversion between two limit conformers constituted by a pair of C_2 -symmetry enantiomers. As a consequence, the orientational behavior of CDC and its associated NMR spectra recorded in a CLC is highly dependent on the sample temperature, while different structures are involved to qualitatively interpret the experimental data according to T (see **Figure 30b, bottom**).

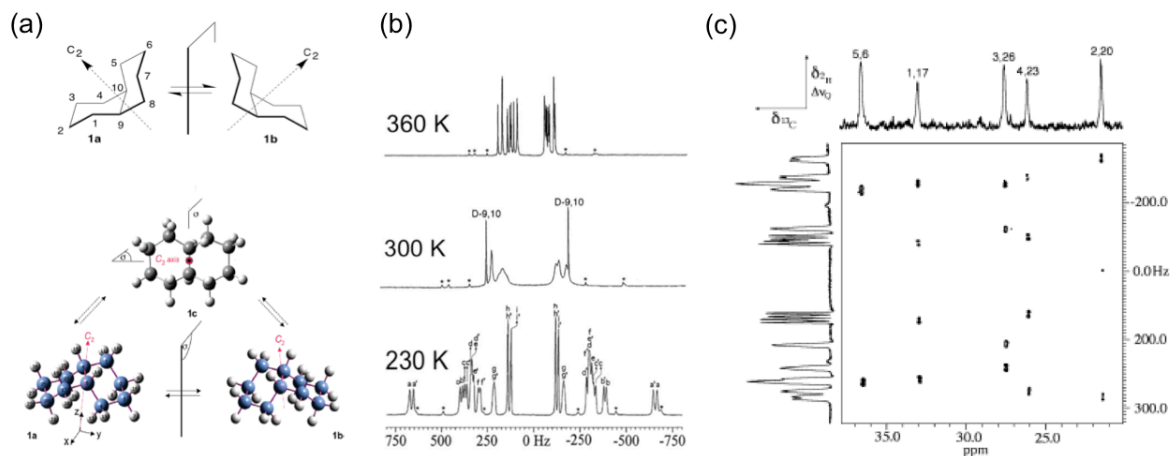


Figure 30. (a) (top) C_2 -symmetry conformers of *cis*-decalin and associated position numbering, (bottom) C_{2v} -symmetry high-energy conformation of *cis*-decalin. (b) 61.4 MHz ^2H 1D-NMR spectra of perdeuterated *cis*-decalin in PBLG recorded at three temperatures. Note the coalescence at 300 K. (c) ^2H - ^{13}C HETCOR 2D spectrum recorded at 243 K. **Figure adapted from refs. [Sarfati et al., 2001; Aroulanda et al., 2009] with permission.**

Experimentally, CDC in PBLG phase can be studied at different temperatures, between 230 and 360 K, using deuterium (perdeuterated compound). [Sarfati et al., 2001] In each case, the ^2H NMR spectra obtained result from averaged NMR observables along the conformational pathway. In **Figure 30b** is presented the variation of ^2H spectrum at three temperature (230, 300 and 360 K). As seen, the coalescence effect is obtained at 300 K. At this temperature, the single high-resolution doublet can be unambiguously assigned to the deuterated sites 9 and 10 located on the bridgehead of CDC because, whatever the temperature, they exhibit no kinetic averaging between the conformational forms 1a and 1b.

The analysis of ^2H 1D NMR spectrum as well as ^2H - ^{13}C HETCOR 2D NMR map (**Figure 29c**) at low temperature (230 K) shows a chiral spectral differentiation between two C_2 -symmetry invertomers while at high temperature (360 K) the spectrum with coherent with a high-energy, C_{2v} -symmetry conformation (in average). The analysis of CDC oriented in the PBLG-based ALC, where all enantiodiscriminations vanish, fully confirms the interpretation of results in the CLC. Thus, a maximum of five ^2H -QDs is expected in ^2H NMR in the CLC, D-9/D-10, D-5, D-4, D-1, D-8, D-5', D-4', D-1', D-8', D-6, D-2, D-7, D-3, D-6', D-2', D-7', D-3, and nine of ^2H -QDs in CLCs, two for each enantiotopic pairs and one for the homotopic pair D-9/D-10.

Determination of the activation barrier energy. As a second illustrative example, we consider the case of (\pm)-1-bromo-2-methyl-3-deuterio-5-(1'-naphthyl)benzene (BMNB), a monodeuterated atropisomer orthosubstituted biaryl, investigated by ^2H - $\{^1\text{H}\}$ 1D NMR in

PBLG, again (see **Figure 31a**). The spectral variation of BMNB-d₁ versus T is displayed in **Figure 31b**. Here, the coalescence phenomenon is observed at 250 K. This temperature indicates a weakly sterically crowded compound.

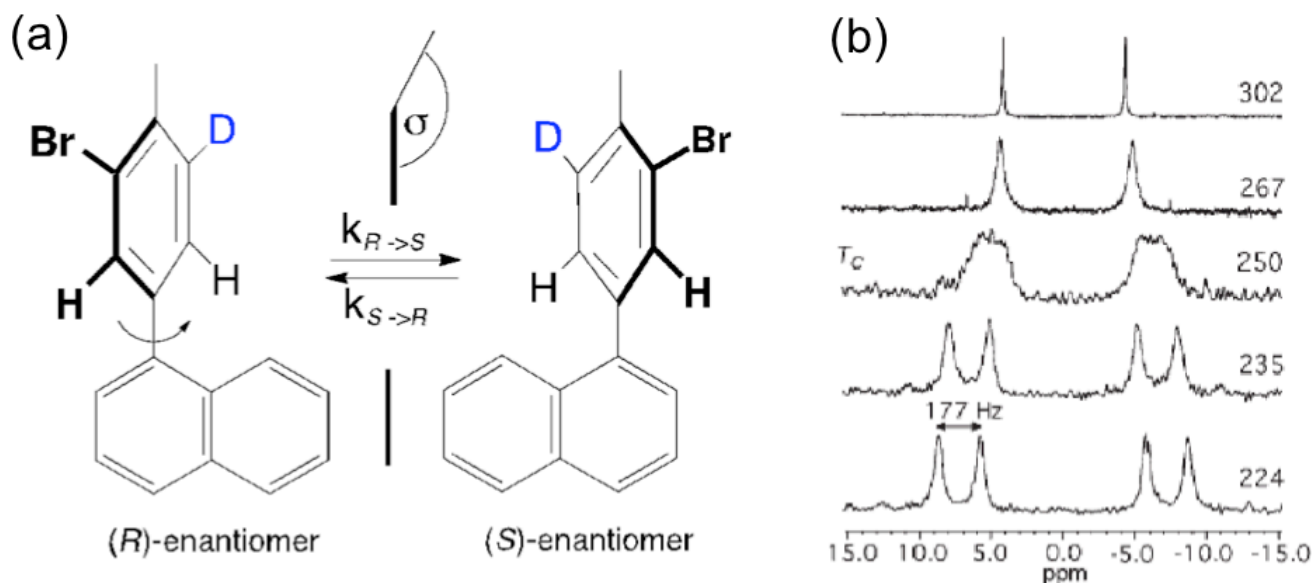


Figure 31. (a) Enantiomeric conformers associated with the (\pm)-1-bromo-2-methyl-3-deuterio-5-(1'-naphthyl)benzene. (b) Associated experimental (left) and simulated (right) 61.4 MHz $^2\text{H}\{-^1\text{H}\}$ 1D-NMR spectra in PBLG versus five temperatures. **Figure adapted from Ref. [Lafon et al., 2007] with permission.**

Determination of thermodynamic parameters from NMR data is possible from the Eyring's equation that described the dependence of the exchange/interconversion rate constant, k , on temperature: [Lafon et al., 2007]

$$k = \frac{RT}{N_A h} \exp\left(-\frac{\Delta G^\ddagger}{RT}\right) \text{ with } \Delta G^\ddagger = \Delta H^\ddagger - T \times \Delta S^\ddagger. \quad (18)$$

where $R = 8.32 \text{ J}\cdot\text{K}^{-1}\cdot\text{mol}^{-1}$, $N_A = 6.02 \times 10^{23} \text{ mol}^{-1}$ and $h = 6.62 \times 10^{-34} \text{ J}\cdot\text{s}$, and T is expressed in K.

Using spectral data measured in simulated ^2H NMR spectra and the analysis of the Eyring plot, namely the natural logarithm of $kN_A h/RT$ against $1/T$ above and below the coalescence temperature: [Lafon et al., 2007] the activation parameters ΔH^\ddagger , ΔS^\ddagger , and subsequently $\Delta G^\ddagger(T)$, can be extracted; the slope and the y-intercept of plot are equal to the ratio $(-\Delta H^\ddagger/R)$ and $(\Delta S^\ddagger/R)$, respectively.

Interestingly, the rate constant, k , and the free energy of activation, ΔG^\ddagger , at the coalescence temperature, T_c , (denoted hereafter $\Delta G^\ddagger(T_c)$) can easily be deduced from the measurement of the half-difference of ^2H quadrupolar splittings, $|\Delta\Delta\nu_Q| = |\Delta\nu_Q^A/2 - \Delta\nu_Q^B|/2$, in the ^2H spectrum

below T_c . At this particular temperature, assuming identical time constant (T_2^*) for the FID decay of both exchanging deuterons, we can write:

$$k = \pi \times \left| \frac{\Delta\nu_Q^A}{2} - \frac{\Delta\nu_Q^B}{2} \right| \quad (19)$$

and

$$\Delta G^\ddagger(T_c) = RT_c \times \ln\left(\frac{RT_c}{N_A h} \times \frac{2\sqrt{2}}{|\Delta\nu_Q^A - \Delta\nu_Q^B|}\right) \quad (20)$$

In practice, the anisotropic $^2\text{H}\{-^1\text{H}\}$ or $\text{NAD}\{-^1\text{H}\}$ spectra measured at T_c can be very different depending on the signs of $\Delta\nu_Q$ for deuterons A and B , as well as the magnitude of $|\Delta\nu_Q^A - \Delta\nu_Q^B|$ compared to $\Delta\nu_Q^A$ and $\Delta\nu_Q^B$. **[Lesot et al., 2006]**

From data measured in simulated NMR spectra (not shown) and the analysis of the Eyring plot, namely the natural logarithm of $kN_A h/RT$ against $1/T$ above and below the coalescence temperature, the activation parameters ΔH^\ddagger , ΔS^\ddagger , and subsequently $\Delta G^\ddagger(T)$, can be extracted from the slope ($-\Delta H^\ddagger/R$) and the y-intercept of plot ($\Delta S^\ddagger/R$). **[Lesot et al., 2006; Bain, 2003]** Thus the coalescence reached at $T = 250$ K corresponds to a value of k equal to $3.2 \cdot 10^2 \text{ s}^{-1}$. The activation parameters of **Eq. 20** derived from the Eyring plot analysis. **[Bain, 2003; Eyring, 1935]** were found to be equal to $\Delta H^\ddagger = 44.7 \pm 0.5 \text{ kJ.mol}^{-1}$, $\Delta S^\ddagger = -18 \pm 2 \text{ J.mol}^{-1}.\text{K}^{-1}$ and $\Delta G^\ddagger(T_c) = 49.0 \pm 0.5 \text{ kJ.mol}^{-1}$.

Reaction monitoring. Another important aspect of “dynamic” NMR spectroscopy is the chemical reaction monitoring by NMR, *in situ* and in real time. The idea is to follow the amount (concentration) of reactant and product(s) *versus* time when the reaction is performed in the NMR tube inside the magnet of the spectrometer. This can be done by integrating/deconvoluting the peak surfaces of reactant(s) and product(s) on spectra of any magnetically active nuclei showing a clear spectral signature (isolated peaks, for instance). Many investigations (inside the tube or in flow) using isotropic solvents and high field NMR, **[Maiwald et al., 2004]** as well as low field NMR **[Dalitz et al., 2012; Gouilleux et al., 2016]** can be found in literature. Investigations using thermotropic liquid crystals as reaction solvents have been also described. **[Leigh, 1991, 2008]**

In 2013, an approach involving anisotropic ^2H 1D NMR and DNA-based chiral LLCs was reported to follow an enzymatic racemization reaction (alanine racemase, an active enzyme) on a deuterated substrate (alanine- d_3) in a scalemic mixture in order to determine its kinetic

parameters (time-dependent parameters) and understanding its mechanism reaction. [Chan-Huot *et al.*, 2013] As this DNA oriented system is enantiodiscriminating, it is possible to distinguish between enantiomer signals of alanine- d_3 , as shown in **Figure 32a**, and hence follow their respective concentrations *versus* time. Interestingly, $^2\text{H}\{-^1\text{H}\}$ NMR of deuterated substrate provides simple analysis of signals. In this example, the larger linewidth for the (*L*)-isomer originates from internal $^2\text{H}\text{-}^2\text{H}$ total couplings that are not equal to zero as for the (*D*)-isomer.

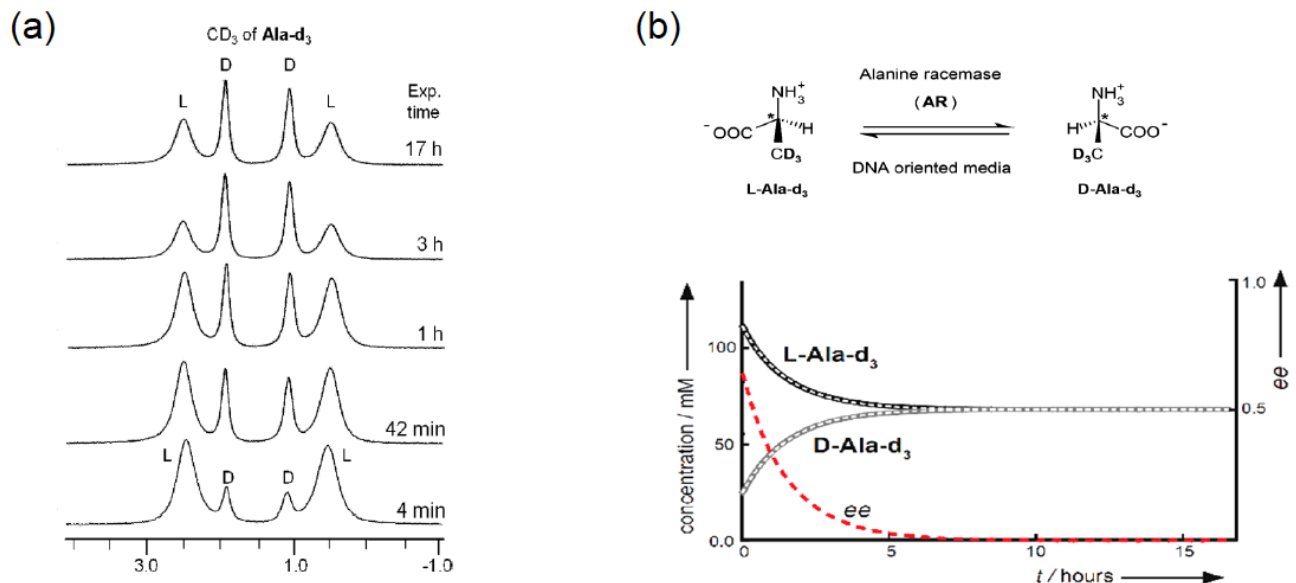


Figure 32. (a) Examples of $^2\text{H}\{-^1\text{H}\}$ 1D signals (same vertical scale) of (*L*)- and (*D*)- d_3 recorded at different time intervals after the introduction of AR in the DNA LLC. (b) (top) Principle of racemisation of alanine- d_3 by AR in DNA-based oriented media. (bottom) Variation of *ee* (red dashed line) and experimental (black and grey continuous lines) and fitted (white dashed lines) concentrations (in mM) of (*L*)- and (*D*)-Ala- d_3 as a function of time (in hours). **Figure adapted from Ref. [Chan-Huot *et al.*, 2013] with permission.**

The time-dependent concentrations permit the evaluation of k_{catL} and k_{catD} (kinetic parameters) for a reversible Michaelis-Menten model, the Michaelis constants K_M and $K_{M'}$ being determined independently. The values of k_{catL} and k_{catD} obtained with this tool are consistent with previous values using circular dichroism, thus showing the potential and robustness of the method proposed.

Ultrafast 2D NMR. The main difficulty of chemical reaction monitoring in real time is the experimental time needed to record spectral data of all compounds in a molecular mixture. This situation can be drastic for extremely fast and/or multiple (cascade) chemical transformations for which the fast identification and reliable quantification of ^2H signals of chiral (or not) products (reactants, (un)stable intermediates, and products) requires 2D-NMR experiments with sub-minute time resolutions or even sub-second time resolutions. Although non-uniform sampling

(NUS) methods, which consist of sparse acquisitions of experimental data (Nyquist's condition not fulfilled) can reduce the experiment times of isotropic or anisotropic 2D-NMR experiments. [Lesot *et al.*, 2015-b; Mobli *et al.*, 2014] The gain in time is not enough for reaching sub-second durations. To overcome these difficulties, ultrafast 2D-NMR experiments, first developed for solution-state NMR, provide an efficient alternative. [Frydman *et al.*, 2003; Giraudeau, 2014] First proposed in 2012 for recording (^1H - ^{13}C)-coupled HSQC 2D spectra in a single PBLG phase. [Giraudeau *et al.*, 2012] The approach has been extended to anisotropic ^2H 2D NMR, and denoted as "ADUF" spectroscopy (see Figure 33). [Lesot *et al.*, 2016] In this particular homonuclear anisotropic ^2H ultrafast 2D-NMR experiments, the usual time (F_1) is replaced by a spatial encoding in QUOSY-like 2D sequences (Q-COSY, Q-resolved and Q-DQ), [Merlet *et al.*, 1999b] thus allowing recording anisotropic ^2H spectra in sub-second experimental times. The

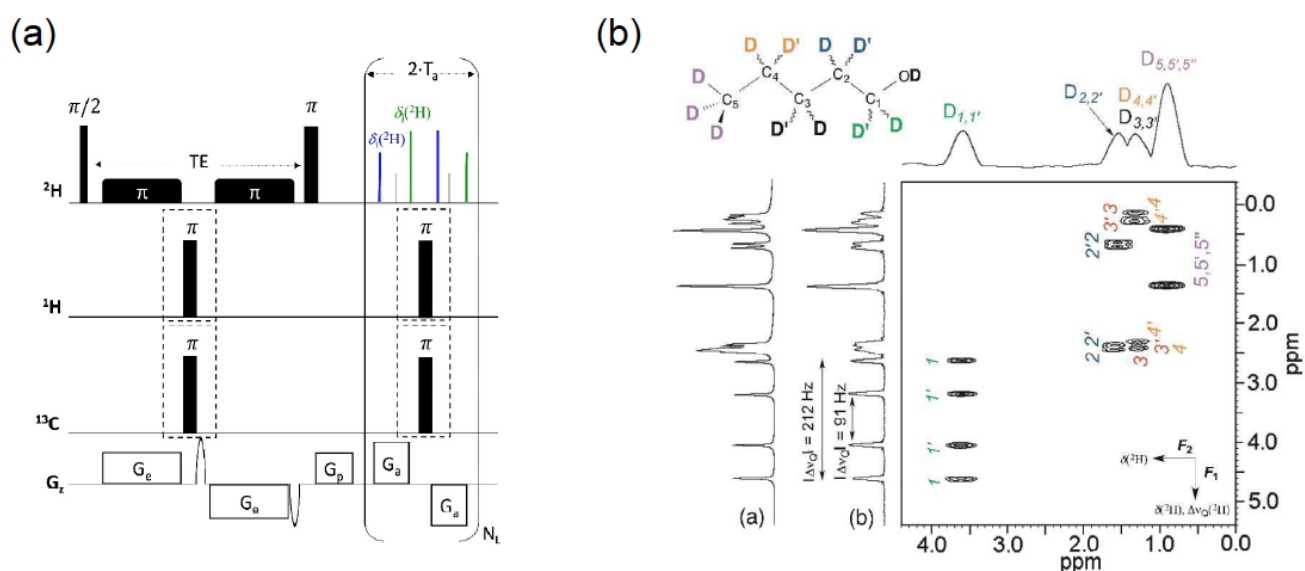


Figure 33. (a) Pulse scheme of the ^2H - $\{^1\text{H}\}$ ultrafast-resolved constant-time pulse NMR sequence. The blocks for ^1H decoupling during the spatial encoding and acquisition periods are shown in dashed boxes. G_e and G_a correspond to the gradients applied during the same periods, respectively. (b) 107.5 MHz single-scan ADUF- $\{^1\text{H}\}$ 2D map (magnitude mode) with F_1 and F_2 projections of $[^2\text{H}_{12}]$ -1-pentanol- d_{12} in the PBLG/ CHCl_3 phase, recorded in ca. 400 ms. The 107.5 MHz ^2H - $\{^1\text{H}\}$ 1D spectrum is also shown as a top projection. **Figures adapted from Ref. [Lesot *et al.*, 2016] with permission.**

choice of various ADUF 2D sequences enlarges the usefulness and applications of the proposed technique. [Gouilleux *et al.*, 2020]

7 Structural value of anisotropic NMR parameters

Among the analytical techniques used routinely in organic chemistry, 1D or 2D NMR spectroscopy is becoming an unavoidable tool for the structural analysis of small molecules, in

particular the determination of the constitution of chiral or non-chiral molecules. [Claridge, 2016] The next challenge is the possibility to establish the 3D spatial structure of a molecule, or in other words determine its configuration and its preferred conformation/s. In isotropic solvents, this task has been historically achieved using scalar couplings (E.g. $^3J_{HH}$ and $^3J_{CH}$), [Haasnoot et al., 1980; Palermo et al., 2010; Marshall et al., 1983] which follow Karplus-based equations to extract dihedral angle information, or the NOE effect to obtain proton-proton distances, [Anet and Boom, 1965; Neuhaus, 2012] These conventional NMR parameters provide structural information of local characters. If or some reason, the chain of J couplings or interproton distances is become disconnected there is no way to correlates the relative configuration of remotely located stereocenters.

For example, to determine the relative configuration of the stereocenters at carbons C-3 and C-17 in the compound in **Figure 34a**, a relay of *J*-couplings and NOE correlation from C-3 to C-17 is enough to achieve this goal. However, if those correlations are interrupted by a linker lacking any 3D structural information (flat in this example) such as that one in the structure on the right is present, there is no way to perform it using *J*-couplings and NOE correlations only. A distance of 7.5 Å (structure on the right) is too far to observe an NOE correlation, when the limit in NMR of small molecules is no more that 4 - 5 Å (see **Figure 34b**).

In this Section, we show the power of anisotropic NMR for the determination of the relative configuration, namely the 3D structure of the molecule. An important number of articles have demonstrated the interest of extracting RDC and/or ^{13}C -RCSAs in the determination of the configuration of molecule of natural compounds, [Liu et al., 2018; Gil et al., 2017-a; Nath et al., 2016; Gil et al., 2014; Boettcher et al., 2012] but the use of ^2H -RQC has been only demonstrated in 2020. [Lesot et al., 2020] RDCs, RCSAs and RQCs do not encode information of the distance between stereocenters, that's why it is necessary to first know how the atoms are connected in the molecule (molecular constitution). However, these anisotropic NMR parameters allow us to determine the relative orientation of stereocenter regardless of the distance between them. Here is where the power of these parameters resides by lifting the limitations imposed by conventional isotropic NMR parameters (scalar couplings and NOE).

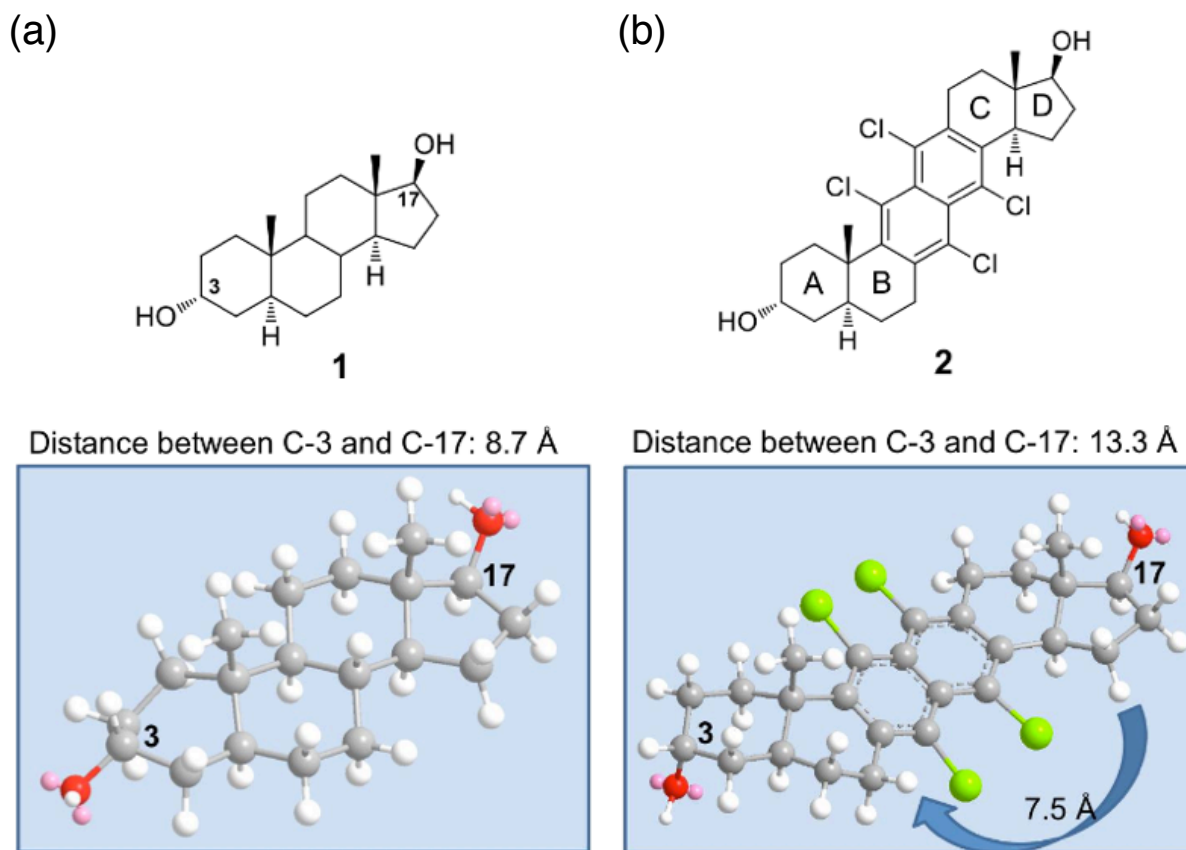


Figure 34. 3D structures of (a) etiocholanediol (1) and (b) a hypothetical derivative (2). **Figures adapted from Ref. [Gil et al., 2017a] with permission.**

7.1 From the molecular constitution to configuration of complex molecules

Principle and process. The main reason to use anisotropic NMR Data is that it exists a univocal relationship between the order-dependent NMR observables (RCSA, RDC or RQC), the Saupe order matrix that describe the orientation of the molecule in the mesophase and the structure of the molecule (see **Figure 34**).

The fit between experimental and back-calculated anisotropic data (from the order matrix for a given (known) geometry) is obtained by varying the elements of Saupe order matrix, $S_{\alpha\beta}$, (using an algorithm based on the principle of singular value decomposition (SVD)) in order to minimize the difference between the two sets of data. **[Losonczi et al., 1999]** **Figure 35** depicted the principle of the calculation. The agreement between the experimental ($Obs_n^{Exptl.}$) and back-calculated ($Obs_n^{Calc.}$) data during the SVD fitting procedure is evaluated by Cornilescu's quality factor, Q , calculated as follows: **[Conilescu et al., 2000; Kramer et al., 2004]**

$$Q = \sqrt{\frac{\sum w_n (\text{Obs}_n^{\text{Exptl.}} - \text{Obs}_n^{\text{Calc.}})^2}{\sum w_n (\text{Obs}_n^{\text{Exptl.}})^2}} \quad (21)$$

where w_n are normalized relative weighting factors. For uniform weighting, w_n is equal to one when a single type of anisotropic data (RCSA, RDC, RQC) used. w_n can be different if various anisotropic data are used simultaneously.

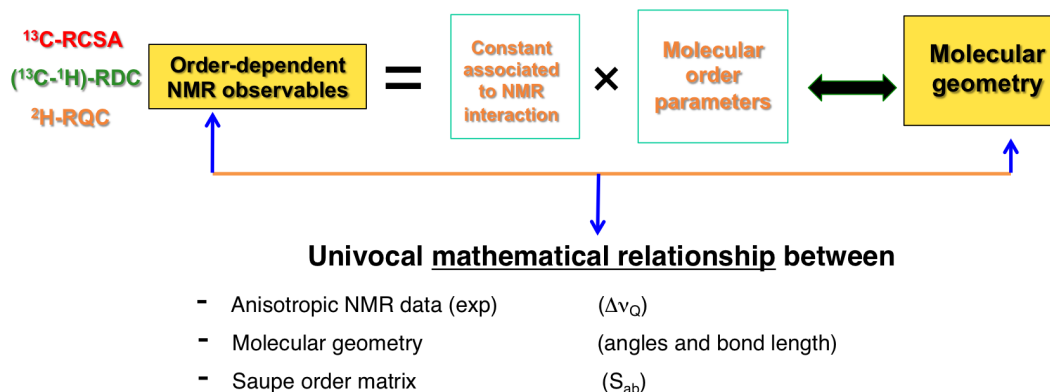


Figure 35. (a) Schematic description of the univocal relationship between a set of experimental anisotropic observables, the molecular geometry and the molecular order parameters (alignment tensor).

In practice, the smaller the value of Q , the better the agreement. The agreement between experimental and predicted value can be graphically presented simply by a correlation plot ($\text{Obs}_n^{\text{Exptl.}}$ vs. $\text{Obs}_n^{\text{Calc.}}$). One example of plot is shown in **Section 7.4**. In practice, Q -values below 0.05 means an excellent agreement between the two set of data for a given geometry. Q -values over 0.1 indicate a smaller confidence between experimental data and structure. The quality of fit between the two set of data can also be evaluated by calculating the standard deviation as:

$$RMSD = \sqrt{\sum w_n (\Delta v_Q^{\text{Exptl.}}(^2\text{H}) - \Delta v_Q^{\text{Calc.}}(^2\text{H}))^2} = \sqrt{\frac{1}{N} \sum (\Delta v_Q^{\text{Exptl.}}(^2\text{H}) - \Delta v_Q^{\text{Calc.}}(^2\text{H}))^2} \quad (22)$$

As for Q -factor, the smaller the value of the RMSD, the better the agreement is.

In the frame of (unknown) relative configuration determination, possible structures of reasonable energy (determined by DFT calculation or other computational approaches as MMFF) must be tested. [Navarro-Vazquez et al., 2018, Troche-Pesqueira et al., 2017] Combining a given set of anisotropic experimental data for a set of diverse, possible relative

configurations results in a variation of the Q-factor, as can be seen in **Figure 36**. [Lesot *et al.* (SI)] In this case, two factors must be considered for a final selection of the configuration: i) the smallest value of Q-factor, ii) the difference to the second smaller Q-factor value.

Note that the case of flexible molecules is more complex to manage because it becomes necessary to consider various conformers with an individual weight in the calculation. In addition, different from isotropic NMR parameters, the value of the anisotropic NMR parameters (RDCs, RCSAs and RQCs) for each conformer depends on their shape and orientation, as will be discussed more in detail in session 7.2.

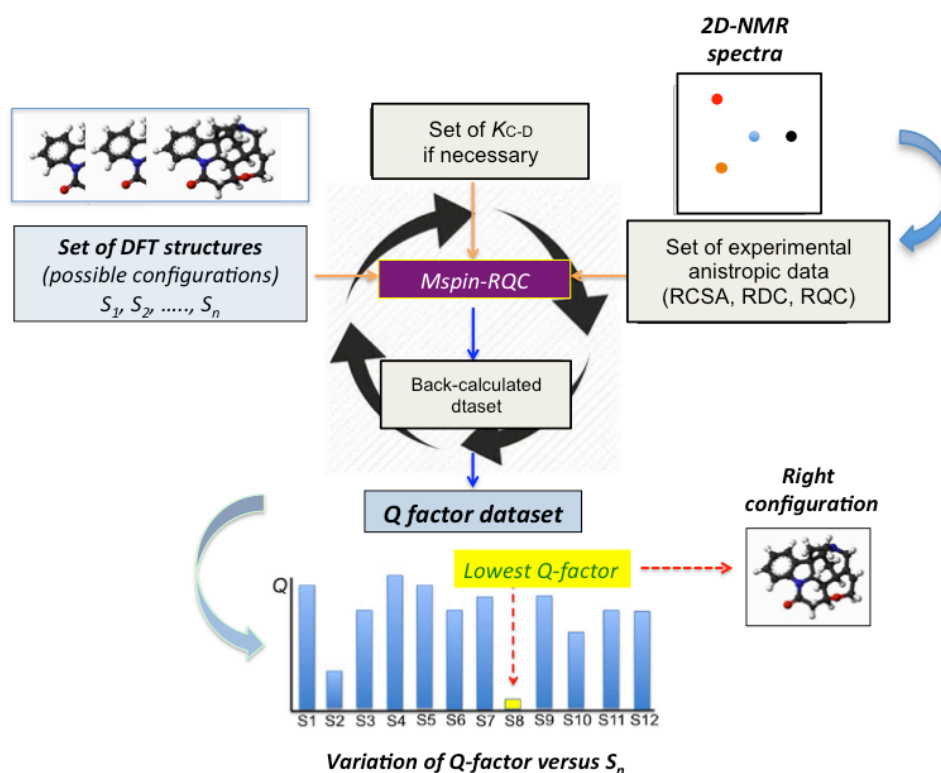


Figure 36. Simplified principle of fitting of experimental anisotropic observable dataset to a set of possible structures. **Figure adapted from ref. [Lesot *et al.*, 2020-b (SI)] with permission.**

Hyphenated programs. From the first exploitable anisotropic data, various computational programs have been developed to exploit the analytical potential of anisotropic data. We can mention the program “SHAPE” initially developed by P. Diehl *et al.* that was suitably modified to handle RDCs and ²H-RQCs as input data. [Diehl *et al.*, 1971; Aroulanda *et al.*, 2003] More two recent two important achievements were proposed with the program MSpin [Navarro-Vazquez *et al.*, 2017; Navarro-Vazquez *et al.*, 2012] as well as the program ConArch+. [Immel *et al.*, 2018; Köck *et al.*, 2020] Both programs use an algorithm based on a single

value decomposition (SVD) process, using RDCs, RCSAs and RDCs as input data. [Berdagué et al., 2021] More interesting, they propose also simple graphical and interfaces that can combined various option such the principal axis system ($S_{a'a'}$, $S_{b'b'}$, $S_{c'c'}$) of the diagonalized Saupe matrix, the inertia tensor axes, ($I_{a'}$, $I_{b'}$, $I_{c'}$), and the Saupe tensor surface representation (see below).

7.2 Contribution of spin-1/2 NMR

Examples using (^{13}C - ^1H)-RDCs. We have selected a few examples where isotropic NMR parameters failed to provide a unique solution to the structural problem, while RDCs lifted the limitation and their correct relative configuration was unambiguously determined. It is very important to highlight that different from isotropic parameter such as J couplings and Chemical Shifts, which can be predicted using semi-empirical or DFT methods, anisotropic NMR parameter cannot be predicted by calculations. The alignment tensor is not known *a priori* and RDCs, RCSAs and RDCs have to be fitted to a pool of candidate structures with the condition that the correct structure must be part of the pool. The fitting procedure will select the best fitting structure and if the correct structure is not present, the best fitting structure will be selected leading to a wrong solution.

Ludartin (see **Figure 37**) is a sesquiterpene lactone first isolated in 1972 from *Artemisia carruthii* by Geissman and Griffin as a mixture with its 11,13-dihydroderivative, [Geissman and Griffin, 1972] and later isolated in pure form from *Stevia yaconensis* var *subeglandulosa*, a plant growing on the mountains of northwestern Argentina. [Sosa et al., 1989] It has been shown to inhibit the aromatase enzyme activity in-vitro, which is involved in hormone dependent breast cancer. [Blanco et al., 1997] In the original publication of 1989, it was pointed out that the chemical shift of H-6 alone was not enough to unambiguously determine the configuration of the 3,4-epoxyguainolide unless both α - and β -epoxide are available for comparison. [Sosa et al., 1989]

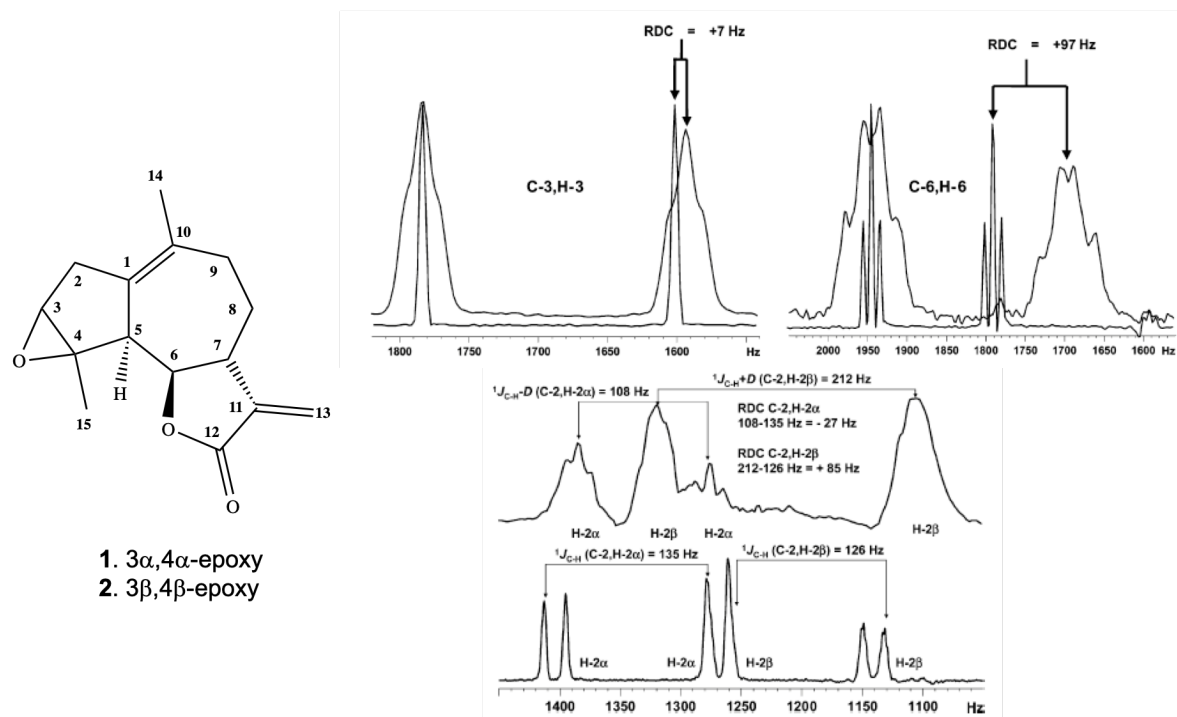


Figure 37. (a) Two possible configurations of the epoxide ring of Ludartine (**1** and **2**). (b) Selected overlapped F_2 traces of the F_2 - ^1H -coupled HSQC 2D spectrum (500 MHz for ^1H and 125 MHz for ^{13}C) in isotropic and anisotropic (self-stretched gel) conditions showing how RDCs were measured (here $^1D_{\text{CH}} = ({}^1T_{\text{CH}} - {}^1J_{\text{CH}})$). **Partially reproduced from Ref. [Gil et al., 2008] with permission.**

Hence, both epoxide isomers were chemically prepared from Ludartine to determine the correct configuration as $3\alpha, 4\alpha$, based on the chemical shifts of H-5 and H-6. In 2008, Ludartine was aligned in a self-stretched PMMA gel swollen in CDCl_3 , and ten proton-carbon ($^1D_{\text{CH}}$) RDCs were measured using an F_2 ^1H -coupled HSQC 2D experiment. Singular value decomposition (SVD) fitting analysis of the RDC data to the 3D structures of both isomers of the epoxide group yielded Q-factors of 0.048 and 0.221 for the $3\alpha, 3\beta$ and $3\beta, 4\beta$, respectively. Hence, based on the lower value of the Q-factor, the correct configuration of the epoxide group of Ludartine was determined as $3\alpha, 3\beta$, clearly showing the structure elucidation power of anisotropic NMR. **[Gil et al., 2008]** Figure 37 also shows the F_2 traces of the associated ^1H F_2 -coupled HSQC 2D experiment. Those experiments were collected using a self-stretched PMMA gels. This experiment was performed at the beginning of the development of the stretched gels technology. It took nearly twenty days to fully swell and stabilize a PMMA rod of 1 cm in length and 0.4 cm of diameter. The homogeneity of the gel was not ideal and far from the quality of current gels. However, the data could be extracted and the RDC analysis done successfully.

Jaborosalactone 32 is a whitanolide (steroidal lactone) isolated from *Jaborosa rotaceae*. Its absolute configuration at C-23 was determined as *R* from the Cotton effect at 218 nm in the

Electronic Circular Dichroism (ECD) spectrum by the chromophore of the α,β -unsaturated γ -lactone group. Its structure was further confirmed by single-crystal X-ray diffraction analysis. [Nicotra et al., 2006] However, in jaborosalactol 24 (see Figure 38), isolated from *Jaborosa parviflora*, this chromophore is absent to perform an ECD analysis due to the conversion of the conjugated γ -lactone into an α,β -epoxy-lactol by the natural chemical machine in the plant. A combined analysis using proton-proton 3J -coupling constants, NOE and molecular modeling resulted in three possible solutions. Jaborosalactol 24 was aligned in a self-stretched PMMA gel swollen in CDCl_3 and fourteen proton-carbon ($^1D_{\text{CH}}$) RDCs were measured using an F_2 ^1H -coupled HSQC experiment. SVD fitting analysis of the RDC data was performed on the three possible candidates obtained by 3J -coupling and NOE analysis leading to a unique solution of 23S, 24S, 25S and 26S relative to the absolute configuration of the main steroidal skeleton. The relative configuration was independently and almost simultaneously confirmed by powder X-ray diffraction analysis leading to a joint publication. [Garcia et al., 2009]

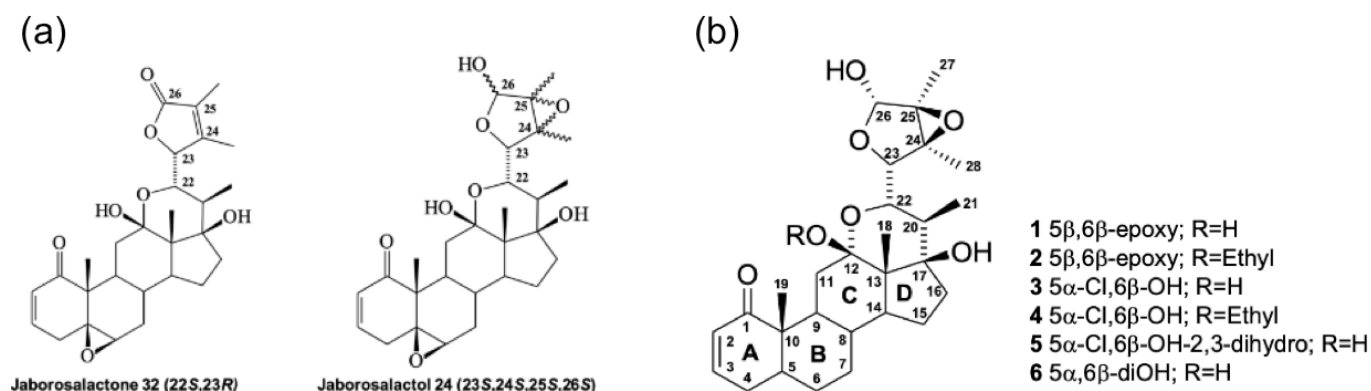


Figure 38. (a) Structure of Jaborosalactol 32 and Jaborosalactol 24. (b) All the structures isolated from *Jaborosa parviflora*, including Jaborosalactol 24 (1). **Figures adapted from Ref. [Garcia et al., 2009] with permission.**

Based on the RDC analysis, the configuration of five other molecular analogs with different substitution pattern in the steroidal skeleton was determined, (see Figure 38b). This was the first report in which the structure a new natural product was determined using RDCs.

Among other interesting compounds studied, the phytochemical analysis of *Xylocarpus rumphii* yielded a series of tetranortriterpenoids that was isolated as hemiacetals, which could not be purified due to the side chain ring opening and closing in solution, hence giving complex spectra. Purification was achieved after acetylation and subsequent separation of the epimeric mixtures of acetates. However, identifying which acetate derivative was the (*R*)- or the (*S*)-epimer at C-23 was not possible using isotropic NMR 1D/2D techniques. Proton H-23 respect to

all the nearby protons in the main skeleton were beyond the maximum distance to observe viable NOE correlations. Acetylation and further separation of the C-23 epimers of mixture **5** (in the publication), yielded epimers **5a** and **5b** pure form. These two epimers were aligned in PMMA/ CDCl_3 using the compression device leading to a ^2H quadrupolar coupling of 17 Hz for chloroform. One-bond (^{13}C - ^1H)-RDCs measured for carbons C-2, C-3, C-5, C-15, C-22, C-23, C-29 and C-30. The structures of **5a** and **5b**, generated by DFT showed only one rotamer of the side chain for each configuration, which facilitated the SVD analysis of RDCs using just a single conformation per configuration. SVD analysis of the RDC data of **5a** with the structure of both epimers yielded Q-factors of 0.081 and 0.177 for the C-23 S and C-23 R configurations, respectively. While the RDC data of **5b** yielded Q-factors of 0.110 and 0.055 for the C-23 S and C-23 R configurations, respectively. [Waratchareeyakul et al., 2017] It is very important to highlight that the 3D structure of both epimer is almost identical, except for the orientation of the acetyl group attached to C-23, and RDCs are able to detect that geometrical difference because they encode for the relative orientation of the C-H bonds involved in the SVD analysis.

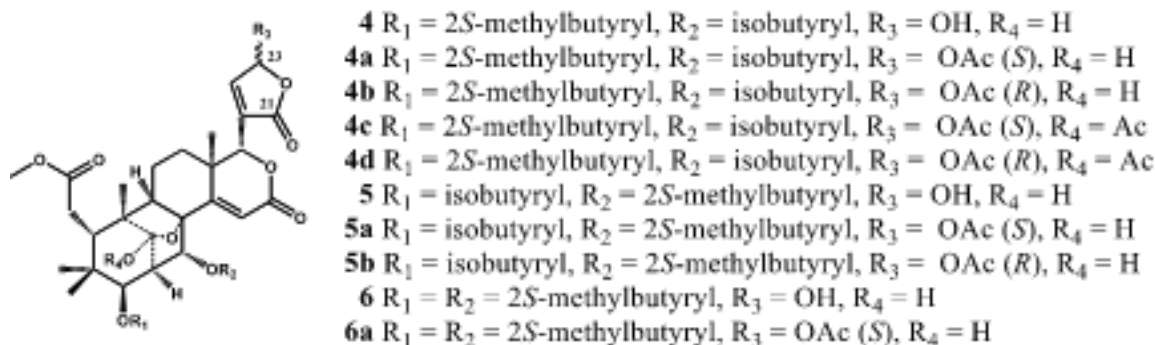


Figure 39. Structure of the compounds isolated from *Xylocarpus rumphii*. Figures adapted from Ref. [Waratchareeyakul et al., 2017] with permission.

Apart from these examples presented above, the analysis of several others structures of natural products were reported in the literature. [Gil et al., 2017a] as well as the determination of molecular constitution by RDCs. [Kummerlöwe et al., 2011-b] Again, for this purpose, the correct structure must be present in the pool of candidates to perform an accurate selection procedure. Thus the reaction of azide-containing 1,5-enyne (**1**) in the presence of electrophilic iodine sources yielded an unknown tricyclic compound (**4**). [Kummerlöwe et al., 2011-b]

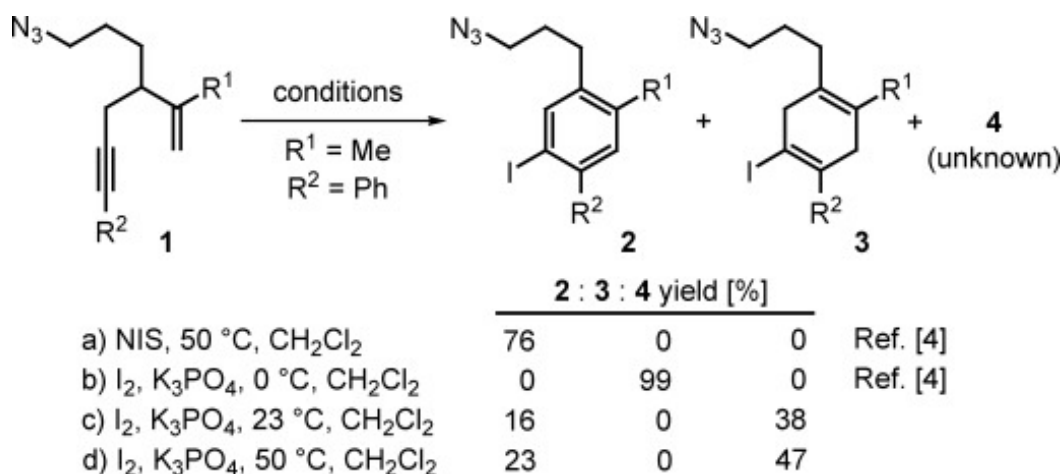


Figure 40. Experimental conditions leading to formation of products noted (**2**), (**3**) and (**4**) from acyclic compound (**1**). Figures adapted from Ref. [Kummerlöwe *et al.*, 2011-b] with permission.

The potential proposed structures of different molecular constitution for **4** are shown in **Figure 40**. Compound **4** was aligned in stretched polystyrene gel swollen in CDCl₃. Twelve (¹³C-¹H)-RDCs were measured using the ¹H F₂-coupled CLIP-HSQC experiment and additional five ²D_{HH} proton-proton geminal RDCs measured with the P.E. HSQC 2D experiment. [Tzvetkova *et al.*, 2007] SVD fitting of the RDCs data to the pool of proposed structures selected the constitution

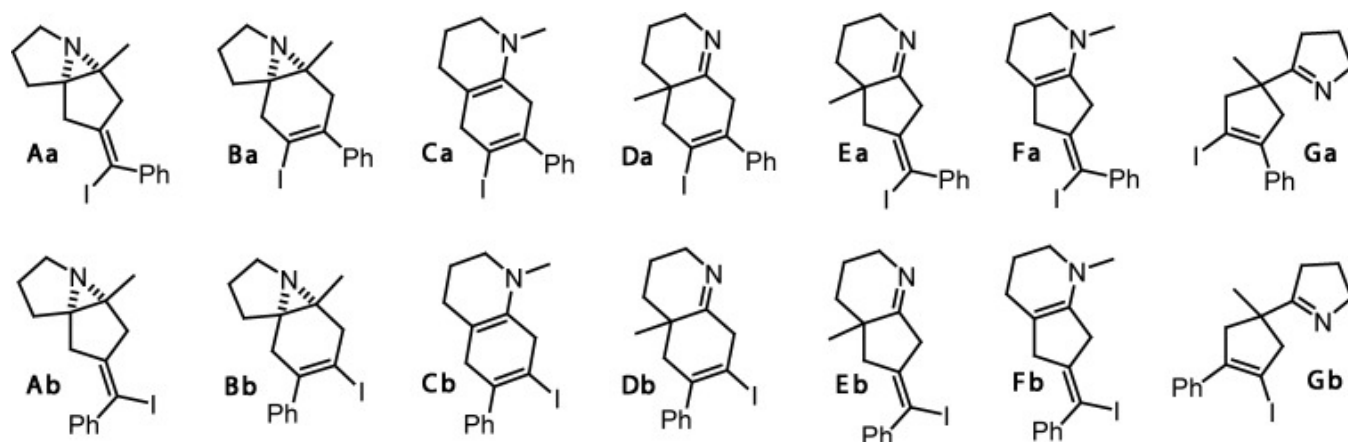


Figure 41. Potential structures of product **4**. Figures adapted from Ref. [Kummerlöwe *et al.*, 2010-b] with permission.

Ba (see **Figure 41**) for compound **4** [Kummerlöwe *et al.*, 2011-b]. Thus far, we presented examples showing how powerful are RDCs to determine molecular configuration and constitution, particularly in cases where isotropic NMR parameters fails to provide a unique solution. These examples deal with rigid molecules, where if flexibility is present, only one conformation dominates the identity of the 3D structure. RDCs, as well as the other two anisotropic parameters (RCSAs and ²H-RQCs) encode information of the relative position in

space of all the atoms in the molecules. This relative position represents the constitution, the configuration and the conformation/s of the molecules as a whole. Determination of conformation by anisotropic NMR parameters is very tricky. For isotropic NMR parameters (J couplings, δ and NOEs), in the presence of a fast exchange of conformers, the NMR response is the result of their population-weighted average, regardless of the orientation of the conformers. E.g., for a two-sites fast exchange conformations system of conformers A and B , the scalar J -coupling and the chemical shift values average as follows:

$$\delta^{\text{aver}} = P_A \times \delta_A + P_B \times \delta_B \quad (23)$$

and

$$J^{\text{aver}} = P_A \times J_A + P_B \times J_B \quad (24)$$

where P_A and P_B are the populations of conformers A and B , respectively, with $P_A + P_B = 1$. But their corresponding RDC values average in multi-tensor approach, according to **Eq. 25**.

$$\overline{D_{ij}^{A+B}} = P_A \left(\frac{k_{ij}}{r_{ijA}^3} \right) \overline{r_{ij}^T} \cdot \widehat{A}_A \cdot \overline{r_{ij}} + P_B \left(\frac{k_{ij}}{r_{ijB}^3} \right) \overline{r_{ij}^T} \cdot \widehat{A}_B \cdot \overline{r_{ij}} \quad (25)$$

where \widehat{A} is the alignment tensor, $\overline{r_{ij}^T}$ is the transposed of vector of $\overline{r_{ij}}$, and $k_{ij} = \left(-\frac{\mu_0}{4\pi} \right) \times \left(\frac{h\nu_i \nu_j}{4\pi^2} \right)$.

Conformers of significantly different shape and rotational diffusion properties will tend to align differently. If a large portion of the molecule dominates the molecular tumbling properties, it is possible to assume that the alignment tensors for conformer A and B are the same.

During the SVD fitting process, the structurally similar parts of the molecule are overlapped (as shown on the right part of the **Figure 42**) and the fittings are performed using a population-weighted average. If the populations are not known, it is possible to find the composition that produces the lowest quality factor value. This is known as the single-tensor approximation.

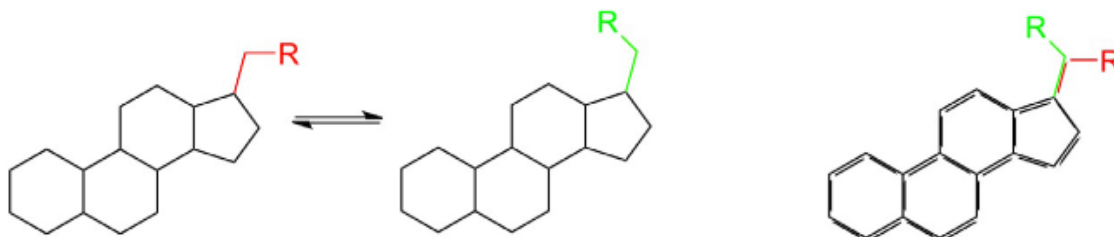


Figure 42. Conformational exchange of two hypothetical compounds. **Figures adapted from Ref. [Gil et al., 2017b] with permission.**

Among, many applications explored, this approximation has been successfully applied to the conformational analysis of cyclic peptides, since the cyclic structure of the backbone of the different conformations share very similar shapes.

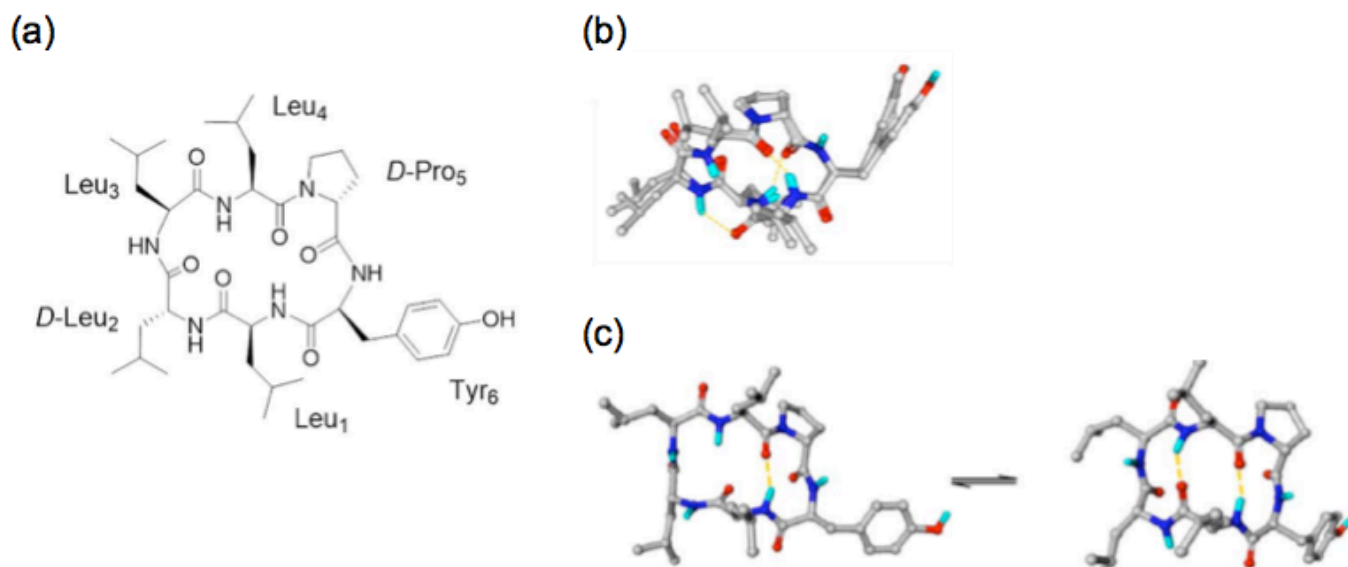


Figure 43. (a) Chemical structure of cyclo-[Leu1-D-Leu2-Leu3-Leu4-D-Pro5-Tyr6]. Preferred conformations of cyclo-[Leu1-D-Leu2-Leu3-Leu4-D-Pro5-Tyr6] in (b) chloroform, and (c) in DMSO. **Figures adapted from Ref. [Farley et al., 2019] with permission.**

The conformational analysis of peptide cyclo-[Leu1-D-Leu2-Leu3-Leu4-D-Pro5-Tyr6] (see **Figure 43a**) was carried out in CDCl_3 and $\text{DMSO-}d_6$. **[Farley et al., 2019]** The analysis was performed using a combination of RDCs, Intramolecular Hydrogen Bond (IMHB) analysis and J -couplings. The peptide was aligned in PMMA/ CDCl_3 and Poly-HEMA/ $\text{DMSO-}d_6$ using the gels reversible compression/relaxation method with the compression device. A total of six $^1D_{\text{CH}}$ and five $^1D_{\text{NH}}$ from the peptide backbone were measured using the ^1H F_1 -coupled J -scaled BIRD(JSB)HSQC 2D experiment. In addition, six $^3J_{\text{NH-H}\alpha}$ coupling constants and temperature coefficients for the five backbone NH groups were measured. The single tensor approximation in combination with the Akaike Information Criterion (AIC) for model selection was used for SVD fitting of the RDC data to the conformational space of thousand DFT optimized structures. The combined analysis, including the J -coupling constants led to the selection of only one conformation in chloroform with three IMHBs (see **Figure 43b**) and two conformations in DMSO with one and two IMHBs, respectively (see **Figure 43c**).

The following example is an interesting and very challenging case for many reasons. It is about an unexpected synthetic by product. It is very small with oval overall shape and aligns

very weakly in gels. Hence, the sample had to be aligned in a stronger aligning medium, such as the lyotropic liquid-crystalline phase (LLC) made of poly- γ -ethyl-L-glutamate (PELG). Attempts to prepare compound **3** from **1** (see **Figure 44**) failed and instead compounds **4** and **5** were produced. [Riveira et al., 2015]

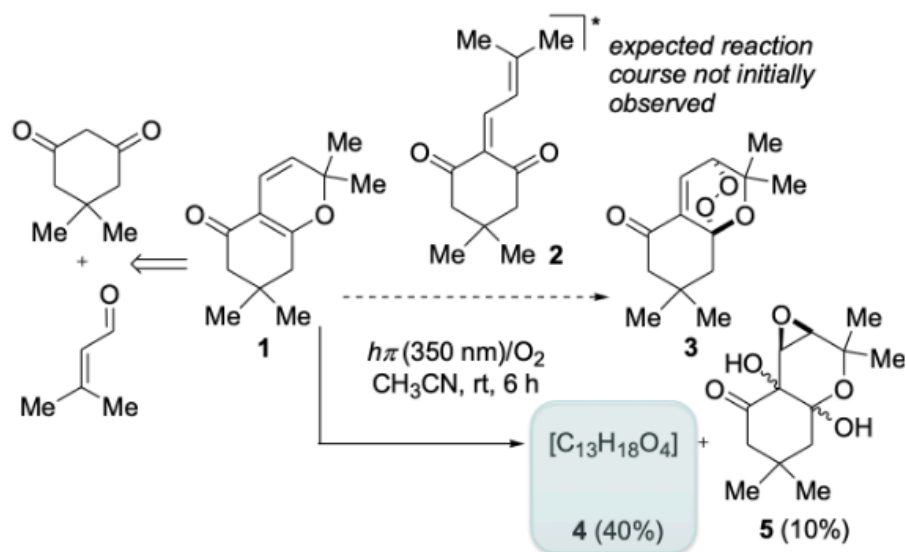


Figure 44. Chemical transformation of (**1**) into unexpected by-product **4**. Figures adapted from Ref. [Riveira, et al., 2015] with permission.

Computer-assisted structure elucidation (CASE) analysis of the 1H and ^{13}C 1D NMR spectra as well as HSQC, HMBC, 1,1-ADEQUATE and 1,n-ADEQUATE 2D NMR spectra of unexpected compound **4** using the structure elucidator program ADC/Labs [ACD/Labs] resulted in only two molecular constitution structures satisfying the atoms connectivity maps, oxirane A and oxetane B (see **Figure 45a**). These two compounds are constitutional isomers. The $^1J_{CH}$ values of the two oxygenated CH groups in A and B would be different enough to distinguish the oxirane from the oxetane structural feature. The DFT predicted values for these $^1J_{CH}$ coupling constants are 181.1 and 188.3 Hz for the oxirane CH bonds and 159.8 and 164.6 Hz for the oxetane CH bonds. The experimental values for compound **4** are 181.2 and 190.5 Hz, clearly indicating that compound **4** is an oxirane and not an oxetane. The sample was aligned in PELG dissolved in $CDCl_3$ and nine (^{13}C - 1H)-RDCs were measured using 1H F_1 -coupled J -SB-HSQC 2D experiment.

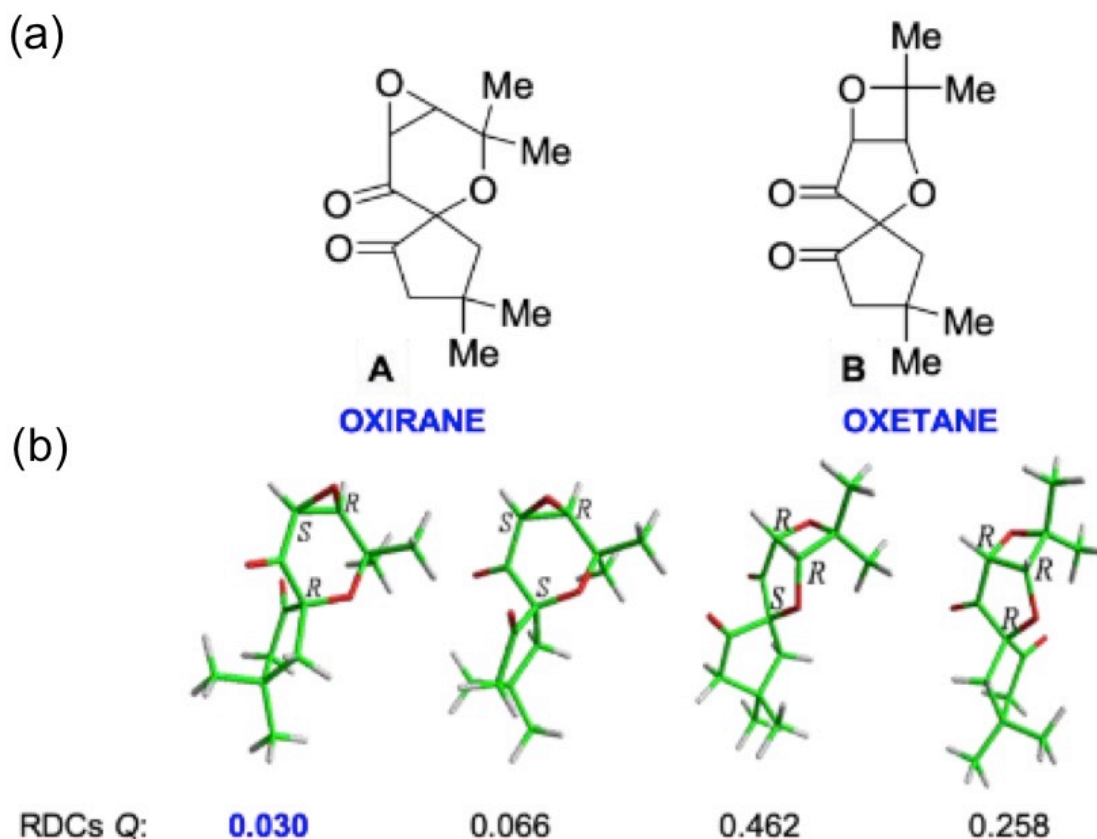


Figure 45. (a) Structure of oxirane (A) and oxetane (B). (b) 3D structure associated to the smallest Q-factors obtained. **Figures adapted from Ref. [Riveira et al., 2015] with permission.**

There are two possible diastereoisomers for both the oxirane A and the oxetane B with two conformations each, as shown in **Figure 45a** above. SVD fitting of the RDCs data using the single tensor approximation led to not only discriminate the oxirane from the oxetane, but also select the correct configuration (**Figure 45b**) with a *Q*-factor value of 0.030. This is a clear example of how RDCs can select in one-shot the constitution, configuration and conformation of a small molecule. In fact, the fitting was performed to select the composition of conformers that produces the lowest *Q*-factor. In this particular case, a ratio of 0.83: 0.17 has been determined.

Examples using ^{13}C -RCSA. As mentioned previously, the development of the application of RCSAs to the structural analysis of small organic molecules was delayed until scientists figured out how to deconvolute RCSAs from isotropic chemical shift contributions. In 2011, the successful measurement of ^{13}C -RCSAs for strychnine (see **Figure 14b**) using a combination of a mechanically stretched polymer gel inside a variable-angle NMR probe was described. **[Kummerlöwe et al., 2011-a]** To prevent interferences from isotropic sample, they used the same sample already anisotropic by stretching the gel inside the rotor. Then, they varied the

angle of the director of the alignment in the gel respect to the magnetic field \mathbf{B}_0 . They monitored the ^2H RQC as function of this angle, scaling the anisotropy down to zero at 54.73° (the magic angle), as shown in **Figure 46**. At the magic angle, the equivalent of isotropic conditions, they measured one-bond proton-carbon $^1J_{\text{CH}}$ coupling constants for strychnine using the F_2 -CLIP-HSQC. At angles $\theta = 0^\circ$ and 65° , they measure the total couplings $^1T_{\text{CH}}$, in order to obtain the $^1D_{\text{CH}}$ values. At the same angles, they also measured 1D ^{13}C NMR spectra (see **Figure 47**).

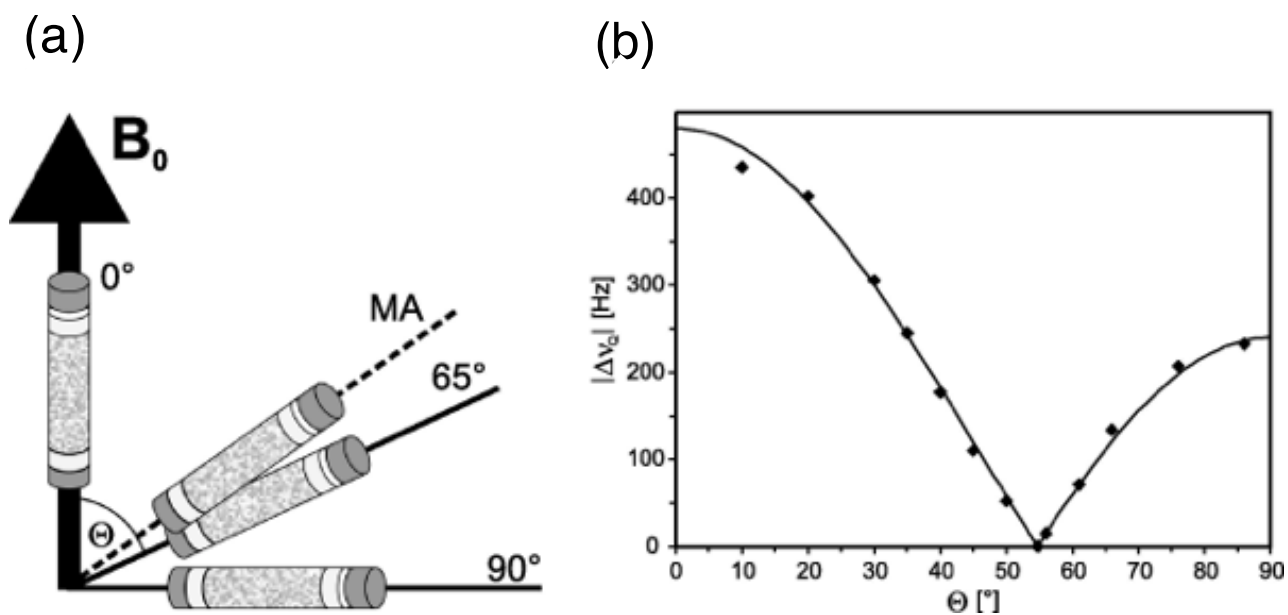


Figure 46. (a) Scaling the anisotropy by varying the angle θ of a mechanically stretched gel with respect to the magnetic field \mathbf{B}_0 , and without the need of sample spinning at the magic angle (MA) at 54.73° . **Figures adapted from Ref. [Kummerlöwe et al., 2011-a] with permission.**

Just by rotation, the anisotropy is changed while the sample maintains exactly the same experimental conditions, not giving room to contributions for isotropic chemical shifts. Since the correct 3D structure of strychnine is well known, the experimental RDCs were used to calculate an accurate alignment tensor. In turn, with this alignment tensor and the DFT calculated CS tensor, ^{13}C -RCSAs were back-calculated for each carbon in the molecules. Then, experimental vs. back-calculated ^{13}C -RCSAs leading to an excellent correlation with an RMSD of 15.9 ppb, as shown in **Figure 48**.

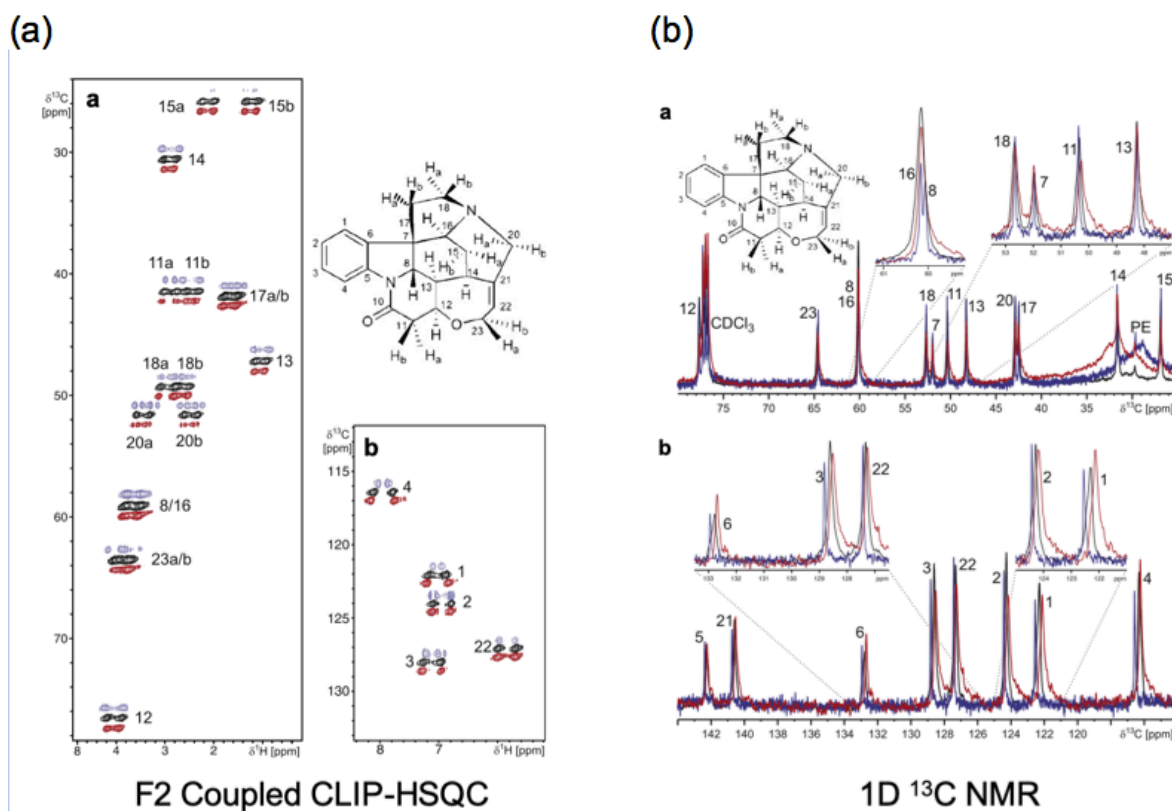


Figure 47. (a) CLIP-HSQC 2D spectrum measured on strychnine in a mechanically stretched PDMS/ CDCl_3 gel at θ angle values of 54.73° (black), 0° (blue, dark gray), and 65° (red, light gray). (b) Aliphatic (top) and aromatic (bottom) regions of $^{13}\text{C}\{-^1\text{H}\}$ 1D spectra with same conditions (same color code). **Figures adapted from Ref. [Kummerlöwe et al., 2011-a] with permission.**

Although this first attempt to accurately measure RCSAs for a small molecule was very successful, the experimental setup, which includes the use of a VASS NMR probe, made its application very impractical and not affordable to everyone.

The same year (2011), a collaborative effort led by several research groups attempted the differentiation of estrone and 13-*epi*-estrone using only RCSAs. [Hallwass et al., 2011] Estrone was aligned in a DMSO-compatible (*S*)-2-acrylamido-1-propanesulfonic acid gel (APS) and the gel was stretched. [Kuchel et al., 2006] $^{13}\text{C}\{-^1\text{H}\}$ 1D NMR spectra were measured at two different degrees of stretching of the gel inside the stretching device. ^{13}C -RCSAs were calculated as the difference in chemical shift for each carbon between the two degrees of alignment. Thus the authors of this article claimed that: “*This approach ensures that the sample composition changes only minimally, if at all, between the different alignment conditions, and the observed chemical shift changes are therefore caused mainly by the RCSAs and by*

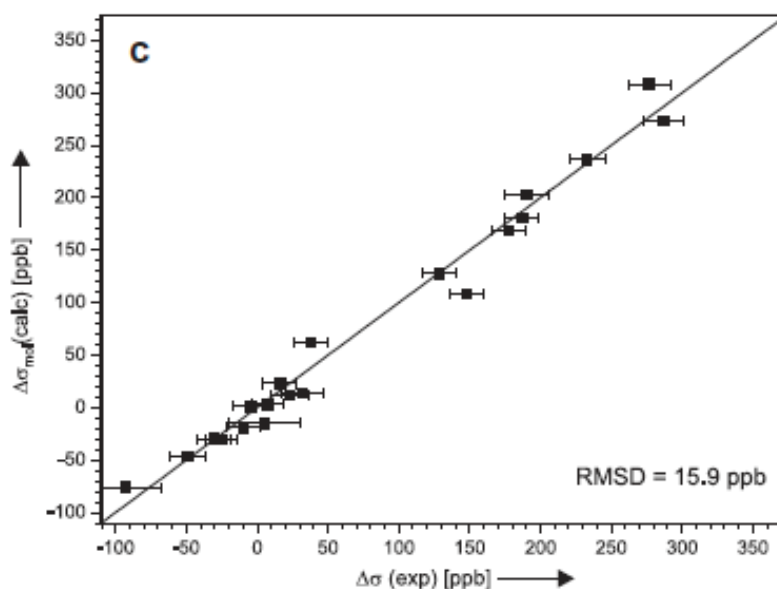


Figure 48. Correlation plot of back-calculated $\Delta\sigma_{\text{mol}}(\text{calc})$ using the *ab-initio* ^{13}C -CSA-tensors and the RDC-derived alignment tensor vs. experimental $\Delta\sigma(\text{exp})$ residual chemical shift anisotropies for strychnine in PDMS/ CDCl_3 corrected by the average uncorrected RCSA value for C-13, C-14, and C-15 as the three nuclei with the smallest theoretically determined CSA tensor. **Figure reproduced from Ref. [Kummerlöwe et al., 2011-a] with permission.**

changes in the overall magnetic susceptibility of the sample, which affects all resonances in the same way.” However, the SVD analysis of fitting only ^{13}C -RCSAs couldn't discriminate the structure of estrone from its C-13 epimer diastereoisomer. Only when combined with RDCs, the discrimination happened but with quite high Q-values (see **Figure 48**).

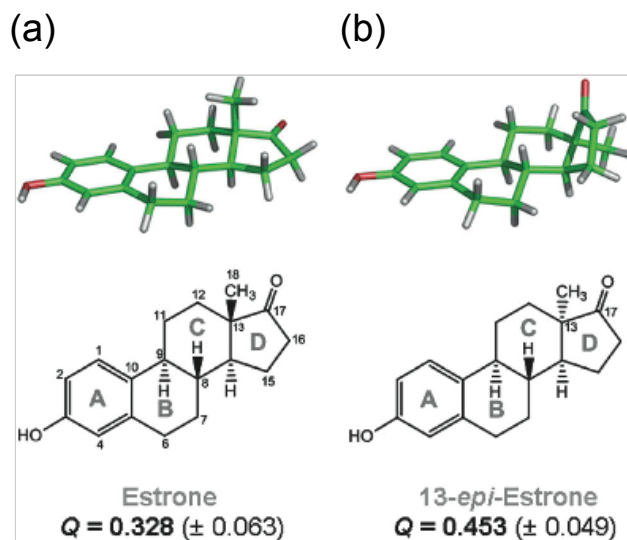


Figure 49. The DFT 3D structure of (a) estrone and (b) 13-*epi*-estrone. **Figures adapted from Ref. [Hallwass et al., 2011] with permission.**

These results discourage NMR spectroscopists from using RCSAs for the determination of molecular configuration in small molecules for a while. It wasn't until five years later (2016) that

a collaborative effort involving Merck & Co. (Rahway, NJ, USA), Carnegie Mellon University (Pittsburgh, PA, USA), Universidade Federal de Pernambuco (Recife, Brazil) and Max Planck Institute for Biophysical Chemistry (Göttingen, Germany), demonstrated using aligning gels and two different devices (compression and stretching) that it was possible to determine the relative configuration of small molecules using only ^{13}C -RCSAs. [Nath *et al.*, 2016] This is a seminal paper that sets the basis to a reliable application of ^{13}C -RCSAs to the structural analysis of small molecules. It is a very complete and robust study in which (^{13}C - ^1H)-RDCs and ^{13}C -RCSAs were accurately measured for estrone, menthol, mefloquine, retrorsine and strychnine in stretched and compressed (PMMA gels swollen in CDCl_3) (see **Figure 50**). We would like to highlight a few important aspects from this piece of work, but we strongly recommend further reading of this seminal article on ^{13}C -RCSAs.

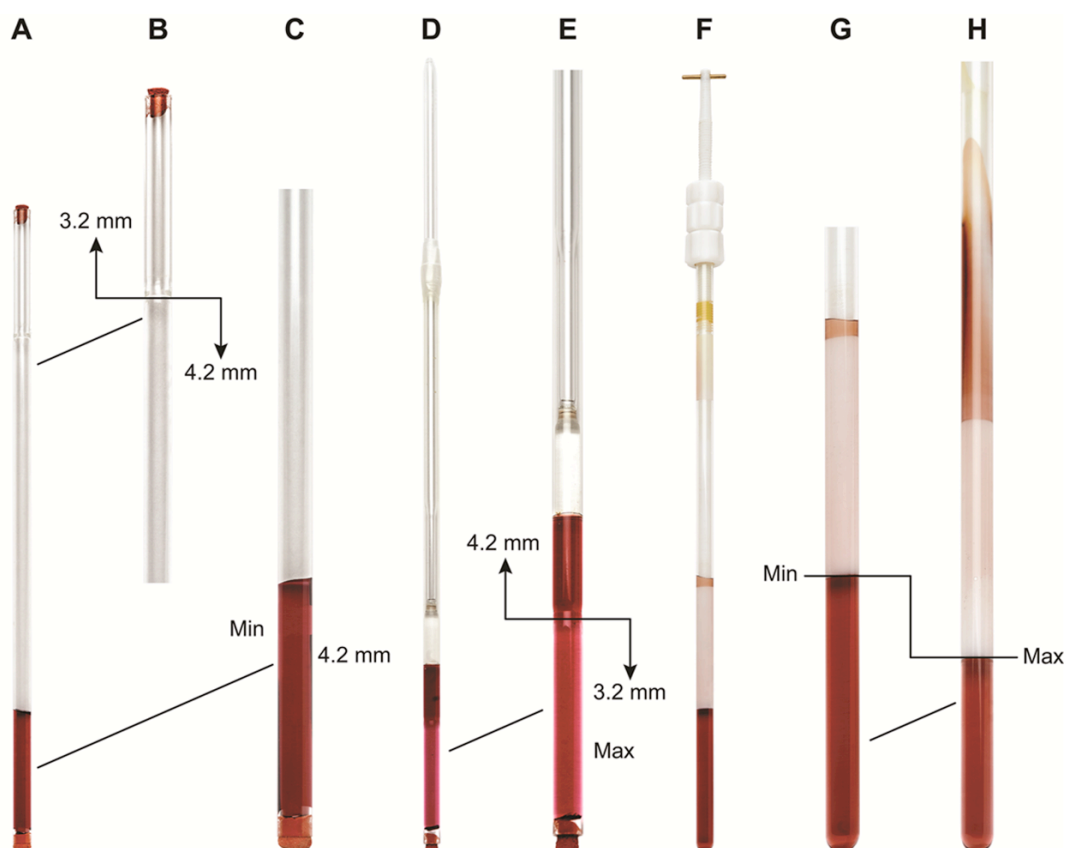


Figure 50. Stretching (left) and compressing (right) device used in this study. **Figures adapted from Ref. [Nath *et al.*, 2016] with permission.**

One important finding is that when the stretching device is used, the difference in ^{13}C chemical shifts between the relaxed and the stretched states is solely due to RCSAs. While,

the same difference between the relaxed and compressed states using the compression device is not only due to RCSAs but also to the addition of a predictable amount of isotropic shift that can be corrected. **[Hallwass et al., 2018]** During the compression, the same active volume is used for strong and weak alignment, yielding similar signal-to-noise for both conditions. However, due to solvent and gel composition changes experienced under the different alignment strengths, the isotropic shift must be compensated. This adjustment can be achieved by a robust post-acquisition correction done during the SVD fitting process **[Hallwass et al., 2018]** The article clearly shows how the Q-factor significantly improves when the isotropic gel shifts is corrected when the compression device is used. This problem only exists when measuring RCSAs. RDCs are straightforwardly collected without problems at all.

Coming back to the analysis of estrone, **Figure 51** shows ^{13}C -RCSAs collected for estrone with both devices. Between the ^{13}C -RCSAs collected with stretched gels (panels a-d) and collected with compressed gels (panels e-h), clear switch in sign is observed. This is because the alignment tensor rotates 90° between stretched and compressed gels and the all RCSAs values are scaled by the trigonometric function, $\cos^2\theta$, as seen above in **Figure 46** for the quadrupolar coupling of the ^2H NMR signal of CDCl_3 . **[Kummerlöwe et al., 2011]** This change in sign by rotation of the alignment tensor was also observed experimentally when the compression method was reported in 2010. **[Gayathri et al., 2010]** It is important to clarify that the stretching device used in this publication is not for variable degree of alignment. It has only two stages for the measurement of RDCs and RCSAs in proteins. **[Liu et al., 2010]** It was adapted for organic solvents. Its setup is not as user-friendly as the compression device. It uses an open-ended tube, which poses a risk of losing the stopper and leak the sample into the NMR probe. As shown in **Figure 52**, the structure of estrone and 13-epi-estrone were clearly differentiated by only RCSAs using stretched and compressed (with gel shift correction) PMMA gels.

As mentioned previously, different from RDCs, the maximum value of RCSAs depends on the anisotropy of the CS Tensor, as well as on the GDO of the alignment medium (see above). This ^{13}C -RCSA is significantly larger ($\sim 4 - 5$ times) for sp^2 compared to sp^3 carbons. The best solution would be to measure the ^{13}C -RCSAs in a stronger alignment medium, such as PBLG. However, at the time of this work in 2016, nobody yet figured out how to compensate for

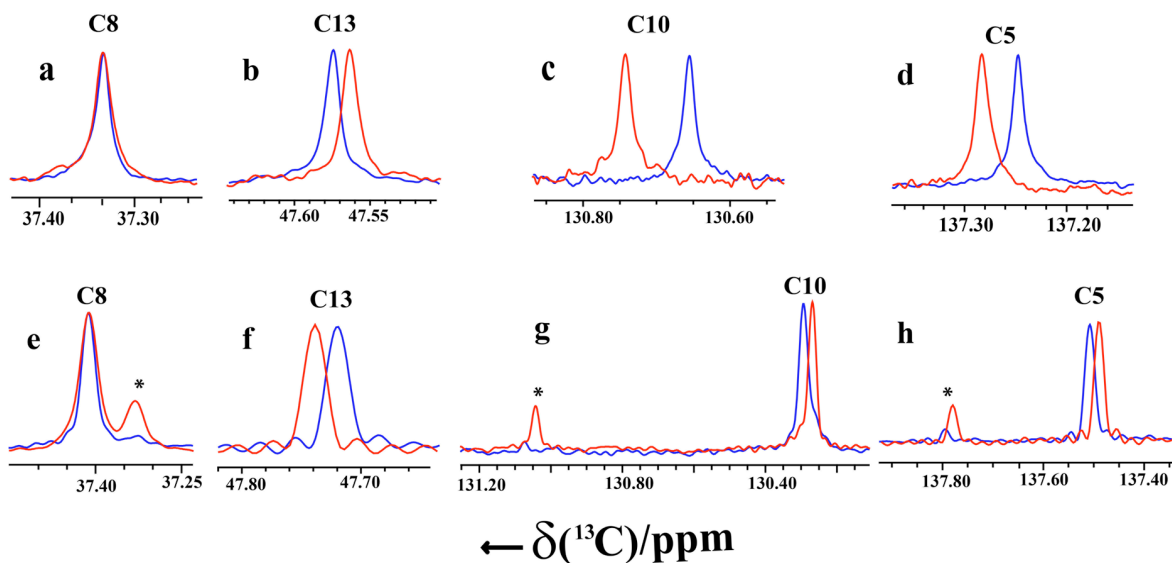
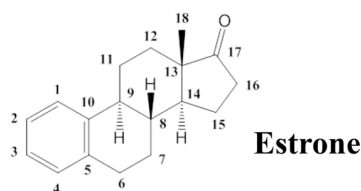


Figure 51. Variation of ^{13}C -RCSAs extracted from 1D NMR spectra of estrone obtained with stretching device (top) at 150.0 MHz and compression device (bottom) at 225.0 MHz of estrone in the narrow-bore (blue) and wide-bore (red) sections of the tube. The C8 resonance shown in panel e was used as the reference resonance. Note the presence of both isotropic (marked with an asterisk) and anisotropic signals for some carbons. **Figure reproduced from Ref. [Nath et al., 2016] with permission.**

isotropic shifts in PBLG. The GDO of PMMA-based gels is on the order 10^{-3} . Hence, an elegant solution was proposed with the introduction of a modified quality factor Q_{CSA} , which was based on the conventional Q-factor, but takes into account the significantly varying chemical shift anisotropy (CSA) values of different carbon atoms, enhancing the capabilities of distinguishing different relative configurations based on ^{13}C -RCSA data only. The Q_{CSA} is calculated as follows: i) the alignment tensor is derived by fitting all ΔRCSAs to the DFT-computed CSA tensor through the singular value decomposition (SVD) method, and ii) a new quality factor, Q_{CSA} , is calculated by scaling both experimental and calculated ΔRCSA values by corresponding atom's chemical shift anisotropies, using the formula given below, where $\text{CSA}_{i,\text{ax}}$ equals $\sigma_{33} - (\sigma_{22} + \sigma_{11})/2$ and the chemical shielding eigenvalues $\sigma_{11} - \sigma_{33}$ are obtained from DFT. The Q_{CSA} factor is defined as:

$$Q_{\text{CSA}} = \sqrt{\frac{\sum \left(\frac{\Delta\text{RCSA}_{i,\text{ax}}^{\text{Exptl.}} - \Delta\text{RCSA}_{i,\text{ax}}^{\text{Calc.}}}{\text{CSA}_{i,\text{ax}}} \right)^2}{\sum \left(\frac{\Delta\text{RCSA}_i^{\text{Exptl.}}}{\text{CSA}_{i,\text{ax}}} \right)^2}} \quad (26)$$

This Q_{CSA} was successfully used in structures containing both sp^2 and sp^3 carbons. E.g. **Figure 53** shows the ^{13}C -RCSAs-assisted configurational analysis of strychnine in stretched and compressed PMMA/ CDCl_3 gels comparing the conventional Q-factor with the new Q_{CSA} quality factors. The diastereomers of strychnine were labeled via the *R*- or *S*-descriptors for the chiral carbons C-7, C-8, C-12, C-13, C-14 and C-16, respectively. Hence, *RSSRRS* represents the correct configuration *7R*, *8S*, *12S*, *13R*, *14R*, *16S* selected by the SVD fitting procedure.

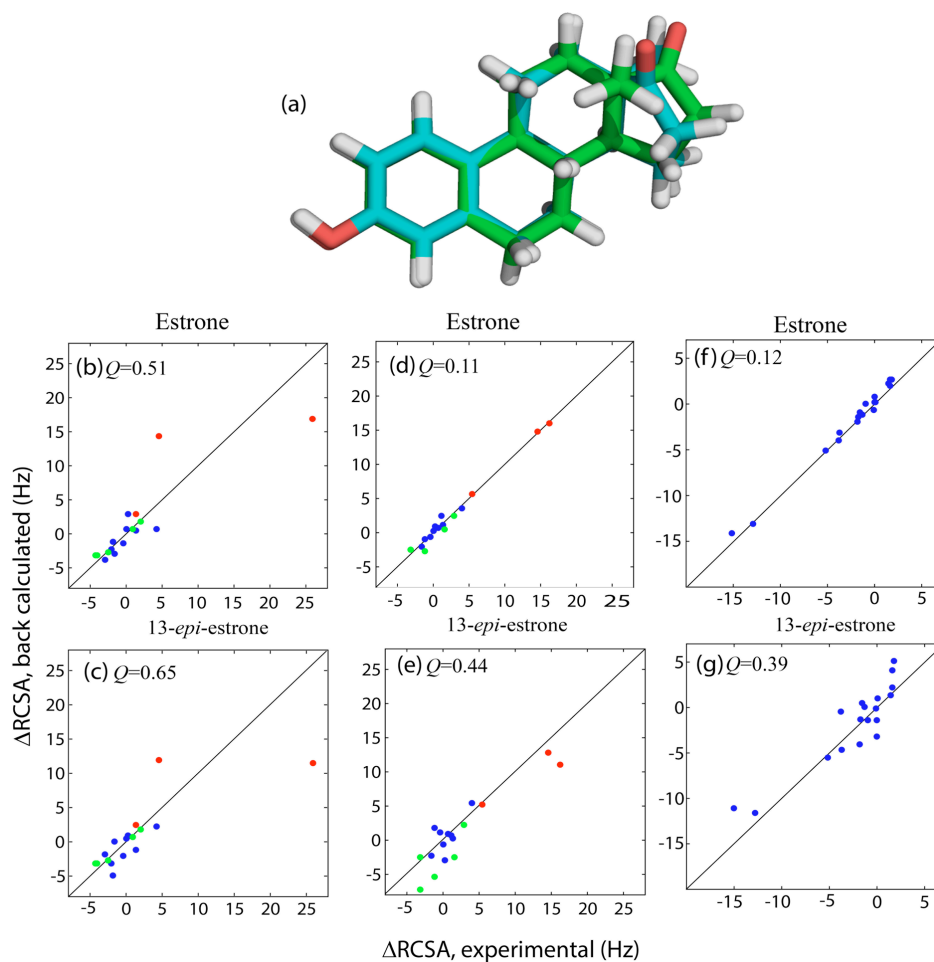


Figure 52. (a) The DFT-computed 3D structural overlay of estrone and 13-*epi*-estrone. (b-g) Comparison of correlation plots $\Delta\text{RCSA}^{\text{Exptl.}}$ and $\Delta\text{RCSA}^{\text{Calc.}}$ values (^{13}C data) for estrone and 13-*epi*-estrone using compression (b-e) and stretching (f-g) devices. Panels (b and c) and (d and e) show ΔRCSA s without and isotropic correction, respectively. Between panels b and c, the *Q*-values do favor the correct configuration ($Q = 0.51$ for estrone vs. $Q = 0.653$ for 13-*epi*-estrone). (d) Effect of the correction of the isotropic shift leading to a better differentiation with *Q* values of 0.11 for estrone and (e) 0.44 for 13-*epi*-estrone. **Figure reproduced with permission from reference [Nath et al., 2016].**

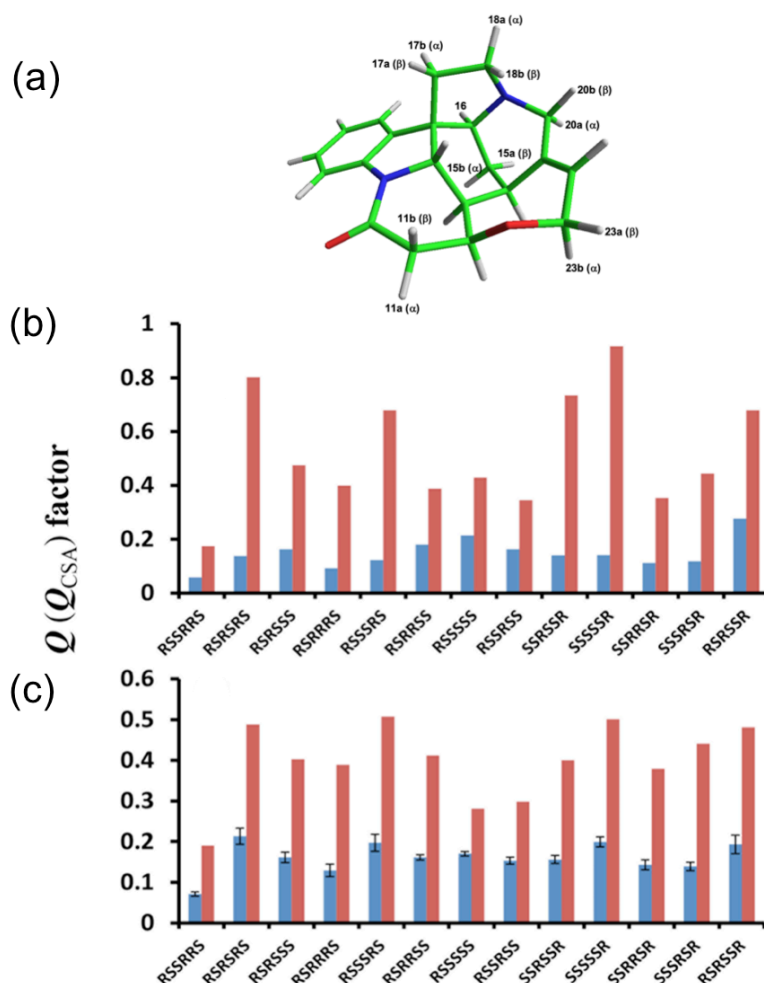


Figure 53. Variation of Q-factor obtained for strychnine with a Δ RCSA-based stereochemical analysis. (a) DFT 3D structure of strychnine. (b) Results from the stretching device: Q (blue) and Q_{CSA} (red) factors calculated for lowest-energy structures of different diastereoisomers from DFT calculation using only Δ RCSAs. (c) Results from the compression device: Q-factors obtained from the analysis of experimental Δ RCSAs and the thirteen possible configurations. **Figure reproduced from Ref. [Nath et al., 2016] with permission.**

Although not described here to avoid redundancy, the correct configuration of menthol, mefloquine and retrorsine was also determined successfully in this work. This work has opened new avenues to reliably applied RCSAs to the structural analysis of synthetic small organic molecules as well as natural compounds. Soon after this publication, another structure elucidation of the fungal metabolite Homodimericin A using computer assisted structure elucidation (CASE) and a combination of isotropic and anisotropic NMR data, which included the first application of ^{13}C -RCSAs to the structural analysis of a natural product. **[Meyer et al., 2016]**

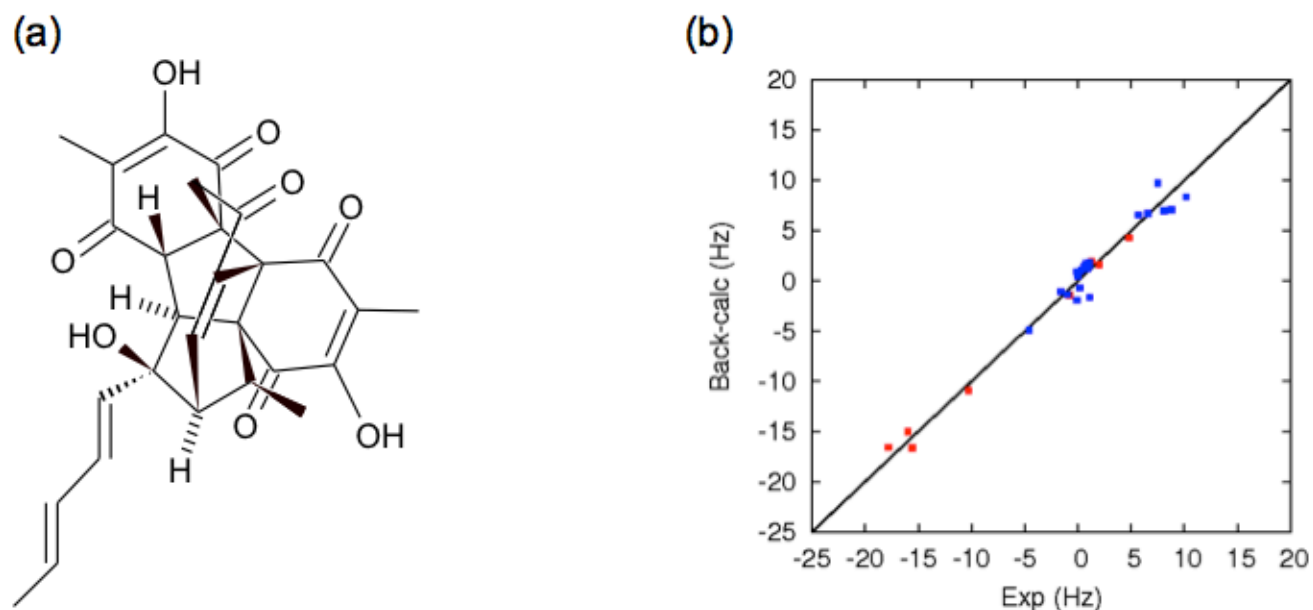


Figure 54. (a) Structure of Homodimericin A. (b) Experimental vs. back-calculated RDCs (red) and RCSAs (blue) [Meyer et al., 2016] reproduced with permission.

Homodimericin A has a twenty-carbon atoms hexacyclic core with a carbon backbone containing eight contiguous stereogenic carbons (see **Figure 54a**). Half of its carbon atoms don't have protons attached, presenting a significant challenge for NMR-based structural analysis. The presence of so many non-protonated carbons sets the perfect scenario to use ^{13}C -RCSAs. RDCs and RCSAs were collected using a poly-HEMA gel swollen in $\text{DMSO-}d_6$ and stretched in the two-stages device [Liu et al., 2010; Nath et al., 2016] described above. The combined SVD fitting of RDCs and RCSAs selected the correct configuration for Homodimericin A with a Q-factor of 0.162 (see **Figure 54b**).

In 2018, a new method to accurately measure RCSAs in PBLG without interferences from isotropic chemical shifts was described. [Liu et al., 2018-b] It consists on adding small amounts of PBLG to the compound's solution (E.g. strychnine) and acquired a $^{13}\text{C}\{^1\text{H}\}$ spectrum after each addition (see **Figure 55**). The method assumes that adding small amounts of PBLG does not introduce isotropic chemical shifts. Tetramethyl silane (TMS) at 4% (v/v) was added for ^{13}C chemical shift referencing. The effect of the bulk susceptibility change at different PBLG concentrations is eliminated by TMS referencing. The method, by using PBLG, significantly enhances the ^{13}C -RCSAs values of carbon atoms with poor anisotropy (low CSA), such as sp^3 carbons. Comparison of ^{13}C -RCSAs measured in PBLG and PMMA gels are provided in **Figure 55**.

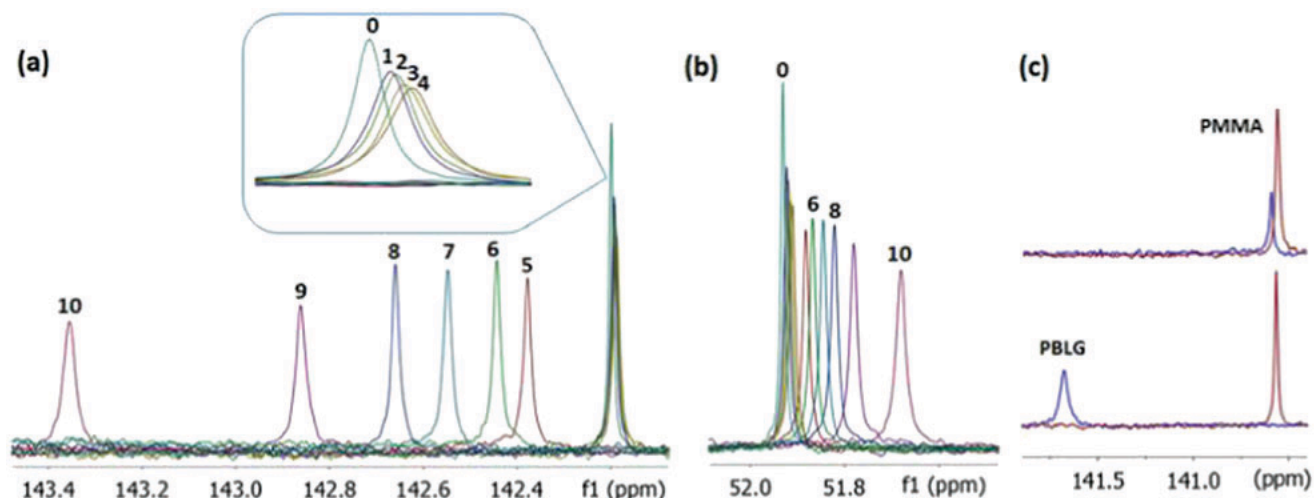


Figure 55. Example of variations of ^{13}C resonances used for the ^{13}C -RCSA measurements. (a) Variation obtained when collected with solution made of 0, 2.1, 4.1, 6.6, 8.8, 11.4, 9, 15.5, 18.4, 22.9, and 34.5% (w/v) of PBLG in CDCl_3 (spectra labelled (0 - 10), respectively). Samples 0 - 4 were acquired with PBLG below its LC-forming critical concentration (isotropic solution spectra), whereas the data for samples 5 - 10 were collected with PBLG mesophase above its critical concentration (C_{crit}) and are increasingly anisotropic in nature. A quaternary sp^2 carbon of strychnine (1a) (C-21) is shown in (a), and the only quaternary sp^3 carbon in strychnine (C-7) is shown in (b). ^{13}C -RCSA shifts in traces 5 - 10 are significantly larger than the change due to $\Delta\Delta\delta_{\text{iso}}$ seen in traces 0 to 4, even for C7 (b), which has a very small DFT-computed CSA of 30 ppm. (c) Top traces: signal of C-21 carbon of strychnine in weakly (red) and strongly (blue) stretched PMMA gel. The RCSA values correspond to the separation between red and blue spectra. Bottom traces: same as top traces with 0% [red, “0” in (a)] and 34.5% PBLG [blue, “10” in (a)]; the actual ^{13}C -RCSA value is actually slightly larger than the separation between red and blue spectra after correcting for $\Delta\Delta\delta_{\text{iso}}$. Although eleven PBLG concentrations were used to study the trend of chemical shift changes, in practice only three concentrations are needed for ^{13}C -RCSA data extraction. **Figure reproduced from Ref. [Liu et al., 2018-b] with permission.**

The configuration of strychnine was straightforwardly determined with this method (data not shown), though most strychnine carbons have enough CSA to measure ^{13}C -RCSAs with PMMA gels, as shown above. [Nath et al., 2016] However, it is noteworthy to mention the power of this method to differentiate caulamidine A from its C-26 epimer (see **Figure 56**). The structure of caulamidine A was previously reported using NMR data that included RDCs and RCSAs collected in a PolyHEMA gel in DMSO. [Milanowski et al., 2018]

This subsequent addition of the PBLG method was intensively used by various research groups. A few examples are described as follows. For complete NMR work, please check the original publications. The structure of dictyospiromide (see **Figure 57**), an antioxidant spirosuccinimide alkaloid from the marine alga, *Dictyota Coriacea*, was determined using a combination of isotropic and anisotropic 1D/2D NMR experiments, complemented with chiroptical, and computational methodologies. Anisotropic NMR parameters provided critical orthogonal verification of the configuration of the difficult to assign spiro carbon and the other stereogenic centers. [Yan et al., 2019] Particularly, the application of ^{13}C -RCSAs led to select

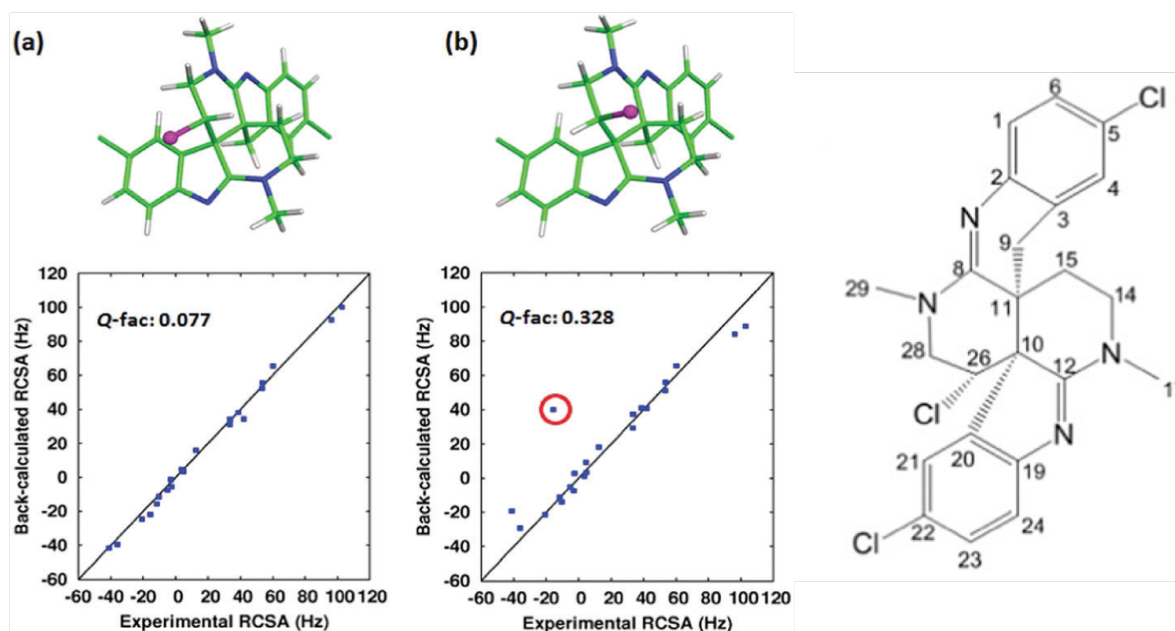


Figure 56. Stereochemical differentiation of caulamidine A using ^{13}C -RCSA data collected in PBLG. (a) The DFT 3D structure of caulamidine A. (b) The energetically feasible C-26-inverted structure. The chlorine atom is represented as a magenta sphere. The outlying point circled in red is the RCSA for the inverted C-26. **Figure reproduced from Ref. [Liu et al., 2018-b] with permission.**

the $1E$, $2R$ with a Q-factor of 0.097, as shown in **Figure 57**. As mentioned earlier, the determining of the configuration of proton-deficient molecules is a challenging problem when using conventional NMR methods (J coupling constants and NOE analysis). Here again, determination of experimental ^{13}C -RCSAs is a powerful alternative option as demonstrated to straightforwardly determine the double-bond configuration (Z/E) of a proton-deficient compounds as thiazolidinedione (see **Figure 58**). [Ndukwe et al., 2019] In this example, ^{13}C -RCSAs selected the E configuration with a Q-factor of 0.068 vs. a Q-factor of 0.404 for the Z isomer.

Another interesting example is provided for Phormidolide A, a natural product isolated from the marine cyanobacterium *Leptolyngbya* sp. (strain ISB3NOV94-8A) that shows a mid-range toxicity in the brine shrimp model. It contains a 16-membered macrocycle linked to a pendant polyol side chain terminating in bromomethoxydiene (see **Figure 59**). In light of discordant results arising from recent synthetic and biosynthetic reports, a rigorous study of the configuration of phormidolide A was reported, which outlined a synergistic effort employing computational and anisotropic NMR investigation, that provided orthogonal confirmation of the reassigned side chain, as well as supporting a further correction of the C-7 stereocenter. [Ndukwe et al., 2020-a]

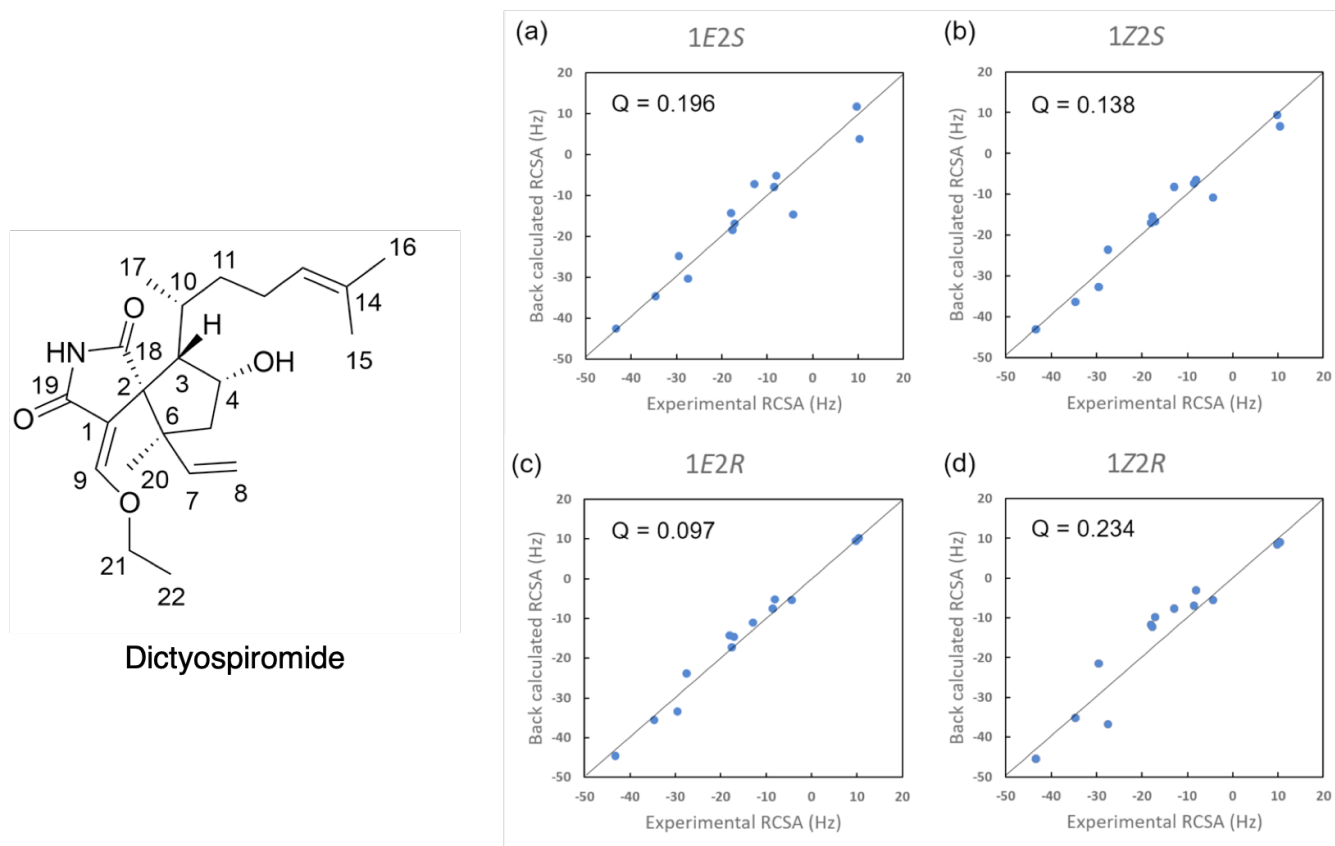


Figure 57. Structure of dictyospiromide and correlation plots of back-calculated vs. experimentally measured ^{13}C -RCSA values for the (a) $1E$, $2S$, (b) $1Z$, $2S$, (c) $1E$, $2R$, and (d) $1Z$, $2R$ isomers. **Partially reproduced from reference [Yan et al., 2019] with permission.**

At this point, it is very clear that the key to measure accurate ^{13}C -RCSAs is to be able to experimentally remove the interferences from isotropic shifts. The stretching gels device described above, [Liu et al., 2010] and the consecutive additions of PBLG method do a very good job to be free of isotropic chemical shift interferences. There was another device developed to remove isotropic chemical shift interferences reported in 2018. [Hellemann et al., 2018] The method was intended as an extension of the compression method, stretching the same gel after it was used compressed to collect RDCs. In practice, the device pushes an already swollen gel through a funnel into the inner part of a 4-mm o.d. NMR tube, and consists of a gel chamber, a funnel, a piston, and a piston driver. Details on the device are shown in **Figure 59**. The piston has a VitonS O-ring, which makes this apparatus compatible with CDCl_3 .

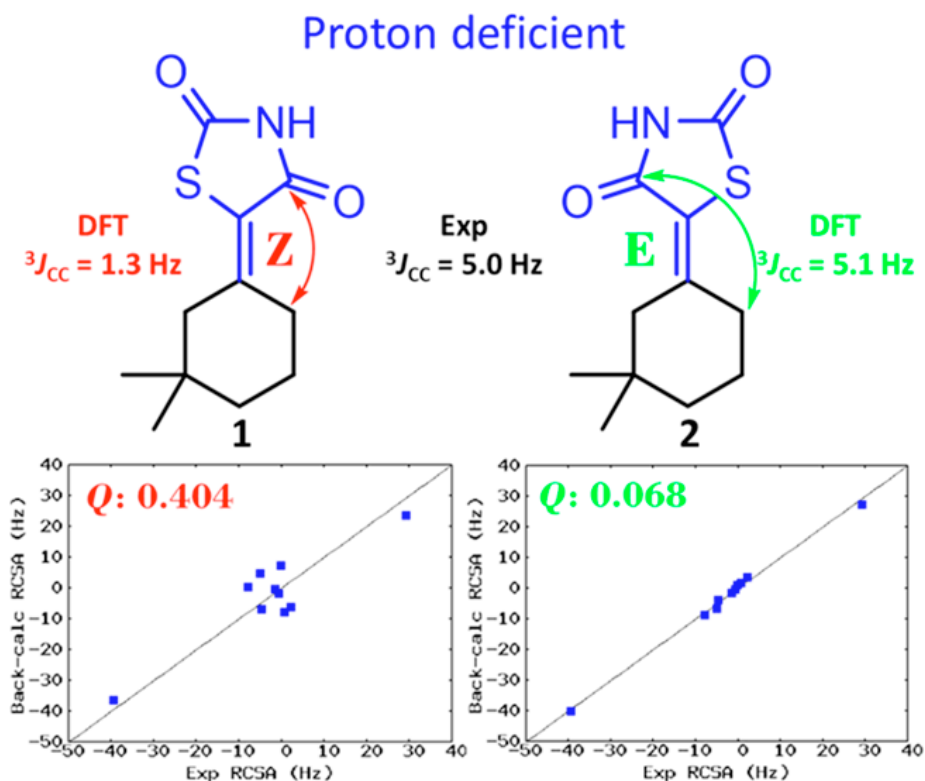


Figure 58. Clear discrimination of the *E* isomer of a proton-deficient analyte, the thiazolidinedione, complemented with experimental vs. calculated ${}^3J_{CC}$ data at ${}^{13}\text{C}$ natural abundance. **Reproduced from Ref. [Ndukwe *et al.*, 2019] with permission.**

The gel chamber, funnel and piston are made out of Teflon. This is a modification of the original device developed to stretch polyacrylamide gels into open-ended 5-mm o.d. tube to align proteins in water. [Chou *et al.*, 2001] Both devices are commercially available. [New Era Enterprise]

As illustrated in **Figure 61a**, the same PMMA gel stick used for the compression device [Gayathri *et al.*, 2010] is first swollen in CDCl_3 in a regular 5-mm o.d. NMR tube. RDCs can be measure in the compressed stage, when anisotropy is created by compression. But, if ${}^{13}\text{C}$ -RCSAs are collected, a post-acquisition correction done during the SVD fitting process is necessary, as mentioned earlier. [Hallwass *et al.*, 2018] The already swollen gel can be further extruded from the gel chamber to a 4-mm o.d NMR tube. In this open-ended 4-mm o.d NMR tube, the gel is stretched and anisotropy is created. This method has the advantage that the 4-mm o.d NMR tube perfectly fits inside a conventional 5-mm o.d NMR tube and is held by a Shigemi tube's cap (see **Figure 59c**). In order to avoid solvent from diffusing into the space between the inner wall of the 5-mm o.d. tube and the outer wall of the 4-mm o.d tube, a tiny

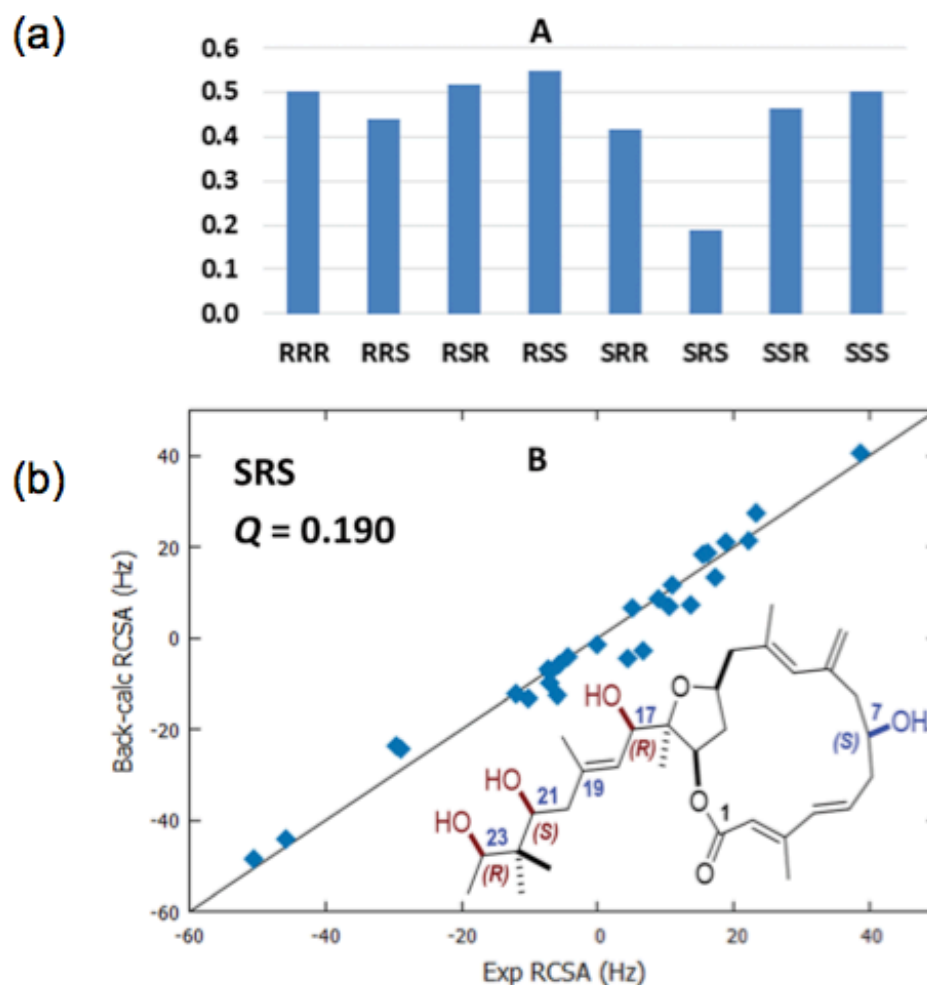


Figure 59. (a) Bar charts of Q-factors of isomeric phormidolide A structures, involving permutational stereo-inversion at position C-7, C-17 and C-21/C-23 (highlighted inset, (B)) leading to structural revision of phormidolide A to SRS. (b) Structure of the S,R,S C24-truncated phormidolide A fragment, and correlation between ^{13}C -RCSAs^{Exptl.} vs. ^{13}C -RCSAs^{Back-calc.} of the revised structure with S,R,S configuration for C-7, C-17 and C-21 stereocenters. **Figure reproduced from Ref. [Ndukwe et al., 2020-a] with permission.**

plug made of Teflon tape is inserted into the bottom open end of the 4-mm o.d. tube. No CDCl_3 isotropic peak is observed and pure ^{13}C -RCSAs can be experimentally measured without isotropic chemical shift interferences. (^{13}C - ^1H)-RDCs and ^{13}C -RCSAs for 10-epi-8-deoxycumambrin B, strychnine and yohimbine were measured and the correct configuration of each compound was successfully selected using only ^{13}C -RCSAs without post-processing gel shift correct during the SVD fitting procedure. **[Hellemann et al., 2018]**

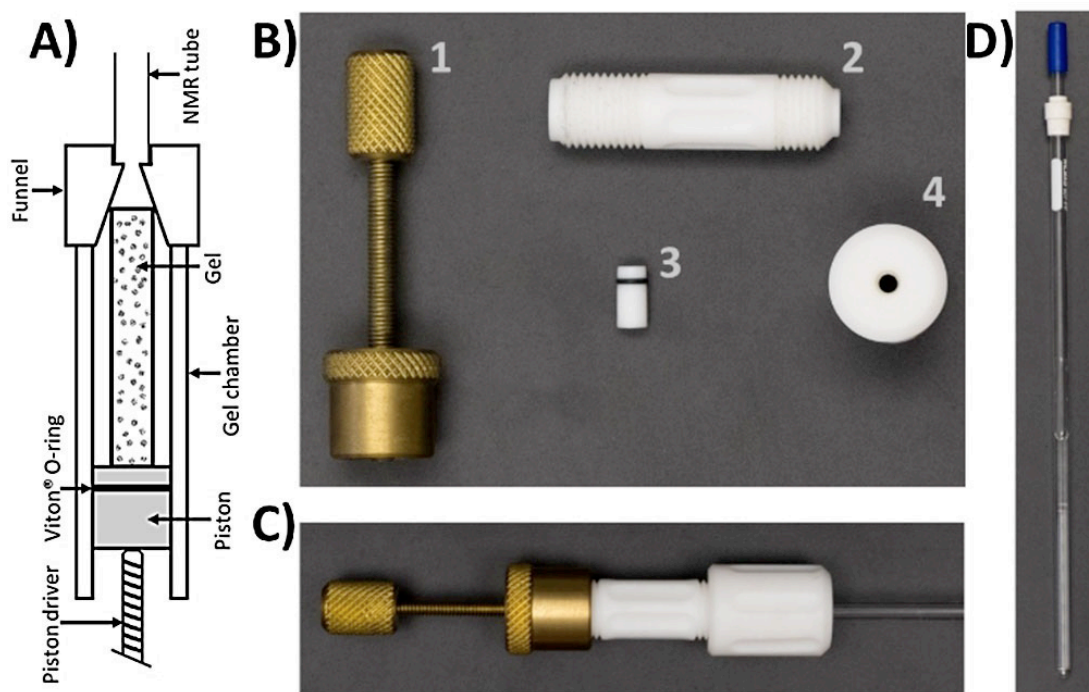


Figure 60. Gels stretching device to measure RCSAs without interference from isotropic chemical shifts. **Figure reproduced from Ref. [Hellemann *et al.*, 2018] with permission.**

The successful application of ^{13}C -RCSAs, particularly to the structural analysis of proton-deficient molecules, created excitement in the community and led to the development of further creative methods to accurately measure ^{13}C -RCSAs without the undesired contribution from isotropic chemical shifts. In this domain, the “one-shot” method, which consists in preparing a PBLG solution in CDCl_3 where both, isotropic and anisotropic conditions co-exist was recently explored and reported. [Recchia *et al.*, 2020] The concentration at which this so-called biphasic condition exists depends on the average molecular weight of the PBLG, as shown in **Figure 62a**.

As shown in **Figure 61b**, this is a very ingenious approach that permits the simultaneous collection of 1D ^{13}C NMR spectra in isotropic and anisotropic condition in exactly the same experimental conditions (concentration, temperature, viscosity, etc.), and hence calculate the ^{13}C -RDCs in “one-shot”. The method was successfully applied to determine the structure of strychnine, neotricone and excelsione. It is interesting to note that despite the recent report of this approach, it has already seen one application. The “one-shot” method permitted also the revision of the structure of a previously reported synthetic product proposed to be the 1*R*,2*S*-cannabidiol epoxide, and was reassigned as cannabielsoin using ^{13}C -RCSAs. [Monroe *et al.*, 2021]

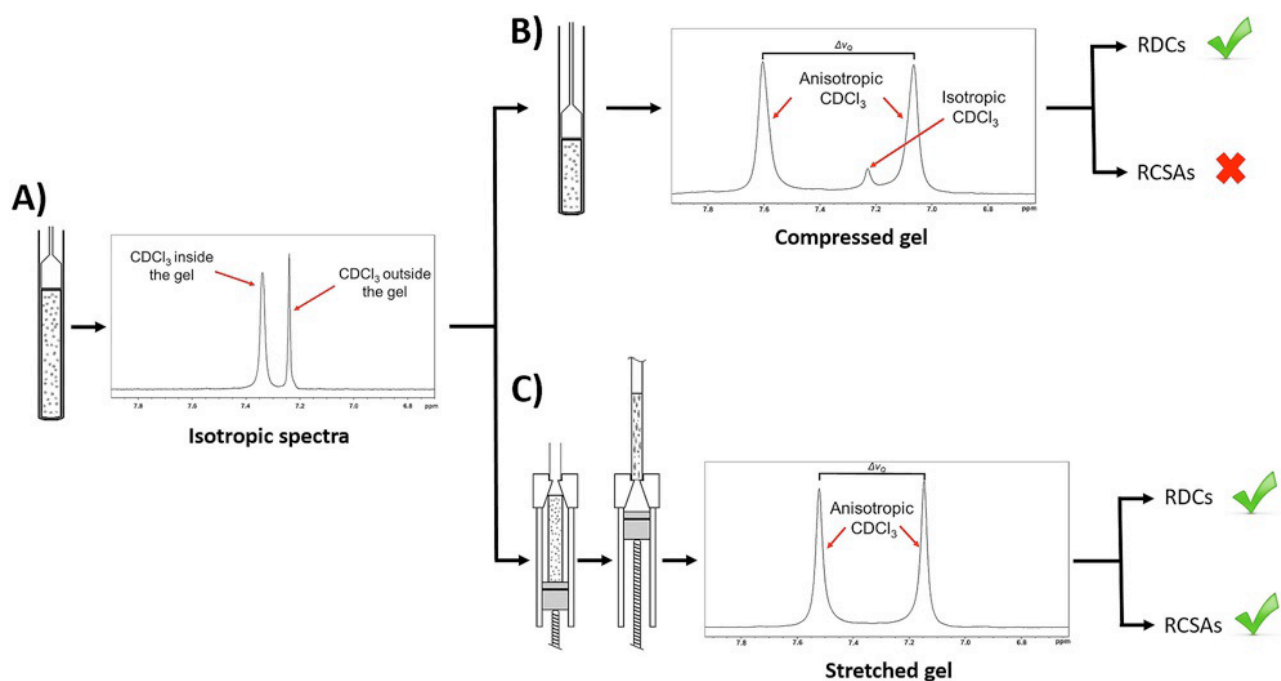


Figure 61. Working flow for the method involving the device shown in **Figure 59**. (a) Swollen of gel in a 5-mm o.d. NMR tube. When relaxed, CDCl_3 shows ^2H NMR isotropic signals from inside and outside the gel. (b) Compressed gel: the ^2H NMR signal of CDCl_3 inside the gel splits into an ^2H -DQ while the signal from outside the gel stay unchanged (a single line) but reduced in intensity. In these conditions, it is possible to collect RDCs but not RCSAs without isotropic chemical shift interferences. (c) Extruded gel through the funnel and stretched inside a 4-mm o.d. NMR tube, no signals from outside the gel are observed. RDCs and RCSAs can be measured accurate without further corrections. **Figure reproduced from Ref. [Hellemann et al., 2018] with permission.**

Discovery of new oriented phases is a continuous challenge. Recently, self-assembled oligopeptide nanotubes (noted AAKLVFF) as a new alignment medium for accurate RDC measurement in methanol was reported. [Lei et al., 2017; Liu et al., 2020] A further step was accomplished with the application of the AAKLVFF-based LLCs phase to measure ^{13}C -RCSAs without interferences from isotropic chemical shifts. [Li et al., 2020] Since anisotropy does not develop immediately after making the solution of AAKLVFF, it is possible to collect ^{13}C - $\{^1\text{H}\}$ NMR spectra in isotropic conditions right after the solution is prepared.

The anisotropy slowly develops in time span of 30 days until a state of equilibrium of the LLC phase is achieved, strong RCSAs can be measured after 10 days. During this period of time, since the experimental conditions are exactly the same, the change in chemical shift is purely due to RCSAs. **Figure 63** shows the evolution of the anisotropy build-up as a function of time of the AAKLVFF phase. This approach was also successfully applied to the determination of relative configuration of the four known natural products ((-)-bilobalide, estrone, limonin, and β -artemether) belonging to different structural classes. In addition, the configuration of marine

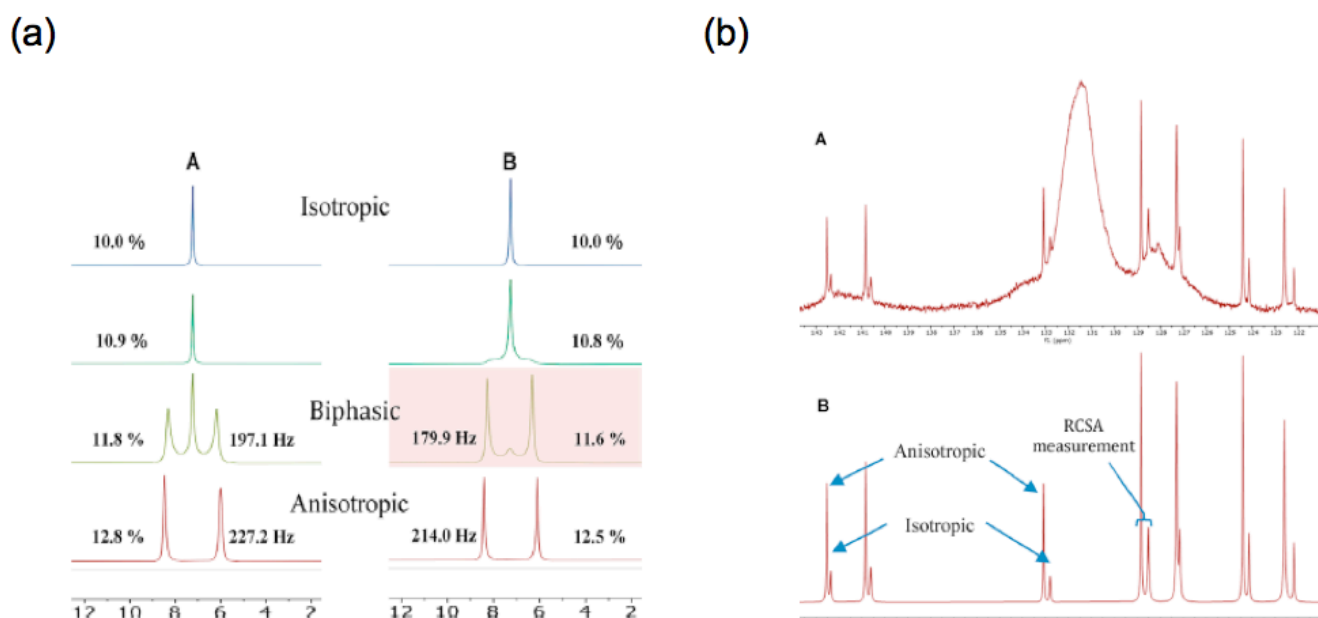


Figure 62. (a) 92.1 MHz ^2H NMR spectra of varying concentrations of two different PBLG (w/v%) with differing molecular weight distributions in CDCl_3 at 300 K. (left PBLG MW of ~ 249 kDa, (right) PBLG MW of ~ 328.5 kDa). (b) Aromatic region expansion of the 150.9 MHz $^{13}\text{C}\{-^1\text{H}\}$ 1D NMR spectrum of strychnine in PBLG (11.6%) showing NMR resonances for seven sp^2 carbons and their respective isotropic and anisotropic NMR resonances. The ratio of anisotropic to isotropic species is proportional to the highlighted ^2H NMR data. **Figures reproduced from Ref. [Recchia et al., 2020] with permission.**

natural product spiroepicoccin A (see **Figure 63**), a rare thiodiketopiperazine whose configuration could not be assigned based on conventional NMR methods, was unambiguously determined.

Magnetic susceptibility-induced alignment in diamagnetic proteins is significantly small, as shown from 1996. [Tjandra et al., 1996] However, in protein/DNA complexes, a significant anisotropic magnetic susceptibility builds-up by constructive addition of the individual magnetic susceptibility tensors of each nucleotide when they orient parallel in the DNA helical B-form. Thus RDCs of several Hertz for the backbone amides and $^{13}\text{C}_\alpha\text{-}^1\text{H}_\alpha$ sites have been measured. [Tjandra et al., 1997-b] Still, the magnetic susceptibility-induced alignment generally remains significantly smaller than what it is desired to measure RDCs with high accuracy for proteins or nucleic acids. [Bax et al., 2003]

Magnetic susceptibility-induced alignment scales with the square of the value of the magnetic field \mathbf{B}_0 . Molecules self-align in solution without the need of any type of alignment media and the alignment can be predicted by DFT calculations. In 2020, this method was applied to measure RDCs and RCSAs (for the first time) on the new marine natural products gymnochrome G (see **Figure 64a**) isolated from the deep-sea crinoid *Hypalocrinus*

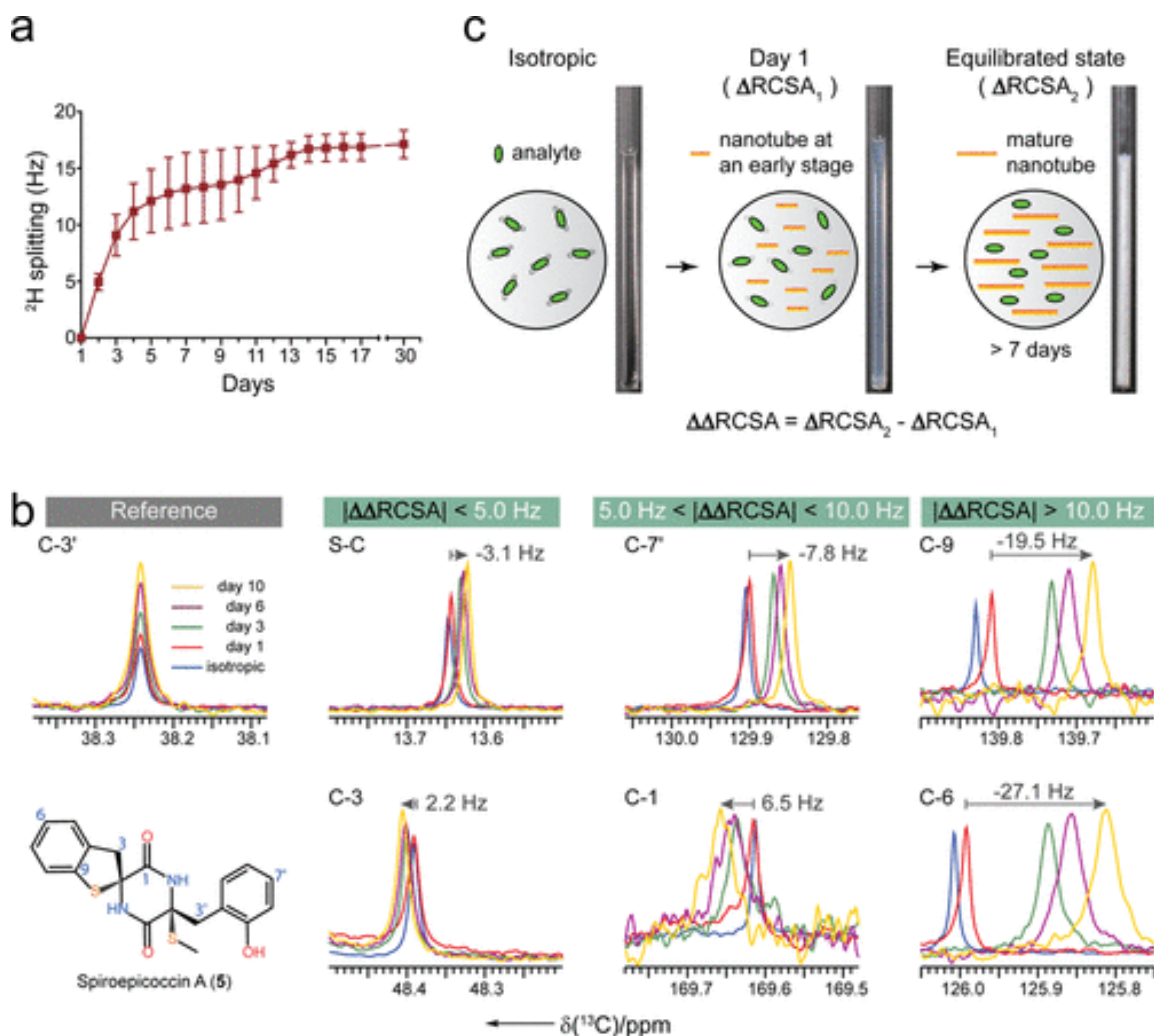


Figure 63. Experimental strategy for the measurement of $\Delta\Delta\text{RCSAs}$ in an AAKLVFF liquid-crystalline phase. (a) Time evolution of ^2H quadrupolar splitting (Hz) measured using eight different samples. (b) Representative $^{13}\text{C}\{-^1\text{H}\}$ signals of aliphatic, aromatic and carbonyl carbons of spiroepicoccin A (5) measured under isotropic conditions (blue), day 1 (red), day 3 (green), day 6 (magenta), and day 10 (yellow). C-3' was defined as the reference. (c) Schematic representation of the experimental procedure for the extraction of $\Delta\Delta\text{RCSAs}$ in an AAKLVFF phase. **Figure reproduced from eproduced from ref. [Li et al., 2020] with permission.**

naresianus featuring a large, proton-deficient aromatic system and two side chains with one stereocenter each. [Karschin et al., 2020] Aromatic rings possess a strongly anisotropic magnetic susceptibility tensor, leading to a large degree of alignment using this approach, as experimentally observed for this compound, but also for the strychnine.

Useful data (proton-proton couplings and extracted ^{13}C chemical shifts) were measured on ^1H and $^{13}\text{C}\{-^1\text{H}\}$ 1D NMR spectra for each compound at two different magnetic field strengths (400 and 950 MHz for ^1H). For strychnine, they acquired $^{13}\text{C}\{-^1\text{H}\}$ and $^1\text{H}\{-^1\text{H}\}$ couplings from CLIP-HSQC 2D spectra. [Karschin et al., 2020]

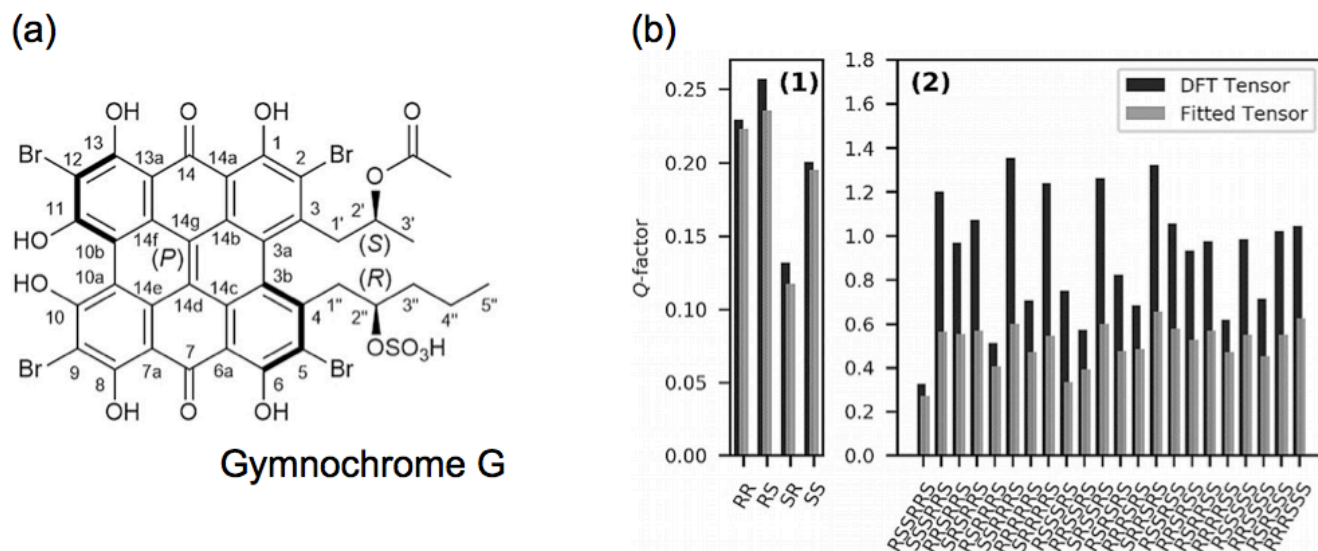


Figure 64. (a) Structure of gymnochrome G. (b) Q-factors for the different configurations of Gymnochrome G (left) and strychnine (right). The values obtained from predicting the alignment tensor with DFT are shown in black, the ones obtained from the fitted alignment tensor are shown in grey. In both cases, the true configuration is correctly identified by the lowest Q-factor. **Figure reproduced from Ref. [Karschin et al., 2020] with permission.**

As mentioned above, this type of alignment scales with the square of the magnetic field \mathbf{B}_0 . While the isotropic component of the chemical shift and the J -couplings stay constant at all magnetic field values, any change in chemical shift and J -couplings observed on anisotropic spectra is due to the contribution of RCSAs and RDCs, respectively. It is a difference experiment, and the larger the difference in \mathbf{B}_0 , the larger the values of RCSAs and RDCs are.

First RDCs measured for small molecules using this method were reported in 1986 for analyzing *o*-dichlorobenzene, [Anet et al., 1986] for analyzing a porphyrin-quinone based molecular cage in 1988, [Lisicki et al., 1988] and hydrogenated fullerenes in 1997. [Alemany et al., 1997] However, this is the first time that RCSAs are reported for small molecules.

The beauty of this method, regardless of the fact that the alignment is very weak and it needs very high-field NMR instruments, resides on the fact that the magnetic susceptibility tensor can be predicted by DFT calculation and the alignment can be predicted. Then, experimental vs. predicted RDCs or RCSAs can be compared. If the molecule is flexible, the magnetic susceptibility tensor for each conformer can be calculated and Boltzmann averaging of RDCs or RCSAs can be predicted from the calculated energies, instead of having to perform SVD fitting to the conformational ensemble using the single tensor approximation. **Figure 59** shows the Q-factors for all diastereomers of predicted and SVD fitted RCSAs for Gymnochrome G and strychnine. In both cases, the correct structure is selected.

At natural abundance, ^1H NMR is 5666 times more sensitive than ^{13}C NMR. Hence, it would be more convenient to measure ^1H - instead of ^{13}C -RCSAs, but on the other side, carbons show stronger anisotropy than protons. It is evident that ^1H -RCSA would be ideal for limited natural product samples at microgram level. Let's see some facts about ^1H -RCSAs. E.g., from DFT calculations, the most anisotropic proton in strychnine is H-18 α with an anisotropy value of 11.900, while the less anisotropic one is H-8 with an anisotropy value of 3.227. LLC phase such as PBLG are a no go for ^1H 1D NMR spectra due to the significant signal's line broadening observed due to their viscosity. The best option would be to use aligning gels. The GDO in aligning gels, such as compressed PMMA, is around 7×10^{-4} . Hence, the maximum ^1H -RCSAs values for H-18 α should be equal to $7 \times 10^{-4} \times (\sigma_{zz} - \sigma^{iso}) = 7 \times 10^{-4} \times (36.86 - 28.93) = 0.00555$ ppm. This value is a constant. It increases therefore in Hertz as the magnetic field B_0 increases in value. To minimize the error, ^1H -RCSAs should be collected at very high magnetic fields. E.g., at 800 MHz, this value corresponds to only 4.44 Hz. For H-8, the same calculations yield a value of only 1.20 Hz. Sound very discouraging. Measuring such small values in Hz accurately and without isotropic shift interferences represent a very challenging task. However, in 2020 it has been reported the successful application of ^1H -RCSAs for the structural analysis of natural products at microgram levels. [Nath et al., 2020] The study was conducted with NMR instruments operating at 700 and 800 MHz with several natural products and ^1H -RCSAs measured with the samples oriented in aligning gels. Among a few known natural products, the relative configuration of a 35- μg sample of the new diterpenoid briarane B-3 isolated from the gorgonian *Briareum asbestinum* collected in the waters off the Yucatan Peninsula of Mexico (see **Figure 65**) was determined. The sample was aligned in a perdeuterated PMMA- d_8 gel stretched in a Hilgenberg's micro stretching device and the ^1H 1D NMR spectra recorded at 800 MHz. Its absolute configuration was determined by ECD. A synergistic combination of anisotropic NMR with chiroptics.

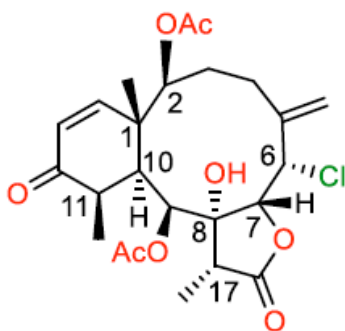


Figure 65. Structure of briarane B-3 along with configuration.

7.3 Configuration determination using spin-1 NMR analysis

A powerful and recent alternative to RDCs and RCSAs is the use of RQCs, because this third anisotropic observable (specific to nuclei with spin $I > 1/2$) encodes also valuable 3D structural information, and correlates the relative orientation of stereogenic centers, regardless of the distance between them in the molecule. As mentioned in **Section 3.3**, RQCs can be effectively exploited for analytical or structural purposes, when the relaxation rates (governed by the quadrupole mechanisms) is relatively low, allowing for high-resolution NMR spectra. This characteristic is typically met with deuterium, with the advantage to be naturally present in all hydrogenated molecules, with $\delta^{\text{iso or aniso}}(^2\text{H}) \approx \delta^{\text{iso or aniso}}(^1\text{H})$, and probing the same molecular directions that the associated ^{13}C - ^1H bond vectors (see **Eq. 12**).

If the analysis of oriented deuterated solutes was abundantly used, **[Dong, 1994]** the detection of first ^2H spectra at natural abundance of a solute has been reported from 1964, **[Diehl and Leipert, 1964]** but isotropic NMR finds interesting developments with the achievement of FT-NMR, as a help to analysis and decipher complex ^1H spectra, since $\delta^{\text{iso}}(^2\text{H}) \approx \delta^{\text{iso}}(^1\text{H})$, **[Briggs et al., 1973]** as simple nuclear probe to understand biosynthesis mechanisms, **[Leopold et al., 1998]** as well as the determination of site-specific ($^2\text{H}/^1\text{H}$) isotopic ratios in molecules by Martin and co-workers from 1981 (see **Section 8**). **[Martin et al., 1981]** Disregarding rather examples of ANAD spectra of liquid crystals (thermotropic), **[Prosser et al., 1996; Tabayashi et al., 1997]** paradoxically, the first results on the utility of ^2H -RQCs recorded at natural abundance level for analyzing solutes in oriented media have been only reported in 1998 **[Khetrapal et al., 1998]**, thirty five years after the first anisotropic ^1H 1D-NMR spectra of a solute, **[Saupe and Englert, 1963]** using also thermotropic systems (achiral nematics), the same year of the first enantiotopic and enantiomeric spectral discriminations in PBLG-based lyotropic CLCs. **[Lesot et al., 1998]** Interestingly, in lyotropic systems, the significant difference of $T_2(^2\text{H})$ values (due to their dynamical range) between the different deuterium sites in the polymer (such as polypeptide and polyacetylene) and in the solute leads to very low-resolution spectra (baseline) and high-resolution ANAD spectra, respectively, and no real interference between the two types of spectral signatures exists.

Analysis of scalemic mixtures by ANAD 2D NMR. Using ANAD QUOSY-type 2D experiments (see **Section 4.2**) to simplify the identification and assignment of ^2H -QDs, the analysis of enantio-isotopomeric mixture associated to prochiral compounds **[Aroulanda et al.,**

2001, 2003; Lesot et al., 2004-b, 2008-c; Sehran et al. 2010] is possible and can be extended to racemic or scalemic mixtures of two enantiomers. **[Lesot et al., 2003, Navarro-Vasquez et al., 2017]**. This is interesting because when RDCs are concerned, the data are generally extracted from two oriented samples, one for each enantiomer, assuming that all experimental conditions are the same.

Simplified schematic protocol showing the principle of molecular structural analysis using the ^2H -RQCs extracted from ANAD 2D-NMR experiments as presented in **Figure 65a**. **[Lesot et al., 2019]** The integrated computational program using SVD algorithm can be “MSpin-RQC” **[Navarro-Vazquez et al., 2017, 2012]** or “ConArch+”. **[Berdagué et al., 2021, Immel et al., 2018]** Note here that the sign of ^2H -RQCs for a given ^{13}C - ^2H bond, not directly accessible from ANAD 1D/2D spectra derived from a rapid analysis of the $^1J(^{13}\text{C}\text{-}^2\text{H})$ and $^1T(^{13}\text{C}\text{-}^2\text{H})$ values extracted from isotropic and anisotropic proton-coupled ^{13}C 1D spectra or with the help of J/D -resolved 2D spectra.

As in case of RDCs and RCSAs, from the analysis of ^2H -RQC data, we can evaluate the difference of average molecular orientation of each enantiomer and the comparison of their alignment tensors (see **Figure 65b**). Such information may provide a quantitative data on the enantiomeric discrimination ability (EDA) of various chiral polymers toward a given analyte or make a comparison of a series of chiral molecules toward a given chiral polymer. **[Berdagué, et al., 2021; Navarro-Vasquez et al., 2017]** Such data are useful to have better insight on the enantiodiscrimination mechanisms in CLCs, with the possibility to correlate the enantio-recognition capabilities to the nature or the structure of chiral polymers (see **Section 7.4**).

In practice, this description is done by calculating the molecular Saupe matrix of each enantiomer, $\{S_{\alpha\beta}\}^{R,S}$ and then compared by evaluating the generalized 9D β angle using **Eq. 26: [Kramer, 2004; Navarro-Vasquez, 2017]**

$$\beta = \arccos \left(\frac{\sum_{\alpha\beta=x,y,z} S_{\alpha\beta}^R S_{\alpha\beta}^S}{\sqrt{\sum_{\alpha\beta=x,y,z} (S_{\alpha\beta}^R)^2} \sqrt{\sum_{\alpha\beta=x,y,z} (S_{\alpha\beta}^S)^2}} \right) \quad (26)$$

The β angle value or the $\cos(\beta)$ value (GCB value) can be used to quantify the enantiodiscrimination efficiency for a enantiomeric pair. Thus, the closer this GCB value is to 1, the closer the positions of the alignment tensors are in space. Conversely, the closer this value

is to 0, the more the positions of the axes of the alignment tensors are different, this second situation corresponds to the maximum enantiodifferentiation and so to an optimum EDA.

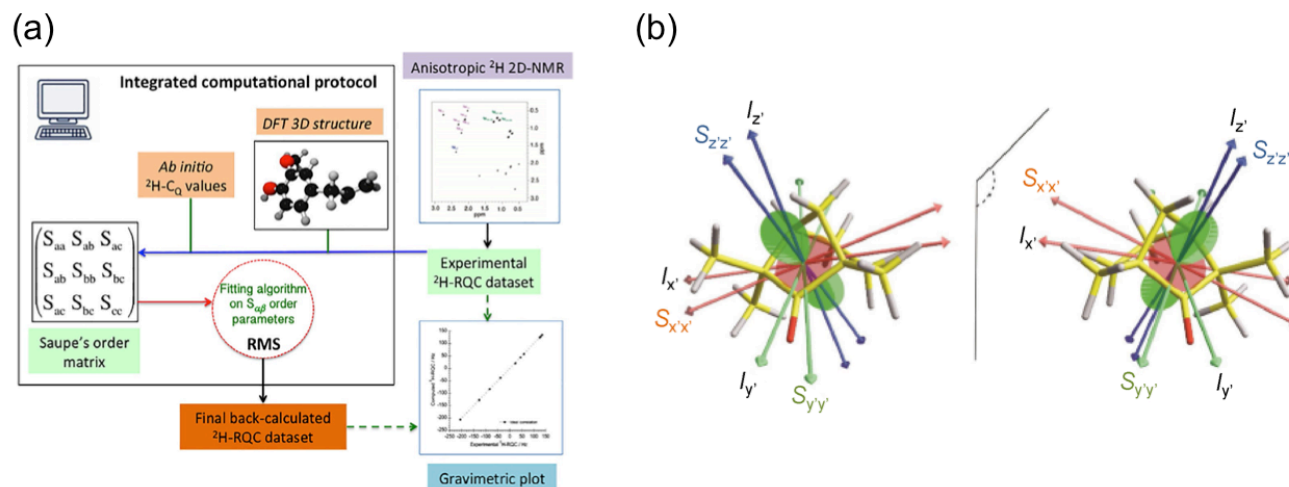


Figure 66. (a) Simplified flowchart showing the principle of molecular structural analysis using the integrated computational program “MSpin-RQC” from the ^2H -RQCs extracted from ANAD 2D-NMR experiments. The correlation plot ($^2\text{H}\text{-RQC}^{\text{Calc.}}$ vs. $^2\text{H}\text{-RQC}^{\text{Exptl.}}$) simply visualizes the quality of fit of experimental data. (b) The principal axis system ($S_{xx'}$, $S_{yy'}$, $S_{zz'}$) of the diagonalized Saupe matrix, the inertia tensor axes, (I_x , I_y , I_z), and the Saupe tensor surface representation (red and green surfaces indicate positive and negative ^2H -RQCs, respectively) for (left) (S)-FCH and (right) (R)-FCH oriented in PBLG/ CHCl_3 . **Figure adapted from ref. [Lesot et al., 2019; Navarro-Vasquez et al., 2017] with permission.**

First analysis of natural drugs by ANAD 2D NMR. In the Sections above, various examples of 3D structural elucidation of natural products or drugs, as well as synthetic compounds of interest based on a unique set of RDCs or RCSAs (or a combination of both), with or without other data sources on the spatial arrangement of atoms in molecules (as nOe) have been proposed, clearly illustrating their analytical potentialities and their contribution to structural issues.

In 2020, a new door was opened with the demonstration that ^2H -RQCs extracted from ANAD spectra could provide reliable and coherent set of anisotropic dataset and hence becoming a promising alternative to RDCs and RCSAs to solve non-trivial structural problems. The performance and scope of this tool was examined for two natural chiral compounds of pharmaceutical interest (artemisinin and strychnine). **Figure 67a** presents the molecular structure, atomic labels and *R/S* descriptors of artemisinin as well as DFT-optimized 3D structures. This rigid molecule possesses seven stereogenic center, leading to 128 (2^7) isomers.

Using the fit procedure shown in **Figure 66**, it has been possible to identify the right molecular relative configuration (1*S*, 4*R*, 5*S*, 6*R*, 7*S*, 10*R*, 11*R*), using either the various ^2H -

RQCs and the average of ^2H -RQCs for each methylene group and their respective prostereogenic methylene directions (α,β), but also the ^2H -RQC data of all deuterium sites. [Lesot *et al.*, 2020-b] The smaller Q-value obtained dropped to 0.017 for all data, while a Q-value of 0.011 was calculated when the average ^2H -RQCs for the diastereotopic site was used. The agreement between experimental and back-calculated RQCs for the smallest Q-factor as shown in **Figure 13-67c** demonstrated the quality of the coherence between the RQC dataset and the spatial arrangements associated to the 1*S*, 4*R*, 5*S*, 6*R*, 7*S*, 10*R*, 11*R* configuration.

The final configuration obtained by the ^2H -RQC protocol is fully consistent with previous reports using RDCs [Navarro-Vázquez *et al.*, 2018] as anisotropic data, as well as with X-ray structure, [Guo, 2016] consequently validating for the first time the robustness of the ANAD-NMR methodology.

Compared to RDC analysis, all monodeuterated isotopomers for a given molecule form independent dilute ^2H -spin systems, and hence in ANAD NMR, the strong coupling effects that frequently hamper the accurate determination of $^1D_{\text{CH}}$ couplings in CH_2 groups no longer exist.

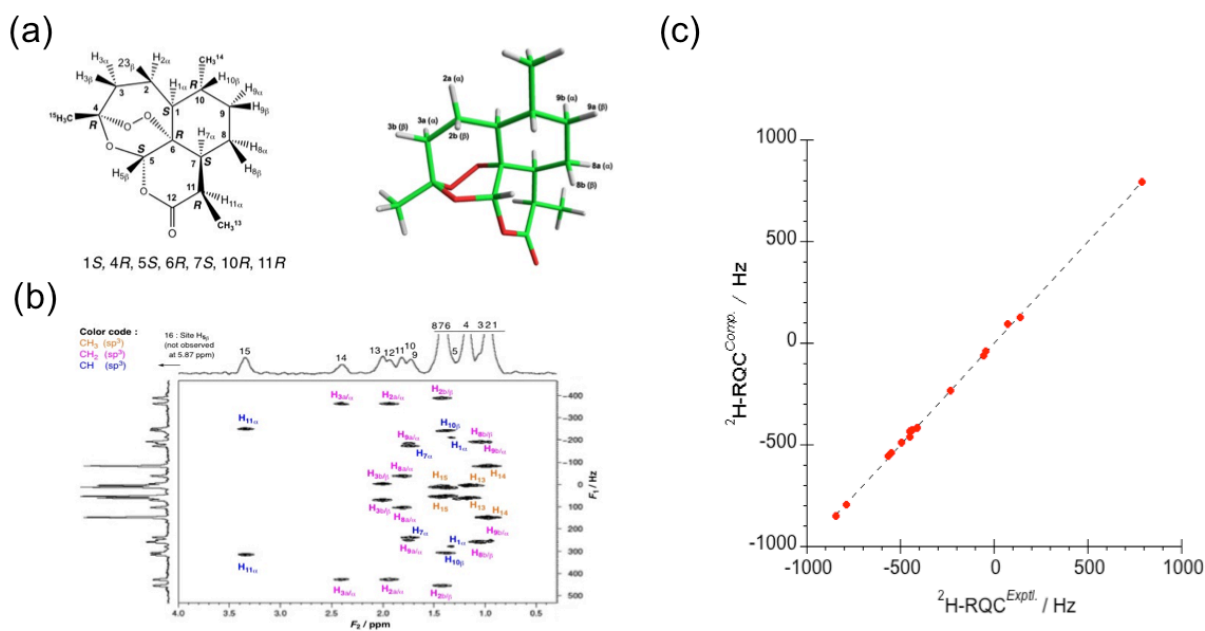


Figure 67. (a) Molecular structure, atomic labels and *R/S* descriptors of artemisinin associated with the (known) absolute configuration, and DFT-optimized 3D structures labeling the $\alpha\beta$ (*a/b*) positions of diastereotopic protons/deuterons. (b) Part of the NAD- $\{^1\text{H}\}$ Q-resolved F_z 2D map (tilted and then symmetrized). (c) Correlation plot between experimental and back-calculated ^2H -RQC values. **Figure adapted from ref. [Lesot *et al.*, 2020-b] with permission.**

From an experimental point of view, the analysis of the ANAD 2D-NMR spectrum recorded in PBLG/ CHCl_3 lead to the unambiguous extraction of fifteen signed ^2H -RQCs out of sixteen

possible sites (see **Figure 67a**). An important deuterium depletion effect (associated with a low $^2\text{H}/^1\text{H}$ isotopic ratio) may lead to a drastic reduction of the ^2H -QD intensity some site, not detected (see **Section 8**). However, the lack of some ^2H -RQCs associated to a molecular structure does systematically not pre-empt the accomplishment of the structural analysis, if a sufficient number of anisotropic data is still experimentally available.

7.4 Determining the absolute configuration of monostereogenic chiral molecules

Determine the absolute configuration (AC) of enantiomeric NMR signals (R/S , M/P , \square/L , Δ/A) with a single stereogenic center using anisotropic NMR in CLCs alone remains a real challenge and a difficult issue because no direct and simple experimental tools exist to do so. **[Berger et al., 2012]** Same situation arises for the signal assignment of enantiotopic elements (pro- R /pro- S) in prochiral molecules.

In 2007, an empirical approach combining NAD 2D-NMR and a PBLG-based mesophase was proposed for assigning the AC of small chiral molecules. **[Ziani et al., 2007]** The key concept of this strategy lies on the fact that recognition phenomena of molecular shape play an important role in global ordering/differentiation mechanisms, and hence analogous molecular structures should be oriented similarly in the same aligned environment. By comparison with molecules in which the AC of enantiomeric signals is known and identified, it becomes possible to propose an AC for the enantiomeric signals of compounds of interest, with an unknown AC.

To date, the most promising alternative to is the development of *ab initio* methods (as Molecular Dynamic (MD) based computational simulations) able to predict molecular alignment. First descriptions were proposed in 1994. **[Helfrich et al., 1994]** The main issue is to correctly evaluate all type of interactions (electronic distribution and molecular shape) between a given analyte and a helically chiral system from the evaluation of interactions between a given analyte and a helically chiral system. **[Alvira et al., 1991; Frank et al., 2010; Nandi et al., 2004; Sager et al 2017; Sehran et al., 2012]** Although some progresses were obtained for predicting orientation behavior of analytes interacting with achiral polypeptide-based achiral systems (PBG), **[Sehran et al., 2012]** and in case of two enantiomers interacting with helical-polymer based CLCs **[Frank et al., 2010; Sager et al., 2017]** the results obtained are rare, and not always convincing in terms of reliability. Thus, MD simulation involving PBLG remains rather fragile because MD has to be performed with a sufficient long time to correctly

evaluate the effect of conformational dynamic of all side chains along the α -helix on the enantiodiscriminating effects. This occurrence needs a formidable calculation power, even whether a small number of polymeric units is considered.

8. Conformational analysis in oriented solvents

The presence of conformational dynamics in flexible molecules, i.e large, low frequency torsional molecular motions, may strongly complicate the interpretation and the correct use of the anisotropic NMR data (as RDCs) compared to the case of rigid compounds. **[Celebre et al, 2003-a,b; Samulski, 2003]** To solve this difficult problem, several (more or less complex) calculation approaches have been proposed so far. To help reader to go further, several solutions were proposed to manage this important problem are briefly outlined below, but a more detailed overview can be found in the Ref. **[Aroulanda and Lesot 2021]**

The simplest possible model, the rotational isomeric state (RIS) model assumes that only a restricted set of minimum-energy structures is populated. **[Flory, 1974]** For instance, the free rotation of methyl groups are described by the three statistically weighted staggered conformers. More realistic models allow for continuous bond rotations. Two main approaches, alone or combined, have been proposed in the past: i) the additive potential (AP) method, an “approximate” approach whose aim is to reduce latest equations to manageable expressions by using some physically justifiable approximations **[Emsley et al, 1982]**, and ii) the maximum entropy (ME) method, an “unbiased” method based on information theory **[Catalano et al, 1991; Di Bari et al, 1988; Stevenson et al, 2003]**. Finally in the last decade were developed hybrid strategies, combining the AP method and a direct probability distribution, DPD, for describing directly the internal potential as sum of Gaussians. **[Celebre et al, 2003-a,b; 2012]**. These models were applied to evaluate the conformational dynamic of small flexible analytes as naproxen or flurbiprofen (enantiopur chiral drugs) in polypeptide (PBLG) mesophases **[Di Pietro et al., 2017-a, 2017-b, 2019]** and a couple of enantiomers of (*R/S*)-1-(4-fluorophenyl)ethan-1-ol, for the first time in 2021. **[Rosachiara et al., 2021]** In this example, it was demonstrated that *R/S*-enantiomers show significant differences in their conformational behaviors, due to the difference of solute-solvent orientational molecular interactions experienced by the (*R*) and (*S*)-isomers in a helical chiral environment as PBLG system. Understanding of chirality-dependent molecular interactions, often involved in a number of important chemical processes

9. Anisotropic ^2H 2D NMR applied to molecular isotope analysis

9.1 The natural ($^2\text{H}/^1\text{H}$) isotope fractionation: principle

The relative abundance of deuterium compared to proton is about 155 ppm, this specific value is known as Vienna-Standard Mean Ocean Water (V-SMOW) value. [IUPAC, Lesot *et al.*, 2020-c] However, in reality the deuterium/proton isotopic ratio can vary from one site to another site of the molecule, thus leading to its molecular isotopic profile.

The chemical origin of the isotopic fractionation comes from a discrimination between light (^1H) and heavy atoms (^2H) that occurs during (bio)chemical processes. [Basov *et al.*, 2019] The determination of isotopic fractionation can provide key data to: i) understand the enzymatic mechanisms, ii) validate the biosynthetic pathways of natural molecules, and iii) authenticate the geographical/botanical origin of bioproducts. [Akoka and Remaud, 2020]

The principle of deuterium isotope fractionation analysis consists in recording $^2\text{H}\{-^1\text{H}\}$ 1D/2D NMR spectra under quantitative conditions (with recycling time $T_R(^2\text{H}) = 5 \times T_i^{(\text{the longest value})}(^2\text{H})$) in the presence of an internal reference (such as Tetramethylurea (TMU)), for which the ($^2\text{H}/^1\text{H}$) isotopic ratio is calibrated and well known. [Martin *et al.*, 1981] The isotope ratio (expressed also in ppm) for each deuterium site is then calculated from the measurement of the peak surfaces in combination with masses of the product and reference, and the stoichiometric ratio according to **Eq. 27**.

$$(^2\text{H}/^1\text{H})_i^{\text{Anal.}} = \left[\frac{A_i^{\text{Anal.}}}{A^{\text{Ref.}}} \right] \times \left[\frac{P^{\text{Ref.}} \times m^{\text{Ref.}} \times M^{\text{Anal.}}}{P_i^{\text{Anal.}} \times m^{\text{Anal.}} \times M^{\text{Ref.}}} \right] \times (^2\text{H}/^1\text{H})_i^{\text{Ref.}} \quad (27)$$

In this equation, $A_i^{\text{Anal.}}$ and $A^{\text{Ref.}}$ are the integrated area of the signals at site i for the analyte and that of the reference, both measured on the isotropic NAD 1D spectra, $P_i^{\text{Anal.}}$ and $P_i^{\text{Ref.}}$ are their stoichiometric numbers of hydrogen at site i (analyte or reference), $M^{\text{Anal.}}$, $M^{\text{Ref.}}$, $m^{\text{Anal.}}$ and $m^{\text{Ref.}}$ are the molecular weights and masses of the analyte and the reference, respectively. Finally, $(^2\text{H}/^1\text{H})_i^{\text{Ref.}}$ is the isotope ratio of chemical reference in the sample (at site i).

This method is well-known as SNIF-NMR® and stands for Site-specific Natural Isotopic Fractionation first explored and then intensively developed by Martin and co-workers. [Martin *et al.*, 1981, 1982] It was an original development of the international company Eurofins. SNIF-NMR was successfully used in several analytical applications, particularly in food analysis.

[Duan *et al.*, 2002; Remaud *et al.* 1997-a, 1997b] However, the method suffers from two drawbacks: i) Significant peaks overlapping due to the low ^2H chemical shift dispersion (in Hz) compared to ^1H ($\gamma(^2\text{H}) = \gamma(^1\text{H})/6.515$), and ii) Impossibility of discriminating enantiotopic sites in prochiral molecules as we can see in the case of the methylene group of ethanol. Interestingly, these problems can be overcome by using NAD- $\{^1\text{H}\}$ NMR in chiral liquid crystals, because we detect a new NMR interaction, the deuterium quadrupolar (RQC). We can spectrally discriminate enantio-isotopomers in a CLC. [Lesot *et al.*, 2020-c] Two illustrative examples are discussed below.

9.2 Case of prochiral molecules: the fatty acid family

The analytical potential of NAD 2D NMR in the framework of the isotope fractionation analysis was first explored in the case of a fragment of prochiral fatty acids, the 1,1'-bis(phenylthio)hexane (BPTH), [Lesot *et al.*, 2004] and then successfully demonstrated on a complete long-chain (C-18) unsaturated fatty acid, the methyl linoleate (ML). [Lesot *et al.*, 2008-c; Sehran *et al.*, 2010] Indeed, for such a prochiral analyte, we were able to spectrally separate all the monodeuterated enantio-isotopomers of the molecule in the PBLG/pyridine mesophase (see **Figure 68b**). As a consequence, it was possible to follow the variation of ($^2\text{H}/^1\text{H}$) isotopic ratios for enantiotopic positions in each methylene group.

As a new molecular isotopic information related to the discrimination of all (*R/S*)-enantioisotopomers, it is possible to determine the bio enantio-isotopomeric excess, ($eie_i(\%)$) for each CH_2 group *i*, according to the equation: [Serhan *et al.*, 2010]

$$eie_i(\%) = 100 \times \frac{|(^2\text{H}/^1\text{H})_i^R - (^2\text{H}/^1\text{H})_i^S|}{(^2\text{H}/^1\text{H})_i^R + (^2\text{H}/^1\text{H})_i^S} \quad (28)$$

It has been evident that the $eie(\%)$ values at the odd-numbered CH_2 positions are larger than those measured at even-numbered CH_2 groups all along the chain (see **Figure 68c**). This observation was explained by the different incorporation mechanisms of hydrogens into the chain during the elongation of fatty acids via the fatty acid synthetase (FAS) enzyme. [Baillif *et al.*, 2009] These new isotope data, only accessible by anisotropic ^2H NMR allowed to better understand the stereochemical aspects of the enzymatic reactions leading to methyl linoleate, and particularly those of Fatty Acid Synthetase (FAS).

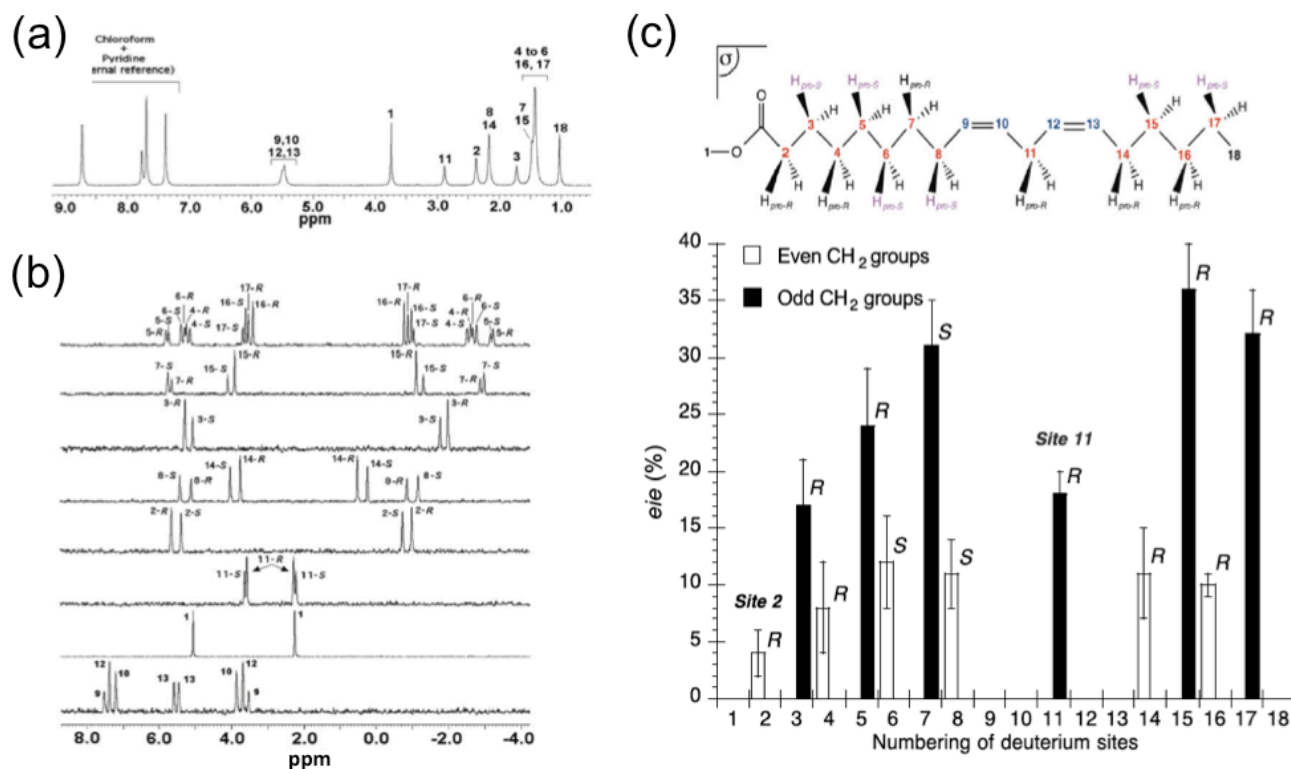


Figure 68. (a) Isotropic 92.1 MHz NAD- $\{^1\text{H}\}$ 1D spectrum of methyl linoleate. Note the high rate of peak overlap. (b) Series of 92.1 MHz NAD- $\{^1\text{H}\}$ 1D sub-spectra of ML in PBLG/pyridine extracted from the ^2H tilted Q-COSY Fz 2D spectrum. The ^2H -QD of methyl 18 is not shown. (c) Variation of $e/e(\%)$ vs. the methylene groups. **Figure adapted from ref. [Serhan et al., 2010] with permission.**

Taking advantage of NMR spectrometer operating at higher field (14.1 T, *i.e.* 92.1 MHz for ^2H) equipped with an electronic modern and a selective ^2H cryogenic probe (5-mm o.d.), the method was then successfully extended to the study of more complex long-chain prochiral FAMES with longer chain, such as C-18 mono or poly unsaturated FAMES, as well as the conjugated unsaturated FAMES (CUFAs) methyl oleate (MO), methyl linolenate (ML), methyl eleostearate (ME), methyl punicate (MP), including the chiral FAME methyl vernoleate (MV). [Lesot et al., 2008, 2011] With such a possibility in hands, it has been possible to experimentally evaluate the possible differences of bioconversion processes of ML to MV involved in the case *Euphorbia lagascae* and *Vernonia galamensis*, two plants that use different enzymatic systems. [Billaut et al., 2012]

The interest of this approach has been also successfully tested for the cases of C-14 to C-18 saturated FAMES (SFA), namely the methyl myristate (MM), methyl palmitate (MP) and methyl stearate (MS) fatty acids. It has been demonstrated that chiral ANAD NMR could provide a robust means of accessing to a larger number of ^2H sites (compared to isotropic NMR). [Sehran et al., 2012] Finally as, a last frontier to be crossed, to examine the ultimate

potentialities of chiral ANAD 2D NMR, the complex case the homogeneous triglycerides (TGs), the last class of lipids was examined (see **Figure 69**). [Lesot *et al.*, 2012] In accordance to Altmann's definition, [Altmann *et al.*, 1967] homogeneous TGs are flexible molecules of C_s symmetry on average containing a plane of symmetry σ . They have two enantiotopic side-chains for which hydrogenated sites are diastereotopic and a central chain (that is diastereotopic relative to the two side chains) containing enantiotopic hydrogenated sites. For clarity, **Figure 69** shows all stereochemical relationships (enantiotopicity and diastereotopicity) of tributyrin (TB), a short-chain TG.

The analysis of the NAD- $\{^1\text{H}\}$ Q-COSY Fz 2D map of TB in PBLG/Py indicates that 95% of the non-equivalent ^2H sites (*i.e.* nineteen ^2H -QDs out of twenty) are spectrally discriminated. In

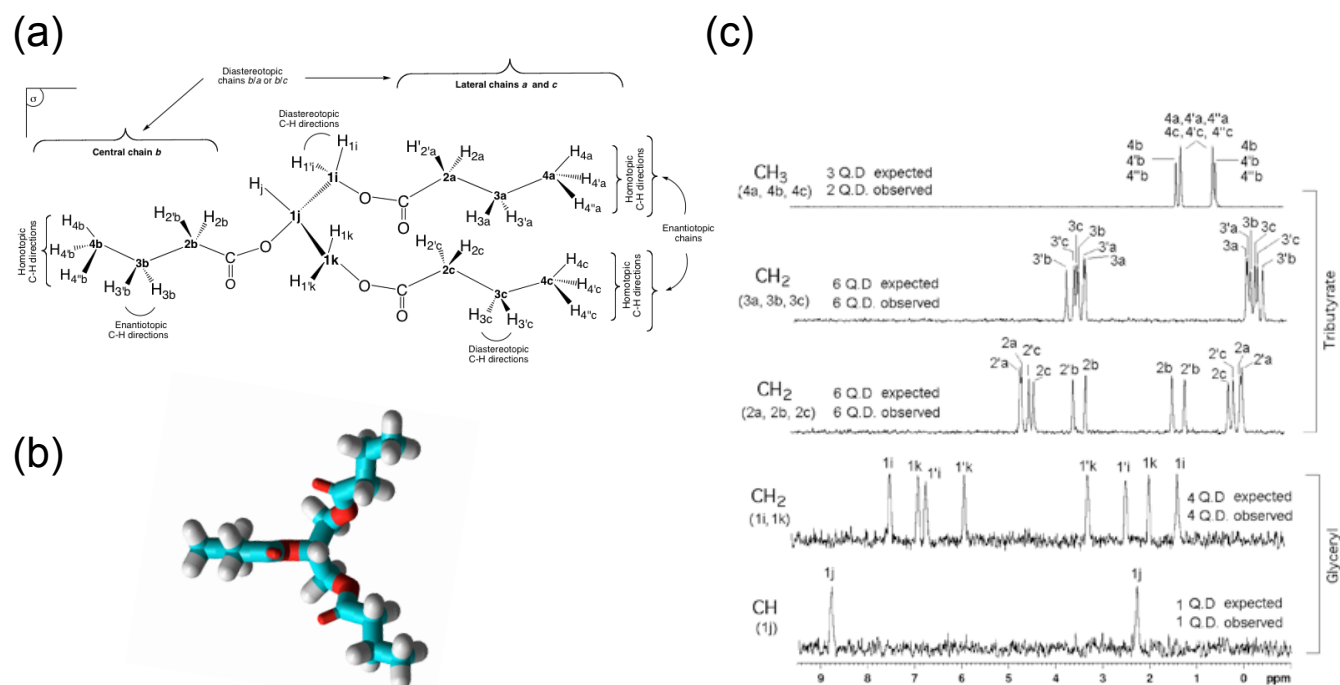


Figure 69. (a) Atomic numbering and stereochemical relationships between the different hydrogenated sites of the glycerol part (sites i, j, k) and methylene (2 and 3) and methyl (4) groups of the three hydrocarbon chains (a, b and c) of TB. Note the different homotopic, enantiotopic and diastereotopic elements in this molecule. (b) 3D structure of TB, top view. (c) Series of 92.1 MHz NAD- $\{^1\text{H}\}$ 1D sub-spectra of TB in PBLG/pyridine extracted from the tilted Q-COSY Fz 2D spectrum. **Figure adapted from ref. [Lesot *et al.*, 2012] with permission.**

this example, the number of differentiated sites is in agreement with the theoretical number expected for a C_s -symmetry molecule (see **Figures 69**), which implies an efficient shape recognition phenomenon. This ability to discriminate all ^2H sites was unfortunately not met in the case of trimyristate (TM), where the discrimination mechanisms that differentiate the central from the two side chains indicate that it is no longer possible to distinguish the side chains (a and c) from the central chain (b) as done for the case of TB. In other words, TM behaves more

as a C_{3v} -symmetry molecule instead of a C_s -symmetry molecule on average. This situation occurs because the ratio ($V_{a,c}/V_b$) of the persistent molecular volume of the side chain ($V_{a,c}$) to the central chain (V_b) strongly tends towards unity. Here the molecular volumes, $V_{a,b,c}$, correspond to the 3D space explored by the moving atoms of each chain. [Lesot et al., 2012]

9.3 New tools for fighting against counterfeiting

The combined application of isotropic ^2H and more recently ^{13}C NMR techniques in a variety of domains of natural products has been intensively investigated. [Jezequel et al., 2017; Zhao et al., 2021] They were used in plant species differentiation, detection of adulteration, and bio-activity evaluation. In 2018, anisotropic ^2H 2D-NMR has been involved in a new challenging analytical domain associated with molecular authenticity/traceability investigations in food products. [Texier-Bonniot et al., 2018] Among possible molecular targets, vanillin, the most widely-used aroma molecule in food industry and an important component of perfumery has been examined for two reasons: i) the price per kilo of natural and synthetic vanillin is extremely different, and therefore the temptation of selling synthetic vanillin at the price of vanillin from natural origin, and ii) the full ^2H isotopic composition of the aromatic core cannot be evaluated by the isotropic ^2H 1D-NMR (two sites over three) because in the case of aromatic deuterium sites $^2\text{H}_a$ and $^2\text{H}_b$ we have $\delta(^2\text{H}_a) = \delta(^2\text{H}_b) \neq \delta(^2\text{H}_c)$.

Using an optimized polypeptide oriented phase (PBLG/ $\text{CHCl}_3/\text{CCl}_4$), the ^2H signal of both sites has been separated on the basis of a difference on the magnitude of the ^2H -RQCs ($|\Delta\nu_Q(\text{C}-^2\text{H}_a)| \neq |\Delta\nu_Q(\text{C}-^2\text{H}_b)|$) (see **Figure 70a**). Interestingly, the assignment for each ^2H -QDs is possible, based on the collinearity of the C-D direction of sites in the aromatic ring of vanillin ($S_{\text{C-H}_a} = S_{\text{C-H}_c}$) leading to equal ^2H -RQCs values for both sites ($|\Delta\nu_Q(\text{C}-^2\text{H}_a)| = |\Delta\nu_Q(\text{C}-^2\text{H}_c)|$) (see **Figure 70b**). Structure of sodium cholate. (b) Structure of strychnine, a (toxic) natural compounds abundantly used as model molecule in the framework of the structure/configuration a)

To test the potential of ANAD NMR in the case of vanillin, we have analyzed different samples of vanillin, both from natural and industrial sources (synthetic or technological bioconversion), to see if we could discriminate them by only using isotopic data of the aromatic ring. Clearly, the access to the isotopic information for all aromatic sites could be an advantage to analytically control the synthetic or natural origin of vanillin.

For this, we have calculated the relative distribution coefficients, $k'_{2H_i (i = a,b,c)}$, of deuterium of three aromatic sites, H_a , H_b and H_c , corresponding to a fraction of peak area, A , and defined as:

$$k'_{2H_i (i = a,b,c)} (\%) = 100 \times \frac{A_{2H_i}}{\sum_{i=a,b,c} A_{2H_i}} \quad (29)$$

In the series of vanillin samples analyzed, it appeared that the ratios vary as $H_a < H_b < H_c$ for the samples of natural origin (bean or from a natural precursor (ferulic acid or lignin)), whereas the two synthetic samples both show $H_a < H_b > H_c$. From these referent isotopic trends, it becomes possible to establish the origin of an unknown sample of vanillin by comparing its distribution coefficients on the three sites with the reference data obtained for known vanillin origin.

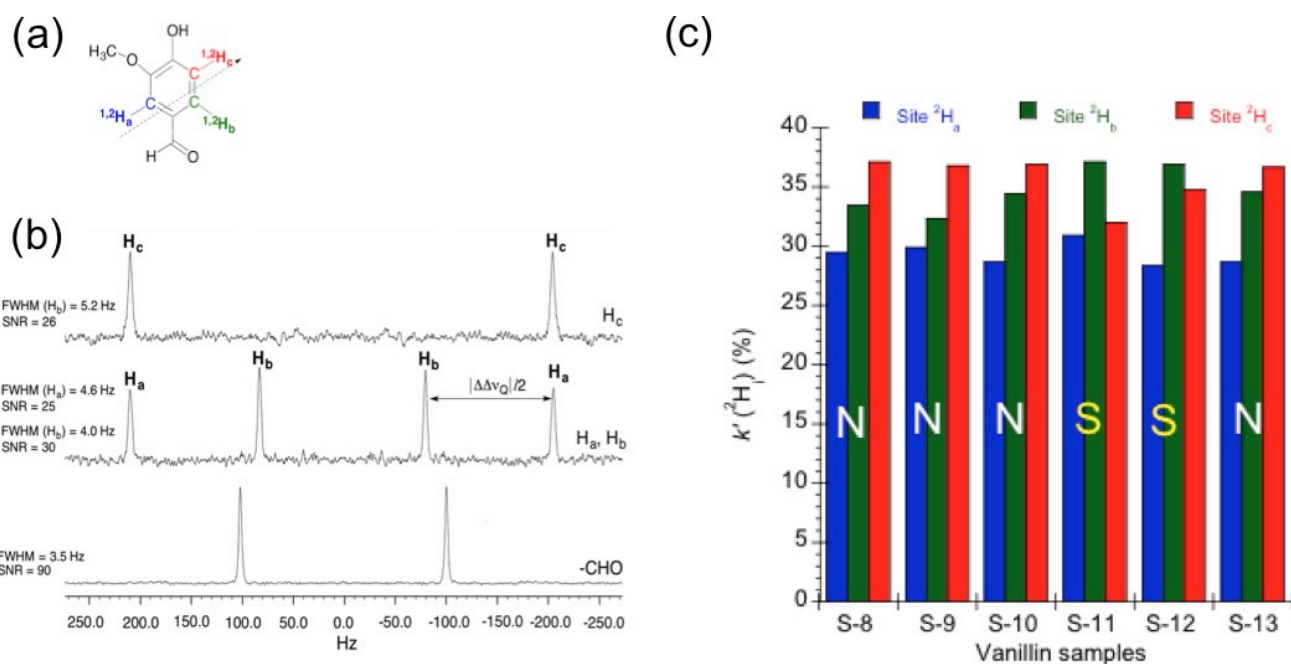


Figure 70. (a) Structure of Vanillin recorded with TMU. (b) Series of 92.1 MHz NAD- $\{^1H\}$ 1D sub-spectra of vanillin in PBLG extracted from the tilted Q-resolved Fz 2D spectrum. Compared to **Figures 68a** and **69b**, all 2H -QDs are centred here on 0 Hz in F_1 dimension. **Figure adapted from ref. [Texier-Bonniot et al., 2018] with permission.**

Access to new isotopic information, it is an important successful example. From a more theoretical standpoint, it has been shown from the analysis of all aromatic isotopic data how the 2H distribution might relate to the biosynthesis of vanillin. **[Texier-Bonniot et al., 2018]** From an applicative viewpoint, these results show that the evaluation of intramolecular 2H isotopic composition of the aromatic ring should enable to discern between natural and

synthetic origin, information that can be used in combination with isotopic data of non-aromatic sites of the molecule.

Exploring the ($^{13}\text{C}/^{12}\text{C}$) isotope fractionation. After a long analytical exploitation of ^2H SNIF-NMR, the possibility of detecting the natural ($^{13}\text{C}/^{12}\text{C}$) isotope fractionation (with a precision of *per mil*) by quantitative $^{13}\text{C}\{-^1\text{H}\}$ 1D NMR was explored and developed in 2000's. [Jezequel *et al.*, 2017, Portaluri *et al.*, 2021; Tenaillon *et al.*, 2004] In 2021, a new page of isotopic analysis by anisotropic NMR was opened with an exploratory experimental study to evaluate the possibility to establish enantiomeric ^{13}C position-specific isotope fractionation (EPSIF), using quantitative ^{13}C in PBLG-based CLC. [Lesot *et al.*, 2021] The idea is to provide a robust NMR tool to answer the intriguing and fundamental question related to chiral induction/amplification at the origin of homochirality in Nature: "*Is there a relationship between enantiomeric and isotopic fractionation of carbon-13 in chiral molecules?*" The main challenge is the ability to record $^{13}\text{C}\{-^1\text{H}\}$ spectra with sufficiently high signal-to-noise ratios to meet the required per-mil precision (‰) in isotope analysis and hence to accurately determine the $^{13}\text{C}/^{12}\text{C}$ isotope ratio", despite the doubling of ^{13}C signals due to the spectral enantiodiscrimination.

Using phenethyl alcohol as molecule model (see **Figure 16**), it was possible to separate the enantiomeric ^{13}C signals in various carbon sites of the analyte, ii) to maximize the spectral resolutions by optimization of the sample composition at 175.1 MHz, iii) to work with a very good repeatability for a series up to seven consecutive replicates; iv) to obtain a rather good long-term reproducible results.

10. Anisotropic NMR in molecular analysis: what you should keep in mind?

Anisotropic NMR using LLCs or alignment gels is a fascinating approach as they offer analytical possibilities and application opportunities that neither the liquid NMR nor the solid-state NMR has. As described here, we have highlighted how the three major anisotropic NMR observables, (RDCs, RSCAs, RQCs) were powerful tools to solve two important, modern problems for chemists: i) the evaluation of enantiomeric purity of chiral mixtures, and ii) the determination of molecular structure of complex synthetic or natural compounds. To be brief, and as a toolkit for any reader, we list below ten important facts and specifics of anisotropic NMR (in weakly aligning media) that every NMR spectroscopists should keep in mind to assess its potential for routine uses:

- i) analytical richness induced by the molecular orientation inside the magnetic field \mathbf{B}_0 ,
- ii) access to order-dependent NMR interactions (RCSA, RDC, RQC) not longer averaged to zero as in liquids,
- iii) spectral advantages to work with weakly orienting phases such as LLC phases and gels, within a range of one order of magnitude in terms of molecular orientation between these two types of media,
- iv) full control of orientation properties by adjusting the molar composition of the sample, the choice/nature of polymer and/or the polarity of organic co-solvent, or simply optimize the sample temperature in \mathbf{B}_0 ,
- v) detection of very weakly abundant nuclei (as ^2H) with reasonable experimental NMR times,
- vi) spectral discrimination enantiomers of chiral molecules to evaluate enantiomeric purity of mixtures as well as differentiate enantiotopic elements in prochiral compounds, when chiral oriented media are used,
- vii) possibility of NMR monitoring of dynamic processes (versus temperature or time) involving chiral objects (conformational equilibria, chemical transformations) with CLC,
- viii) analysis of site-specific isotopic profile using ^2H or ^{13}C NMR,
- ix) determination of molecular relative configuration because all anisotropic NMR observables encode valuable 3D structural information,
- x) and finally, the interest of diversifying the sources of molecular data using nD NMR for solving many challenging analytical problems met by chemists.

From the first pioneering work by Saupe and Englert and later Sackmann and coworkers in the early 1960's, which first opened the doors of the anisotropic NMR spectroscopy in ALCs [**Saupe and Englert, 1963**] and then in CLCs, [**Sackmann et al., 1968**] respectively, numerous methodological and/or technological developments (NMR sequences, variable angle spinning sample (VASS) NMR probes, new oriented systems, etc.) were proposed during three fertile decades of continuous progress. Combining with recent instrumental NMR achievements, they provide various keys to fully exploit the potential of NMR in oriented media and solve important analytical issues for a large community of chemists.

Clearly, after three decades dominated by thermotropic systems, an important rebirth of NMR in oriented solvents has occurred with the advent of (chiral or not) weakly alignment environments such as organic or water-compatible LLCs in the 1990's. Among future challenges associated with the next developments of anisotropic NMR in these specific

systems, two important challenges can be mentioned. The first one concerns the increasing of sensitivity of anisotropic NMR, particularly the detection of low abundant nuclei as deuterium. [Griesinger et al., 2012] The second one concerns the possibility of proposing robust computational model to predict the molecular orientation of a solute and the complex mechanisms of enantiodiscrimination phenomena using molecular dynamics. [Helfrigh et al., 1994; Celebre et al., 2001, 2019; Frank et al., 2015; Ibanez de Opakua et al; 2020; Sager et al., 2020; Tzvetkova et al., 2019] The final objective of this second challenge would be the possibility of predicting the absolute configuration of chiral mono- or poly-stereogenic molecules without the help of any analytical tool other than NMR. [Berger et al., 2012]

11. References and notes

ACD labs, <https://www.acdlabs.com>.

Akoka, S., and Remaud, G.S. (2020). NMR-based isotopic and isotopomic analysis. *Prog. Nucl. Magn. Reson.* 120-121: 1-24.

Aleman, L.B., Gonzalez, A., Billups, W.E., Willcott, M.R., Ezell, E., and Gozansky, E. (1997). Alignment effects in high field proton NMR spectra of the hydrogenated fullerenes $c_{60}H_2$ and $c_{60}H_4$: Evidence for residual anisotropic dipole-dipole couplings. *J. Org. Chem.* 62: 5771-5779.

Altmann, S.I. (1967). The summary of nonrigid molecules: the Schrödinger supergroup. *Proc Roy Soc. (London)*, A298: 184-203.

Alvira, E., Breton, J., and Plata, J. (1991). J. Chiral discrimination - a model for the interaction between a helicoidal system and an amino-acid molecule. *Chem. Phys.* 155: 7-18.

Anet, F.A.L. (1986). Magnetic alignment effects in the 500-MHz proton NMR spectrum of *o*-dichlorobenzene in acetone- d_6 . *J. Am. Chem. Soc.* 108: 1354-5.

Anet, F.A.L., and Bourn, A.J.R. (1965). Nuclear magnetic resonance spectral assignments from nuclear overhauser effects. *J. Am. Chem. Soc.* 87: 5250-5251.

Aroulanda, C., and Lesot, P. (2022). Molecular enantiodiscrimination by NMR in chiral oriented systems: Concept, tools and applications. *Chirality*, article online. DOI: 10.1002/chir.23386.

Aroulanda, C., Zimmermann, H., Luz, Z., and Lesot, P. (2011). Enantiotopic discrimination in the deuterium NMR spectrum of solutes with S_4 symmetry in chiral liquid crystals. *J. Chem. Phys.* 134: 134502-1/8.

Aroulanda, C., Lafon, O., and Lesot, P. (2009). Enantiodiscrimination of flexible cyclic solutes using deuterium NMR spectroscopy in polypeptide chiral mesophases: Investigation of *cis*-decalin and THF. *J. Phys. Chem. B.* 113: 10628-10640.

Aroulanda, C., Lesot, P., Merlet, D., and Courtieu J. (2003). Structural ambiguities in bridged ring systems resolved using natural abundance deuterium NMR in chiral liquid crystals. *J. Phys. Chem. A.* 107: 10911-10918.

Aroulanda, C., Sarfati, M., Courtieu, J., and Lesot, P. (2001-a). Investigation of enantioselectivity of three polypeptide liquid-crystalline solvents using NMR spectroscopy. *Enantiomer.* 6: 281-287.

- Aroulanda, C., Merlet, D., Courtieu, J., and Lesot, P. (2001-b).** NMR experimental evidence of the differentiation of enantiotopic directions in C_s and C_{2v} molecules using partially oriented, chiral media. *J. Am. Chem. Soc.* 123: 12059-12066.
- Auger, C., Lesage A., Caldarelli, S., Hodgkinson P., and Emsley, L. (1998).** Assignment and measurement of deuterium quadrupolar couplings in liquid crystals by deuterium-carbon NMR correlation spectroscopy. *J. Phys. Chem. B*, 120: 3718-3723.
- Baczko, K., Larpent, C., and Lesot, P. (2004).** New amino acid based on anionic surfactants and their use as enantiodiscriminating lyotropic liquid crystalline NMR solvent, *Tetrahedron: Asymmetry* 15: 971-982.
- Baillif, V., Robins, R.J., Le Feunten, S., Lesot, P., and Billault, I. (2009).** Investigation of fatty acid elongation and desaturation steps in *Fusarium Lateritium* by quantitative two-dimensional deuterium NMR spectroscopy in Chiral Oriented Media. *J. Biol. Chem.* 284: 10783-92.
- Bain, A.D.** Chemical exchange in NMR. (2003). *Prog. Nucl. Magn. Reson. Spectrosc.* 43: 63-103.
- Basov, A., Fedulova, L., Vasilevskaya, E., and Dzhimak, S. (2019).** Possible mechanisms of biological effects observed in living systems during $^2H/^1H$ isotope fractionation and deuterium interactions with other biogenic isotopes. 24: 4101-4123. DOI: 10.3390/molecules24224101.
- Bax, A.** Weak alignment offers new NMR opportunities to study protein structure and dynamics. (2003). *Protein Sci.* 12: 1-16.
- Bayle, J.-P., Courtieu, J., Gabetty E., Loewenstein A., and Péchiné J.-M. (1992).** Enantiomeric analysis in a polypeptide lyotropic liquid-crystal through proton decoupled deuterium NMR. *New J. Chem.* 16: 837-838.
- Becker, J., and Luy, B. (2015).** CLIP-ASAP-HSQC for fast and accurate extraction of one-bond couplings from isotropic and partially aligned molecules. *Magn. Reson. Chem.* 53: 878-885.
- Beguin, L., Giraud, N., Ouvrard, J.-M., Courtieu, J., and Merlet, D. (2009).** Improvements to selective refocusing phased (SERFph). *J. Magn. Reson.* 199: 41-47.
- Beguin, L., Courtieu, J., Ziani, L., and Merlet, D. (2006).** Simplification of the H-1 NMR spectra of enantiomers dissolved in chiral liquid crystals, combining variable angle sample spinning and selective refocusing experiments. *Magn. Reson. Chem.* 44: 1096-1101.
- Berdagué, P., Gouilleux, B. Nolls, M., Immel, S. Reggelin, M., and Lesot, P. (2021).** Study and quantification of enantiodiscrimination power of four polymeric chiral LLCs using NAD 2D-NMR, submitted.
- Berger, R., Courtieu, J., Gil R.R., Griesinger C, Köck M., Lesot, P., Luy, B., Merlet, D., Navarro-Vazquez, A., Reggelin, M, Reinscheid, U.M., Thiele, C.M., and Zweckstetter, M. (2012).** Is the determination of absolute configuration possible by using residual dipolar couplings from chiral-non-racemic alignment media? - A critical assessment. *Angew. Chem., Int Ed.* 51: 2-5.
- Billault, I., Ledru, A., Ouetrani, M., Serhan, Z., Lesot, P., and Robins, R.J. (2012).** Probing substrate-product relationships by natural abundance deuterium 2D NMR spectroscopy in liquid-crystalline solvents: the case of the epoxidation of linoleate to vernoleate by two different plant enzymes. *Anal. Bioanal. Chem.* 402: 2985-2998.
- Bilz, A., Stork, T.G., and Helmchen, G. (1997).** New chiral solvating agents for carboxylic acids: discrimination of enantiotopic nuclei and binding properties. *Tetrahedron: Asymmetry* 8: 3999-4002.
- Blanco, J.G., Gil, R.R., Alvarez, I., Patrio, L.C., Genti-Raimondi, and S., Flury, A. (1997).** A novel activity for a group of sesquiterpene lactones: inhibition of aromatase. *FEBS Lett.* 409: 396-400.

- Boettcher, B., and Thiele, C.M. (2012).** Stereochemistry of molecules determined from residual dipolar couplings. Eds. Harris, R.K., and Wasylishen, R.E. *Encyclopedia of NMR*, 8: 4736-4747.
- Brandes, R., and Kearns, D.R. (1986).** Magnetic ordering of DNA liquid crystals. *Biochemistry*, 25: 5890-5885.
- Briggs, J.M., Farnell, L.F., and Randall, E.W. (1973).** Proton-noise-decoupled deuterium resonance at natural abundance by Fourier transform. *Chem. Commun.* 70-71.
- Burnell, E.E., and Delange, C.A. (Eds.) (2003).** *NMR of Oriented Liquids*. Springer Science. Dordrecht.
- Canlet, C., Merlet, D., Lesot, P., Meddour, A., Loewenstein, A., and Courtieu, J. (2000).** Deuterium NMR stereochemical analysis of threo-erythro isomers bearing remote chiral centres in racemic and non-racemic liquid crystalline solvents. *Tetrahedron: Asymmetry*, 11: 1911-1918.
- Canet, I., Courtieu, J., Loewenstein, A., Meddour, A., and Péchiné, J.-M. (1995).** Enantiomeric analysis in a polypeptide lyotropic liquid crystal by deuterium NMR, *J. Am. Chem. Soc.* 117: 6520-6526.
- Catalano, D., Di Bari, L., and Veracini C.A. (1991).** A maximum-entropy analysis of the problem of the rotameric distribution for substituted biphenyls studied by ¹H nuclear magnetic resonance spectroscopy in nematic liquid crystals. *J. Chem. Phys.* 94: 3928-3935.
- Celebre, G., De Luca, G., D'Urso, C., and Di Pietro, M.E. (2019).** Helical solutes orientationally ordered in anisotropic media composed of helical particles: Formulation of a mean torque potential sensitive to P and M chirality as a tool for the assignment of the absolute configuration of enantiomers. *J. Mol. Liq.* 288: 111044 (1-5).
- Celebre, G., De Luca, G., and Di Pietro, M.E. (2012).** Conformational distribution of trans-stilbene in solution investigated by liquid crystal NMR spectroscopy and compared with in vacuo theoretical predictions. *J. Phys. Chem. B.* 116: 2876-2885.
- Celebre, G., De Luca, G., Emsley, J.W., Foord, E.K., Longeri, M., Lucchesini, F., and Pileio G. (2003-a).** The conformational distribution in diphenylmethane determined by nuclear magnetic resonance spectroscopy of a sample dissolved in a nematic liquid crystalline solvent. *J. Chem. Phys.* 118: 6417-6426.
- Celebre, G., and Longeri, M. (2003-b).** NMR studies of solutes in liquid crystals: Small flexible molecules, Eds. Burnell, E.E., de Lange C.A., Kluwer Academic Publisher, Dordrecht, Chap. 14.
- Celebre, G. (2001).** On the anisotropic intermolecular potential of biaxial apolar solutes in nematic solvents: Monte Carlo predictions and experimental data. *J. Chem. Phys.* 115: 9552-9556.
- Chan-Huot, M., Lesot, P., Pelupessy, P., Duma, L., Duchambon, P., Bodenhausen, G., Toney, M.D., Reddy, V., and Suryaprakash, N. (2013).** 'On-the-fly' kinetics of enzymatic racemization using deuterium NMR in DNA-based, oriented chiral solvents. *Anal. Chem.* 85: 4694-4697.
- Chou, J.J., Gaemers, S., Howder, B., Louis, J.M., and Bax, A.** A simple apparatus for generating stretched polyacrylamide gels, yielding uniform alignment of proteins and detergent micelles. (2001). *J. Biomol. NMR.* 21: 377-382.
- Claridge, T.D.W. (2016).** *High-Resolution NMR Techniques in Organic Chemistry*, 3rd Edition. Elsevier Science B.V. Amsterdam, Neth. ISBN: 978-0-08-099986-9, DOI: 10.1016/b978-0-08-099986-9.00002-6.
- Cornilescu, G., and Bax, A. (2000).** Measurement of proton, nitrogen, and carbonyl chemical shielding anisotropies in a protein dissolved in a dilute liquid-crystalline phase. *J. Am. Chem. Soc.* 122: 10143-10154.
- Courtieu, J., Bayle, J.-P., and Fung, B.M. (1994).** Variable-angle sample-spinning NMR in liquid-crystals, *Prog. Nucl. Magn. Reson. Spectrosc.* 26: 141-169.
- Dalitz, F., Cudaj., M. Maiwald, M., and Guthau, G. (2012).** Process and reaction monitoring by low-field NMR spectroscopy. *Prog. Nucl. Magn. Reson.* 60: 52-70.

- Deloche, B., Samulski, E.T. (1981). Short-range nematic-like orientational order in strained elastomers: A deuterium magnetic resonance study. *Macromolecules* 14: 575-581.
- Di Bari, L., Forte, C., Veracini, C.A., and Zannoni C. (1988). An internal order approach to the investigation of intramolecular rotations in liquid crystals by NMR: 3-phenyl-thiophene in PCH and phase IV. *Chem. Phys. Lett.* 143: 263-269.
- Didier, D., Meddour, A., Bezzenine-Lafollée, S., and Collin, J. (2010). Samarium iodobinaphtholate: An efficient catalyst for enantioselective aza-michael additions of O-benzylhydroxylamine to N-alkenoyloxazolidinones. *Eur. J. Org. Chem.* 14: 2678-2684.
- Diehl, P., Henrichs, P. M., and Niederberger, W. (1971). A study of the molecular structure and of the barrier to methyl rotation in o-chlorotoluene partially oriented in the nematic phase. *Mol. Phys.* 1: 139-145.
- Diehl, P., and Leipert, T. (1964). Deuteronen-kernresonanzspektroskopie, *Helv. Chim. Acta.* 47: 545-557.
- Di Pietro, M.E., Sternberg, U., and Luy, B. (2019). Molecular dynamics with orientational tensorial constraints: A New approach to probe the torsional angle distributions of small rotationally flexible molecules. *J. Phys. Chem. B*, 123: 8480-8491.
- Di Pietro, M.E., Celebre, G., Aroulanda C., Merlet D., and De Luca, G. (2017). assessing the stable conformations of ibuprofen in solution by means of residual dipolar couplings. *Eur. J. of Pharma. Sci.* 106: 113-121.
- Di Pietro, M.E., Aroulanda C., Celebre, G., Merlet D., and De Luca, G. (2015). The conformational behaviour of naproxen and flurbiprofen in solution by NMR spectroscopy. *New J. Chem.* 39: 9086-9097.
- Dirat, O., Kouklovsky, C.Y., Langlois, P. Lesot, P., and Courtieu, J. (2010). Double diastereoselection in asymmetric [2+3] cycloadditions reactions of chiral oxazoline n-oxides and application to the kinetic resolution of a racemic α,β -unsaturated δ -lactone, *Tetrahedron: Asymmetry.* 10: 3197-3207.
- Dong, R.Y., Ed. (2012). NMR spectroscopy in liquid crystalline and ordered phases. In book: *Encyclopedia of Analytical Chemistry*. Meyers R.A. (Ed.), John Wiley & sons. DOI: 10.1002/9780470027318.a9297.
- Dong, R.Y. Ed. (2010). *NMR Spectroscopy of Liquid Crystals*. New Jersey, World scientific.
- Dong, R.Y. (2004). *Advances in NMR studies of liquid crystals*. *Ann. Rep. on NMR Spectr.* 53: 67-155.
- Dong, R.Y. (1996). In book: *Encyclopedia of NMR*, Eds. Harris R.K., and Grant D.M. J. Wiley & Sons, Chichester, pp. 2752-2759.
- Duan, J.-R., Billault, I. Mabon, F., and Robins, R.J. (2002). Natural deuterium distribution in fatty acids isolated from peanut seed oil: A site-specific study by quantitative ^2H NMR spectroscopy, *ChemBioChem.* 3: 752-759.
- Dupont, Dupont elastomercompagny, <http://www.dupontelastomers.com/products/kalrez/indsemi.asp>.
- Eliel, E.L., and Wilen, S.H. (1994). *Stereochemistry of organic compounds*, John Wiley & Sons, New York.
- Emsley, J.W., and Feeney, J. (1995). Milestones in the first fifty years of NMR, *Prog. Nucl. Magn. Reson. Spectrosc.* 2: 1-9.
- Emsley, J.W., Luckhurst, G.R., and Stockley, C.P. (1982). A theory of orientational ordering in uniaxial liquid crystals composed of molecules with alkyl chains. *Proc. R. Soc. London, Ser. A.* 381: 117-138.
- Emsley, J.W., and Lindon, J.C. (Eds.). (1975). Chap. 2, in book: *NMR Spectroscopy Using Liquid Crystal Solvents*, Pergamon Press, Oxford.
- Enthart, A., Freundenberger, J.C., Furrer, J., and Luy, B. (2008). The CLIP/CLAP-HSQC: Pure absorptive spectra for the measurement of one-bond couplings. *J. Magn. Reson.* 192: 314-22.

- Eyring, H. (1935). Activated complex in chemical reactions. *Chem. Rev.* 17: 65-77.
- Facke, T., and Berger, S. (1995). SERF, A new method for H,H spin-coupling measurement in organic-chemistry, *J. Magn. Reson. A*, 113: 114-116.
- Farjon J., and Giraud, N. (2018). Analyses of enantiomeric mixtures using chiral liquid crystals. *Current Opinion in Colloid & Interface Science.* 33: 1-8.
- Farjon, J., and Merlet, D. (2010). SERF-filtered experiments: New enantio-selective tools for deciphering complex spectra of racemic mixtures dissolved in chiral oriented media. *J. Magn. Reson.* 210: 24-30.
- Farley, K.A., Che, Y., Navarro-Vazquez, A., Limberakis, C., Anderson, D., Yan, J., Shapiro, M., Shanmugasundaram, V., and Gil, R.R. (2019). Cyclic peptide design guided by residual dipolar couplings, *j*-couplings, and intramolecular hydrogen bond analysis. *J. Org. Chem.*, 84: 4803-4813.
- Farley, K., Koos, M.R.M, Che, Y., Horst, R., Limberakis, C., Bellenger, J., Lira, R., Gil-Silva, L., and Gil, R.R. (2021). Cross-linked poly-4-acrylomorpholine: a flexible and reversibly compressible aligning gel for anisotropic NMR analysis of peptides and small molecules in water. *Angew. Chem., Int. Ed.* 60: 26314-26319.
- FDA, FDA directives, <https://www.fda.gov/>.
- Flory, P.J. (1974). Foundations of rotational isomeric state theory and general methods for generating configurational averages. *Macromolecules.* 7: 381-392.
- Frank, A.O., Freudenberger, J.C., Shaytan A.K., Kessler H., and Luy, B. (2010). Direct prediction of residual dipolar couplings of small molecules in a stretched gel by stochastic molecular dynamics simulations. *Magn. Reson. Chem.* 53: 213-217.
- Freudenberger, J. C., Knoer, S., Kobzar, K., Heckmann, D., Paululat, T., Kessler, H., and Luy, B. (2005). Stretched poly(vinyl acetate) gels as NMR alignment media for the measurement of residual dipolar couplings in polar organic solvents. *Angew. Chem., Int. Ed.* 44: 423-426.
- Freudenberger, J.C., Spitteller, P., Bauer, R., Kessler, H., and Luy, B. (2004). Stretched poly(dimethylsiloxane) gels as NMR alignment media for apolar and weakly polar organic solvents: an ideal tool for measuring RDCs at low molecular concentrations. *J. Am. Chem. Soc.* 126: 14690-14691.
- Frydman L., Lupulescu, A., and Scherf, T. (2003). Principles and features of single scan two-dimensional NMR spectroscopy, *J. Am. Chem. Soc.* 125: 9204-9217.
- Fujita, S. (2010). Systematic characterization of prochirality, prostereogenicity, and stereogenicity by means of the sphericity concept. *Tetrahedron.* 56: 735-740.
- Gao, L., Perato, S., Garcia-Argote, S., Taglang, C., Miguel Martinez-Prieto, L., Chollet, C., Buisson, D. Dauvois, D., Lesot, P. Chaudret, B. Rousseau, B., Feuillastre, S., and Pieters. G. (2018). Ruthenium-catalyzed hydrogen isotope exchange of (C_{sp^3})-H bonds directed by a sulfur atom. *Chem. Commun*, 54: 2986-2989.
- Garcia, M.E., Woodruff, S.R., Helleman, E., Tsarevsky, N.V., and Gil, R.R. (2017). Di(ethylene glycol) methyl ether methacrylate (DEGMEMA)-derived gels align small organic molecules in methanol. *Magn. Reson. Chem.* 55: 206-209.
- García, M.E., Pagola, S., Navarro-Vazquez, A., Phillips, D.D., Gayathri, C., Krakauer, H., Stephens, P.W., Nicotra V.E., and Gil, R.R. (2009). Stereochemistry determination by powder X-ray diffraction analysis and NMR spectroscopy residual dipolar couplings. *Angew. Chem., Int. Ed.*, 48: 5670-5674.

Gayathri, C., Tsarevsky N.V., and Gil, R.R. (2010). Residual dipolar couplings (RDCs) analysis of small molecules made easy: fast and tuneable alignment by reversible compression/relaxation of reusable PMMA gels. *Chem. Eur. J.* 16: 3622-3626.

Geissman, T.A., and Griffin, T.S. (1972). Sesquiterpene lactones of *Artemisia Carruthii*. *Phytochemistry*. 11: 833-835.

Gil, R.R., and Navarro-Vazquez, A. (2017-a). Application of residual dipolar couplings to the structural analysis of natural products. In book : *From Modern NMR Approaches to the Structure Elucidation of Natural Products*, 2, 117-176. Royal Society of Chemistry Cambridge (UK). Eds. Williams, A.J., Martin, G.E., and Rovnyak, D. ISBN: 978-1-84973-383-0.

Gil, R.R. (2017-b). Residual dipolar couplings in small-molecules NMR, in *Encyclopedia of spectroscopy and spectrometry*. Lindon, J.C. Tranter, G.E., and Koppenaal D. (Eds.), 3rd Ed., Vol. 3, 946-955.

Gil, R.R. Griesinger, C., Navarro-Vazquez, A., and Sun, H. (2014). Structural elucidation of small organic molecules assisted by NMR in aligned media. Edited by Cid, Maria-Magdalena; Bravo, Jorge. *From Structure Elucidation in Organic Chemistry*, 279-323. Wiley-VCH Verlag GmbH & Co. KGaA. Weinheim, Germany. ISBN: 978-3-527-66461-0, DOI: 10.1002/9783527664610.ch8.

Gil, R.R., Gayathri, C., Tsarevsky, N.V., and Matyjaszewski, K. (2008). Stretched poly(methyl methacrylate) gel aligns small organic molecules in chloroform. Stereochemical analysis and diastereotopic proton NMR assignment in lidartin using residual dipolar couplings and ³J coupling constant. *J. Org. Chem.* 73: 840-848.

Gil-Silva, L.F., Santamaria-Fernandez, R., Navarro-Vazquez, A., and Gil, R.R. (2016). Collection of NMR scalar and residual dipolar couplings using a single experiment. *Chem. Eur. J.* 22: 472-476.

Giraud, N., Beguin, L., Courtieu, J., and Merlet, D. (2010). Nuclear magnetic resonance using a spatial frequency encoding: application to J-edited spectroscopy along the sample. *Angew. Chem., Int. Ed.* 49: 3481-3484.

Giraudeau, P., and Frydman, L. (2014). Ultrafast 2D NMR: an emerging tool in analytical spectroscopy. *Ann. Rev. Anal. Chem.* 7: 129-161.

Giraudeau, P., Montag, T., Charrier, B., and Thiele, C.M. (2012). Fast access to residual dipolar couplings by single-scan 2D NMR in oriented media. *Magn. Reson. Chem.* 50: S53-S57.

Gouilleux, B., Meddour, A., and Lesot, P. (2020). ²H QUOSY 2D-NMR Experiments in weakly aligning systems: From the conventional to the ultrafast approach. *ChemPhysChem*. 21: 1548-1563.

Gouilleux, N., Charrier, B., Akoka, S., Felpin, F.-X., Rodriguez-Zu-Biri, M., and Giraudeau P. (2016). Ultrafast 2D NMR on a benchtop spectrometer: Applications and perspectives. *TRAC-Trends in Anal. Chem.* 83: 65-75.

Griesinger, C., Bennatia, M., Viethn, H.M, Luchinat, C., Parigi, G., Höferd, P., Engelked, F., Glasere, S.J., Denysenkov, V., and Prisne, T.F. (2012). Dynamic nuclear polarization at high magnetic fields in liquids. *Prog. Nucl. Magn. Reson. Spectrosc.* 64: 4-28.

Guo, Z. (2016). Artemisinin anti-malarial drugs in China Zongru Guo. *Acta Pharm. Sin. B*, 6: 115-124.

Haasnoot, C.A.G., De Leeuw, F.A.A.M., De Leeuw, H.P.M., and Altona, C. (1980). The relation between proton-proton NMR coupling constants and substituent electronegativities. An empirical generalization of the Karplus equation. *Tetrahedron*, 36: 2783-92.

Haberz, P., Farjon, J., and Griesinger, C. (2005). A DMSO-compatible orienting medium: Towards the investigation of the stereochemistry of natural products. *Angew. Chem., Int. Ed.* 44: 427-429.

Hallwass, F., Teles, R.R., Hellemann, E., Griesinger, C., Gil, R.R., and Navarro-Vazquez, A. (2018). Measurement of residual chemical shift anisotropies in compressed polymethylmethacrylate gels. Automatic compensation of gel isotropic shift contribution. *Magn. Reson. Chem.* 56: 321-328.

Hallwass, F., Schmidt, M., Sun, H., Mazur, A., Kummerlöwe, G., Luy, B., Navarro-Vázquez A., Griesinger C, and Reinscheid UM. (2011). Residual chemical shift anisotropy (RCSA): A tool for the analysis of the configuration of small molecules. *Angew. Chem., Int. Ed.* 50: 9487-9490.

Hansmann, S., Schmidts, V., and Thiele, C.M. (2017). Synthesis of poly- γ -S-2-methylbutyl-L-glutamate and poly- γ -S-2-methylbutyl-D-glutamate and their use as enantiodiscriminating alignment media in NMR spectroscopy. *Chem. Eur. J.* 23: 9114-9121.

Helfrich, J., Hentschke, J., and Apel, U.M. (1994). Molecular-dynamics simulation study of poly(γ -benzyl L-glutamate) in dimethylformamide. *Macromolecules.* 2: 472-482.

Hellemann, E., and Gil, R.R. (2018). New stretching method for aligning gels: its application to the measurement residual chemical shift anisotropies (RCSAs) without the need for isotropic shift correction. *Chem. Eur. J.* 24: 3689-3693.

Hirschmann, M., Schwab, M., and Thiele C.M. (2019). Molecular weights: The key of lyotropic liquid crystalline of poly- β -benzyl-L-aspartate. *Macromolecules.* 52: 6025-6034.

Ibanez de Opakua, A., Klama, F., Ndukwe, I.E., Martin, G.E., Williamson, R.T., and Zweckstetter, M. (2020). Determination of complex small-molecule structures using molecular alignment simulation. *Angew. Chem., Int. Ed.* 59: 617-6176.

Immel, S., Köck, M., and Reggelin, M. (2018). Configurational analysis by residual dipolar coupling driven floating chirality distance geometry Calculations. *Chem. Eur. J.* 24: 13918-13930.

IUPAC. (1976). Presentation of NMR data for publication in chemical journals - B. Conventions relating to spectra from nuclei other than protons. *Pure Appl. Chem.* 45: 217-220.

IUPAC. (1972). Recommendations for the presentation of NMR data for publication in chemical journals. *Pure Appl. Chem.* 29: 627-628.

Jackman, H., Marsden, S.P., Shapland, P., and Barrett, S. (2007). Isotopic labeling for determination of enantiomeric purity by ^2H NMR spectroscopy. *Org Lett.* 9: 5179-5182.

Jézéquel, T., Joubert, V., Giraudeau, P., Remaud, G.S., and Akoka, S. (2017). The new face of isotopic NMR at natural abundance. *Magn. Reson. Chem.* 55: 77-90.

Jezirowski, S., and Thiele, C.M. (2018). Poly- γ -p-biphenylmethyl-glutamate as enantiodifferentiating alignment medium for NMR spectroscopy with temperature-tunable properties. *Chem. Eur. J.* 24: 15631-15637.

Kaden, P., Freudenberger, J.C., and Luy, B. (2012). Noncovalently and covalently cross-linked polyurethane gels as alignment media and the suppression of residual polymer signals using diffusion-filtered spectroscopy. *Mag. Reson. Chem.* 50(S1): S22-S28.

Karschin, N., Wolkenstein, K., and Griesinger, C. (2020). Magnetically induced alignment of natural products for stereochemical structure determination via NMR. *Angew. Chem., Int. Ed.* 59: 15862-15864.

Khetrapal, C.L., Ramanathan, K.V., Suryaprakash, N., and Vivekanandan, S. (1998). Natural abundance ^2H NMR spectra of molecules oriented in liquid crystals. *J. Magn. Reson.* 135: 265-266.

Kobzar, K., Kessler, H., and Luy, B. (2005). Stretched gelatin gels as chiral alignment media for the discrimination of enantiomers by NMR spectroscopy. *Angew. Chem., Int. Ed.* 44: 3145-3147.

Köck, M., Reggelin, M., and Immel, S. (2020). The advanced floating chirality distance geometry approach - how anisotropic NMR parameters can support the determination of the relative configuration of natural products. *Marine Drugs.* 18: 330-352.

Kovacs, H., Moskau, D., and Spraul, M. (2005). Cryogenically cooled probes - a leap in NMR technology. *Prog. Nucl. Magn. Reson. Spectrosc.* 4: 131-155.

Kramer, F., Deshmukh, M. V., Kessler, H., and Glaser, S.J. (2004). Residual dipolar coupling constants: An elementary derivation of key equations. *Concepts Magn. Reson.* 21A: 10-21.

Kuchel, P.W., Chapman, B.E., Boghda, Mueller, N., Bubb, W.A., Philp, D.J., and Torres, A.M. (2006). Apparatus for rapid adjustment of the degree of alignment of NMR samples in aqueous media: Verification with residual quadrupolar splittings in ^{23}Na and ^{133}Cs spectra. *J. Mag. Res.* 180: 256-265.

Kummerlöwe, G., Auernheimer, J., Lendlein, A., and Luy, B. (2007). Stretched poly(acrylonitrile) as a scalable alignment medium for DMSO. *J. Am. Chem. Soc.* 129: 6080-6081.

Kummerlöwe, G., and Luy, B. (2009-a). Residual dipolar couplings for the configurational and conformational analysis of organic molecules. *Ann. Rep. NMR Spectrosc.* 68: 193-232.

Kummerlöwe, G., Udaya Kiran, M., and Luy, B. (2009-a). Covalently cross-linked gelatin allows chiral distinction at elevated temperatures and in DMSO. *Chem. Eur. J.* 15: 12192-12195.

Kummerlöwe, G., Grage, S.L.; Thiele, C.M., Kuprov, I., Ulrich, A.S., and Luy, B. (2011-a). Variable angle NMR spectroscopy and its application to the measurement of residual chemical shift anisotropy. *J. Magn. Reson.* 209: 19-30.

Kummerlöwe, G., Crone, B., Kretschmer, M., Kirsch, Stefan F., and Luy, B. (2011-b). Residual Dipolar Couplings as a Powerful Tool for Constitutional Analysis: The Unexpected Formation of Tricyclic Compounds. *Angew. Chem., Int. Ed.* 50: 2643-2645, S2643/1-S2643/25.

Kummerlöwe, G., McCord, E.F., Cheatham, S.F., Niss, S., Schnell, R.W., and Luy, B. (2010). Tunable alignment for all polymer gel/solvent combinations for the measurement of anisotropic NMR parameters. *Chem. Eur. J.* 16: 7087-7089.

Lafon, O., Lesot, P., Fan C.A., and Kagan, H.B. (2007). Analysis of intramolecular dynamic processes in enantiomeric diaryl atropisomers and related derivatives through ^2H NMR in polypeptide liquid crystals. *Chem. Eur. J.* 13: 3772-3786.

Lafon, O., Lesot, P., Rivard, M., Chavarot, M., Rose-Munch, F., and Rose, E. (2005) Enantiomeric analysis of planar chiral (η^6 -arene) chromium tricarbonyl complexes using NMR in oriented solvents organometallics. 24: 4021-4028.

Lafon, O., Berdagué, P., and Lesot, P. (2004). Use of two-dimensional correlation between ^2H quadrupolar splittings and ^{13}C CSA's for assignment of NMR spectra in chiral nematics, *Phys. Chem. Chem. Phys.* 6: 1080-1084.

Lei, X., Qiu, F., Sun, H., Bai, L., Wang, W.X., Xiang, W., and Xiao, H. (2017). A self-assembled oligopeptide as a versatile NMR alignment medium for the measurement of residual dipolar couplings in methanol. *Angew. Chem., Int. Ed.* 56: 12857-12861.

Leigh, W.J., Workentin, M.S. Demus, D., and Vill, V. (2008). Liquid crystals as solvents for spectroscopic, chemical reaction, and gas chromatographic applications. In book: *Handbook of Liquid Crystals Set.* Demus, D., Goodby, J., Gray, G.W., Spiess, H.-W., and Vill, V. (Eds.). DOI: 10.1002/9783527619276.ch9da.

Leigh, W.J. (1991). Thermotropic liquid crystals as chemical reaction media. In book: *Liquid Crystals - Applications and Uses*, pp. 357-408. DOI: 10.1142/9789814360449_0007.

Leopold, M.F., Epstein, W.W., and Grant, D.M. (1998). Natural abundance deuterium NMR as a novel probe of monoterpene biosynthesis: Limonene. *J. Am. Chem. Soc.* 111: 616-617.

- Lesot, P., Berdagué P., Silvestre V., and Remaud, G. (2021). Exploring the enantiomeric ^{13}C isotope fractionation: Challenges and anisotropic NMR-based analytical strategy. *Anal. Bioanal. Chem.* 413: 6379-6392.
- Lesot, P., Aroulanda, C., Berdagué, P., Meddour, A., Merlet, D., Farjon, J, Giraud, N., and Lafon, O. (2020-a). Three fertile decades of methodological developments and analytical challenges. *Prog. Nucl. Magn. Reson. Spectrosc.* 116: 85-154.
- Lesot, P., Gil, R.R., Berdagué, P., and Navarro-Vazquez, A. (2020-b). Residual quadrupolar couplings: crossing the current frontiers in the relative configuration analysis of natural products. *J. Nat. Prod.* 83: 3141-3148.
- Lesot, P. (2020-c). Determination of the natural deuterium distribution of fatty acids by application of ^2H 2D-NMR in liquid crystals: fundamentals, advances, around and beyond. *Liquid Crystals*, 47: 1886-1910.
- Lesot, P., Berdagué, P., Meddour, A., Kreiter, A., Noll, M., and Reggelin, M. (2019-a). ^2H and ^{13}C NMR-based enantiodetection using polyacetylene versus polypeptide aligning media: versatile and complementary tools for chemists. *ChemPlusChem.* 84: 144-155.
- Lesot, P. (2019-b). Nuclear Magnetic Resonance Spectroscopy | Hydrogen Isotopes: ^2H NMR, *Encyclopedia of Analytical Science*, 3rd Ed., pp 152-167. DOI: 10.1016/B978-0-12-409547-2.14084-3.
- Lesot, P., and Lafon, O. (2017). Natural abundance ^2H NMR spectroscopy, in book: *Encyclopedia of Spectroscopy and Spectrometry*. Lindon, J., Tranter G.E., and Kopenaal D.W. (Eds.). Elsevier / Academic Press. 3rd Ed., Vol. 3, 1-14.
- Lesot, P., Berdagué, P., and Giraudeau, P. (2016). Detection of quadrupolar nuclei by ultrafast 2D-NMR: exploring the case of deuterated analytes aligned in chiral oriented solvents. *Chem. Commun.* 52: 2122-2125.
- Lesot, P., Aroulanda, C., Zimmermann, H., and Luz Z. (2015-a). Enantiotopic discrimination in the NMR spectrum of prochiral solutes in chiral liquid crystals. *Chem. Soc. Rev.* 44: 230-275.
- Lesot, P., Kazimierczuk, K., Trebosc, J., Amoureux, J-P., and Lafon, O. (2015-b). Fast acquisition of multidimensional NMR spectra of solids and mesophases using alternative sampling methods. *Magn Reson Chem.* 53: 927-939.
- Lesot, P., Lafon O., and Berdagué, P. (2014). Correlation 2D-NMR experiments involving both ^{13}C and ^2H Isotopes in oriented media: methodological developments and analytical applications. *Magn. Reson. Chem.* 52: 595-613.
- Lesot, P., Serhan, Z., Aroulanda, C., and Billault, I. (2012-a). Analytical contribution of NAD 2D-NMR spectroscopy in polypeptide mesophases to the investigation of triglycerides. *Magn. Reson. Chem.* 5: S2-S11.
- Lesot, P., and Lafon, O. (2012-b). Experimental detection of achiral and chiral naturally abundant ^{13}C - ^2H isotopomers by 2D-NMR in liquids and chiral oriented solvents. *Anal. Chem.* 84: 4569-73.
- Lesot, P., Venkateswara Reddy, U., and Suryaprakash, N.S. (2011-a). Exploring the enantiodiscrimination potentialities of DNA-based orienting media using deuterium NMR spectroscopy. *Chem. Commun.* 47: 11736-11738.
- Lesot, P., Serhan, Z., and Billault, I. (2011-b). recent advances in the analysis of the site-specific isotopic fractionation of metabolites such as fatty acids using anisotropic natural abundance ^2H NMR spectroscopy: application on conjugated linolenic methyl esters. *Anal. Bioanal. Chem.* 399: 1187-1200.
- Lesot, P., and Lafon, O., and (2008-a). Enantiomeric analysis using natural abundance deuterium 3D NMR spectroscopy in polypeptide chiral oriented media. *Chem. Phys. Lett.* 458: 219-222.

Lesot, P., Lafon, O., Aroulanda, C., and Dong, R. (2008-b). ^2H NMR studies of two-homopolypeptide lyotropic mesophases: Toward the quantification of solute-fiber interactions. *Chem. Eur. J.* 14: 4082-4092.

Lesot, P., Baillif, V., and Billault, I. (2008-c). Combined analysis of four C-18 unsaturated fatty acids using natural abundance deuterium 2D-NMR spectroscopy in chiral oriented solvents. *Anal. Chem.* 80: 2963-2972.

Lesot, P., and Courtieu J. (2007). Natural abundance deuterium NMR spectroscopy: developments and analytical applications in liquids, liquid crystals and solid phases. *Prog. Nucl. Magn. Reson. Spectrosc.* 55: 128-159.

Lesot, P., Lafon, O., Kagan, H.B., and Fan, P. (2006). Study of molecular rotational isomerism using deuterium NMR in chiral oriented solvents. *Chem. Commun.* 389-391.

Lesot, P., Lafon, O., Courtieu, J., and Berdagué, P. (2004-a). Analysis of the ^{13}C NMR spectra of molecules, chiral by isotopic substitution, dissolved in a chiral oriented environment: Toward the absolute assignment of the pro-R/pro-S character of enantiotopic ligands in prochiral molecules. *Chem. Eur. J.* 10: 3741-3746.

Lesot, P., Aroulanda, C., and Billault, I. (2004-b). Exploring the analytical potential of NMR spectroscopy in chiral anisotropic media for the study of the natural abundance deuterium distribution in organic molecules. *Anal. Chem.* 76: 2827-2835.

Lesot, P., Sarfati, M., and Courtieu, J. (2003). Natural abundance deuterium NMR spectroscopy in polypeptide liquid crystals as a new and incisive means for enantiodifferentiation of chiral hydrocarbons. *Chem. Eur. J.* 9: 1724-1745.

Lesot, P., Merlet, D., Sarfati, M., Courtieu, J., Zimmermann, H., and Luz, Z. (2002). Enantiomeric and enantiotopic analysis of cone-shaped compounds with C_3 and C_{3v} symmetry using NMR spectroscopy in chiral anisotropic solvents, *J. Am. Chem. Soc.* 124: 10071-10082.

Lesot, P., Merlet, D., Loewenstein, A., and Courtieu, J. (1998). Enantiomeric visualisation using proton-decoupled natural abundance deuterium NMR in poly(γ -benzyl-L-glutamate) liquid crystalline solutions. *Tetrahedron: Asymmetry*, 9: 1871-1881.

Lesot, P., Merlet, D., Courtieu, J., Emsley, J.W., Rantala, T.T., and Jokisaari, J. (1997). Calculation of the molecular ordering tensors of (\pm)-3-butyn-2-ol in an organic solution of poly(γ -benzyl-L-glutamate). *J. Phys. Chem. A.* 101: 5719-5724.

Lesot, P., Merlet, D., Meddour, A., Courtieu, J., and Loewenstein, A. (1995-a). Visualization of enantiomers in a polypeptide liquid-crystal solvent through carbon-13 NMR spectroscopy. *J. Chem. Soc, Faraday Trans.* 91: 1371-1375.

Lesot, P., Gounelle, Y., Merlet, D., Loewenstein, A., and Courtieu, J. (1995-a). Measurement and analysis of the molecular ordering tensors of two enantiomers oriented in a polypeptide liquid crystalline system, *J. Phys. Chem. A.* 99: 14871-14875.

Li, X.-L., Chi, L.-P., Navarro-Vazquez, A., Hwang, S., Schmieder, P., Li, X.-M., Li, X., Yang, S.-Q., Lei, X., Wang, B.-G., and Sun, H. (2020). Stereochemical Elucidation of Natural Products from Residual Chemical Shift Anisotropies in a Liquid Crystalline Phase. *J. Am. Chem. Soc.* 142: 2301-2309.

Lisicki, M.A., Mishra, P.K., Bothner-By, A.A., and Lindsey, J.S. (1988). Solution conformation of a porphyrin-quinone cage molecule determined by dipolar magnetic field effects in ultra-high-field NMR. *J. Phys. Chem.* 92: 3400-3403.

Liu, H., Chen, P., Li, X.L., Sun, H., and Lei, X. (2020). Practical aspects of oligopeptide AAKLVFF as an alignment medium for the measurements of residual dipolar coupling of organic molecules. *Magn. Reson. Chem.* 58: 404-410.

Liu, Y., Navarro-Vázquez, A., Gil, R.R., Griesinger, C., Martin, G.E., and Williamson, R.T. (2018-a). Application of anisotropic NMR parameters to the confirmation of molecular structure. *Nature Protocol*. 14: 217-247.

Liu, Y., Cohen, R.D., Gustafson, K.R., Martin, G.E., and Williamson, R.T. (2018-b). Enhanced measurement of residual chemical shift anisotropy for small molecule structure elucidation. *Chem. Commun*. 54, 4254-4257.

Liu, Y., and Prestegard, J.H. (2010). A device for the measurement of residual chemical shift anisotropy and residual dipolar coupling in soluble and membrane-associated proteins. *J. Biomol. NMR*, 47: 249-258.

Losonczi, J.A., Andrec, M., Fischer, M.W.F., and Prestegard, J.H. (1999). Order matrix analysis of residual dipolar couplings using singular value decomposition. *J. Mag. Res.* 138: 334-342.

Luy, B., Kobzar, K., Knoer, S., Furrer, J., Heckmann, D., and Kessler, H. (2005). Orientational properties of stretched polystyrene gels in organic solvents and the suppression of their residual ^1H NMR signals. *J. Am. Chem. Soc.* 127: 6459-6465.

Luy, B. (2010). Distinction of enantiomers by NMR spectroscopy using chiral orienting media. *J. of the Indian Institute of Science*. 90: 119-132.

Luy, B., Kobzar, K., and Kessler, H. (2004). An easy and scalable method for the partial alignment of organic molecules for measuring residual dipolar couplings. *Angew. Chem., Int. Ed.* 43: 1092-1094.

Luz, Z. (2003). *Dynamic NMR in liquid crystals and liquid crystalline solutions*, Eds. Burnell, E.E., de Lange, C.A., Kluwer Academic Publisher, Dordrecht, Chap. 19.

Luz, Z. (1983). Dynamic of molecular processes by NMR in liquid crystalline solvents. *Israel J. Chem.* 23: 305-313.

Maiwald, M., Holger H. Fischer, H.H., Kim Y.-K., Albert, K., and Hasse, H. (2004). Quantitative high-resolution on-line NMR spectroscopy in reaction and process monitoring. *J. Mag. Res.* 166135-146.

Mangoni, A., Esposito, V., and Randazzo, A. (2003). Configuration assignment in small organic molecules via residual dipolar couplings. *Chem. Commun.* 154-155.

Marathias, V.M., Tate, P.A., Papaioannou, N., and Masefski, W. (2010). An improved method for determining enantiomeric excess by ^{13}C -NMR in chiral liquid crystal media, *Chirality* 22: 838-843.

Marshall, J.L. (1983). Carbon-carbon and carbon-proton NMR couplings: Applications to organic stereochemistry and conformational analysis. In book: *Methods in Stereochemical Analysis*, Vol. 2. Verlag Chemie. Weinheim, Germany.

Martin M.L., and Martin, G.J. (1990). In book: *NMR Basic Principles and Progress*, Ed. P. Diehl, Springer-Verlag Vol. 23, pp. 1-61.

Martin, G.J., Martin, M.L., Mabon F., and Bricout, J. (1982). A new method for the identification of the origin of natural products. Quantitative ^2H NMR at the natural abundance level applied to the characterization of anetholes, *J. Am. Chem. Soc.* 104: 2658-9.

Martin, G.J., and Martin, M.L. (1981). Deuterium labelling at the natural abundance level as studied by high-field quantitative H-2 NMR. *Tetrahedron Lett.* 22: 3525-8.

Meddour, A., Atkinson, D., Loewenstein, A., and Courtieu, J. (1998). Enantiomeric analysis of homologous series of secondary alcohols by deuterium NMR spectroscopy in a chiral nematic liquid crystal: influence of molecular geometry on chiral discrimination. *Chem. Eur. J.* 4: 1142-1147.

Meddour, A., Berdagué, P., Hedli, A., Courtieu, J., and Lesot, P. (1997). Proton-decoupled carbon-13 NMR spectroscopy in a lyotropic chiral nematic solvent as an analytical tool for the measurement of the enantiomeric excess, *J. Am. Chem. Soc.* 119: 4502-4508.

- Meddour, A., Canet, I., Loewenstein, A., Péchiné, J.-M., and Courtieu, J. (1994).** Observation of enantiomers, chiral by virtue of isotopic substitution, through deuterium NMR in a polypeptide liquid crystal. *J. Am. Chem. Soc.* 116: 9652-9656.
- Merle, C., Kummerlöwe, G., Freudenberger, J. C., Halbach, F., Stoewer, W., von Gostomski, C.L., Hoepfner, J., Beskers, T., Wilhelm, M., and Luy, B. (2013).** Crosslinked poly(ethylene oxide) as a versatile alignment medium for the measurement of residual anisotropic NMR parameters. *Angew. Chem., Int. Ed.* 52: 10309-10312.
- Merlet, D. Beguin, L. Courtieu, J., and Giraud, N. (2011).** Spin-spin coupling edition in chiral liquid crystal NMR solvent, *J. Magn. Reson.* 209: 315-322.
- Merlet, D., Emsley, J.W. Lesot, P., and Courtieu, J. (1999-a).** The relationship between molecular symmetry and second-rank orientational order parameters for molecules in chiral liquid crystalline solvents. *J. Chem. Phys.* 111: 6890-6896.
- Merlet, D., Ancian, B., Courtieu, J., and Lesot, P. (1999-b).** Two-dimensional deuterium NMR spectroscopy of chiral molecules oriented in a polypeptide liquid crystal: Application for the enantiomeric analysis through natural abundance deuterium NMR. *J. Am. Chem. Soc.* 121: 5249-5258.
- Merlet, D., Ancian, B., Smadja, W., Courtieu, J., and Lesot, P. (1998).** Analysis of the natural abundance deuterium NMR spectra of enantiomers in chiral liquid crystals through 2D auto-correlation experiments. *Chem. Commun.*, 2301-2302.
- Mevers, E., Sauri, J., Liu, Y., Moser, A., Ramadhar, T.R., Varlan, M., Williamson, R.T., Martin, G.E., and Clardy, J. (2016).** Homodimericin A: A complex hexacyclic fungal metabolite. *J. Am. Chem. Soc.* 138: 12324-12327.
- Milanowski, D.J., Oku, N., Cartner, L.K., Bokesch, H.R., Williamson, R.T., Sauri, J., Liu, Y., Blinov, K.A., Ding, Y., Li, X.-C., Ferreira, D., Walker, L.A., Khan, S., Davies-Coleman, M.T., Kelley, J.A., McMahon, J.B., Martin, G.E., and Gustafson, K.R. (2018).** Unequivocal determination of caulamidines A and B: Application and validation of new tools in the structure elucidation toolbox. *Chem. Sci.* 9: 307-314.
- Mislow, M., and Raban, M. (1967).** in book: *Topics in Stereochemistry, Vol. 1*, Eds. Allinger, N.L., and Eliel, E.L., John Wiley & sons, New York.
- Mobli, M., and Hoch JC. (2014).** Nonuniform sampling and non-Fourier signal processing methods in multi-dimensional NMR. *Prog. Nucl. Magn. Reson. Spectrosc.* 83: 21-41.
- Monroe, A.Z., Gordon, W.H., Wood, J.S., Martin, G.E., Morgan, J.B., and Williamson, R.T. (2021).** Structural revision of a Wnt/ β -catenin modulator and confirmation of cannabielsoin constitution and configuration. *Chem. Commun.* 57: 5658-5661.
- Nandi, N. (2004).** Role of secondary level chiral structure in the process of molecular recognition of ligand: Study of model helical peptide. *J. Phys. Chem. B.* 108: 789-797.
- Nath, N., Schmidt, M., Gil, R.R., Williamson, R.T., Martin, G.E., Navarro-Vazquez, A., Griesinger, C., and Liu, Y. (2016).** Determination of relative configuration from residual chemical shift anisotropy. *J. Am. Chem. Soc.* 138: 9548-9556.
- Nath, N., Fuentes-Monteverde, J.C., Pech-Puch, D., Rodriguez, J., Jimenez, C., Noll, M., Kreiter, A., Reggelin, M., Navarro-Vazquez, A., and Griesinger, C. (2020).** Relative configuration of micrograms of natural compounds using proton residual chemical shift anisotropy. *Nat. Commun.* 1: 4372-4381. DOI: 10.1038/s41467-020-18093-5.
- Naumann, C., and Kuchel, P.W. (2009).** NMR (pro)chiral discrimination using polysaccharide gels. *Chem. Eur. J.* 15: 12189-12191.
- Naumann, C., and Kuchel, P.W. (2008).** Prochiral and chiral resolution in ^2H NMR spectra: Solutes in stretched and compressed gelatin gels. *J. Phys. Chem. A.* 112: 8659-8664.

Naumann, C., Bubb, W.A., Chapman, B.E., and Kuchel, P.W. (2007). Tunable-alignment chiral system based on gelatin for NMR spectroscopy. *J. Am. Chem. Soc.* 129: 5340-5341.

Navarro-Vázquez, A, Gil, R.R., and Blinov, K. (2018). Computer-Assisted 3D structure elucidation (CASE-3D) of natural products combining isotropic and anisotropic NMR parameters. *J. Nat. Prod.* 81: 203-210.

Navarro-Vazquez, A., Berdagué, P., and Lesot, P. (2017). Integrated computational protocol for analyzing quadrupolar splittings from natural abundance deuterium NMR spectra in (chiral) oriented media. *ChemPhysChem.* 18: 1252-1266.

Navarro-Vázquez, A. (2012). MSpin-RDC. A program for the use of residual dipolar couplings for structure elucidation of small molecules. *Magn. Reson. Chem.* 50: S73-S79.

Ndukwe, I.E., Brunskill, A., Gauthier, D.R., Zhong, Y-L., Martin, G.E., Williamson, R.T., Reibarkh M., and Liu, Y. (2019). ¹³C NMR-based approaches for solving challenging stereochemical problems. *Org. Lett.* 21: 4072-4076.

Ndukwe, I.E., Wang, X., Lam, N.Y. S., Ermanis, K., Alexander, K.L.; Bertin, M.J., Martin, G.E., Muir, G., Paterson, I., Britton, R., Goodman, J.M., Helfrich, E.J.N., Piel, J., Gerwick, W.H., and Williamson, R.T. (2020-a). Synergism of anisotropic and computational NMR methods reveals the likely configuration of phormidolide A. *Chem. Commun.* 56: 7565-7568.

Neuhaus, D. (2012). Nuclear Overhauser Effect. *Encyclopedia of NMR.* 6: 3020-3035. Harris, R.K., and Wasylishen, R.E. (Eds.).

New Era Enterprise. <http://newera-spectro.com/gel-presses>.

Nicotra, V.E., Ramacciotti, N.S., Gil, R.R., Oberti, J.C., Feresin, G.E.; Guerrero, C.A., Baggio, R.F., Garland, M. T., and Burton, G. (2006). Phytotoxic Withanolides from *Jaborosa rotacea*. *J. Nat. Prod.* 69: 783-789.

Palermo, G., Riccio, R., and Bifulco, G. (2010). Effect of electronegative substituents and angular dependence on the heteronuclear spin-spin coupling constant ³J_{C-H}: An empirical prediction equation derived by density functional theory calculations. *J. Org. Chem.* 75: 1982-1991.

Palomino, M., Khudr, H., Courtieu, J., Merlet, D., and Meddour, A. (2012). The use of exchangeable nuclei to observe enantiomers through deuterium NMR in chiral liquid crystalline solvents. *Magn. Reson. Chem.* 50: S12–S16.

Parenty, A., Campagne, J.-M., Aroulanda, C., and Lesot, P. (2002). Routine use of natural abundance deuterium NMR in a polypeptidic chiral oriented solvent for determination of the enantiomeric composition of chiral building blocks. *Org. Lett.* 4: 1663-1666.

Phillips, A.R., and Sharman, G.J. (2004). The measurement of high enantiomeric excesses in chiral liquid crystals using ¹⁹F NMR and exchangeable protons in ²H NMR. *Chem. Commun.* 1330-1331.

Portaluri, V., Thomas F., Jamin, E., Akoka, S., and Remaud G. (2021). Authentication of agave products through isotopic intramolecular ¹³C content of ethanol: optimization and validation of ¹³C quantitative NMR methodology *ACS Food Sci. Technol.* 1: 1316-1322.

Prosser, R.S., Heaton, N.J., and Kothe, J. (1996). Application of the quadrupolar Carr-Purcell-Meiboom-Gill pulse train for sensitivity enhancement in deuterium NMR of liquid Crystals. *J. Magn. Reson. B.* 112: 51-56.

Queffelec, C., Boeda, F., Pouilhès, A., Meddour, A., Kouklovsky, C., Hannedouche, J., Collin, J., and Schulz, E. (2011). Enantioselective intramolecular hydroamination of secondary amines catalyzed by easily accessible ate and neutral rare-earth complexes, *ChemCatChem.* 3: 122-126.

Reach directive, https://ec.europa.eu/environment/chemicals/reach/reach_en.htm

Recchia, M.J.J., Cohen, R.D., Liu, Y., Sherer, E.C., Harper, J.K.; Martin, G.E., and Williamson, R.T. (2020). "One-shot" measurement of residual chemical shift anisotropy using poly- γ -benzyl-L-glutamate as an alignment medium. *Org. Lett.* 22: 8850-8854.

Reinitzer, P. (1888). Beiträge zur kenntnis des cholesterins, *Monasth. Chem.* 9: 421-441.

Reinsperger, T., and Luy, B. (2014). Homonuclear BIRD-decoupled spectra for measuring one-bond couplings with highest resolution: CLIP/CLAP-RESET and constant-time-CLIP/CLAP-RESET. *J. Magn. Reson.* 239: 110-120.

Reinsperger, T., and Luy, B. (2008). CLIP-ASAP-HSQC for fast and accurate extraction of one bond couplings from isotropic and partially aligned molecules. *J. Magn. Reson.* 239: 110-120.

Reller, M. Svenja Wesp, Koos M.M.M, Reggeline M., and Luy B. (2017). Biphasic liquid crystal and the simultaneous measurement of isotropic and anisotropic parameters by spatially resolved NMR spectroscopy. *Chem Eur J.* 23: 13351-13359.

Remaud, G.S., Martin, Y.-L., Martin, G.G., and Martin G.J. (1997). Detection of sophisticated adulterations of natural vanilla flavors and extracts: application of the SNIF-NMR method to vanillin and p-hydroxybenzaldehyde. *J. Agric. Food Chem.* 45: 859-866.

Remaud, G., Debon, A.A., Martin, Y.-L., Martin G.G., and Martin, G.J. (1997). Authentication of bitter almond oil and cinnamon oil: application of the SNIF-NMR method to benzaldehyde. *J. Agric. Food Chem.* 45: 4042-4048.

Riveira, M.J., Trigo-Mourino, P., Troche-Pesqueira, E., Martin, G.E., Navarro-Vazquez, A., Mischne, M.P., and Gil, R.R. (2015). Self-sensitized photooxygenation of ^2H -Pyrans: Characterization of unexpected products assisted by computed structural elucidation and residual dipolar couplings. *J. Org. Chem.* 80: 7396-7402.

Robyr, P., and Meier, B.H. (2000). Deuterium-carbon NMR correlation spectroscopy: A tool for structural characterization of solids. *Chem. Phys. Lett.* 327: 319-324.

Sylva, M.S. (2017). Recent advances in multinuclear NMR spectroscopy for chiral recognition of organic compounds, *Molecules.* 22: 247-268.

Sackmann, E., Meiboom, S., and Snyder, L.C. (1968). Nuclear magnetic resonance spectra of enantiomers in optically active liquid crystals, *J. Am. Chem. Soc.* 90: 2183-2184.

Sager, E., Tzvetkova, P., Gossert, A.D., Piechon, P., and Luy, B. (2020). Determination of configuration and conformation of a reserpine derivative with seven stereogenic centers using molecular dynamics with RDC-derived tensorial constraints. *Chem. Eur. J.* 26: 14435-14444.

Salvino, R.A. De Luca, G., and Celebre, G. (2021). Assessing the chirality-dependent conformational distribution of small flexible opposite enantiomers dissolved in weakly ordering enantiopure media by means of liquid crystal NMR techniques. *J. Mol. Liquids*, article online. DOI: 10.1016/j.molliq.2021.117994.

Samulski, E.T. (2003). Very flexible solutes: Alkyl chains and derivatives, Eds. Burnell, E.E., de Lange C.A., Kluwer Academic Publisher, Dordrecht, Chap. 13.

Sandström, D., and Zimmermann, H. (2000). Correlation of deuterium quadrupolar couplings and carbon-13 chemical shifts in ordered media by multiple-quantum NMR. *J. Phys. Chem. B.* 104: 1490-1493.

Sarfati, M., Aroulanda, C., Courtieu, J., and Lesot, P. (2001). Enantiomeric recognition of chiral invertomers through NMR in chiral oriented solvents: a study of the cis-decalin. *Tetrahedron: Asymmetry.* 12: 73-744.

Sass, H.-J., Musco, G., Stahl, S.J. Wingfield, P.T., and Grzesiek, S. (2000). Solution NMR of proteins within polyacrylamide gels: diffusional properties and residual alignment by mechanical stress or embedding of oriented purple membranes. *J. Biomol. NMR.* 18: 303-309.

Sau, S.P., and Ramanathan, K.V. (1997). Visualization of enantiomers in the liquid-crystalline phase of a fragmented DNA solution. *J. Phys. Chem. B.* 113: 1530-1535.

Saupe, A., and Englert, G. (1963). High-resolution nuclear magnetic resonance spectra of orientated molecules. *Phys. Rev. Lett.* 11: 462-464.

Schwab, M., Schmidts, V., and Thiele, C.M. (2018). Thermoresponsive alignment media in NMR spectroscopy: Helix reversal of a co-polyaspartate at ambient temperatures. *Chem. Eur. J.* 24: 14373-14377.

Schwab, M., Herold, D., and Thiele, C.M. (2017). Polyaspartates as thermoresponsive enantiodifferentiating helically chiral alignment media for anisotropic NMR spectroscopy. *Chem. Eur.* 23: 14576-14584.

Serhan, Z., Aroulanda, C., and Lesot, P. (2016). Investigation of solute-fiber affinity and orientational ordering of norbornadiene interacting with two-polypeptide chiral liquid-crystalline solvents by NAD NMR. *J. Phys. Chem. A,* 120: 6076-6088.

Serhan, Z., Billault, I., Borgogno, A., Ferrarini, A., and Lesot, P. (2012). Analysis of NAD 2D-NMR spectra of saturated fatty acids in polypeptide aligning media by experimental and modeling approaches. *Chem. Eur. J.* 18: 117-126.

Serhan, Z., Martel, L., Billault, I., and Lesot, P. (2010). Complete determination of site-specific bio-enantiomeric excesses in linoleic acid using natural abundance deuterium 2D NMR in polypeptide mesophase. *Chem Commun.* 46: 6599-601.

Shaka, A.J., Keeler, J., and Freeman, R. (1983). Evaluation of a new broadband decoupling sequence: WALTZ-16, *J. Magn. Reson.* 53: 313-340.

Smadja, W., Auffret, S., Berdagué, P., Merlet, D., Canlet, C., Courtieu, J., Legros, J.-Y., Boutros, A., and Fiaud, J.-C. (1997). Visualisation of axial chirality using ^2H - $\{^1\text{H}\}$ NMR in poly(γ -benzyl-L-glutamate), a chiral liquid crystal solvent. *Chem. Commun.* 2031-2032.

Solgadi, A., Meddour, A., and Courtieu, J. (2004). Enantiomeric discrimination of water-soluble compounds using deuterium NMR in a glucocon/buffered water/n-hexanol chiral lyotropic liquid crystal. *Tetrahedron: Asymmetry.* 15: 315-1318.

Sosa, V.E., Oberti, J.C., Gil, R.R., Ruveda, E.A., Goedken, V.L., Gutierrez, A.B., and Herz, W. (1989). 10-Epideoxycumambrin B and other constituents of *Stevia yaconensis* var. *subeglandulosa*. *Phytochemistry,* 28: 1925-1929.

Souza, A.A., Gil, R.R., and Parella, T. (2017). Highly resolved HSQC experiments for the fast and accurate measurement of homonuclear and heteronuclear coupling constants. *J. Mag. Res.,* 282, 54-61.

Stevensson, B., Sandström, D., and Maliniak, A. (2003). Conformational distribution functions extracted from residual dipolar couplings: A hybrid model based on maximum entropy and molecular field theory. *J. Chem. Phys.* 119: 2738-2746.

Strzelecka, T.E., and Rill, R.L. (1987). Solid State ^{31}P NMR Studies of DNA liquid crystalline phases. The isotropic to cholesteric transition. *J. Am. Chem. Soc.* 109: 4513-4518.

Tabayashi, K., and Akasaka, K. (1997). Natural abundance ^2H NMR for liquid crystal studies. application to 4'-(hexyloxy)-4-cyanobiphenyl. *J. Phys. Chem. B.* 101: 5108-5111.

Tenailleau, E., Lancelin, P., Robins, R.J., and Akoka, S. (2004). Authentication of the origin of vanillin using quantitative natural abundance C-13 NMR, *J. Agric. Food Chem.* 52: 7782-7787.

Texier-Bonniot, T., Berdagué, P., Robins, R., Remaud, G., and Lesot, P. (2018). Analytical contribution of deuterium 2D-NMR in oriented solvents to $^2\text{H}/^1\text{H}$ isotopic characterization: The case of Vanillin. *Flavour Frag J.* 34: 217-29.

Thiele, C.M., and Bermel, W. (2012). Speeding up the measurement of one-bond scalar (^1J) and residual dipolar couplings (^1D) by using non-uniform sampling (NUS). *J. Magn. Reson.* 216: 134-143.

Tjandra, N., and Bax, A. (1997-a). Direct measurement of distances and angles in biomolecules by NMR in a dilute liquid crystalline medium. *Science.* 278: 1111-1114.

Tjandra, N., Omichinski, J.G., Gronenborn, A.M., Clore, G. M. and Bax, A. (1997-b). Use of dipolar ^1H - ^{15}N and ^1H - ^{13}C couplings in the structure determination of magnetically oriented macromolecules in solution. *Nat. Struc. & Mol. Biol.* 4: 732-738.

Tjandra, N., Grzeisek, S., and Bax, A. (1996). Magnetic field dependence of nitrogen-proton J splittings in ^{15}N -enriched human ubiquitin resulting from relaxation interference and residual dipolar coupling. *J. Am. Chem. Soc.* 118: 6264-6272.

Tolman, J.R., Al-Hashimi, H.M., Kay, E. and Prestegard, J.H. (2001). Structural and Dynamic Analysis of Residual Dipolar Coupling Data for Proteins. *J. Am. Chem. Soc.* 123: 1416-1424.

Tracey, A.S., and Radley, K. (1984). Effects of composition on cholesteric behavior in the lyotropic mesophase system of potassium N-dodecanoyl-L-alaninate. *J. Phys. Chem.* 88: 6044-6048.

Tracey, A.S., and Diehl, P. (1975). The interaction of D- and L-alanine with an optically active model membrane system. *FEBS Lett.* 59: 131-132.

Trigo-Mouriño, P., Navarro-Vazquez, A., Ying, J., Gil, R.R., and Bax, A. (2011). Structural discrimination in small molecules by accurate measurement of long-range proton-carbon NMR residual dipolar couplings. *Angew. Chem., Int. Ed.* 50: 7576-7580.

Trigo-Mouriño, P., Merle, C., Koos, M.R. M., Luy, B., and Gil, R.R. (2013). Probing spatial distribution of alignment by deuterium NMR imaging. *Chem. Eur. J.* 19: 7013-7019.

Troche-Pesqueira, E., Anklin, C., Gil, R.R., and Navarro-Vazquez, A. (2017). Computer-assisted 3D structure elucidation of natural products using residual dipolar couplings. *Angew. Chem., Int. Ed.* 56, 3660-3664.

Tycko, R., Blanco, F.J., and Ishii, Y. (2000). Alignment of Biopolymers in Strained Gels: A new way to create detectable dipole-dipole couplings in high-resolution biomolecular NMR. *J. Am. Chem. Soc.* 122: 9340-9341.

Tzvetkova, P., Sternberg U., Gloge, T., Navarro-Vázquez A., and Luy B. (2019). Configuration determination by residual dipolar couplings: accessing the full conformational space by molecular dynamics with tensorial constraints. *Chem. Sci.* 10: 8774-8791.

Tzvetkova, P., Luy, B., and Simova, S. (2011). Chemical shift anisotropy-based measurement of enantiomeric excess for selected tetrasubstituted pyrrolidines. In book: *Topics in Chemistry and Material Science Vol. 5*, pp. 70-77 of *Current Issues in Organic Chemistry*, Eds. Nikolova, R.D., Simova, S., Denkova, P., Vayssilov, G.N., Heron Press Ltd, Birmingham.

Tzvetkova, P., Simova, S., and Luy, B. (2007). P.E. HSQC: A simple experiment for simultaneous and sign-sensitive measurement of ($^1\text{J}_{\text{CH}} + \text{D}_{\text{CH}}$) and ($^2\text{J}_{\text{HH}} + \text{D}_{\text{HH}}$) couplings. *J. Mag. Res.* 186: 193-200.

Veracini, C. (1985). In book: *Nuclear Magnetic Resonance of Liquid Crystals*, NATO ASI Series.

Waratchareeyakul, W., Hellemann, E., Gil, R.R., Chantrapromma, K., Langat, M.K., and Mulholland, D.A. (2017). Application of residual dipolar couplings and selective quantitative NOE to establish the structures of tetranortriterpenoids from *Xylocarpus rumphii*. *J. Nat. Prod.* 80: 391-402.

Wenzel, T.J. (2018). In book: *Differentiation of Chiral Compounds using NMR Spectroscopy*. 2nd Ed. John Wiley & sons, Hoboken, USA.

Wenzel, T.J., and Chisholm, C.D. (2011). Assignment of the absolute configuration of polyfunctional compounds by NMR using chiral derivatizing agents. *Prog. Nucl. Magn. Reson. Spectrosc.* 59: 1-63.

Wenzel, T.J. (2007). In book: *Discrimination of chiral compounds using NMR Spectroscopy*. Eds. Smyth, H.D.C., and Donovan, M.J., Wiley Interscience. New York. DOI: 10.1080/03639040701662677.

Yan, P., Li, G., Wang, C., Wu, J., Sun, Z., Martin, G.E., Wang, X., Reibarkh, M., Sauri, J., and Gustafson, K.R. (2019). Characterization by empirical and computational methods of dictyospiromide, an intriguing antioxidant alkaloid from the marine Alga *Dictyota Coriacea*. *Org. Lett.* 21: 7577-7581.

Zhao, J., Wang, M., Saroja, S.G., and Khan, I.A. (2021). NMR technique and methodology in botanical health product analysis and quality control. *J. of Pharm. and Biomed. Anal.* 207: 114376, 1-27.

Ziani, L., Lesot, P., Meddour, A., and Courtieu, J. (2007). Empirical determination of the absolute configuration of small chiral molecules using natural abundance ²H NMR in chiral liquid crystals. *Chem Commun.* 45: 4735-4739.